

**REPUBLIC DEMOCRATICS OF ALGERIA**

**MINISTER OF HIGHER EDUCATION AND SCIENTIFIC RESEARCH**

**University of Saad Dahlab Blida 1**

**Faculty of Technology**

**Department of Civil Engineering**



**Specialty: Geotechnical Engineering**

**FINITE ELEMENT ANALYSIS OF SLOPE STABILITY- BY  
NEW NUMERICAL PROCEDURE (SDIM)**

**Candidates :**

**Cumbe Edson Da Graça Manuel**

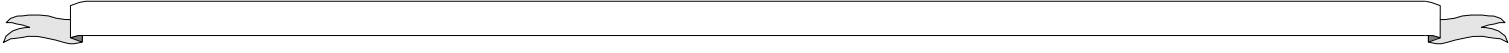
**Sitoe Crimildo Maria Antonio**

**Supervisor:**

**Prrofessor: DJILALI Amar Bouzid**

PROMO: 2019-2020

Blida, 2020



“Simple can be harder than complex: You have to work hard to get your thinking clean to make it simple. But it’s worth it in the end because once you get there, you can move mountains.”

— Steve Jobs

## **ACKNOWLEDGEMENTS**

The development of this research, at the end of the master's cycle would not be possible without the support of some relevant parties. Therefore, we intend to thank all those who have always supported us and contributed to the realization and implementation of this final stage of our training, the Master in Geotechnical Engineering in this institution Blida University.

In this way we would like to thank: our families, because all this has been possible thanks to the effort and dedication they have always had. To our Professor Doctor Djilali Amar Bouzid for his availability, his understanding and his confidence to give us this topic and take charge of this project, under his guidance towards the development of our work, always express his enriching opinions for the growth of this end-of-cycle project and enrichment of our training. To all the teachers who have contributed to our training throughout the degree (license) and the master, for all the knowledge, dedication and contribution to our personal and educational growth. To the friends with whom we have developed the practice of the internship and who have always been present, with all the support, affection and understanding.

Thank you very much to all!

## *Dedications 1*

I dedicate my dissertation work to my family and many friends. A special feeling of gratitude to my loving parents, Manuel Bernardo Cumbe and Eugenia da Graça Salomão whose words of encouragement and push for tenacity ring in my ears. My sisters Katia, Sheila and Ivone have never left my side and are very special, also especially thanks to my brothers Dercio and Hilario who always shared supported me right when I needed the most. I also dedicate this dissertation to my many friends and my Grandmothers Isabel Chipissene Dique and Florencia M. Marrengule who have supported me throughout the process. I will always appreciate all they have done, especially to the supervisor Dr. Amar Bouzid for helping me develop my technology skills and understanding of the matter, to my colleague for the many hours of proofreading and helping me to master the leader dots. To my aunties and cousins who have been my best cheerleaders.

*Edson da Graca M. Cumbe*

## **Dedication 2**

With the expression of my gratitude, I dedicate this modest work to those who, have been always with me, parents, brothers and friends, they have been there supporting me.

I dedicate this work in particular to my father Marcos Antonio Siteo who has always been there to pressure me, doing the work of every father that is to provide and teach the child to seek wisdom and knowledge, I also dedicate my mother who was also there for me bear and give me strength to continue, my heart praises God for everything that provided me.

*Crimildo Maria A. Siteo*

## Abstract

The assessment of slope stability factor by a finite element analysis using the shear strength reduction method (SRM) is one of the most powerful methods that have been proposed as a competitive to the conventional limit equilibrium methods (LEM) in the last two decades

. Although the SRM enjoys several advantages, it owns unfortunately many shortcomings. As an alternative, a new finite element approach called stress deviator increasing method (SDIM) is proposed in this paper. The new approach assesses the slope stability by incrementally increasing the mobilized principal stress deviator until the soil failure is reached. The incremental increasing of the factor that controls the expansion of principal stress Mohr's circles in the SDIM, follows the reverse path as that of reducing factor in the SRM. The numerical procedure is based then on a rigorous formulation as it preserves the definition of the safety factor consistent with that of LEM and maintains the progressive development of the shear stress on same plane on which the shear strength will occur at failure. The proposed method deals with the actual material by using the real strength parameters ( $c$ ,  $\phi$ ) and  $\psi$  rather than those reduced by a factor. The results of SDIM encoded in a computer code called *S<sup>4</sup>DINA* were thoroughly assessed against those of both SRM and LEM.

**Key words:** Slope stability, Factor of safety, SDIM, Plastic strain, S<sup>4</sup>DINA

---

## Résumé

L'évaluation du facteur de stabilité de la pente par une analyse par éléments finis en utilisant la méthode de réduction de la résistance au cisaillement (SRM) est l'une des méthodes les plus puissantes qui ont été proposées comme compétitive par rapport aux méthodes conventionnelles d'équilibre limite (LEM) au cours des deux dernières décennies. Bien que le SRM bénéficie de plusieurs avantages, il présente malheureusement de nombreuses lacunes. Comme alternative, une nouvelle approche par éléments finis appelée méthode d'augmentation des déviateurs de contrainte (SDIM) est proposée dans cet article. La nouvelle approche évalue la stabilité de la pente en augmentant progressivement le déviateur de contrainte principal mobilisé jusqu'à ce que la rupture du sol soit atteinte. L'augmentation incrémentielle du facteur qui contrôle l'expansion des cercles de Mohr de contrainte principale dans le SDIM, suit la voie inverse comme celle du facteur de réduction dans le SRM. La procédure numérique repose alors sur une formulation rigoureuse car elle préserve la définition du facteur de sécurité cohérente avec celle du LEM et maintient le développement progressif de la contrainte de cisaillement sur le même plan sur lequel la résistance au cisaillement se produira à la rupture. La méthode proposée traite du matériau réel en utilisant les paramètres de résistance réelle ( $c$ ,  $\phi$ ) et  $\psi$  plutôt que ceux réduits d'un facteur. Les résultats du SDIM codé dans un code informatique appelé *S<sup>4</sup>DINA* ont été soigneusement évalués par rapport à ceux du SRM et du LEM.

**Mot-clé :** Stabilité des pentes, Facteur de sécurité, SDIM, Déformation Plastic, *S<sup>4</sup>DINA*

---

يعد تقييم عامل استقرار المنحدر من خلال تحليل عنصر محدود باستخدام طريقة تقليل مقاومة القص (SRM) أحد أقوى الطرق التي تم اقتراحها على أنها منافسة لطرق توازن الحد التقليدية (LEM) في العقد الماضيين. على الرغم من أن SRM تتمتع بالعديد من المزايا، إلا أنها تمتلك للأسف العديد من السلبيات.

كبديل، تم اقتراح نهج جديد للعناصر المحدودة يسمى طريقة زيادة انحراف الضغط (SDIM) في هذه المقالة العلمية. يقوم النهج الجديد بتقييم استقرار المنحدر عن طريق زيادة انحراف الضغط الرئيسي المعبأ بشكل تدريجي حتى يتم الوصول إلى فشل التربة.

الزيادة التدريجية للعامل الذي يتحكم في توسع الضغط الرئيسي لدوائر Mohr في SDIM، يتبع المسار العكسي مثل عامل الاختزال في SRM.

يعتمد الإجراء العددي بعد ذلك على صياغة صارمة لأنها تحافظ على تعريف عامل الأمان المتسق مع ذلك الخاص بـ LEM ويحافظ على التطور التدريجي لضغط القص على نفس المستوى الذي ستحدث عليه مقاومة القص عند الفشل.

تتعامل الطريقة المقترحة مع المادة الفعلية باستخدام معلمات القوة الحقيقية (C،  $\phi$ ) و  $\psi$  بدلاً من تلك التي يتم تقليلها بواسطة عامل.

تم تقييم نتائج SDIM المشفرة في رمز كمبيوتر يسمى S ^ 4 DINA بدقة مقابل نتائج كل من SRM و LEM.



# Summary

ACKNOWLEDGEMENTS .....	2
<i>Dedications 1</i> .....	3
<b>Dedication 2</b> .....	4
Abstract.....	5
Résumé .....	6
List of Tables.....	15
General Introduction .....	16
1 Introduction.....	19
1.2 Theoretical determination of the pressure coefficient of the earth at rest .....	19
1.3 Importance of in situ stresses .....	19
1.4 Soil mass with horizontal surface .....	20
1.5 . Magnitude and measurement of in situ stresses .....	20
1.6. Definition of the coefficient of earths pressure at rest $K_0$ .....	21
1.7. Expressions of the coefficient of earths pressure at rest $K_0$ .....	21
1.8 . Loading conditions .....	22
1.9. Unloading conditions .....	23
1.10. Over-consolidated soil .....	23
1.11. Isotropic linear elasticity .....	23
1.12. INITIAL STRESSES IN SLOPING GROUND.....	24
Conclusion.....	26
2.1.1 Introduction.....	28
2.2.1 Fellenius method .....	28
2.3.1 Bishop's method.....	29
2.4.1 Bishop's Method Simplified.....	30
2.5.1 Janbu's Method .....	30
2.6.1 Spencer's method.....	31
2.7.1 Method of Lowe and Karafiath.....	33
2.8.1 Morgenstern and Price's Method.....	33
Conclusion.....	34
3.1.1 Introduction.....	36
3.1.2 The Strength Reduction Method (SRM).....	36
3.1.3 The SRM Drawbacks .....	37
3.1.4 Advantages of the SRM.....	40
3.2.1 Gravity Increase Method (GI) .....	41
3.2.2 Determination of the factor of safety .....	42

3.2.3 Drawbacks (GIM) .....	42
3.3.1 Finite element methods for slopes .....	43
3.3.2 Brief description of the finite element model .....	43
3.4.1 Finite Elements Limit Analysis (FELA) .....	44
3.4.2 Safety factor obtained from finite element analysis .....	46
Conclusion .....	48
4. Introduction .....	50
4.1 . New method for the slope stability analysis: Increasing of the mobilized principal stress deviator	50
4.1.2 The computer Program S4DINA : Computational procedure .....	54
4.2.1 Spurious zones of plastic strains and the importance of visualizing plastic deformation areas	58
4.2.2 Comparative analysis involving the slope safety factor and contours of plastic deformation zones	59
Conclusion .....	61
5.1. Introduction.....	63
5.2. Parametrical Study.....	63
5.3. Input Soil Parametric .....	64
5.4. Comparison between the results of calculation of LEM and SDIM.....	67
5.5. Analyses of the influence of the input parametric .....	67
5.6 Iteration Number, Slope with Foundation and without foundation. ....	67
Associated flow rule. ....	67
Non-associated.....	68
5.6.1. Iteration Number, Slope without Foundation.....	69
5.7. Analyses of the plastic zones and stress contours in a slope stability problem. ....	71
5.7.1. Associated flow rule. ....	71
a) Number of iterations 100.....	71
b) Number of iterations 200.....	72
c) Number of iterations 300.....	73
d) Number of iterations 400.....	74
e) Number of iterations 500.....	75
f) Number of iterations .....	76
g) Number of iterations 700.....	77
h) Number of iterations 800.....	78
i) Number of iterations 900.....	79
j) Number of iterations 1000.....	80
k) Number of iterations 1100.....	81
l) Number of iteration 1200 .....	82
m) Number of iterations 1300.....	83
n) Number of iterations 1400.....	84

o)	Number of iterations 1500.....	85
5.7.2.	Non-Associated flow rule.....	86
a)	Number of Iterations 100 .....	87
b)	Number of iterations 200.....	88
c)	Number of iterations 300.....	89
d)	Number of iterations .....	90
e)	Number of iterations 500.....	91
f)	Number of iterations 600.....	92
g)	Number of iterations 700.....	93
h)	Number of iterations 800.....	94
i)	Number of iterations 900.....	95
j)	Number of iterations 1000.....	96
k)	Number of iterations 1100.....	97
l)	Number of iterations 1200.....	98
m)	Number of iterations 1300 .....	99
n)	Number of iterations 1400.....	100
o)	Number of iterations 1500.....	101
5.8.	Deformation Parametric .....	102
5.8.1.	Young's Modulus Analyses .....	102
	Associated flow rule. ....	102
5.8.2.	Associated flow rule .....	103
a)	Young's Modulus E=1000 kN/m <sup>2</sup> .....	105
b)	Young's Modulus E=5000kN/m <sup>2</sup> .....	106
c)	Young's Modulus E=10000kn/m <sup>2</sup> .....	107
d)	Young's Modulus E=100000KN/m <sup>2</sup> .....	108
5.8.3.	Non-Associate flow rule. ....	109
5.8.4.	Non associated flow rule. ....	109
a)	Young's Modulus E=1000kN/m <sup>2</sup> .....	110
b)	Young's Modulus E=5000kN/m <sup>2</sup> .....	111
c)	Young's Modulus E=10000kn/m <sup>2</sup> .....	112
d)	Young's Modulus E=100000kn/m <sup>2</sup> .....	113
5.8.5.	Poisson ratio Evaluation.....	114
	1.2 Analyse of Poisson ratio on slope with Foundation and without foundation.....	114
5.8.6.	Associated flow rule. ....	114
5.8.7.	Associated flow rule. ....	115
a)	Poisson Ratio 0.10.....	116
b)	Poisson Ratio 0.15.....	117

c) Poisson Ratio 0.20.....	118
d) Poisson Ratio 0.25.....	119
e) Poisson Ratio 0.30.....	120
f) Poisson Ratio 0.35.....	121
g) Poisson Ratio 0.40.....	122
h) Poisson Ratio 0.45.....	123
i) Poisson Ratio 0.49.....	124
<b>5.8.8. Non associated flow rule .....</b>	<b>125</b>
<b>Non-Associated flow rule .....</b>	<b>126</b>
a) Poisson Ratio 0.10.....	127
b) Poisson Ratio 0.15.....	128
c) Poisson ratio 0.20.....	129
d) Poisson Ratio 0.25.....	130
e) Poisson ratio 0.30.....	131
f) Poisson Ratio 0.35.....	132
g) Poisson Ratio 0.40.....	133
h) Poisson Ratio 0.45.....	134
i) Poisson Ratio 0.49.....	135
<b>5.9.2. Associated flow rule with foundation. ....</b>	<b>137</b>
<b>5.9.3. Non-associated without foundation .....</b>	<b>143</b>
<b>Conclusion.....</b>	<b>149</b>
<b>Conclusion.....</b>	<b>150</b>
<b>References .....</b>	<b>151</b>



Figure 5.11 48 Strain contours corresponding to the step of failure for 900 iterations, with the foundation	95
Figure 5.11 49 Strain contours corresponding to the step of failure for 900 iterations, without the foundation.	96
Figure 5.11 50 Strain contours corresponding to the step of failure for 1000 iterations, with the foundation	96
Figure 5.11 51 Strain contours corresponding to the step of failure for 1000 iterations, without the foundation.	97
Figure 5.11 52 Strain contours corresponding to the step of failure for 1100 iterations, with the foundation	97
Figure 5.11 53 Strain contours corresponding to the step of failure for 1100 iterations, without the foundation	98
Figure 5.11 54 Strain contours corresponding to the step of failure for 1200 iterations, with the foundation	98
Figure 5.11 55 Strain contours corresponding to the step of failure for 1200 iterations, without the foundation	99
Figure 5.11 56 Strain contours corresponding to the step of failure for 1300 iterations, with the foundation.	99
Figure 5.11 57 Strain contours corresponding to the step of failure for 1300 iterations, without the foundation	100
Figure 5.11 58 Strain contours corresponding to the step of failure for 1400 iterations, with the foundation.	100
Figure 5.11 59 Strain contours corresponding to the step of failure for 1400 iterations, without the foundation	101
Figure 5.11 60 Strain contours corresponding to the step of failure for 1500 iterations, with the foundation.	101
Figure 5.11 61 Strain contours corresponding to the step of failure for 1500 iterations, without the foundation.	102
Figure 5.11 62 Evaluation of the young's Modulus variation. Associated .....	103
Figure 5.11 63. Evaluation of the young's Modulus variation. Associated .....	104
Figure 5.11 64 Strain contours corresponding to the step of failure for E=1000 kN/m <sup>2</sup> , with the foundation.	105
Figure 5.11 65 Strain contours corresponding to the step of failure for E=1000 kN/m <sup>2</sup> , without the foundation.	105
Figure 5.11 66 Strain contours corresponding to the step of failure for E=5000 kN/m <sup>2</sup> , with the foundation	106
Figure 5.11 67 Strain contours corresponding to the step of failure for E=5000 kN/m <sup>2</sup> , without the foundation.	106
Figure 5.11 68 Strain contours corresponding to the step of failure for E=1000 kN/m <sup>2</sup> , with the foundation.	107
Figure 5.11 69 Strain contours corresponding to the step of failure for E=10000 kN/m <sup>2</sup> , without the foundation.	107
Figure 5.11 70 Strain contours corresponding to the step of failure for E=100000 kN/m <sup>2</sup> , with the foundation	108
Figure 5.11 71 Strain contours corresponding to the step of failure for E=1000 kN/m <sup>2</sup> , without the foundation.	108
Figure 5.11 72 Evaluation of the young's Modulus variation. Non-associated .....	109
Figure 5.11 73 Evaluation of the young's Modulus variation. Non-associated .....	110
Figure 5.11 74 Strain contours corresponding to the step of failure for E=1000kN/m <sup>2</sup> , with the foundation	110
Figure 5.11 75 Strain contours corresponding to the step of failure for E=1000 kN/m <sup>2</sup> , without the foundation.	111
Figure 5.11 76 Strain contours corresponding to the step of failure for E=5000 kN/m <sup>2</sup> , with the foundation.	111
Figure 5.11 77 Strain contours corresponding to the step of failure for E=5000 kN/m <sup>2</sup> , without the foundation.	112
Figure 5.11 78 Strain contours corresponding to the step of failure for E=10000 kN/m <sup>2</sup> , with the foundation.	112
Figure 5.11 79 Strain contours corresponding to the step of failure for E=10000 kN/m <sup>2</sup> , without the foundation.	113
Figure 5.11 80 Strain contours corresponding to the step of failure for E=100000 kN/m <sup>2</sup> , with the foundation.	113
Figure 5.11 81 Strain contours corresponding to the step of failure for E=100000 kN/m <sup>2</sup> , without the foundation	114
Figure 5.11 82 Evaluation of the Poisson ratio variation. Associated.....	115
Figure 5.11 83 Evaluation of the Poisson ratio variation. Associated.....	116
Figure 5.11 84 Strain contours corresponding to the step of failure for v=0.10, with the foundation. ...	116
Figure 5.11 85 Strain contours corresponding to the step of failure for v=0.10, without the foundation	117
Figure 5.11 86 Strain contours corresponding to the step of failure for v=0.15, with the foundation. ...	117
Figure 5.11 87 Strain contours corresponding to the step of failure for v=0.10, without the foundation.	118
Figure 5.11 88 Strain contours corresponding to the step of failure for v=0.20, with the foundation ....	118
Figure 5.11 89 Strain contours corresponding to the step of failure for v=0.20, without the foundation.	119
Figure 5.11 90 Strain contours corresponding to the step of failure for v=0.25, with the foundation. ...	119
Figure 5.11 91 Strain contours corresponding to the step of failure for v=0.25, without the foundation	120
Figure 5.11 92 Strain contours corresponding to the step of failure for v=0.30, without the foundation	120
Figure 5.11 93 Strain contours corresponding to the step of failure for v=0.30, without the foundation.	121
Figure 5.11 94 Strain contours corresponding to the step of failure for v=0.35, with the foundation. ...	121
Figure 5.11 95 Strain contours corresponding to the step of failure for v=0.35, without the foundation.	122
Figure 5.11 96 Strain contours corresponding to the step of failure for v=0.40, with the foundation. ...	122

Figure 5.11 97 Strain contours corresponding to the step of failure for $\nu=0.40$ , without the foundation.	123
Figure 5.11 98 Strain contours corresponding to the step of failure for $\nu=0.45$ , without the foundation	123
Figure 5.11 99 Strain contours corresponding to the step of failure for $\nu=0.45$ , with the foundation ....	124
Figure 5.11 100 Strain contours corresponding to the step of failure for $\nu=0.49$ , with the foundation ..	124
Figure 5.11 101 Strain contours corresponding to the step of failure for $\nu=0.49$ , without the foundation	125
Figure 5.11 102 Evaluation of the Poisson ratio variation. Non-Associated .....	126
Figure 5.11 103 Evaluation of the Poisson ratio variation. Non-Associated .....	127
Figure 5.11 104 Strain contours corresponding to the step of failure for $\nu=0.10$ , with the foundation .	127
Figure 5.11 105 Strain contours corresponding to the step of failure for $\nu=0.10$ , without the foundation	128
Figure 5.11 106 Strain contours corresponding to the step of failure for $\nu=0.15$ , with the foundation ..	128
Figure 5.11 107 Strain contours corresponding to the step of failure for $\nu=0.15$ , without the foundation.	129
Figure 5.11 108 Strain contours corresponding to the step of failure for $\nu=0.20$ , with the foundation ..	129
Figure 5.11 109 Strain contours corresponding to the step of failure for $\nu=0.20$ , without the foundation.	130
Figure 5.11 110 Strain contours corresponding to the step of failure for $\nu=0.25$ , with the foundation ..	130
Figure 5.11 111 Strain contours corresponding to the step of failure for $\nu=0.25$ , without the foundation.	131
Figure 5.11 112 Strain contours corresponding to the step of failure for $\nu=0.30$ , with the foundation ..	131
Figure 5.11 113 Strain contours corresponding to the step of failure for $\nu=0.30$ , without the foundation.	132
Figure 5.11 114 Strain contours corresponding to the step of failure for $\nu=0.35$ , with the foundation ..	132
Figure 5.11 115 Strain contours corresponding to the step of failure for $\nu=0.35$ , without the foundation.	133
Figure 5.11 116 Strain contours corresponding to the step of failure for $\nu=0.40$ , with the foundation. ..	133
Figure 5.11 117 Strain contours corresponding to the step of failure for $\nu=0.40$ , without the foundation.	134
Figure 5.11 118 Strain contours corresponding to the step of failure for $\nu=0.45$ , with the foundation. .	134
Figure 5.11 119 Strain contours corresponding to the step of failure for $\nu=0.45$ , without the foundation.	135
Figure 5.11 120 Strain contours corresponding to the step of failure for $\nu=0.49$ , with the foundation ..	135
Figure 5.11 121 Strain contours corresponding to the step of failure for $\nu=0.49$ , without the foundation.	136
Figure 5.11 122 Evaluation of the Finite elements variation. Associated .....	137
Figure 5.11 123 Evaluation of the Finite elements variation. Non-Associated .....	143

# List of Tables

Table 3 1 Soil Parametric.....	43
Table 5 2 1. Rapport of the Results of the effect of the Number of Iteration for FS of the 3 methods. ....	67
Table 5 2 2 Rapport of the Results of the effect of the Number of Iteration for FS of the 3 methods .....	68
Table 5 2 3 Rapport of the Results of the effect of the Number of Iteration for FS of the 3 methods .....	69
Table 5 2 4 Rapport of the Results of the effect of the Number of Iteration for FS of the 3 methods. ....	86
Table 5 2 5 Results of Evaluation of the young's Modulus variation. Associated. ....	102
Table 5 2 6 Results of Evaluation of the young's Modulus variation. Associated .....	103
Table 5 2 7 Results of Evaluation of the young's Modulus variation. Non-associated .....	109
Table 5 2 8 Results of Evaluation of the young's Modulus variation. Non-associated .....	109
Table 5 2 9 Results of Evaluation of the Poisson ratio variation. Associated .....	114
Table 5 2 10 Results of Evaluation of the Poisson ratio variation. Associated .....	115
Table 5 2 11 Results of Evaluation of the Poisson ratio variation. Non-Associated .....	125
Table 5 2 12 Results of Evaluation of the Poisson ratio variation. Non-Associated .....	126



## Introduction

The principles of slope stability, using the Finites Elements Methods (FEM) have been developed over the past seventy years, from which practical problems are addressed. Although the slope failure mechanism can be difficult to predict, the principles used in a review of the Standards of Practice are relatively straight forward.

Slopes in soils and rocks are ubiquitous in nature and in man-made structures. Highways, dams, dikes, canals, and piles are built by tilting the side faces of the ground, as building slopes is usually less expensive than building walls. Natural forces (wind, water, snow, etc.) modify the topography of the Earth, often have unstable slopes. The failures of natural slopes (landslides) and artificial slopes have caused numerous deaths and destruction, economic losses and environmental damage. Some failures are sudden and catastrophic; others are insidious. Some failures are widespread; others are localized.

Geotechnical engineers should pay special attention to geology, surface drainage, groundwater, and shear strength of soils when evaluating slope stability. However, we are handicapped by the geological variability of soils and the methods of obtaining reliable values of shear strength. Slope stability analyzes are based on simplifying assumptions, and the design of a stable slope relies heavily on experience and careful site investigation.

An analysis of the stability of a slope begins with the assumption that the stability of a slope is the result of descending or moving (i.e. gravitational) and resistant (or ascending) forces. These forces act in equal and opposite directions. Resistance forces must be greater than moving forces for a slope to be stable. The relative stability of a slope (or its stability at a given time) is generally transmitted by geotechnical engineers through a safety factor  $F_s$ . And so, over the years, this factor has been found to be effective on the basis of the method used for its identification, but this is not always shown to be true in the results, since it is based on reducing the internal forces of the soil, that is, devaluation of soil conditions tends to show results that do not match the soil condition.

### OVERVIEW OF THE CHAPTERS

The first chapter of this paper we are going to talk about the theories behind the calculation of the  $K_0$  coefficient of the earth at rest (in-situ-stresses).

In the second chapter, we will be reviewing some limit equilibrium methods to calculate the factor of safety, hence we will be describing each method and demonstrating its formulations that lead to the calculation of the factor of safety.

The third is focus in stability of slope using finite elements method, in this chapter we are going to describe these methods strength reduction method (SRM), gravity increasing method (GIM) and finite elements analyses

(FELA), and meticulously show how they function also present their formulations that are going to lead us into the calculation of the factor of safety.

The fourth chapter in this paper is a review of the SDIM (STRESS DEVIATOR INCREASING METHOD) and computer program called S<sup>4</sup>DINA (Soil Stability Study by Stress Deviator Increasing using Numerical Analysis), were this method will be presented with its formulations.

The last chapter we will be performing a parametrical studies where we are going to verify the applicability and functionality of the program S<sup>4</sup>DINA and SDIM, comparing this method to those from LEM (Bishops and Morgenstern-Price).

---

**CHAPTER I:**

**THE IN-SITU STRESSES**

# **1 Introduction**

Before we make a calculation in geotechnical engineering, it is very important for us to start by determining the initial stresses. It is preponderant to calculate the initial stresses because generally the majority of the problems that we find in geotechnical engineering depend on it. The initial stresses depend on the nature, land geometry, geological history and the deposit conditions.

The first researcher that proposed the expression of calculating the initial stresses was Jacky, and a part of his formulation was based in empiric expressions, taken from laboratory experience. The aim of this chapter is to present some synthesis that are going to lead us to the calculation of the initial stresses in slope.

## **1.2 Theoretical determination of the pressure coefficient of the earth at rest**

The initial state of the stresses in the soil, specifically in the slopes depend on several factors such as: the geometry of the slope, the loading and geological history of the soil, the presence of water in the soil and the state of equilibrium of the slope. These factors can make it easier for us to predict how the soil on the slope will behave.

In the case of soil masses with a horizontal surface, the principal stresses correspond to the horizontal stress and the vertical stress. The effective vertical stress is given by the pressure due to the weight of the earth above the point considered. The effective horizontal stress is more difficult to determine because it depends on both the type of soil and the loading history. In the presence of a mass of soil with a sloping geometry, determining the initial stress field becomes a problem of a high level of difficulty.

## **1.3 Importance of in situ stresses**

The importance of geological and topographical setting in relation to natural slopes was the major factor for the understanding of soils behaviour as it leads us to more accurate predictions in such ways that today, newer methods are emerging and this information is the essential for their validation.

As it has been defined the geology is the science of earth's history, composition, and structure. This science has existed long before the advance of soil engineering. General surficial geology of the area includes the study of slopes, tributary valleys, landslides, springs and seeps, sinkholes, exposed rock section, origin of deposit, and the nature of unconsolidated overburden. Hence this allowed engineer to get more familiarized with the initial stress for natural slope design.

With that said, topography is defined as the features of plain or region. Then for this last branch is very important due to its contribution into knowing the earth surfaces features with which paired with geology gives better mechanical parametric to work with while trying to build a numerical models for soil study in this case an earth slope, all this leads to point where its proved that slope stability depends upon the slope's angle, rock and soil formations, evidence of past slope movement, and drainage features.

Geology and topography survey both play a very important role into a design of an analytical model that will feature all of the characteristics of the soil in place where will be implanted the slope, hence this will be governed by in situ stresses measurement. The slope stability depends upon the strength of the soil before excavation and after excavation. This induced stresses gotten after excavation are a function of the slope angle and the in situ stresses which existed before excavation.

Because of the capital importance of the in situ stresses, designers of earth structures have been incorporating this information into their models for better predictions in such way that today a model without this parameters on it may not be taken in consideration for bigger projects as tunnels, underground openings, where this knowledge is relevant to the understanding of soil or rock behaviour which allowed operators or designers to control this operations choosing for each step of a project what kind of method is applicable by only regarding the in situ stresses. In recent years engineer have been facing serious stability problems caused by the excavations which leads them to give a better look into the lateral ground stresses that by the removal of the soil after an openings cause a lot problems, such as rock burst in rock masses or landslide in soil this have showed to engineers that mechanical behaviour of soil is dependent on the stresses paths and this fact is important for a proper understanding of the role of in situ stress in geotechnical problems.

The numerical approach that has been built to study the stresses evolution, has led engineer into a better understanding of geotechnical issues due to its versatility and powerful predictions that conduct a path which in further development can be made in order to turn this tools more accurate regarding the studied soil. Finite elements have got a huge attention since it's allowed a more complex models to be studied and accurate predictions over the year have been made, in such way that even this method is getting more powerful over years. Right before this tools for slope studies have been made in which those slopes study were based on the assumption in situ horizontal and vertical principal stresses.

#### **1.4 Soil mass with horizontal surface**

The initial stress of the ground in a slope can be a complex study bringing several aspects. For this, we will analyze this phenomenon more clearly, starting with the analysis of the horizontal stress of the ground at rest ( $K_0$ ), which turns out to be the most common starting point.

#### **1.5. Magnitude and measurement of in situ stresses**

In this chapter an initial state of stress was defined in terms of the parameter  $k$  for total stresses and the parameter  $K_0$  for effective stresses.

Consistent with accepted practice two important assumptions were made, namely:

The vertical and horizontal normal stresses at any point are principal stresses when the ground surface is horizontal and the vertical normal stress at any point is equal to the corresponding overburden pressure at that same point.

As we know earth structure can be tricky to assume that they are stable in long-term by that not always these assumption can be taken as granted to a good stabilization since the tectonics movements can cause a variation of the orientation of the principal normal stresses both vertical and horizontal so its kind unpredictable. Again it may sometimes be inaccurate to assume the vertical normal stress to be equal to the overburden pressure particularly in rock masses. Where the sloping ground with a given uniform inclination to the horizontal, the description stresses which is considered in some. For the present let us consider the magnitude of initial stresses based on assumption considered above.

### **1.6. Definition of the coefficient of earths pressure at rest $K_0$**

$K_0$  is the ratio of the initial and vertical stresses given by the vertical and horizontal stress equations (1.1). This coefficient depends on the characteristics of the soil and in some cases, on the history of the stresses to which the massif is subjected.

In 1962 researchers Bishop and Henkel added that the coefficient of rest also depends on the type of soil and the degree of saturation to the list of factors that influence the state of the initial stresses. The resting earth pressure coefficient  $K_0$  could also be related to the history of deformations and to the microstructure of the soil.

$$K_0 = \frac{\sigma'_{h0}}{\sigma'_{v0}} \quad (1.1)$$

### **1.7. Expressions of the coefficient of earths pressure at rest $K_0$**

Many researchers in this field have been interested in the determination of the pressure coefficient of earths at rest by the development of theories and empirical, semi-empirical or analytical formulas based on the analysis of the stress state of a pressure of ground. The various formulas proposed are linked to certain intrinsic parameters of the soil and can be classified as follows:

- Soil loading history (normally consolidated or over-consolidated);
- The nature of the soil (clay, sand, etc.);
- The loading and unloading conditions.

The different methods of determining the pressure coefficient of the earth at rest are classified according to their loading history, which can be compared to the geological history of the site.

## 1.8. Loading conditions

Jacky (1944) in this way theoretically studied the stability of a massif with the Mohr-Coulomb criterion and established the value of the ratio of horizontal stresses  $e$  of vertical stresses at limit equilibrium he obtained:

$$K_0 = \frac{1 - \sin\phi}{1 + \cos\phi} \left( 1 + \frac{2}{3} \sin\phi' \right) \quad (1.2)$$

This expression is usually simplified and we use the following approximate formula, called Jaky's formula (1944) (1.7):

$$K_0 = 1 - \sin\phi' \quad (1.3)$$

Jaky's formula applies to normally consolidated soils without restriction due to their nature (sand, silt, clay, etc.). Hendron (1963), with theoretical considerations drawn from the assembly of quartz spheres, He arrived at an expression relating the pressure coefficient of the earth at rest to the coefficient of Friction ( $f$ ) between quartz spheres (1.8). The expression is applicable only to sands, which are normally consolidated sands.

$$K_0 = \left( \frac{1-f}{2(1+f)} \right) \quad (1.4)$$

The expression of the coefficient of friction  $f$  (1.9), taken from the work of Thurston and Deresiewicz (1959), allows to express the pressure coefficient of the earths at rest  $K_0$  exclusively as a function of the angle of internal friction (1.10).

$$\sin\phi = \frac{1}{3} \cdot \frac{4}{9} \sqrt{6f} \quad (1.5)$$

Brooker and Ireland (1965), after comparison with experimental data from a series of tests on 5 clays (tested with the oedometer), made a slight readjustment on Jaky's formula (1.7). Indeed, they consider the simplified Jaky equation more suited to granular soils and propose a slightly modified expression (1.11) for cohesive soils.

$$K_0 = 0.95 - \sin\phi' \quad (1.6)$$

Although the equation of Brooker and Ireland (1965) seems close to the simplified equation of Jaky, it is, by calculation, closer to its first formulation (1.6) than to the formula Simplified by Jaky (1.7). (Figure 1.4)

This finding would certainly explain this slight modification to the Jaky equation.

Schmidt (1966) revises the formula proposed by Brooker and Ireland (1965) (1.11) because they judge the experimental data of the tests on the 5 clays "reasonably better represented" by the new expression (1.12):

$$K_0 \approx 1 - \sin(1.2\phi') \quad (1.7)$$

Bishop (1948) refers to the degree of mobilization of the angle of internal friction. He finds,

Through his experiments, the higher the porosity, the lower the mobilized friction angle and consequently the value of  $K_0$  may be suspected of increasing.

## 1.9. Unloading conditions

Unloading corresponds to the action of reducing the loads placed on the ground, in this way by reducing the vertical stress, it also causes a decrease in horizontal stress.

The study carried out by researcher Schmidt in 1967 on loading and unloading revealed a correspondence between the last point of the loading curve and the first point of the unloading curve. The pressure coefficient of the earth at rest during unloading  $K_0$  at the start of unloading is therefore the same as that of the soil normally consolidated during loading ( $K_0$ ).

Hendron's expression (1.14) links coefficient of earth's pressure at rest  $K_0$  in unloading ( $K_0$ ), with:

- The ratio 
$$\frac{\sigma_{vmax}}{\sigma_v} \quad (1.8)$$

## 1.10. Over-consolidated soil

Over-consolidation is a phenomenon that is mainly noted in clay soils. An over-consolidated clay is a normally consolidated clay which, having undergone an important loading during its history, is found discharged by a geological (or other) mechanism. The earth pressure coefficient  $K_0$  can also be obtained in the laboratory during a compression test which simulates the conditions under which the sample was located in the soil. These conditions are characterized by the total vertical stress in place and by zero lateral strains. The tests are triaxial drained tests with zero lateral strain or oedometric tests with measurement of the lateral stress (Serratrice and Flavigny, 1993). The vertical stress applied to the specimen varies so as to simulate the loadings and successive discharges undergone by the soil during its history.

## 1.11. Isotropic linear elasticity

The soil being a three-phase material, it was necessary to facilitate the study by the formulation of the isotropic linear environment where we have the same deformation in all directions, because this phenomenon does not correspond to reality, but it brings us closer to analytical values with which we can easily work, the pressure coefficient of the earths at rest can be associated with the Poisson's ratio by the equation (1.4).

$$K_0 = \frac{\nu}{1-\nu} \quad (1.9)$$

Where  $\nu$  is the Poisson's ratio of the soil. It is the same for the expressions deduced from the more complex constitutive laws, like laws of elastoplastic type.

(1.4) is easily demonstrated by using an oedometric condition

$$\sigma = \sigma_1 = \lambda tr \epsilon \delta + 2\mu \begin{pmatrix} \epsilon \alpha \\ 0 \\ 0 \end{pmatrix} \quad (1.9)$$

$$\sigma_1 = \lambda \epsilon \alpha + 2\mu \epsilon \quad (1.9.1)$$



$$\sigma_3 = \lambda \epsilon_a \quad \Rightarrow \quad \frac{\sigma_3}{\sigma_1} = \frac{\lambda}{\lambda + 2\mu} = \frac{E\nu}{(1+\nu)(1-2\nu)} \frac{1}{\frac{E\nu}{(1+\nu)(1-2\nu)} + \frac{E}{(1+\nu)}} \quad (1.9.2)$$

$$\Rightarrow \frac{\sigma_3}{\sigma_1} = \frac{E\nu}{(1+\nu)(1-2\nu)} \frac{1}{\frac{E}{1+\nu} \left(1 + \frac{\nu}{(1-2\nu)}\right)} \frac{E\nu}{(1-\nu)(1-2\nu)} \frac{1+\nu}{E \left(\frac{1-\nu}{1-2\nu}\right)} \quad (1.9.3)$$

$$\Rightarrow \frac{\sigma_3}{\sigma_1} = \frac{\nu}{1-\nu} \quad (1.9.4)$$

The stresses  $\sigma_3$  and  $\sigma_1$  can be assimilated to the vertical and horizontal stresses because of the weight of the ground  $\sigma'_{v0}$  and  $\sigma'_{h0}$  already exposed on equation. By substituting the stresses  $\sigma_3$  and  $\sigma_1$  by the stresses  $\sigma'_{v0}$  and  $\sigma'_{h0}$ , we obtain the equation (1.4).

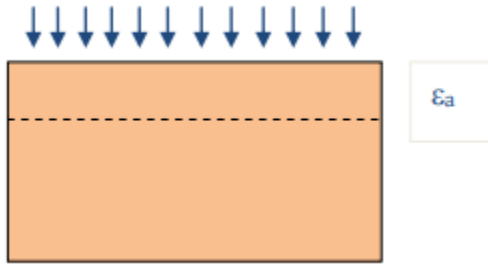


Figure 1 1 Soil sample under oedometric conditions.

This clearly shows that the weakness of this formulation is shown by the fact that we are forced to consider the elastic behavior . Which does not express the reality of the soil.

## 1.12. INITIAL STRESSES IN SLOPING GROUND

As the concept given by Taylor to conjugate stresses for uniform natural slopes by considering a small element or point at depth  $z$  below the surface of the slope of a uniform  $\beta$  (where  $\beta$  is the slope angle), such case gives a total stress on planes parallel to the slope that it's called  $\sigma_\beta$  and the total stress on planes parallel to the slope that will act in vertical direction and is burden above the element. This stresses can are given as:

$$\sigma_v = \gamma z \cos\beta \quad \sigma_\beta = k \gamma z \cos\beta \quad (1.10)$$

These stresses are not normal stresses but have both shear and normal components. Therefore consideration of an effective stress ratio such as  $k_0$  requires care. However where  $\beta = 0$ . Therefore the description of  $K$  as a conjugate stress ratio which becomes a total stress ratio for  $\beta = 0$  is quite adequate. When pore water pressure is zero  $k$  becomes the effective principal stress ratio  $k_0$  when  $\beta = 0$  as showed in the figure

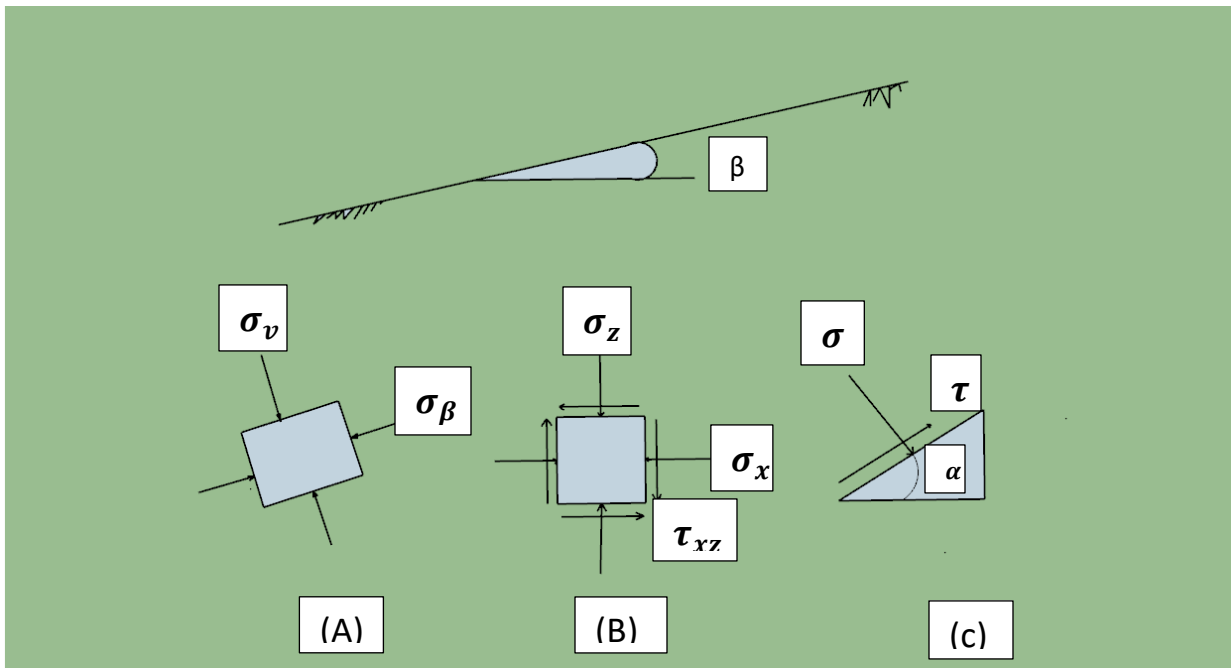


Figure 1.2 stresses within a long uniform natural slope (a) conjugate stresses (b) normal and shear stresses on an element (c) stresses on a plane at any arbitrary inclination.

Considering the stresses components in the X-Z plane we have the from (1.4.1) two normal stresses and a shear stresses (Fig 1.2.1 b)

$$\sigma_z = \gamma z (1 + \sin^2 \beta)$$

$$\sigma_x = K \gamma z \cos^2 \beta$$

$$\tau_{xz} = K \gamma z \sin^2 \beta \cos \beta$$

## Conclusion

In this chapter we analyze the contributing factors for the provision of studies of slope stabilization, where running on about some researches made in this topic. with which we came to the conclusion that the stabilization of these structures is only possible if we observe some details or information of the terrain under study (in-situ stresses, when we can make accurate predictions on soils behavior these component/parameters of soil have huge impact in short and long term stabilization to mention parameters such as the coefficient of earth pressure at rest, which should be the starting point through which we cannot pass over if the study of the existing pressures on the soil depend on this factor. and when talking about sloping ground this task is very complex, to make this task more accessible the finite elements guarantee that we can carry out the analyzes. in the next chapters we will delve into this last aspect. It's important to calculate the initial stresses in geotechnical engineering before we go forward with other calculations.

Initial stresses are the masterpieces of finite element method (FEM) specially speaking about slope stability, because we need them for the medialization, nother than less the soil coefficient of soil at rest is one of the first most important feature to look for, since this can be easily calculated by using the method illustrated in this chapter for the horizontal surfaces, while for sloping ground any effort must be taken and carefully analysed by Finite elements methods that will be showed in later chapters. By this time we know that soil behaviour can be mastered by knowing the exact in-situ stresses. We also realised that the initial stresses have an influence in the development of plastic deformation.

---

# CHAPTER II

## LIMIT EQUILIBRIUM METHODS FOR DETERMINING THE FACTOR OF SAFETY

## 2.1.1 Introduction

Over the years, several methods have been developed for solving slope stability problems, one of which has been the adoption of a security value that allows the structure to be in equilibrium, either due to internal forces or to external forces that will be exerted on it. This value has seen over the years several methods created in order to achieve good security results. So the factor of safety counts with tens of equilibrium method for its determination. This chapter will be devoted to some of the methods for determining the safety factor:

### 2.2.1 Fellenius method

Fellenius in 1927 proposed a method limited to circular slip surfaces or in general, he assumes that the forces between slices can be neglected, because they are parallel to the bases of the slices. This method doesn't take in consideration the Newton's principle of equality of action and reaction, however, he suggests that the resultant of the forces acting on each slice is zero in the normal direction. See figure 1 noting that he considered that each slices is independent of each other's. So the balance of forces in projection on the normal to the slip line is considered to be:

$$N_i = W_i \cos \alpha_i \quad (2.1)$$

And also for the global equilibrium of moments what can be found directly by the expression of F will be given as a result:

$$F = \frac{1}{\sum W_i \sin \alpha_i} \left[ \sum_1^n W_i \cos \alpha_i \operatorname{tg} \varphi_i + C_i \frac{b_i}{\cos \alpha_i} \right] \quad (2.2)$$

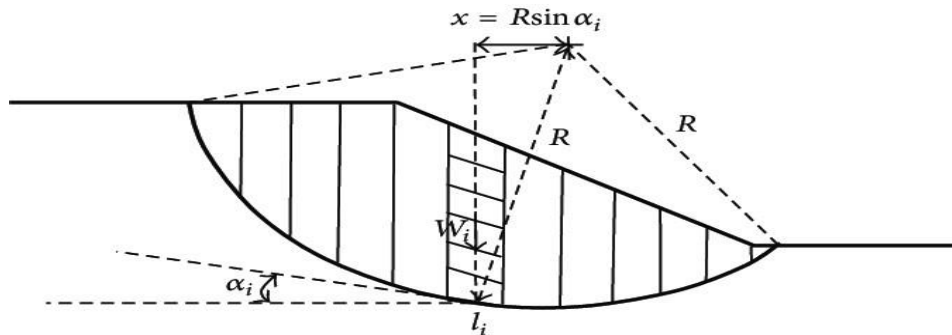


Figure 2 1 Illustration of the Fellenius method.

We notice that the equation making it possible to define F is the same as that given by the method of Bishop for a circular slip line but the normal forces  $N_i$  have a different expression, c which leads to a different allocation of constraints based on slices.

The security expression determined by the Fellenius method is often used as the basis values for the iterations necessary to find the value of F by the Bishop method.

Note:

If the medium is purely coherent ( $\varphi = 0$ ).

In this case the efforts ( $R_i = N_i$ ) all passing through the center of the slip circle, for methods using this type of slip line give:

$$F = \frac{1}{\sum W_i \sin \alpha_i} \left[ \sum \frac{c_i b_i}{\cos \alpha_i} \right] \quad (2.3)$$

If we consider the medium as homogeneous.  $\gamma$  Constant and  $b = b_i$  (slice width) constant

$$\begin{aligned} \sum W_i \sin \alpha_i &= \sum \gamma h b_i \sin \alpha_i \\ \frac{c}{\gamma H} \left[ \frac{\sum 1 / \cos \alpha_i}{\sum \frac{h_i \sin \alpha_i}{H}} \right] &= N_s \frac{c}{\gamma H} \end{aligned} \quad (2.4)$$

From where:  $N_s$  depends only on the geometry of the slope it is independent of the mechanical characteristics of the medium (to be compared to the formula of Taylor).

This methods gives lower safety factors - imprecise for flat slopes with high pore pressures; only for circular sliding surfaces; assume that the normal force on the basis of each slice is  $W \cos \alpha$ ; an equation (moment of equilibrium of the whole mass), an unknown (safety factor).

### 2.3.1 Bishop's method

This is a method of calculating circular slip. Bishop assumed that the safety factor is constant along the sliding surface. This method was first presented in 1955. In this case where the slip line is circular, the vertical equilibrium is written as follows:

$$\sum_{i=1}^n \{ (V_i - V_{i+1}) \left[ \frac{\sin \alpha_i - \frac{tg \varphi_i}{F} \cos \alpha_i}{\cos \alpha_i + \frac{tg \varphi_i}{F} \sin \alpha_i} \right] \} \quad (2.5.1)$$

$$\sum_{i=1}^n \left\{ \left( W_i - \frac{c_i b_i}{F} tg \alpha_i \right) \left[ \frac{\sin \alpha_i - \frac{tg \varphi_i}{F} \cos \alpha_i}{\cos \alpha_i + \frac{tg \varphi_i}{F} \sin \alpha_i} \right] - \frac{c_i b_i}{F} \right\} \quad (2.5.2)$$

And so this system can be solved by equilibrium equations.

- - n balances relating to the balance of the tranches
- - n equations relating to 'horizontal balance of the slices
- - the global moment equation.

For the following unknowns:

- $N_i$  : let n values
- $(V_i - V_{i+1})$ : n values also
- $F$ : Unkown

This method is Precise only for circular sliding surfaces; satisfies the vertical balance and overall balance of the moment; assumes that the lateral forces on the slices are horizontal;  $N + 1$  equations and unknowns

### 2.4.1 Bishop's Method Simplified

Due to the great difficulty in implementing the detailed method, Bishop made additional assumptions to make the application of his method more affordable. He therefore assumed that for everything  $i, (V_i + V_{i+1}) = 0$  which is equivalent to considering only horizontal inter-slice forces. And the safety coefficient is obtained by iterating the equation (2.6):

$$F = \frac{1}{\sum W_i \sin \alpha_i} \left[ \sum \left[ \frac{c_i b_i}{\cos \alpha_i} + tg \varphi_i \left[ \frac{W_i + (V_i + V_{i+1}) - c_i \frac{b_i}{F} tg \alpha_i}{m_a} \right] \right] \right] \quad (2.6)$$

Note, however, that we do not verify all the equations of statics since we are satisfied with:

- n equations relating to the vertical balance of each slice
- The equation of the global moment F or the unknowns that its normal forces N and the safety factor F

We therefore do not check the horizontal balance of the slices or the balance of moments for each slice.

This method is the most used and which gives results very similar to the detailed method.

Precise method; only for circular sliding surfaces; satisfies the vertical balance and overall balance of the moment; assumes that the lateral forces on the slices are horizontal; N + 1 equations and unknowns.

### 2.5.1 Janbu's Method

This method was developed to respond to the moments when the sliding surface deviates too much from the non-circular shape, Janbu's (1954-1957) proposes to consider the force and the equilibrium moment of a typical vertical slice and the force of 'balance of all the slipped mass.

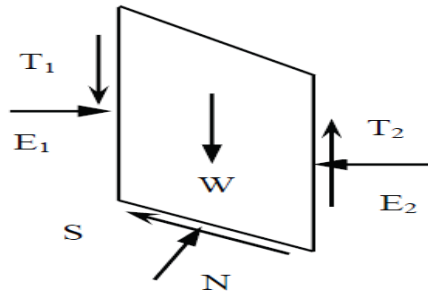


Figure 2.2 Illustration of the Janbu's method.

Horizontal equilibrium gives us F:

$$F = \frac{\sum b_i S_i \frac{1}{\cos \alpha_i^2}}{\sum (W_i \Delta V_i) tg \alpha_i} \quad (2.7)$$

With

$$S_i = \frac{c_i + \frac{W_i + \Delta V_i}{b_i} tg \varphi_i}{1 + \frac{tg \alpha_i tg \varphi_i}{F}} \quad (2.8)$$

The forces inter trances can be calculated by the following equilibrium equations:

$$H_i - H_{i+1} = \Delta H_i = (W_i + \Delta V_i)tg\alpha_i - \frac{S_i b_i}{F} \frac{1}{\cos\alpha_i^2} \quad (2.9)$$

$$V_i = -H_i tg\alpha_{it} + h_{it} \frac{\Delta H_i}{b_i} \quad (2.10)$$

In which

- $\Delta H_i$  : is the difference of the normal forces alongside two successive slices,
- $\Delta V_i$  : is the difference of the forces parallel to the sides of two successive slices,
- $\alpha_{it}$  ,  $h_{it}$  : define the direction and position of the push line.

Using equations 1.3, while proceeding section by section, allows us to obtain the force values  $H_i$  and  $V_i$  of all slices.

This method satisfies all equilibrium conditions: applicable to any form of sliding surface; assumes heights of lateral forces above the base of the slice (varying from slice to slice); digital convergence problems more frequent than some other methods; precise method; Equations and unknowns 3N.

### 2.6.1 Spencer's method

Spencer to consider inter-slices efforts as parallel to each other; that is to say:

$$\frac{V_i}{H_i} = tg\theta_i = \lambda \quad (2.11)$$

$\lambda$  Is a parameter to be determined: the method is this time again exact for this  $\theta_i$  must be between the angle of the slope  $\beta$  and the angle  $\alpha_i$  what does the base of slice i do with the horizontal.

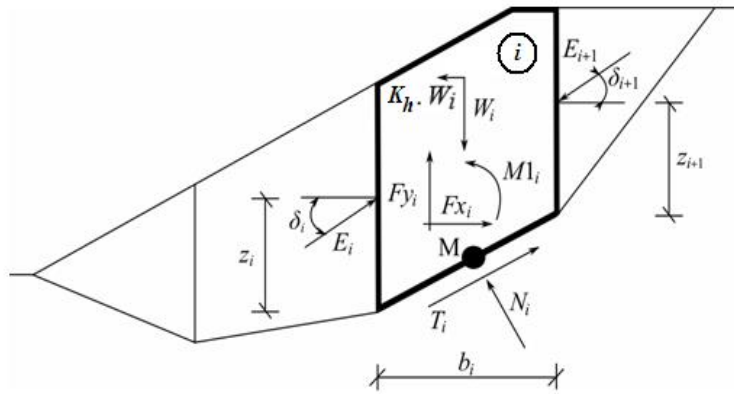


Figure 2.3 Illustration of Spencer's method.

$Q_i$  represents the result of inter-unit forces. It makes an angle equal to  $(\alpha - \theta)$  with the base of the slice i.

We will find:

$$T_i = \frac{C_1}{F} \frac{b_i}{\cos\alpha_i} + N_i \frac{tg\varphi_i}{F} \quad (2.12)$$

At equilibrium, the projection of forces parallel to the base of the slice gives:

$$T_i - Q_i \cos(\alpha_i - \theta_i) - W_i \sin\alpha_i = 0 \quad (2.13)$$



In the same way the projection of the forces on the normal at this base:

$$N_i - Q_i \sin(\alpha_i - \theta_i) - W_i \cos \alpha_i = 0 \quad (2.14)$$

Let us replace  $T_i$  by its value. So we Get:

$$\frac{C_1 b_i}{F \cos \alpha_i} + N_i \frac{tg \varphi_i}{F} - Q_i \sin(\alpha_i - \theta_i) - W_i \cos \alpha_i = 0 \quad (2.15)$$

Soit

$$C_1 \frac{b_i}{\cos \alpha_i} + N_i \frac{tg \varphi_i}{F} - F Q_i \sin(\alpha_i - \theta_i) - F W_i \cos \alpha_i = 0$$

$$N_i - Q_i \sin(\alpha_i - \theta_i) - W_i \cos \alpha_i = 0 \quad (2.15.1)$$

By << eliminating >>  $N_i$  between these two expressions we can calculate Q

$$Q = \frac{\frac{C_1 b_i}{F \cos \alpha_i} + \frac{tg \varphi_i}{F} W_i \cos \alpha_i - W_i \sin \alpha_i}{\cos(\alpha - \theta) \left[ 1 + \frac{tg \varphi_i}{F} tg(\alpha - \theta) \right]} \quad (2.16)$$

We must multiply the primary equation by  $-tg \varphi$  and add up

At this moment it is considered that the forces outside the slope are in equilibrium, then the vector sum of the inter-slice forces must be zero. What gives us:

$$\sum Q_i \cos \theta_i = 0 \quad (2.17)$$

$$\sum Q_i \sin \theta_i = 0$$

So if the sum of the moments of the external forces with respect to a center of rotation is zero, then the sum of the moments of the inter-slice forces with respect to this center must also be zero. What gives us:

$$\sum Q_i R \cos(\alpha_i - \theta_i) = 0 \quad (2.18)$$

If we admit that the sliding surface is circular and R is the radius (therefore R = a constant) the preceding equation can be written:

$$\sum Q_i \cos(\alpha_i - \theta_i) = 0 \quad (2.19)$$

For a given problem, the equations must be solved (2.17 and 2.19.).

Spencer considers the inter-slice efforts to be parallel to each other, that is to say  $\theta = \text{constant}$  equation 2.17 reduces to:

$$\sum Q_i = 0$$

So we go to solving only two equations instead of three.

This method satisfies all equilibrium conditions: applicable to any form of sliding surface; assumes that the inclinations of the lateral forces are the same for each slice; lateral force inclination is calculated in the solution process so that all conditions for equilibrium is satisfied; Precise method; Equations and unknowns 3N.

$$\sum Q_i \cos \theta_i = 0$$

$$\sum Q_i \sin \theta_i = 0$$

$$\sum Q_i = 0$$

### 2.7.1 Method of Lowe and Karafiath

Lowe and Karafiath assume that the inter-slice forces are tilted at an angle equal to the average of the ground surface and the base angles of the slices. This simplification leaves  $(4n-1)$  unknowns and does not satisfy the moment equilibrium.

Usually the most accurate of the balance of power methods; applicable to any form of sliding surface; suppose that the inclinations of the lateral forces are average of the slope surface and sliding surface (varying from one slice to another); satisfies the vertical and horizontal force balance;  $2N$  equations and unknowns.

### 2.8.1 Morgenstern and Price's Method

The method employed by Morgenstern and Price (1965) is similar to Spencer's method except that it assumes that the inclination of the inter-slice forces can vary by an arbitrary function  $f(x)$  and this method also satisfies both forces and moments (Fig.2.3).

Assume Spencer's equation:

$$\frac{V_i}{H_i} = tg\theta_i = \lambda \quad (2.20)$$

So for Morgenstern and Price (1965) based on this same equation added to this a function of forces as a sequence:

$$\frac{V_i}{H_i} = tg\theta_i = \lambda f(x_i) \quad (2.21)$$

$\theta$  being the angle made by the resulting inter-slice force with respect to the horizontal.

By choosing the function  $f(x)$  beforehand, we obtain  $(n-1)$  additional equation and a parameter to be determined. The problem is therefore statically determined with  $(4n-1)$  equation for  $(4n-1)$  unknowns. This method poses big problems of numerical computation at the level of the convergence of the safety factor.

This method Satisfies all equilibrium conditions: its applicable to any form of sliding surface; assumes that the inclinations of the lateral forces follow a prescribed pattern, called  $f(x)$ ; side the inclinations of force may be the same or may vary from one slice to another; lateral force tilts are calculated in the solution process so that all conditions for equilibrium is satisfied; precise method; Equations and unknowns  $3N$ .

## **Conclusion**

In conclusion, we can say the Bishops and Morgenstern-Price methods are the most used in the practice of engineering, because they give us precise results and with the minimum of parameters to be determined. They are applicable to any form of sliding surface. Both methods are the most used because of their accuracy results since they both give very close value of factor of safety. This makes it easier to analyze the factor of safety and gives us some security that other methods do not provide. Also these methods are easy to work with.

In principle, the stability of excavation slopes should be evaluated for both the end-of-construction and the long-term conditions. The long-term condition is usually critical. The stability of an excavated slope decreases with time after construction as pore water pressures increase and the soils within the slope swell and become weaker. As a result, the critical condition for stability of excavated slopes is normally the long-term condition, when increase in pore water pressure and swelling and weakening of soils is complete. If the materials by which the excavation is made are so highly permeable that these changes occur completely as construction proceeds, the end-of-construction and the long-term conditions are the same. These considerations lead to the conclusion that an excavation that would be stable in the long-term condition would also be stable at the end of construction. This methods help designer to get good results which the stabilization can be satisfied, but these methods have the drawbacks since they cannot give the designer a precision of the slide line for stresses path of the proposed studied and they tend to weakening the soil in order to get the smallest factor of safety. In the next chapters this matter will be covered and we will be presenting the new proposed method that deals with actually soil parameters.

---

# CHAPTER III

## STABILITY OF SLOPES BY THE FINITE ELEMENT METHOD

### 3.1.1 Introduction

The majority of slope stability analyses performed in practice still use traditional limit equilibrium, involving the methods of slices that during many years were unchangeable. This changed when Wittman and Bailey set a criteria of emerging methods to become readily to engineers.

The Finite Element method represents a very powerful approaches that is alternative for slope stability analyses which is accurate, versatile and requires fewer assumptions, especially, regarding the failure mechanism. Slope failure in finite element model occurs naturally through the zones in which the shear strength of the soil is insufficient to resist the shear stresses. In this chapter we will see some methods that are used in finite element method (Strength Reduction Method, Gravity loading and Finite Element limit Analysis).

### 3.1.2 The Strength Reduction Method (SRM)

The principle behind the shear strength reduction technique, which was proposed in finite element slope stability analysis it consists in reducing  $c$  and  $\phi$  until the slope failure occurs, in which slope failure is defined as the fracture shear strain develops from the toe at the top of the slope. The overall factor of safety for a slope can be determined as the ratio of the total shear strength along the failure surface of a slope to the total shear stress along the same failure surface, in general the factor of security it can be determined as the ratio of the total shear stress along the same failure surface is expressed:

$$FOS^{overall} = \frac{\int (c + \sigma^m \tan \phi) dl}{\int \tau^m dl} \quad (3.1)$$

where  $\sigma^m$  and  $\tau^m$  are respectively the mobilized normal and shear stresses and  $dl$  is the differential arc length. If the failure surface is known a priori, the conventional way of the application of the finite element analysis is able to compute the FOS of equation (3.1) which represents the global factor of safety of the entire slope. At various points along the failure surface, a local factor of safety can be defined:

$$FOS^{local} = \frac{\tau^f}{\tau^m} \quad (3.2)$$

Where  $\tau^f$  is the shear strength and  $\tau^m$  is the mobilized shear stress at the same point along the potential failure surface (Pasternak and Gao 1988).

Since there is no predefined failure surface in the finite element method, the scalar of expression (3.2) can be regarded at any arbitrary point from the discretized medium as the ultimate value of a trial factor given by the following equation:

$$F^{Trial} = \frac{\tau^f}{\tau^{Trial}} \quad (3.3)$$

Where  $\tau^{Trial}$  is any arbitrary shear stress located between  $\tau^m$  and  $\tau^f$ , which tends to  $\tau^m$  when  $F^{Trial}$  tends to  $FOS^{local}$ . As the strength reduction method was originally proposed in conjunction with Mohr-Coulomb failure

criterion (Figure 1), the factor  $F^{Trial}$  termed strength reduction factor can geometrically satisfy the following equation:

$$F^{Trial} = \frac{c}{c^{Trial}} = \frac{\tan \phi}{\tan \phi^{Trial}} \quad (3.4)$$

Where  $c$  and  $\phi$  are the effective soil strength parameters. Trial values for strength parameters can be determined by:

$$c^{Trial} = \frac{c}{F^{Trial}} \quad \text{and} \quad \phi^{Trial} = \arctan \left( \frac{\tan \phi}{F^{Trial}} \right) \quad (3.5)$$

The search of the slope stability factor by the strength reduction technique consists of reducing progressively the original soil strength parameters namely  $c$  and  $\phi$  by increasing  $F^{Trial}$  according to the equations (3.5). When  $F^{Trial}$  is gradually increased, at a certain number of stress points (Gauss points in this paper), the failure envelope becomes tangential to their stress Mohr's circles. At this stage, plastic states are established at these stress points but the global convergence of the iterative process is still occurring. Here the ratio of shear strength to the mobilized shear stress previously defined by the equation (3.2), is called the stress-point based factor of safety  $FOS_{SRM}^{sp}$  and determined within the scope of the SRM as :

$$F^{Trial} = FOS_{SRM}^{sp} = \frac{\tau^f}{\tau_{SRM}^m} \quad (3.6)$$

$FOS_{SRM}^{sp}$  is in fact a local factor of safety as previously stated. By further increasing of  $F^{Trial}$ , when the stresses equilibrium can no longer be established by a sudden substantial changes in displacements or by a connection of plastic shear band, the soil collapse is said to occur and then, the reached value of  $F^{Trial}$  is the value of the global soil stability factor  $FOS_{SRM}$ . Consequently,  $FOS_{SRM}$  can neither be represented geometrically nor it can be quantified analytically as it is evaluated in the global sense. It can be seen as the stress-point based factor of safety  $FOS_{SRM}^{sp}$  of the last stress point that triggered the failure mechanism.

Had it not been to the linearity of Mohr-Coulomb failure envelope, the  $F^{Trial}$  would never be considered as a factor of safety  $FOS_{SRM}$  when the rotated failure line becomes tangential to the in-situ stress Mohr's circles.

### 3.1.3 The SRM Drawbacks

Although, many researchers confirmed the deviation of  $FOS_{SRM}$  from  $FOS_{LEM}$  in many slope configurations, a research study which seriously criticized the SRM had not been found in the literature and unfortunately always the LEM which had been incriminated for lack of accuracy. In the author's opinion, the SRM has its inherent drawbacks:

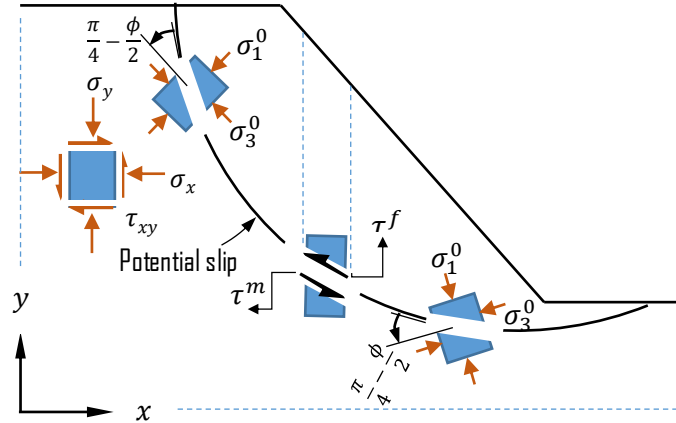


Figure 3. 1 Stress state in a sloping ground and orientation of principal stresses with respect to the slip line. Djillali Amar Bouzid- Finite Element Analysis of a Slope Stability by Incrementally Increasing the Mobilized Principal Stress Deviator. <https://orcid.org/0000-0003-2991-6533>

According to the theory of slip lines, it is generally accepted that the soil failure occurs at an inclination of an angle  $\Gamma (= \frac{\pi}{2} + \frac{\phi}{2})$ , with respect to the major principal stresses directions (Figure 3.1). In order to define an accurate expression for the slope stability factor, it is mandatory to evaluate both the mobilized shear stress necessary for the slope equilibrium and the available shear strength on the same slip surface. For simplicity and for a better illustration, let's consider a stress point in a cohesion less medium ( $c = 0$ ) where the stress state is defined by its effective principal stresses  $\sigma_1^0$  and  $\sigma_3^0$ , which are respectively the major and minor principal stresses illustrated by Figure 3. Taking into account the inclination  $(\frac{\pi}{2} + \frac{\phi}{2})$ , the mobilized shear and normal stresses are respectively  $\tau_{ac}^m$  and  $\sigma_{ac}^m$  and are indicated by the segments  $\overline{ab}$  and  $\overline{ba}$  on Figure 3 (the subscript  $ac$  stands for the accurate value). Obviously, the available shear strength corresponding to  $\sigma_{ac}^m$  is  $\tau_{ac}^f$  and it is indicated by the segment  $\overline{ad}$  on Figure 3. In this situation, the stress-point based factor of safety is  $FOS_{ac}^{sp} = \tau_{ac}^f / \tau_{ac}^m = \overline{ad} / \overline{ab}$ . However, the failure envelope in its pivoting process (around point  $o$  in Figure 3) for reducing strength, defines an inaccurate pair of stresses when it becomes tangent to the mobilized principal stresses Mohr' circle  $c_1$ . These stresses which are  $\tau_{SRM}^m$  and  $\sigma_{SRM}^m$  and indicated respectively by the segments  $\overline{ef}$  and  $\overline{oe}$  on Figure 3, act on a surface inclined by angle  $\Delta (= \frac{\pi}{2} + \frac{\phi^{trial}}{2})$  with respect to the directions of the mobilized principal stresses. As the angle  $\Delta$  differs from the angle  $\Gamma$ , a different value of shear strength corresponds to  $\sigma_{SRM}^m$ . This shear strength  $\tau_{SRM}^f$  is indicated by the segment  $\overline{eg}$  and consequently the stress point-based factor of safety is evaluated as

$FOS_{SRM}^{sp} = \tau_{SRM}^f / \tau_{SRM}^m = \overline{eg} / \overline{ef}$ . A close inspection of the Figure 3 and using some geometrical simple rules, it is easy to see that:

$$FOS_{SRM}^{sp} = \frac{\overline{eg}}{\overline{ef}} = \frac{\overline{ad}}{\overline{ac}} < \frac{\overline{ad}}{\overline{ab}} = FOS_{ac}^{sp} \quad (3.7)$$

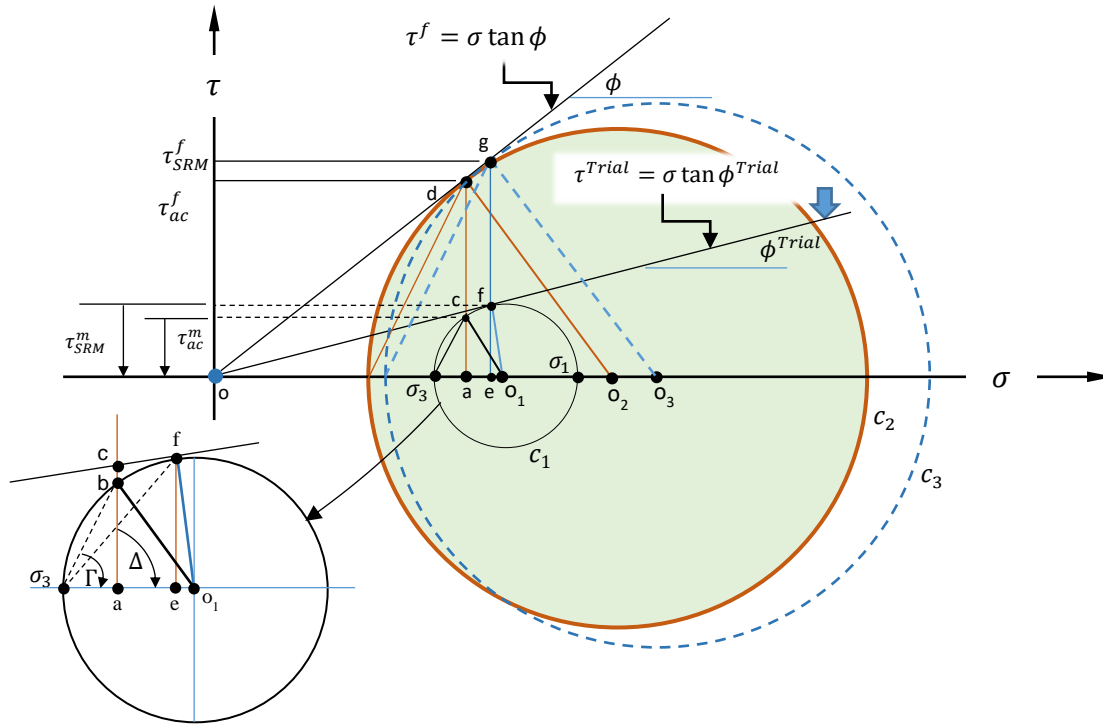


Figure 3. 2 State of stresses at a given stress point from the modeled medium. (Djillali Amar Bouzid- Finite Element Analysis of a Slope Stability by Incrementally Increasing the Mobilized Principal Stress Deviator. <https://orcid.org/0000-0003-2991-6533>)

The equation (3.7) holds true because  $\overline{ac}$  is greater than  $\overline{ab}$  regardless the value of the internal friction angle  $\phi$  as long as it differs from zero. For purely cohesive materials the two stress point-based factors of safety become equal as we will see next. The author can conclude that the SRM slightly underestimates the factor of safety. This underestimation gets bigger when the internal friction angle gets larger and the cohesion gets smaller.

During the whole deformation process of a material obeying Mohr-coulomb's yield criterion the inequality  $\sin \phi \geq 1 - 2\nu$  (where  $\nu$  is the material Poisson's ratio) must be satisfied. If this condition (termed the  $\phi - \nu$  condition) is violated, abnormal zones of plastic strains appear and are overestimated (Zheng et al. 2005). By reducing  $c$  and  $\tan \phi$ , while keeping  $\nu$  invariant, the  $\phi - \nu$  condition is violated at a certain deformation step. At that moment, plastic strains might happen in depth and consequently inaccurate values for  $FOS_{SRM}$  are obtained.

In order to overcome this and to satisfy the  $\phi - \nu$  condition within the prescribed values of the reducing factor, Zheng et al. (2005) proposed to reduce the Poisson's ratio according to the trial value of the internal friction angle:



$$\nu^{Trial} = \frac{1}{2} \left[ 1 - \left( \frac{\sin \phi^{Trial}}{\beta} \right) \right] \text{ where } \beta = \frac{\sin \phi}{1-2\nu} \quad (3.8)$$

By doing so, one of the most important deformation parameter  $\nu$  is affected and consequently the elastic stress-strain relationships are affected either. This may lead to inaccurate slope shape configurations. Furthermore, this would have not only implications on the deformation process but on the plastic deformations either, since they depend on the value of pseudo time which relies in turn on  $\nu$ .

In general, a non-associated flow rule with a dilatancy angle  $\psi$  smaller than  $\phi$  is adopted in the SRM. By applying the SRM to a problem of earth pressure, Nordal 2008 showed that this may result in numerical instabilities with no clear illustration the collapse mechanism. Furthermore, Krabenhof et al. 2012 observed that the failure surface tends to deviate towards the boundaries rather than remaining on the usual path from slope toe to its top. To overcome this situation in the case of an associated plasticity, Tschuchnigg et al. 2015 proposed to reduce the angle of dilatancy the same way the two other strength properties are reduced, but in the non-associated flow rule, the angle  $\psi$  is kept constant as long as it is smaller than  $\phi^{Trial}$ . However, once  $\phi$  falls to the value of  $\psi$  both are reduced simultaneously. This solution has been proposed without providing any solid justification, showing that the SRM suffers from the plastic flow rule.

Computational speed and time can be an issue; Requires more material input parameters; Deformation properties, elasto-plastic stress-strain behaviour; Requires more numerical modelling expertise than is commonly taught to geotechnical engineers; Inexperience with the method; Definition of instability of solution; Definition of convergence can be result of numerical instability (and not physical instability); Sensitivity or probabilistic analysis is time consuming.

### 3.1.4 Advantages of the SRM

With passing time, the SRM becomes a confirmed tool for slope stability assessment, not only in the academia but even in geotechnical engineering practice. In this regard, Griffiths and Lane 1999, pointed out that the SRM should be considered as a powerful alternative to the traditional LEM. This widespread use is probably due to the following advantages:

1. The SRM is applicable to complicated geometries with complex boundary and loading conditions.
2. No assumption needs to be made in advance about the critical failure surface. The latter occurs ‘naturally’ through the zones within the soil in which the shear strength is unable to sustain the applied shear stresses.
3. Since it is formulated on the displacement-based FE analysis, the SRM is able to provide information about the parameters such as displacements, strains and stresses from the initial positions up to the threshold of failure.
4. The SRM has gained popularity and consequently has been implemented in many geotechnical engineering codes such as PLAXIS (PLAXIS 2004).

5. Accounts for various material stress-strain behaviour.

### 3.2.1 Gravity Increase Method (GI)

The gravity increase method keeps the shear strength parameters unchanged. In this methodology, gravitational acceleration is gradually adjusted until the slope it reaches the critical failure state. At this point, the ratio of the applied gravitational acceleration to the standard gravitational acceleration is safety factor of the slope.

Similarly, the gravity increase method can be achieved by adjusting the density of rock and soil masses with the gravitational acceleration kept unchanged.

The analysis of stability by the gravity increase method assumes the external forces increase due to increasing gravity  $\mathbf{g}$  and the equilibrium solution satisfying equation, can no longer be obtained. Monotonically increasing gravity brings external forces on the edge of stability when the strength of the soil is reached.

Gravity increases according to the formula:

$$\mathbf{g} = \mathbf{g} \cdot t \quad (3.9)$$

Where:

$\mathbf{g}$  - A prescribed vector specifying the direction of gravity loading and its rate of Increase with time, and  $t$  is a parametric time variable.

Prescribed in this manner, gravitational acceleration vector  $\mathbf{g}(t)$  increases and the limit analysis problem reduces simply to finding the largest time  $t = t_{limit}$  for which a global equilibrium solution exists. The limiting acceleration due to gravity in the system is then:

$$\mathbf{g}_{limit} = \mathbf{g} \cdot t_{limit} \quad (3.10)$$

The present work applies gravity in a single increment to an initially stress-free slope. Others have shown that under elastic conditions, sequential loading in the form of incremental gravity application or embanking, affects strains but not stresses (Clough and Woodward, 1967). In nonlinear analyzes, it is recognized that the stress paths followed due to sequential excavation may be quite different from those followed under a gravity "turn on" procedure; however, the safety factor appears unchanged when using single elasto-plastic models (Borja et al. 1989; Smith & Griffiths, 1998).

In comparing our results with limiting equilibrium solutions which generally ignore sequence loading, experience has shown that the predicted safety factor is insensitive to the form of application of gravity when using the elastic-perfectly plastic Mohr-Coulomb models.

The factor of safety can be sensitive to sequence loading when implementing more complex constitutive laws, such as those that attempt to accurately reproduce volumetric changes in an undrained or partially drained environment. For example, Hicks and Wong (1988) showed that an efficient stress trajectory could have a great influence on the safety factor of an undrained slope.

### 3.2.2 Determination of the factor of safety

The factor of safety (FOS) of soil slope is defined here as the factor by which the original shear strength parameters must be divided in order to bring the slope to the point of failure. The factored shear strength parameters  $C_f$  and  $\varphi_f$ , are therefore given by:

$$C_f = \frac{c}{F^{Trial}} \quad (3.11)$$

$$\varphi_f = \arctg\left(\frac{\tan\phi}{F^{Trial}}\right) \quad (3.12)$$

Where SRF is a strength reduction factor, this method is referred to as the shear strength reduction technique and allows for the interesting option of applying different strength reduction factors to the  $c'$  and  $\tan\phi'$  terms. In this method however, the same factor is always applied to both terms. To find the “true” factor of safety is necessary to initiate a systematic search for the value of SRF that will just cause the slope to fail. When this value has been found,  $FOS=SRF$ .

This definition of factor of safety it is the same as that used in traditional limit equilibrium methods, namely the ratio of restoring to driving moments.

Since gravitational loading induces slope failure, the gravity-based factor of safety against slope failure is given by:

$$F_{sgi} = \frac{g_{limit}}{g_{actual}} \quad (3.13)$$

Where:

$g_{actual}$  – Representative actual acceleration due to gravity in the slope analysed, i.e. 9.81 m/s<sup>2</sup>.

The value of the safety factor is greater than unity for a stable slope. The higher value of safety factor, the more stable the slope it is.

It has been found that a good measure of slope safety is to associate  $g_{limit}$  with the abrupt increase of acoustic emission rate or a dramatic increase in the nodal displacement within the elements.

### 3.2.3 Drawbacks (GIM)

The gravity increase method (GIM) has an inherent defect that may result in an incorrectly calculated safety of factor or result in a failure to obtain the expected outcome.

In this study, the error source of GIM was quantitatively analyzed through theoretical derivation to address this problem. Hence, the modified gravity increase method (MGIM), which can eliminate the error in GIM, was developed by adding a correction factor to the friction angle during the gravity increase procedure. The MGIM was comparatively studied by applying the GIM, shear strength reduction method, and MGIM to homogeneous

slope models under different dimensions, and an ACADS (Australian computer Aided design society) test was introduced to validate the applicability of the MGIM to heterogeneous slopes. The analyses proved that the MGIM does not have the inherent defect present in the GIM, and can provide accurate results in the stability analysis of both homogeneous slope and heterogeneous slopes with various slopes angle height. Finally, the MGIM and GIM were applied to the numerical analysis of a geotechnical centrifugal model test of a soil slope. The results indicate that MGIM is capable of capturing the deformation and failure characteristics of geotechnical centrifugal test of soil slopes.

### 3.3.1 Finite element methods for slopes

### 3.3.2 Brief description of the finite element model

#### The parameters needed to draw Soil model

Table 3 1 Soil Parametric.

$\phi'$	Friction Angle
$c'$	cohesion
$\psi'$	Dilatancy Angle
$E'$	Young Modulus
$\nu'$	Poisson ratio
$\gamma'$	Volumic weight

The angle of expansion  $\psi$  affects the change in soil volume during yield. It is well known that the actual volume change exhibited by a soil during yield is quite variable. For example, a medium-dense material during shear might initially exhibit some decrease in volume ( $\psi' < 0$ ), followed by an expanding phase ( $\psi' < .0$ ), eventually leading to yield under constant volume conditions ( $\psi' = 0$ ). Clearly, this kind of detailed volumetry modeling goes beyond the perfectly plastic model elasticity used in this study, where a constant expansion angle is involved. The question then arises as to which value to use. If  $\psi' = \phi'$ , then the plasticity rule is “associated” and direct with the theorems of classical plasticity can be done. This is also the case where when the flow rule is associated, the stress and velocity characteristics coincide, so more agreement can be expected between the failure mechanisms predicted by the finite elements and critical failure surfaces generated by the equilibrium limit methods. Despite these potential advantages of using an associated flow rule, it is also well known that flow rules associated with friction soil models predict much greater expansion than ever observed in reality. This in turn results in an increase in the prediction failure load, especially in problems like load bearing capacity (Griffiths, 1982). This shortcoming has led some of the most successful constituent soil models to incorporate non-associated plasticity elements (Molenkamp, 1981; Hicks & Boughrarou, 1998).

The analysis of slope stability is relatively unconfirmed, so the choice of the expansion angle is less important. Since the main objective of the present study is accurate prediction of slope safety factors, a compromise value of  $\psi = 0$ , corresponding to a non-associated flow rule with zero volume change during yield, was used throughout. Throughout this article. It will be shown that this value of  $\psi'$  allows model to provide reliable safety factors and reasonable indication of the location and shape of potential failure surfaces. The parameters  $c'$  and  $\phi'$  refer to the angle efficiency of cohesion and friction of the soil. Although a number of failure criteria have been suggested to model soil strength (Griffiths, 1990), the Mohr-Coulomb criterion remains one of the most widely used in geotechnical practice. In terms of principal stresses and assuming a compression by convention of negative sign, the criterion can be written as follows:

$$F = \left(\frac{\sigma_1 + \sigma_3}{2}\right) \sin \phi' - \left(\frac{\sigma_1 - \sigma_3}{2}\right) - c' \cos \phi' \quad (3.14)$$

Where  $\sigma_1$  and  $\sigma_3$  are the main and minor effective constraints.

The failure function F can be interpreted as follows:

F < 0 stresses inside the failure envelope (elastic)

F = 0 emphasizes the envelope of failure (efficiency)

F > 0 requests outside the failure envelope (assignor and must be redistributed)

The elastic parameters  $E'$  and  $\nu'$  refer to Young's modulus and Poisson's ratio of the soil. The value of Young's modulus can be related to the compressibility of the soil measured in a one-dimensional oedometer (Lambe & Whitman, 1969):

$$E' = \frac{(1+\nu')(1-2\nu')}{m_v(1-\nu')} \quad (3.15)$$

Where  $m_v$  is the coefficient of volume compressibility.

Although the actual values given to the elastic parameters have a profound influence on the deformations calculated before failure, they have little influence on the factor of safety expected in the analysis of slope stability.

Thus, in the absence of meaningful data for  $E'$  and  $\nu'$  they can be given nominal values.

The total unit weight  $\tilde{\alpha}$  assigned to the soil is proportional to the nodal self-weight loads generated by gravity.

In summary, the most important parameters in the FE slope stability analysis are the same as they would be in a traditional approach, namely, the total unit weight  $\tilde{\alpha}$ , the shear strength parameters  $c'$  and  $\phi'$  and the geometry of the problem.

### 3.4.1 Finite Elements Limit Analysis (FELA)

The finite element code is used for all the displacement finite element analyzes discussed in this part. It is well known that the type of element, the discretization of the mesh and the convergence tolerances have a pronounced influence on the safety factor obtained from the finite element method by displacement. Therefore, the influence of these parameters was minimized by the use of high order elements (Sloan & Randolph, 1982), fine meshes and

tight tolerances. In the finite element code, the safety factor is obtained through the reduction of resistance method (SRM); in other words, an analysis is carried out with properties of resistance mobilized for the angle of friction  $\phi$  and the cohesion  $c$ , followed by a progressive decrease of  $\tan\phi$  and  $c$  (assuming a Mohr - Coulomb failure criterion).

This results in stress states which violate the resistance criterion which are iteratively solved using the same stress point algorithm used for a standard elastoplastic in a numerical calculation, leading to a redistribution of the stresses in the system up to that balance can no longer be established and failure is achieved. However, careful inspection of the failure mechanisms and movement of the checkpoints is necessary to avoid misinterpretation. It should be noted that this procedure only works for simple failure criteria such as Mohr - Coulomb. If the force is a function of state variables, e.g. density, a more complex algorithm is required, as pointed out by Potts & Zdravkovic (2012). In fact, it is one of the objectives of this part to show that the simple resistance reduction procedure works for classical failure criteria by comparing it with rigorous limit analysis solutions. The safety factor (denoted  $F_s$ ) obtained from the procedure is defined by:

$$F_s = \frac{\tan\phi'}{\tan\phi'_{\text{modifie}}} = \frac{c'}{c'_{\text{modifie}}} \quad (3.14)$$

Where

This is the effective cohesion,  $\phi'$  is the effective friction angle.

One issue that needs to be addressed in moving finite element analysis of failure is the definition of the flow rule. Typically, a flow rule not associated with dilatancy angle "less than friction angle" is used, but this can lead to numerical instability without a clear indication of the failure mechanism. This problem has been studied by Nordal (2008) in the context of a land pressure problem. When using finite element structured meshes with an unassociated flow rule, it has been observed that the failure surface tends to propagate along the element boundaries (Krabbenhoft et al. 2012). This is accompanied by strong oscillations of the resulting safety factor during the resistance reduction procedure, which is the consequence of a non-unique failure mechanism, thus making it difficult (or in some cases, even impossible) to set a value, unique for that quantity. In the finite element code used in this study the flow rule in the force reduction procedure is treated as follows: for the associated plasticity, the dilatancy the angle  $\psi'$  is gradually reduced in the same way as the friction angle  $\phi$ , while for the case not associated with  $\psi' < \phi'$ ,  $\psi'$  are kept constant as long as the reduced value for  $\phi'$ , is greater than  $\psi'$ . Once  $\phi'$  drops to the value of  $\psi'$ , the two are then reduced simultaneously in subsequent iterations. This is only relevant in the following for analyzes under drained conditions, where extreme cases have been rather than using values based on proof experiments. Undrained analyzes are usually performed with

$$\psi' = 0.$$

To model unassociated plasticity in limit analysis, Davis (1968) suggested the use of reduced resistance parameters,  $c^*$  and, in combination with an associated flux rule of the form

$$c^* = \beta \cdot c' \quad (3.15)$$

$$\tan\varphi' = \beta \cdot \tan\varphi' \quad (3.16)$$

Where

$$\beta = \frac{\cos\psi' \cdot \cos\varphi'}{1 - \sin\psi' \cdot \sin\varphi'} \quad (3.17)$$

Thus, in what follows, all analyzes referred to as Davis approach have  $c$  and  $\varphi'$  as input parameters. Davis argued that the flow rule will have no influence on the ultimate limiting load unless the problem is kinematic stress, and only for these situations should his approach be applied. As discussed by Sloan (2013), however, it is not straightforward to identify such cases in practice, but it is generally accepted that in slope stability analysis, the flow rule should not significantly influence on the calculated safety factor (Cheng et al., 2007). This hypothesis will be studied later, where it will prove doubtful for steep slopes with high friction angles.

### 3.4.2 Safety factor obtained from finite element analysis

The upper and lower limit theorems of plasticity are powerful tools for predicting the stability of geotechnical problems. Finite element formulations of these theorems have developed significantly over the past two decades, and it is now possible to apply them to a wide variety of complex engineering problems.

Finite element analysis is particularly powerful when upper bound and lower bound estimates are calculated of the true collapse load (for the idealized material) is in upper and lower brackets. The difference between the two bounds then provides an exact measure of the error in the solution, and can be used to refine the meshes until a sufficiently accurate estimate of the collapse load is found. These formulations used in this game come from the methods originally developed by Sloan (1988, 1989) and Sloan & Kleeman (1995), and further improved by Lyamin & Sloan (2002a, 2002b) and Krabbenhoft et al. (2005, 2007). A detailed description of the formulation of the FELA methods used in this article, including the process of adaptive mesh refinement and resistance reduction, is given in Sloan (2013). If a load-based safety factor is desired, which is defined as the ratio of the limit load to the actual load, the solution can be obtained from a single pair of lower bound analyzes. However, if the safety factor is to be expressed in terms of material strength, which is defined as the ratio of the strength of the mobilized material to the actual strength of the material, a strength reduction process should be performed as described in Sloan (2013). This involves several analyzes of the upper and lower limits, each with resistance parameters. Once a state is found where the calculated collapse of the load matches the actual applied load, the limit resistance parameters are derived.

#### 3.4.1 Comparison of SRM and FELA methods and their advantages

Finite element analysis provides lower limits of the factor of safety and can therefore estimate the error in the solution (for the idealized material adopted). Because displacement finite element analysis is increasingly used to calculate safety factors by means of the resistance reduction technique (SRFEA), results from this are compared with those from FELA in order to prove that resistance reduction techniques can be applied in practice. This was found to be the case by comparing the results for slope stability and tunnel face issues when adopting an associated

flow rule, a limit analysis assumption. In SFREA, we would hardly have adopted an associated flow rule; however, the influence of the expansion angle on the calculated safety factors obtained from SRFEA is considered minor for the slope stability problems. Although this is true in many cases, it has been shown in this article that for high friction angles (.408) and steep slopes with low safety coefficient, this is no longer the case and the flux rule can have a significant influence on the result. Importantly, these cases also lead to instabilities, precise determination of the influence of the difficult flow rule. It was therefore investigated whether the approach suggested by Davis (1968), which modifies the resistance parameters to account for plasticity's but performs the analysis as an associated one, can be recommended. Although it is possible because the assumptions are on the safe side, this approach can give estimates of the factor of safety that might be considered conservative. Further investigations are currently underway to overcome this problem of reliably identifying the factor of safety by means of SRFEA involving unassociated flow. Finally, it was emphasized that care should be taken when comparing the safety factors obtained and analyzing the total stress for undrained conditions.



## Conclusion

In this chapter we presented the Strength Reduction Method, Gravity Increase method and Finite Element Limit Analysis, as we can see in the project we made some comparisons between some methods the analytical results.

The location of the critical slip plane of a slope is accurately determined by using the finite element analysis. Unlike the traditional methods, finite element method does not require an arbitrary partitioning of the critical surface selection prior to calculations.

Finite-element limit analysis provides rigorous upper and lower bounds on the factor of safety and can therefore estimate the error in the solution (for the idealized material adopted). Because displacement finite-element analysis is increasingly used to calculate factors of safety by means of the strength reduction technique (SRM), results from this method are compared with those from FELA in order to prove that strength reduction techniques can be safely applied in practice. This has been shown to be the case by comparing the results for slope stability problems when adopting an associated flow rule, an intrinsic assumption of limit analysis. In SFREA one would hardly adopt an associated flow rule; however, the influence of the dilatancy angle on the calculated factors of safety obtained from SRFEA is considered to be minor for slope stability problems. Although true in many cases, it has been shown in this chapter that for high friction angles and steep slopes with low factors of safety, this is no longer the case and the flow rule may have a significant influence on the results. Importantly, these cases also lead to numerical instabilities, making an accurate determination of influence of the flow rule difficult. It has therefore been investigated whether the approach suggested by Davis (1968).

---

# CHAPTER IV

FINITE ELEMENT ANALYSIS OF A SLOPE STABILITY BY  
INCREMENTALLY INCREASING THE MOBILIZED  
PRINCIPAL STRESS DEVIATOR.

## 4. Introduction

In this section we will introduce the method that was created by Amar Bouzid, to solve slope stability problems by the means of finite elements. Hence this chapter will be a full undercover of the method called SDIM and will also be presenting the computational procedure of the programme created to validate this method called S<sup>4</sup>DINA. All features of the programme will be displayed graphical in order to make the reviewer follow the step by step process that will occur during the slope analysis using this Method and Program.

As announced by the author the new approach assesses the slope stability by incrementally increasing the mobilized principal stress deviator until the soil failure is reached. The gradual increasing of the factor controls the expansion of principal stress Mohr's circles in the SDIM. The numerical procedure is based then on a rigorous formulation as it preserves the definition of the safety factor consistent with that of LEM and maintains the progressive development of the shear stress on same plane on which the shear strength will occur at failure. The proposed method deals with the actual material by using the real strength parameters  $(c, \phi)$  and  $\psi$  rather than those reduced by a factor.

### 4.1. New method for the slope stability analysis: Increasing of the mobilized principal stress deviator

Naturally, the slope stability failure takes place because of the variation of effective stresses due to an increasing in applied surcharge loading or pore pressure for instance.

In order to keep the concept the stress level and the local factor of safety consistent, and consequently preserving either the mobilized normal stress  $\sigma^m$  and slip orientation identical at equilibrium and at failure state, the mobilized Mohr's circle is brought on the verge of failure by maintaining the tangential line at the level of  $\sigma^m$  parallel to the failure envelope (Figure 4.1). This is cannot be carried out by rotating the failure envelope about a fixed point, but however, by translating this line parallel to its original position.

Initially at any point of the discretized medium (stress or Gauss point in the FEM jargon), the major and the minor effective principal stresses are respectively  $\sigma_1^0$  and  $\sigma_3^0$ . These stresses may result from the soil self-weight only or the combination of the latter with any applied loading on the slope crest. The mobilized stress pairs acting on the plane making an angle  $(\frac{\pi}{4} + \frac{\phi}{2})$  with the major principal direction, are  $(\sigma^m, \tau^m)$  and  $(\sigma^m, \tau^{Trial})$  (Figure 4) corresponding respectively to the initial situation and to any intermediate situation before failure. This plane becomes the plane of failure when the initial Mohr's circle reaches the failure envelope at the end of the process, The new idea behind this method was inspired from the concept Rankine (1857) used when he developed the theory of lateral earth pressures against a retaining wall. By allowing the latter to move far away or against the retained soil, the major principal stress was kept constant while the minor principal stress was allowed to increase progressively by the fact of the wall movement, to reach finally its ultimate value. By this way, Rankine developed his theory for the two earth pressures states (active and passive). In Rankine's problem there was a unique stress

path, however in a slope stability problem, both principal stresses change and consequently an infinite number of stress paths may be followed. Two important key elements may enable us to reduce all the possibilities to only one. Firstly, and according to the original definition of the safety factor, the shear strength or the mobilized shear stress correspond to same mobilized normal stress ( $\sigma^m$ ) at any point in the discretized medium. Secondly, the shear stress corresponding to the mobilized normal stress occurs on the same plane, which becomes for the ultimate Mohr's circle, the sliding plane.

The objective of the following derivation is to explain the numerical procedure leading to the definition of a stress point-based factor of safety  $FOS_{SDIM}^{sp}$  within the present method called Stress (Deviator Increasing Method (SDIM)). The overall slope safety factor  $FOS_{SDIM}$  obviously depends on the precision of  $FOS_{SDIM}^{sp}$  in every stress point but its value is determined by the global slope failure.)

The idea is then, to expand the initial principal stresses Mohr's circle in such a way that the segment ( $O_0i$ ) remains parallel to the corresponding segment in the subsequent Mohr's circles ( $O_t t$ ) (Figure 4.1), ensuring that both mobilized shear stress  $\tau^m$  and trial shear stress  $\tau^{Trial}$  occur on the same sliding plane and holding the definition of the factor of safety in terms of shear stresses satisfied. In these conditions, and assuming a compression-positive sign convention, the major principal stress should be increased and the minor principal stress should be decreased. The new set of stresses is:

$$\sigma_1^{Trial} = \sigma_1^0 + \Delta\sigma_1^{Trial} = \sigma_1^0 \left( 1 + \frac{\Delta\sigma_1^{Trial}}{\sigma_1^0} \right) = A^{Trial} \sigma_1^0 \quad (4.1)$$

$$\sigma_3^{Trial} = \sigma_3^0 - \Delta\sigma_3^{Trial} = \sigma_3^0 \left( 1 - \frac{\Delta\sigma_3^{Trial}}{\sigma_3^0} \right) = B^{Trial} \sigma_3^0 \quad (4.2)$$

The determination of  $A^{Trial} = \left( 1 + \frac{\Delta\sigma_1^{Trial}}{\sigma_1^0} \right)$  and  $B^{Trial} = \left( 1 - \frac{\Delta\sigma_3^{Trial}}{\sigma_3^0} \right)$  are the key elements in the method of increasing the stress deviator.

The magnitude of expansion, that is the rate of  $\sigma_1^0$  increasing and the rate of  $\sigma_3^0$  decreasing is controlled by  $F^{Trial}$ . This factor called here the Mohr's circle expansion factor, is defined as the ratio of shear stress magnitudes by:

$$F^{Trial} = \frac{\tau^{Trial}}{\tau_{SDIM}^m} \quad (4.3)$$

Where  $\tau_{SDIM}^m$  is the mobilized shear stress and  $\tau^{Trial}$  is any shear stress between in-situ and failure states. If  $D_0$  and  $S_0$  stand respectively for the in-situ principal stresses deviator and principal stresses sum, they can be defined at any point from the analyzed continuum as:

$$D_0 = \sigma_1^0 - \sigma_3^0 \text{ and } S_0 = \sigma_1^0 + \sigma_3^0 \quad (4.3)$$

Using Mohr's circles radii,  $F^{Trial}$  can be written as:

$$F^{Trial} = \frac{A^{Trial} \sigma_1^0 - B^{Trial} \sigma_3^0}{\frac{D_0}{2}} \quad (4.4)$$

The equation (4.4) becomes:

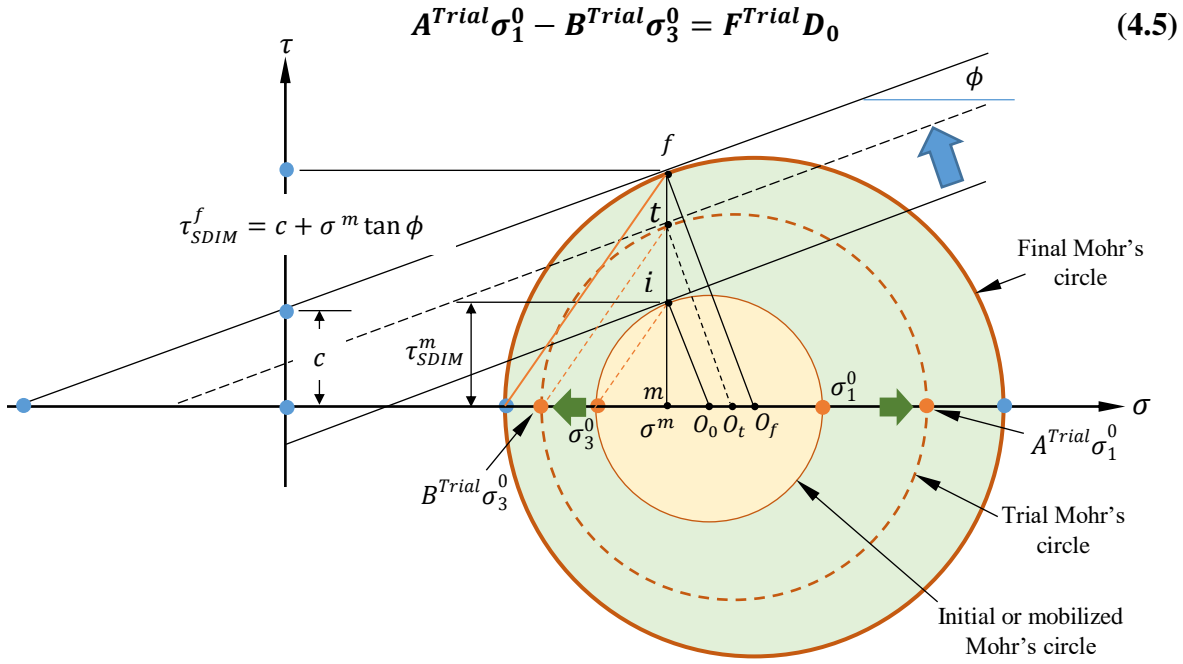


Figure 4. 1 Evolution of principal stresses in the Stress Deviator Increasing Method (SDIM). (**Djillali Amar Bouzid**-Finite Element Analysis of a Slope Stability by Incrementally Increasing the Mobilized Principal Stress Deviator. <https://orcid.org/0000-0003-2991-6533>).

Since the factor  $F^{Trial}$  is increased, its ultimate value corresponds to the factor of safety  $FOS_{SDIM}^{SP}$  and hence the increased major principal stress  $A^{Trial}\sigma_1^0$  and the decreased minor principal stress  $B^{Trial}\sigma_3^0$  reach respectively the failure stresses  $\sigma_1^f$  and  $\sigma_3^f$ .

From Figure (4.1),  $F^{Trial}$  is also defined as:

$$F^{Trial} = \frac{m O_t}{m O_0} = \frac{\frac{A^{Trial}\sigma_1^0 + B^{Trial}\sigma_3^0}{2} - \sigma^m}{\frac{S_0}{2} - \sigma^m} \quad (4.6)$$

The equation (4.6) becomes:

$$A^{Trial}\sigma_1^0 + B^{Trial}\sigma_3^0 = F^{Trial} S_0 + 2\sigma^m(1 - F^{Trial}) \quad (4.7)$$

The expression of  $\sigma^m$  can be deduced from the Figure (4) as:

$$2\sigma^m = S_0 - D_0 \sin \phi \quad (4.8)$$

By replacing the equation (4.8) into the equation (4.7) one gets:

$$A^{Trial}\sigma_1^0 + B^{Trial}\sigma_3^0 = S_0 + D_0(F^{Trial} - 1) \sin \phi \quad (4.9)$$

Resolving concurrently the equations (4.5) and (4.9), it is easy to find the stress factoring parameters:

$$A^{Trial} = \frac{S_0 + D_0 F^{Trial}(1 + \sin \phi) - D_0 \sin \phi}{2\sigma_1^0} \quad (4.10)$$

$$B^{Trial} = \frac{S_0 + D_0 F^{Trial}(\sin \phi - 1) - D_0 \sin \phi}{2\sigma_3^0} \quad (4.10)$$

Since  $A^{Trial}$  and  $B^{Trial}$  may have singular values when the in-situ principal stresses are equal to zero, it is then, better to return to the equations (4.1) and (4.2) and define the trial values of the principal stresses:

$$\sigma_1^{Trial} = \frac{S_0 + D_0 F^{Trial} (1 + \sin \phi) - D_0 \sin \phi}{2} \quad (4.11)$$

$$\sigma_3^{Trial} = \frac{S_0 + D_0 F^{Trial} (\sin \phi - 1) - D_0 \sin \phi}{2} \quad (4.12)$$

On one side,  $\sigma_1^0$  is increased regardless its starting value to become  $\sigma_1^{Trial}$  by increasing progressively  $F^{Trial}$ , on the other side  $\sigma_3^0$  is decreased regardless its starting value to become  $\sigma_3^{Trial}$  by increasing progressively  $F^{Trial}$ . When these trial stresses reach their ultimate values, the magnitude of  $F^{Trial}$  is considered the stress point-based factor of safety  $FOS_{SDIM}^{SP}$ .

For a purely cohesive soil ( $\phi = 0$ ), the equations (4.13) and (4.14) reduce to the following :

$$\sigma_1^{Trial} = \frac{S_0 + D_0 F^{Trial}}{2} = \sigma_1^0 + \frac{D_0}{2} (F^{Trial} - 1) \quad (4.13)$$

$$\sigma_3^{Trial} = \frac{S_0 - D_0 F^{Trial}}{2} = \sigma_3^0 - \frac{D_0}{2} (F^{Trial} - 1) \quad (4.14)$$

(4.6) Since  $F^{Trial}$  controls the expansion (if  $F^{Trial} > 1$  the trial Mohr's circle expands outside the mobilized Mohr's circle, and if  $0 < F^{Trial} < 1$ , the trial Mohr's circle expands inside the mobilized Mohr's circle), the amount  $\frac{D_0}{2} (F^{Trial} - 1)$  added to the major principal stress  $\sigma_1^0$  is subtracted from the minor principal stress  $\sigma_3^0$  (Figure 4.2b). The evolution the Mohr's circle corresponding to  $\sigma_1^{Trial}$  and  $\sigma_3^{Trial}$  is then isotropic (Figure 4.2b). In this kind of soils, the failure envelope line in the SRM, falls straight fully horizontal on the Mohr's circle (Figure 4.2a), while in the SDIM (present method) the Mohr's circle expands isotopically to attain the failure envelope. Consequently, for purely cohesive soils, both methods then are expected to yield the same value of factor of safety.

The proposed method (SDIM) can be viewed as a method which preserves the validity of the safety factor definition by imposing a correct stress path to reach failure. Firstly, the procedure maintains the progressive development of the shear stress on same plane on which the shear strength will occur at failure. Secondly, it deals hence with the actual material, by employing its real strength parameters ( $c$ ,  $\phi$ ) and  $\psi$  rather than those reduced by a factor.

Unlike, the SRM which brings the failure envelope to the stress point in-situ Mohr's circle, the proposed method SDIM expands the latter by gradually increasing  $F^{Trial}$ . For a certain value of this factor, some stress points undergo plastic flow when their  $FOS_{SDIM}^{SP}$  are reached and the overall factor of safety is not known as long as the solution of the algebraic systems of equations is still converging. By a further increasing of  $F^{Trial}$  and when a non-convergence is established the last value of  $F^{Trial}$  is assumed to be the overall factor of safety  $FOS_{SDIM}$ . Therefore, the accuracy of  $FOS_{SDIM}$  depends obviously of the accuracy of  $FOS_{SDIM}^{SP}$ .

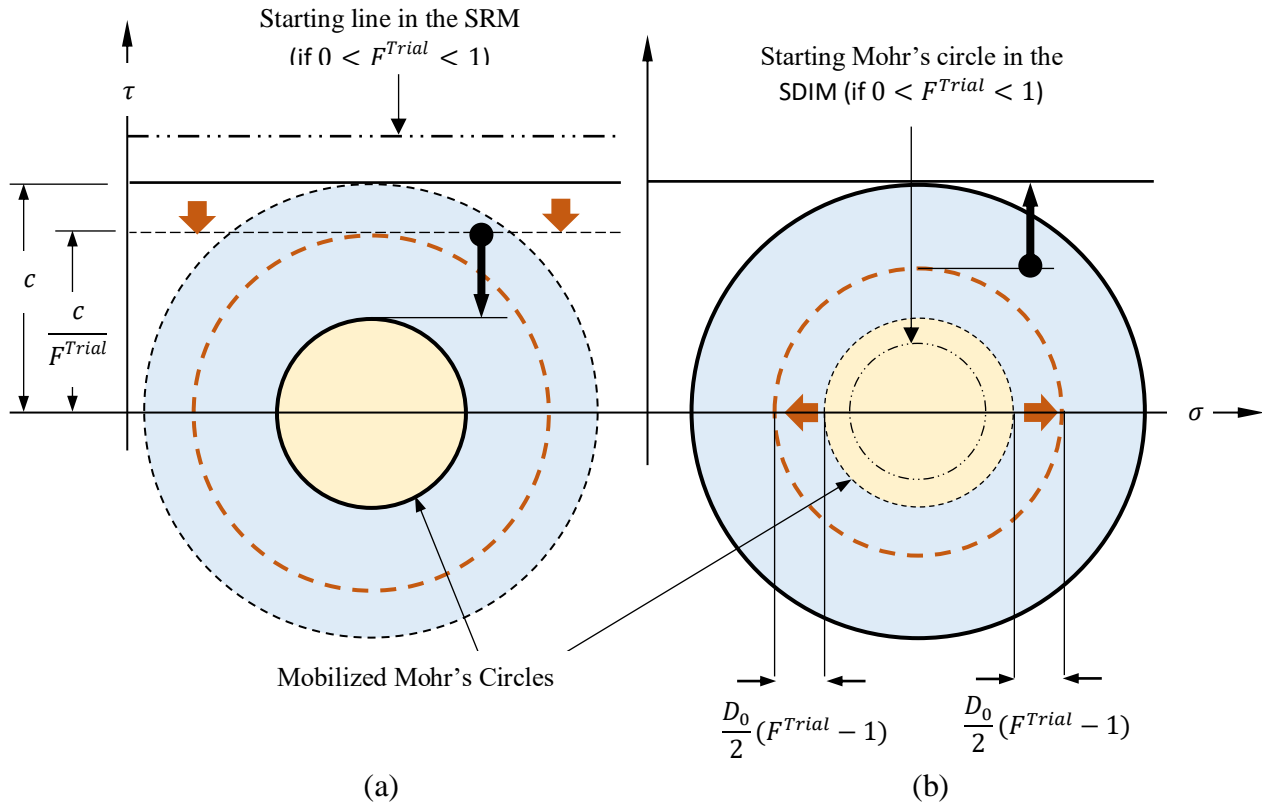


Figure 4. 2 Computational process I in a purely cohesive material (a) in the srm, the failure envelope line falls horizontally on the mobilized mohr's circle, (b) in the sdim, the mobilized mohr's circle expands isotropically.

#### 4.1.2 The computer Program S<sup>4</sup>DINA : Computational procedure

The theoretical developments described in the previous section have been implemented in a Fortran computer program called S<sup>4</sup>DINA (*Soil Stability Study by Stress Deviator Increasing using Numerical Analysis*). The finite element discretization of a typical slope domain is depicted in Figure 6. The eight-noded quadrilateral element was employed to mesh the entire region of a slope containing an embankment and a foundation layer. This element which possesses a quadratic field of displacements performs well in analysing problems such as those of slope stability (Smith et al. 2014). Applied boundary conditions to the soil are pinned supports at the bottom of the slope with no displacements in both horizontal and vertical directions ( $u = v = 0$ ) and roller supports on both sides of the mesh with no movement in the horizontal direction ( $u = 0$ ). The element heights were obtained by a uniform division of the embankment total height by the FEs number modelling the embankment in the vertical direction  $Y$  and the division of the foundation depth by the number of FEs modelling the foundation layer according to  $Y$ . The elements widths in the embankment were obtained by dividing both embankment top distance and embankment bottom distance by the number of finite elements discretizing the embankment according to the  $X$  coordinate. The generation of the elements coordinate was performed on the basis of the inclination of the lines connecting the nodes.

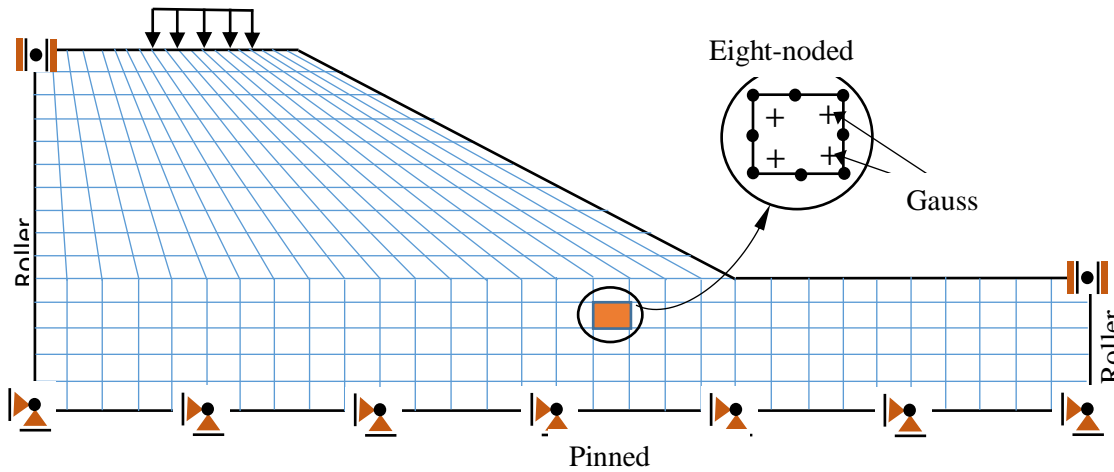


Figure 4. 3 Mesh used in <sup>4</sup>DINA.

Although the modelling with the adopted mesh is rather crude, the obtained results were reasonably accurate as we will see next. A more performant mesh should contain unstructured high order triangles or a combination between eight-noded elements and six-noded triangular elements. The latter are preferred as they can adequately model the shape of the sloping ground. The optimization of the finite element mesh is beyond the scope of this paper, and it is left to a future work.

Before starting the description of the computer program S<sup>4</sup>DINA and how the present procedure was implemented in the finite element code, it is worth to provide some additional information that may enable the reader a better comprehension. The slope geomaterial is dealt with as a visco-plastic material and its behaviour is described according to the visco-plastic procedure as given by (Zienkiewicz and Corneau 1974). The procedure is explained in detail by Smith et al. 2014. The computer program begins by reading the geometrical characteristics of the FE mesh (mesh dimensions, number of elements, etc.), boundary conditions, soil deformation and strength properties relevant to the Mohr-Coulomb failure criterion, and certain parameters relative to the visco-plastic computations such as the pseudo time  $\Delta T$ , the maximum number of iterations  $Iters^{mas}$  and tolerance of convergence  $TOL^{conv}$ . After the formulation of the stiffness matrix for each element using the deformation parameters ( $E, \nu$ ), the global stiffness matrix  $[K]$  for the entire discretized medium is then assembled. The in-situ stresses due to gravity in the initial conditions combined with any other stresses which are the result of any applied external loading, are calculated for all elements in Gauss points. For the initial stresses due to gravity, the  $K_0$  procedure is not valid for a domain with a sloping ground. Instead a deformation process is triggered by gravity loading. This involves, the resolution of the following system:

$$[K]\{U\} = \{R\}^0 \quad (4.15)$$

$$\{R\}^0 = \sum_{i=1}^{N_{elem}} \{f^e\} + \{P\}^{EXT} \text{ With } \{f^e\} = \int_{v^e} [N]^T \gamma dv^e \quad (4.16)$$



Expressions in which,  $Nelem$  is the total number of finite elements,  $[K] = \sum_{i=1}^{Nelem} [k^e]$  is the global stiffness matrix, whereas  $[k^e] = \int_{v^e} [B]^T [D] [B] dv^e$  is the element stiffness matrix.  $\{P\}^{EXT}$  is the global loading vector resulting from the external agencies.  $[N]^T$  is the transpose of the shape functions matrix and  $\{\gamma\} = \begin{Bmatrix} 0 \\ -\gamma \end{Bmatrix}$  the gravity vector composed from the soil unit weight  $\gamma$ .

By resolving the system (4.17), the nodal displacements and the stresses  $\sigma_x^0$ ,  $\sigma_y^0$  and  $\tau_{xy}^0$  at Gauss points are determined all over the slope area. The shear stresses exist in both embankment and foundation layer and are remarkably high in the vicinity of the sloping ground. On the basis of this set of stresses, the principal stresses and the orientation angle  $\alpha$  of their principal planes with respect to the axes of coordinates  $(X, Y)$ , are computed in the same locations by:

$$\sigma_1^0 = \frac{\sigma_x^0 + \sigma_y^0}{2} + \sqrt{\left(\frac{\sigma_x^0 - \sigma_y^0}{2}\right)^2 + (\tau_{xy}^0)^2} \quad (4.17)$$

$$\sigma_3^0 = \frac{\sigma_x^0 + \sigma_y^0}{2} - \sqrt{\left(\frac{\sigma_x^0 - \sigma_y^0}{2}\right)^2 + (\tau_{xy}^0)^2} \quad (4.18)$$

$$\tan(2\alpha) = \frac{-2\tau_{xy}^0}{(\sigma_x^0 - \sigma_y^0)} \quad (4.19)$$

At this point, the computed values of  $\sigma_1^0$ ,  $\sigma_3^0$  and  $\alpha$  are the backbone elements of SDIM since the present method is based on the expansion of the principal stress Mohr's circle. Once these stresses and their planes are known at every stress point, the program S<sup>4</sup>DINA proceeds with a large loop over a set of the prescribed values of the increasing factor  $F^{Trial}$  (see flowchart of Figure 4.4). The discrete values of this parameter can be either generated by the user or computed internally by the program. The second option is adopted in S<sup>4</sup>DINA and the user can check more than 950 values starting by 0.50, and incremented by 0.01, allowing thus to obtain a factor of safety within two decimals first and another procedure to refine the FOS for three decimals. The trial principal stresses values  $\sigma_1^{Trial}$  and  $\sigma_3^{Trial}$  that result from the process of stress deviator increasing and necessary to generate the Cartesian stresses for checking Mohr-Coulomb failure criterion can be determined now by the equations (4.13) and (4.14). Since the algebraic system of equations is resolved according to global system of coordinates  $(X, Y)$  it is mandatory to find the Cartesian stresses corresponding to the principal stresses  $\sigma_1^{Trial}$  and  $\sigma_3^{Trial}$ . A simple transformation gives:

$$\sigma_x^{Trial} = \frac{\sigma_1^{Trial} + \sigma_3^{Trial}}{2} + \frac{\sigma_1^{Trial} - \sigma_3^{Trial}}{2} \cos 2\alpha \quad (4.20)$$

$$\sigma_y^{Trial} = \frac{\sigma_1^{Trial} + \sigma_3^{Trial}}{2} - \frac{\sigma_1^{Trial} - \sigma_3^{Trial}}{2} \cos 2\alpha \quad (4.21)$$

$$\tau_{xy}^{Trial} = -\left(\frac{\sigma_1^{Trial} - \sigma_3^{Trial}}{2}\right) \sin(-2\alpha) \quad (4.22)$$

The purpose of computing the quantities given by the previous equations constitute another feature of the proposed method. Indeed, they serve to compute the equivalent stress loading vector in each finite element  $\{p^e\}$  as:

$$\{p^e\} = \int_{v^e} [B]^T \{\sigma^{Trial}\} dv^e \text{ and } \{P\}^{ESL} = \sum_{i=1}^{Nelem} \{p^e\} \quad (4.23)$$

Where  $\{P\}^{ESL}$  is the global equivalent stress loading vector,  $[B]^T$  is the transpose of strain field-nodal displacement matrix, whereas  $\{\sigma^{Trial}\}$  is the stress vector containing the stresses defined by the equations (4.22-4.24), that is  $\{\sigma^{Trial}\} = [\sigma_x^{Trial} \ \sigma_y^{Trial} \ \tau_{xy}^{Trial}]^T$ . There is no contribution of  $\sigma_z^{Trial} = \nu(\sigma_x^{Trial} + \sigma_y^{Trial})$  in the loading system, since all elements of the fourth column in the matrix  $[B]^T$  are zero. However, its contribution in checking the yield criterion is not trivial.

Another imbricated loop starts just after the calculation of the equivalent stress loading vector. Within a maximum number of iterations  $Iters^{max}$ , the following system of equations is resolved:

$$[K]\{U\}^j = \{R\}^j \quad \text{with} \quad \{R\}^j = \{P\}^{ESL} + \{P\}^{BLj} \quad (4.24)$$

Equation in which  $\{P\}^{BLj}$  is the vector of body loads which varies from an iteration to another. It is given by:

$$\{P\}^{BLj} = \sum_{i=1}^{Nelem} \int_{v^e} [B]^T [D] \Delta T (\delta \epsilon^{VP})^j dv^e \quad (4.25)$$

For Mohr-Coulomb failure criterion, the pseudo time  $\Delta T$  is given by:

$$\Delta T = \frac{4(1+\nu)(1-2\nu)}{E[1-2\nu+(\sin \phi)^2]} \quad (4.26)$$

The constant stiffness method is adopted in this program. It uses repeated elastic solutions to achieve convergence by iteratively varying the loads on the system. At this point the SDIM differs significantly from the SRM. In the latter,  $\{R\}^0$  of equation (4.17) is kept as the first term in the loading vector (4.26). If stress distribution is necessary, body loads should be considered. Here, the body load vector is not formulated the same way as in the SRM. In the SRM it is composed from plastic strains after checking stresses against a fictive yield criterion resulting from reduced strength parameters according to each value of  $F^{Trial}$  whereas,  $\{P\}^{BLj}$  in the present method (SDIM) is generated in each iteration after checking stresses whose deviators were expanded according  $F^{Trial}$  against the real Mohr-Coulomb yield function formulated by the effective soil strength parameters  $c$  and  $\phi$ . Inside this loop and for each iteration a convergence test is assessed. This is given by:

$$\eta = \frac{|u^j - u^{j-1}|}{|u^j|_{max}} < TOL^{conv} \quad (4.27)$$

Where  $u^j$  the nodal displacement in the current iteration is,  $u^{j-1}$  is the nodal displacement in the previous iteration,  $|u^j|_{max}$  is the maximum value of the nodal displacement in the current iteration and  $TOL^{conv}$  is the convergence tolerance. When the iterative process fails to converge within the prescribed number of iterations, the slope failure is said to occur and then the value of  $F^{Trial}$  is considered the SDIM factor of safety  $FOS_{SDIM}$ .

## 4.2.1 Spurious zones of plastic strains and the importance of visualizing plastic deformation areas

The finite element analysis of a slope stability problem, using the combination of Mohr-coulomb criterion and continuum mechanics equations of plane strain problems can give birth to an abnormal phenomenon producing large areas of plastic strains. This, in many situations mislead the deformation process to indicate a premature slope collapse with an underestimated safety factor, especially if a non-convergence criterion is employed to assess the value of FOS.

To understand how these plastic zones occur, let's consider a half-infinite space loaded only by gravity. Mohr-Coulomb elasticity condition gives:

$$[\sigma_1(1 - \sin \phi) - \sigma_3(1 + \sin \phi)] \leq 2 c \cos \phi \quad (4.29)$$

Where  $\sigma_1 = \gamma z$  and  $\sigma_3 = k_0 \gamma z$  are the principal stresses caused by the unit weight at a given depth  $z$ . The use of plane strain equations leads to an earth pressure coefficient at rest  $k_0 = \frac{\nu}{1-\nu}$  where  $\nu$  is the soil Poisson's ratio. Replacing the expressions of the principal stresses and the lateral earth pressure coefficient at rest into the inequality (4.30), the elasticity condition becomes:

$$\gamma z \left[ \frac{(1-2\nu) - \sin \phi}{(1-\nu)} \right] \leq 2 c \cos \phi \quad (4.30)$$

Since both  $(1 - \nu)$  and  $z$  are  $> 0$ , two possibilities are to be considered:

- If  $\frac{(1-2\nu) - \sin \phi}{(1-\nu)} \leq 0$ , which means that  $\sin \phi \geq (1 - 2\nu)$  (called the  $\phi - \nu$  inequality condition (Zheng et al. 2005)) the inequality (4.31) is verified everywhere since  $z$  is positive and consequently the elasticity condition (inequality 4.30) holds true at any point from the medium indicating thus that the whole medium is in an elastic state.
- If  $\frac{(1-2\nu) - \sin \phi}{(1-\nu)} > 0$  which means that  $\sin \phi < (1 - 2\nu)$ , the depth of interest  $z$  is less than a thickness  $H$  according to the inequality :

$$z < H = \frac{2 (1-\nu) c \cos \phi}{\gamma [(1-2\nu) - \sin \phi]} \quad (4.31)$$

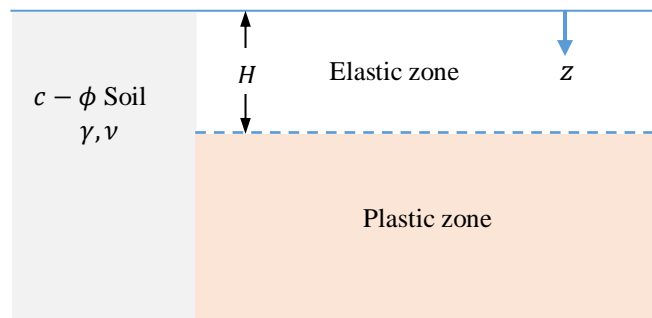


Figure 4. 4. The depth beyond which an abnormal layer of plastic strains can appear in a semi-infinite medium. The condition  $\sin \phi < (1 - 2\nu) k$

keeps the holding the elasticity conditions true only in an upper layer of thickness  $H$  (Figure 4.5). Obviously the elastic zone thickness depends on the magnitudes of  $\nu$ ,  $c$  and  $\phi$ . The lower layer extending to infinity is plastically damaged which is physically irrational (Zheng et al. 2005). This abnormal plasticity layer should not exist since the medium is in overabundant equilibrium.

The above equations are only valid for a semi-infinite space. However, for a slope stability problem, the anomalous region of plastic strains is curved with irregular shapes that follow the sloping ground. As it is difficult to establish the area expression analytically, the option for the numerical method is possible since the four plastic strains increments are available in each integration point. Many researchers (Maji 2017 and Zheng et al. 2005) agreed to use of equivalent plastic strain as an appropriate scalar to represent the plastic state at any given point.

This parameter is computed as:

$$\bar{\epsilon}_p = \sum_i (\Delta \bar{\epsilon}_p)_i \quad (4.32a)$$

$$\text{with} \quad (\Delta \bar{\epsilon}_p)_i = \sqrt{\{\Delta \epsilon_p\}_i^T \{\Delta \epsilon_p\}_i} \quad (4.32b)$$

$(\Delta \bar{\epsilon}_p)_i$  is the incremental equivalent plastic strain evaluated from the components of the vector of plastic strains  $\{\Delta \epsilon_p\}_i$  at a given loading step  $i$ .  $\bar{\epsilon}_p$  is the accumulation of the incremental equivalent plastic strains from all loading steps.  $\bar{\epsilon}_p$  which is computed in each Gauss point is an excellent indicator for the plasticity conditions when treating a slope stability problem.

Focussing on the computation of the slope stability factor is not enough to decide whether the slope has really collapsed and the factor of safety has been accurately determined. Checking for the violation of the  $\phi - \nu$  inequality with the use of a visualization technique to plot the plastic deformation contours are necessary steps to care for in order to ensure that the finite element computations have been normally performed.

#### **4.2.2 Comparative analysis involving the slope safety factor and contours of plastic deformation zones**

It is well established that the accuracy of FOS computed by the finite element method, relies on several factors. These factors may include, the nature of finite element employed, the total number of elements in FE mesh, the mesh density in the slope region where the failure line is expected to occur, the prescribed maximum number of iterations, the convergence tolerance allowed in the finite element computations, the type of flow rule adopted and obviously the value of Poisson's ratio.

The primary target of this section is seeking the relative accuracy when compared to both LEM and SRM or to any other rigorous method. The SRM results were obtained by the use of the Fortran computer program code P64 from the textbook by Smith et al. 2014. In order to create the same conditions of comparison and hence a reliable comparison, slight modifications were performed on the code P64 which is called MSGP64 (Modified Smith and Griffiths P64) in this paper. Firstly, the routine which performs the generation of the mesh in S<sup>4</sup>DINA was implemented in MSGP64 to exclude any effect of the nature and the number of finite elements on the outcomes.

Secondly, the sequence of  $F^{Trial}$  values, implemented internally to control the process of Mohr's circles expansion in S<sup>4</sup>DINA were similarly adopted in MSGP64 as factors for reducing the strength parameters. Thirdly and similarly to what has been programmed in S<sup>4</sup>DINA, a supplementary routine for computing the equivalent plastic strains was also encoded in MSGP64. The process of stress correction is the same as was stated earlier. The LEM factors of safety appearing in the comparison examples were obtained using the computer code SLIDE 6.0. The comparison is restricted to the most accurate slice methods, the Bishop and Morgenstern-Price methods.

## Conclusion

As reviewed early SDIM as the potential to help slope designer or geotechnical engineers deal with this problems with more efficacy and with precise data displayed by the programs that comes to paired with this Method S<sup>4</sup>DINA and mitigate future problems in order to save life's and money. By working in means of progressively increasing a factor called Mohr's circle expansion factor until the slope failure is reached, borrowing thus, and the reverse path of the SRM which consists of reducing the soil strength parameters. The slope failure is said to occur when the iterative process fails to converge within the prescribed range of the maximum number of iterations.

SDIM tends to use a very strict rules in order to provide the best results and more accurate factor of safety. It gives the engineer a clear view of the dangerous zones with a high precision for the best interpretations of the results. Making designer life easier and making sure that the factor of safety provided is related to the real soil parametric took from in-situs tests analysis. In this chapter we studied the bases of the new method called SDIM-stresses deviator increasing Method that comes paired with its program called S<sup>4</sup>DINA that will be reviewed in the next chapter. This program will be studied in order to validate all that have been mentioned in this chapter. The basis of SDIM are solid and with a very good results by the end of it.

To verify that the data have been input correctly, a cross section of the problem being analysed should be drawn to scale and include all the required data. The input data should be checked against the drawing to ensure the data in the input file are correct.

Automatic searches will be performed for circular or noncircular slip surfaces. The automatic search procedures used S<sup>4</sup>DINA is designed to aid the designer into getting the best results for any type of surfaces form so since the method is applicable to any form of surfaces like slice methods of Morgenstern-Price fore stance SDIM takes advantages of providing the precise strain stresses path.

---

# CHAPTER V

## APPLICATION OF THE PROGRAM S<sup>4</sup>DINA AND PARAMETRIC STUDY

## 5.1. Introduction

In this chapter we get to conclude our work by exposing the study's that have been conducted in order to get able to make accurate evaluation of the safety coefficient using both Numerical analyses. For the following chapter we worked with the following material (software) In order to carry out the parametric study:

- Rocscience SLIDE 6.0
- TECPLOT
- SDINAR
- Origin Pro

**SLIDE 6.0** for the factor of safety from the LE Methods, while **TECPLOT** for drawing plastic zones and stress contours in a slope stability problem and **S<sup>4</sup>DINA** to conduct a Slope Stability Analysis by Finite Element Modelling and we used **Origin Pro** to Build graphical representation of the analyses that will be showed further in this chapter for a better appreciation of the method even the table of the results will be represented to compare it.

## 5.2. Parametrical Study.

For the analyses of the new method SDIM was verified by comparing results with the existing slice method using examples in the literature. The slope stability and safety were evaluated with this new method and the effects of different factors on soil slope safety and stability were analysed. These results indicate Finite elements Analysis provides a very close value from those given by the LE method in slope stability analysed and for that, the analyse was conducted using an associated analyse and non-associated since the LEM uses associated analyses as its standard while S<sup>4</sup>DINA gives the designer a choice of associating or not.

So for the association we assumed that  $\psi = 19.6^\circ$  and non-associated will be zero  $\psi = 0^\circ$ .

### 5.1 1Table Soil characteristics.

SOIL	C(kn/m2)	$\varphi^\circ$	$\gamma$ (kn/m3)	$\psi^\circ$
	3	19.6°	20	19.6°

The model profile that have been used for this evaluation is displayed bellow for the respective profile with foundation and without foundation model. The drawing was designed on the designate software Slide 6.0 the same models that will be used on S<sup>4</sup>DINA to make sure that the evaluation taken in count the same configuration.

1. Case 1 we have studied a profile that included the Slide surfaces within its foundation and the profile description are displayed in picture in other to show off the measurement that have been taken in consideration for this study.



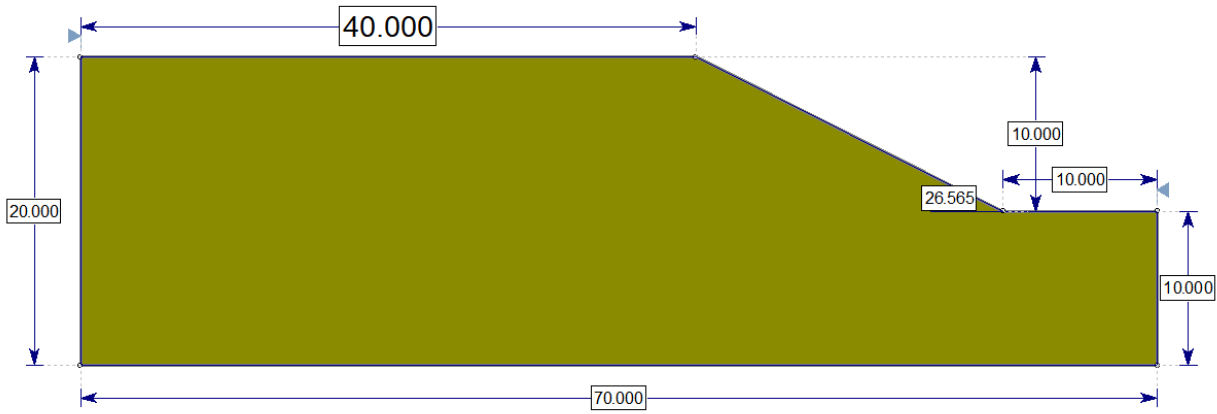


Figure.5 1

Slope with foundation Profile.

- Case 1 in this part we have took out the foundation in order to study the slope itself, the profile that will be followed was taken in consideration for the analyses to better understand the studied of the disassembled parts of the project to get better and precision of the general and partial factor of safety.

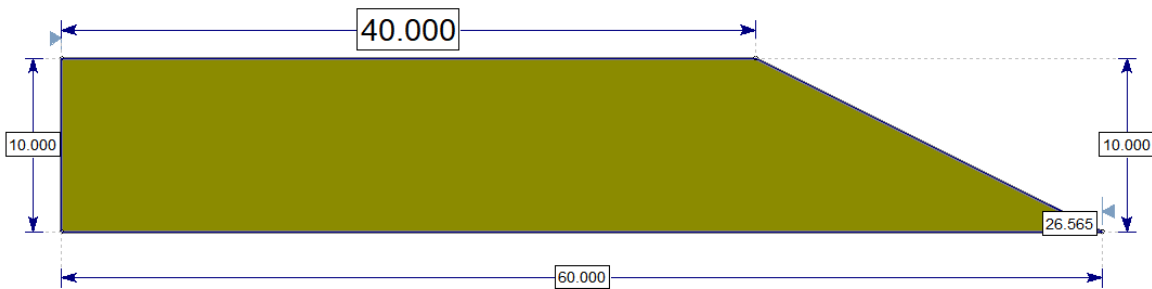


Figure 5.2 1 Slope without foundation Profile.

### 5.3. Input Soil Parametric

In this part we show the inputted parametric that we have taken in consideration in both software's SLIDE 6.0 and S<sup>4</sup>DINA for Study propose:

Case 1) Slide 6.0. for this software in both cases where the slope with foundation and without foundation the that input that file will be the same, as showed in the interface below.

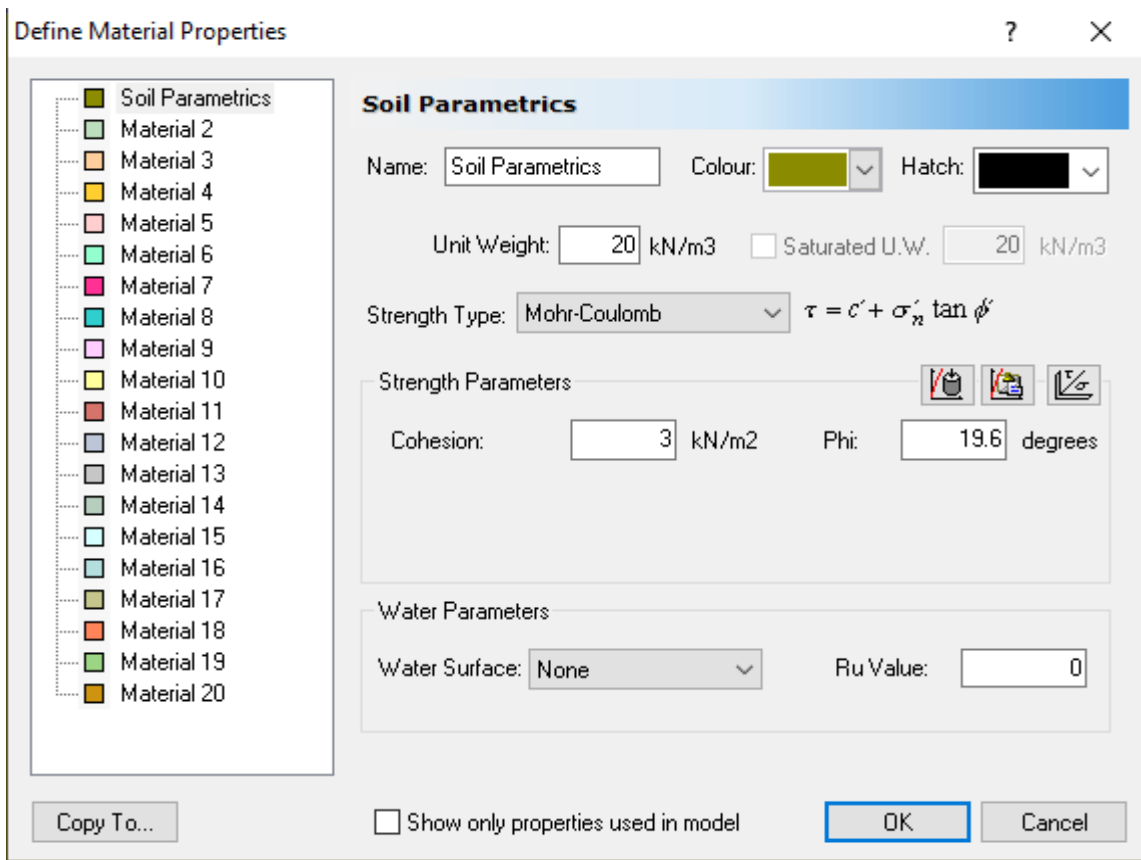


Figure 5.3 1 Soil parametric in Slide 6.0 Input Data file.

Case 2) S<sup>4</sup>DINA, in this case we will include two input that files for the slope with Foundation and without foundation profile since the work in S<sup>4</sup>DINA will be taken by the off MSDV COMPILER. Therefore we will also display two input files since we said early that in S<sup>4</sup>DINA we can perform a study's that are associated or note by the use of psi.

A) Slope profile with foundation Data file. **Associated.**

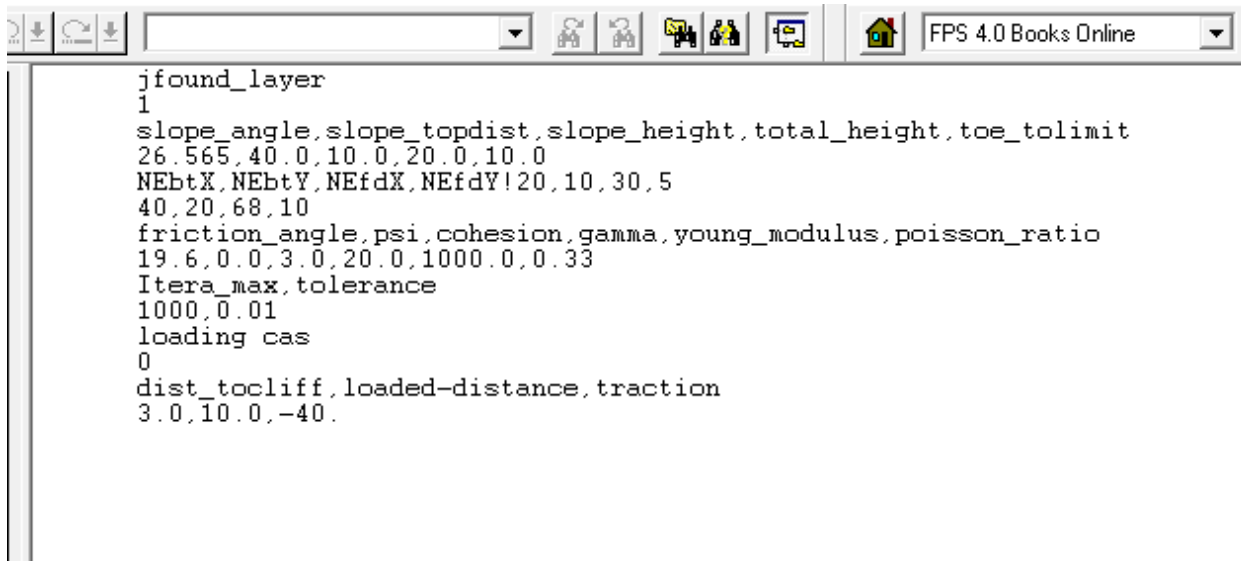
```

jfound_layer
1
slope_angle,slope_topdist,slope_height,total_height,toe_tolimit
26.565,40.0,10.0,20.0,10.0
NEbtX,NEbtY,NEfdX,NEfdY|20,10,30,5
40,20,68,10
friction_angle,psi,cohesion,gamma,young_modulus,poisson_ratio
19.6,19.6,3.0,20.0,1000.0,0.33
Itera_max,tolerance
1000,0.01
loading cas
0
dist_tocliff,loaded-distance,traction
3.0,10.0,-40.

```

Figure 5.4 1 Associated Profile of the slope with foundation on SDINAR data file

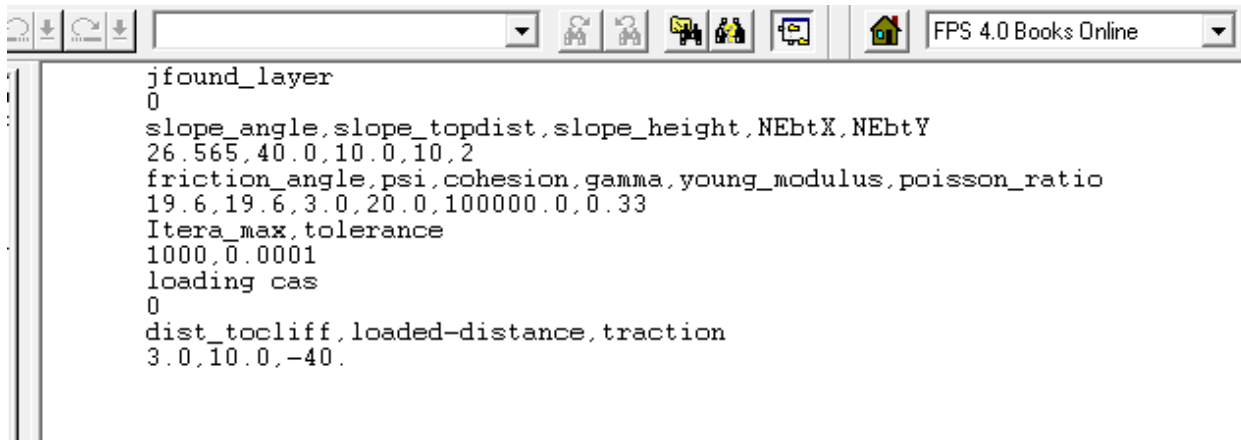
A.1) in this case we can clearly see that the value of psi is taken to zero, means that this calculation will be **non-associated**.



```
jfound_layer
1
slope_angle,slope_topdist,slope_height,total_height,toe_tolimit
26.565,40.0,10.0,20.0,10.0
NEbtX,NEbtY,NEfdX,NEfdY!20,10,30,5
40,20,68,10
friction_angle,psi,cohesion,gamma,young_modulus,poisson_ratio
19.6,0.0,3.0,20.0,1000.0,0.33
Itera_max,tolerance
1000,0.01
loading cas
0
dist_tocliff,loaded-distance,traction
3.0,10.0,-40.
```

Figure 5.5 1 non-Associated Profile of the slope with foundation on SDINAR data file.

**B) Slope profile without foundation input Data file. Associated**



```
jfound_layer
0
slope_angle,slope_topdist,slope_height,NEbtX,NEbtY
26.565,40.0,10.0,10,2
friction_angle,psi,cohesion,gamma,young_modulus,poisson_ratio
19.6,19.6,3.0,20.0,100000.0,0.33
Itera_max,tolerance
1000,0.0001
loading cas
0
dist_tocliff,loaded-distance,traction
3.0,10.0,-40.
```

Figure 5.6 1 Associated Profile of the slope without foundation on SDINAR data file.

**B.1) Slope profile without foundation input Data file. Non-Associated**

```

jfound_layer
0
slope_angle,slope_topdist,slope_height,NEbtX,NEbtY
26.565,40.0,10.0,10,2
friction_angle,psi,cohesion,gamma,young_modulus,poisson_ratio
19.6,0.0,3.0,20.0,100000.0,0.33
Itera_max,tolerance
1000,0.0001
loading cas
0
dist_tocliff,loaded-distance,traction
3.0,10.0,-40.

```

Figure 5.7 1 Non-Associated Profile of the slope without foundation on SDINAR data file

### 5.4. Comparison between the results of calculation of LEM and SDIM

This analyses will conducted by phases, fort the first part we will be testing the influence of the Calculation parametric to know how do they can influence the results of the factor of safety to be obtain since S<sup>4</sup>DINA take all parametric in consideration, and we further get to make evaluation of the deformation parametric in order to understand how can they also influence to the slope stability analyses. We will be displaying the results got in S<sup>4</sup>DINA while of slide 6.0 are constant because for its parametric study have no influence on the results.

### 5.5. Analyses of the influence of the input parametric

In this parte we will analyse the effects of the parametric that are required within the S<sup>4</sup>DINA while for Slide 6.0 those are not required, to start this first parte we will begin with Calculation parametric (Interaction number and Number of Finite elements) and further we will analyse the Deformation parametric (E- Young’s Modulus and Poisson Ratio).

**Iteration**, in the context of computer programming, is a process wherein a set of instructions or structures are repeated in a sequence a specified number of times or until a condition is met.

### 5.6 Iteration Number, Slope with Foundation and without foundation.

#### Associated flow rule.

Table 5 2 1. Rapport of the Results of the effect of the Number of Iteration for FS of the 3 methods.

INTERATION	BS	MP	SDIM
100			0.957
200			0.979
300			0.989
400			0.990
500			0.991

600	0.999	0.997	0.991
700			0.991
800			0.991
900			0.991
1000			0.992
1100			0.992
1200			0.992
1300			0.992
1400			0.992
1500			0.992

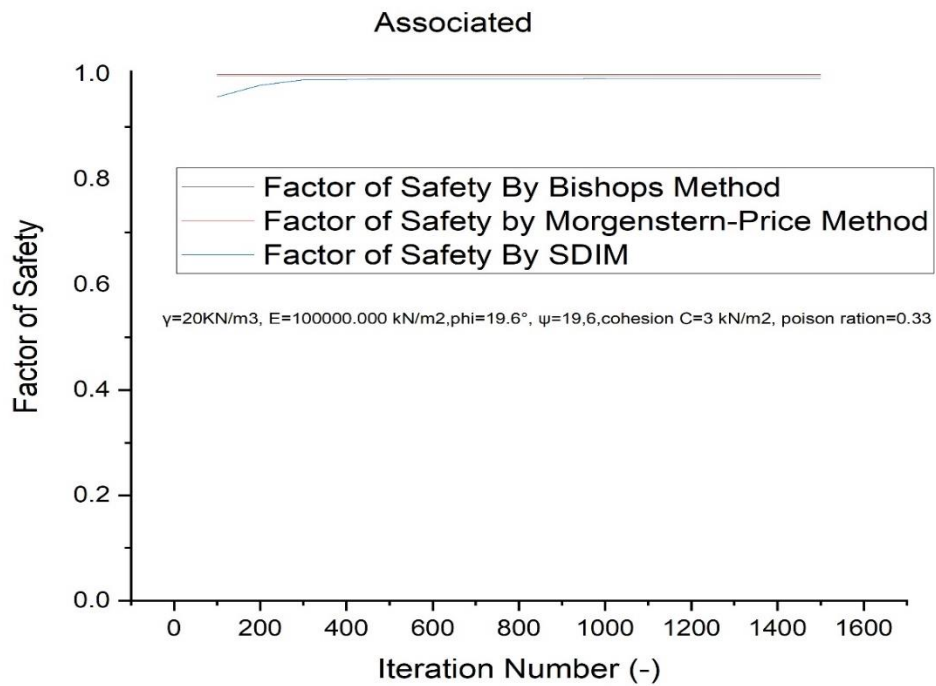


Figure 5.8 1 Iteration Number for the slope with foundation, associated

**Non-associated**

Table 5 2 2 Rapport of the Results of the effect of the Number of Iteration for FS of the 3 methods

Iteration	BS	MP	SDIM
100			0.914
200			0.914
300			0.938
400			0.949
500			0.951
600			0.953

700	0.999	0.997	0.954
800			0.955
900			0.956
1000			0.957
1100			0.958
1200			0.959
1300			0.959
1400			0.959
1500			0.959

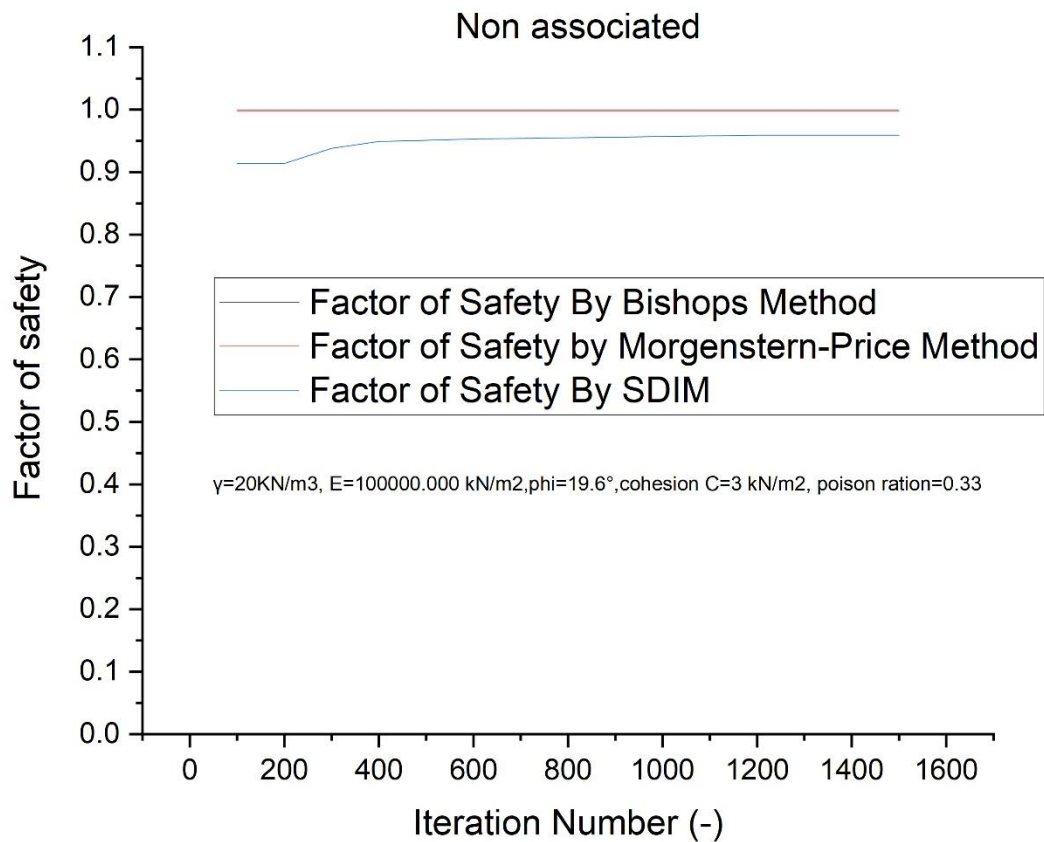


Figure 5.9 1. Iteration Number for the slope with foundation, non-associated

### 5.6.1. Iteration Number, Slope without Foundation

#### a) Associated

Table 5 2 3 Rapport of the Results of the effect of the Number of Iteration for FS of the 3 methods

Interactions	BS	MP	SDIM
100			0.949
200			0.969

300			0.978
400			0.982
500			0.983
600			0.985
700			0.985
800	0.989	0.984	0.986
900			0.986
1000			0.986
1100			0.987
1200			0.987
1300			0.987
1400			0.987
1500			0.987

**Associated**

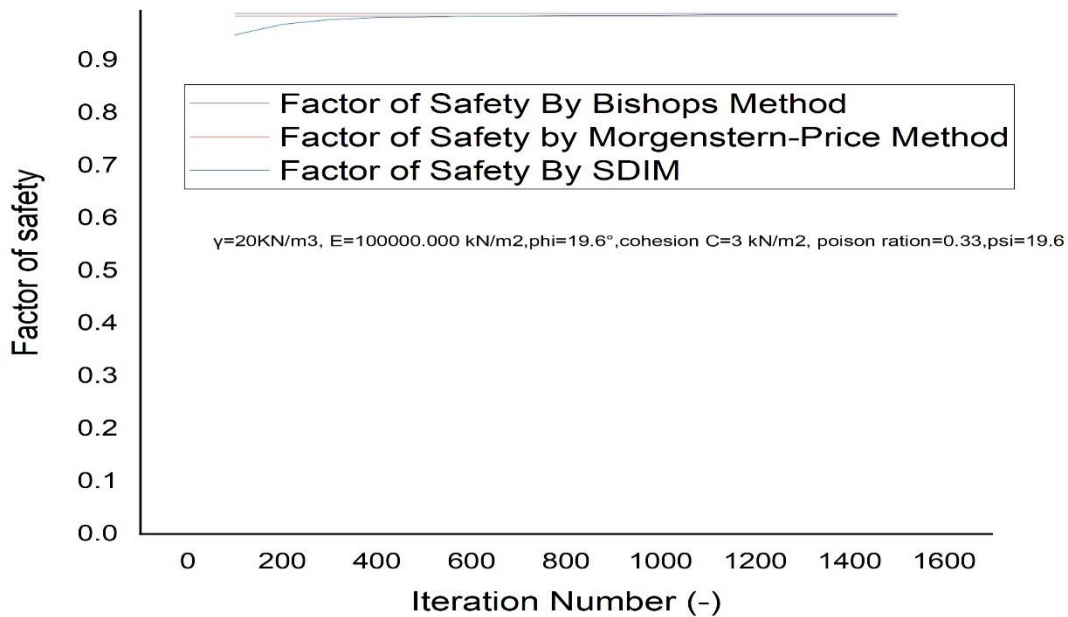


Figure 5.10 1 Iteration Number for the slope without foundation, associated.

The variation of the Number of Iteration have a big influence on the factor of safety that will be displayed as result, starting from a 100 iterations we got a underestimated value of factor cause by the lack of iteration for the correspondent geometry since at this set number the program could get into the convergence, it can be cleared viewed on the plastic counters.

Also when the assumption for the calculations is with associated flow rule the factor of safety factor got from SDIM and LEM are very closed from each other, when applying the non-associated flow rule we found the a lack of resistance of soil and the factor of factor tends to be far from LEM.

## 5.7. Analyses of the plastic zones and stress contours in a slope stability problem.

In this part we will be analysing the plastic zones and stress contours in a slope stability problem got with this new procedure SDIM. As mentioned early in this chapter, for the drawing we used Tecplot, into this we focusing on testing the parametric that have inputted early on this same chapter, we have gather the coordinates from SDINAR Rapport file order to get this date into an extension .dat to be able to run it on tecplot. We will displaying in this the both the slope features, with foundation and a slope without foundation.

### 5.7.1. Associated flow rule.

#### a) Number of iterations 100.

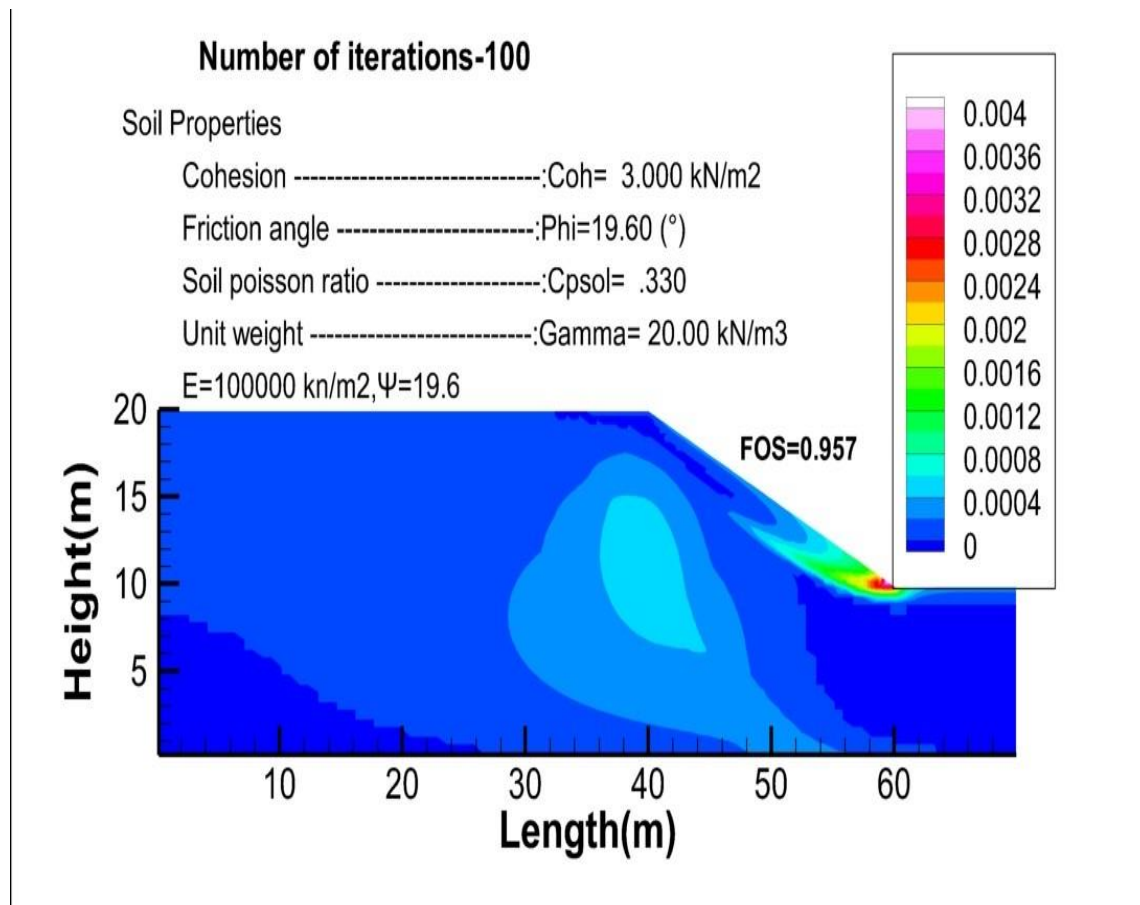


Figure 5.11 1 Strain contours corresponding to the step of failure for 100 iterations, with the foundation.

At this step is clear the appearance of small slip line by toe and clear see a start of deformation which can mislead engineers into thinking that the failure process has begun while isn't true because at this set of iterations there is no convergence and the deformation process is far from being reach. The same behaviour will be seen on the non-associated flow rule. To rectify this further increasing of the number of iteration is needed.



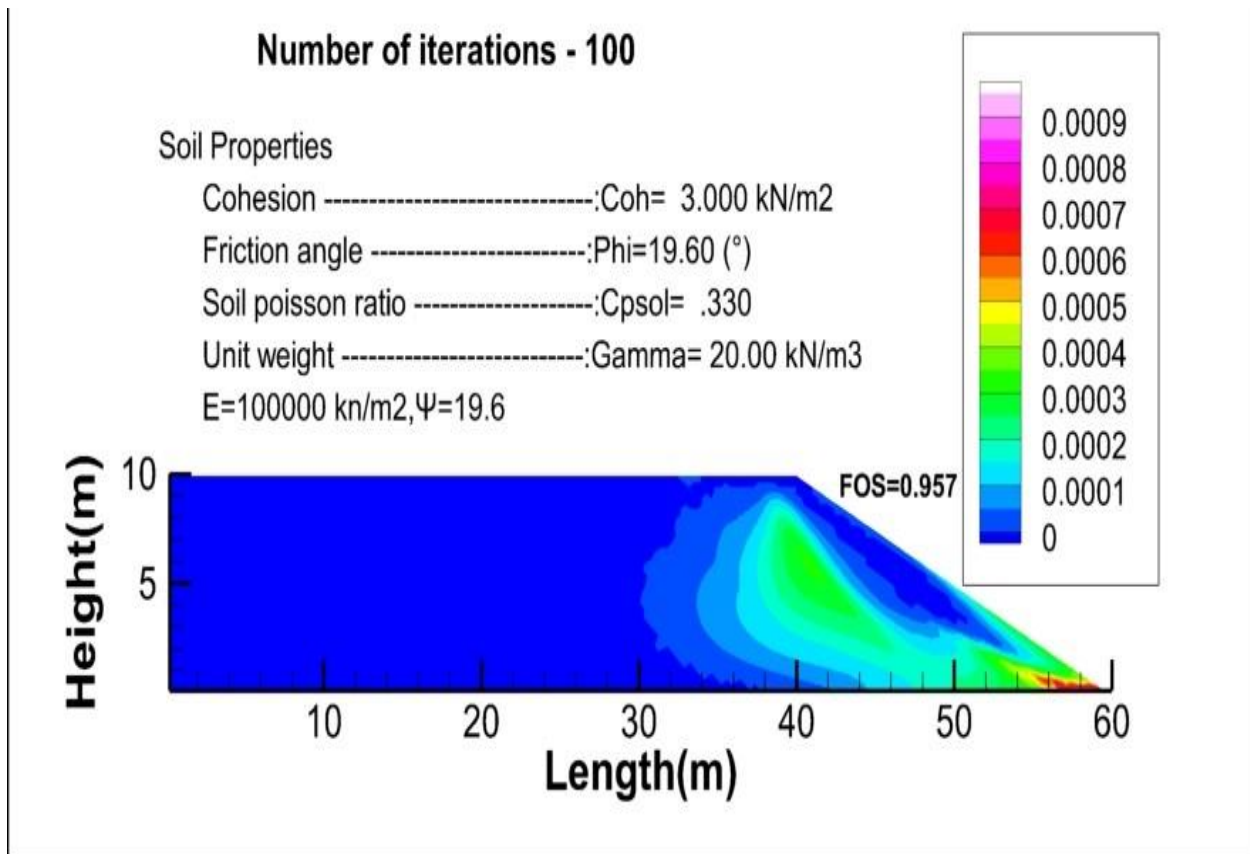


Figure 5.11 2 Strain contours corresponding to the step of failure for 100 iterations, without the foundation.

**b) Number of iterations 200**

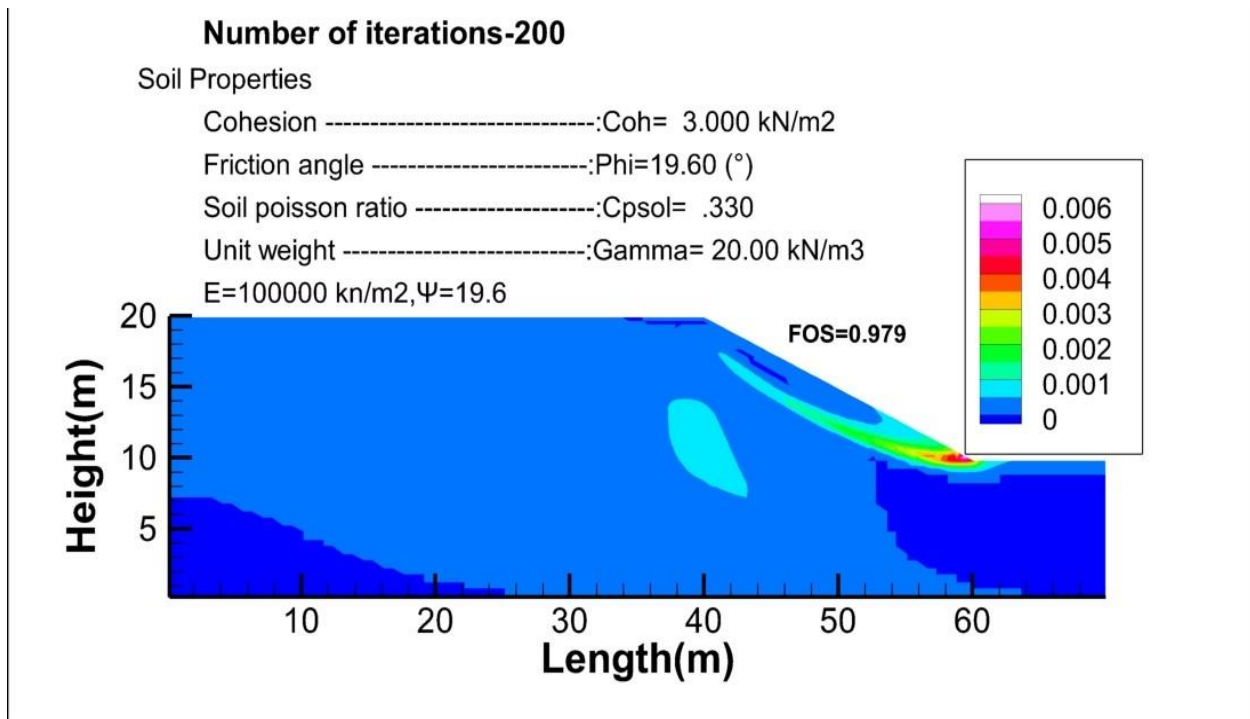


Figure 5.11 3 Strain contours corresponding to the step of failure for 200 iterations, with the foundation.

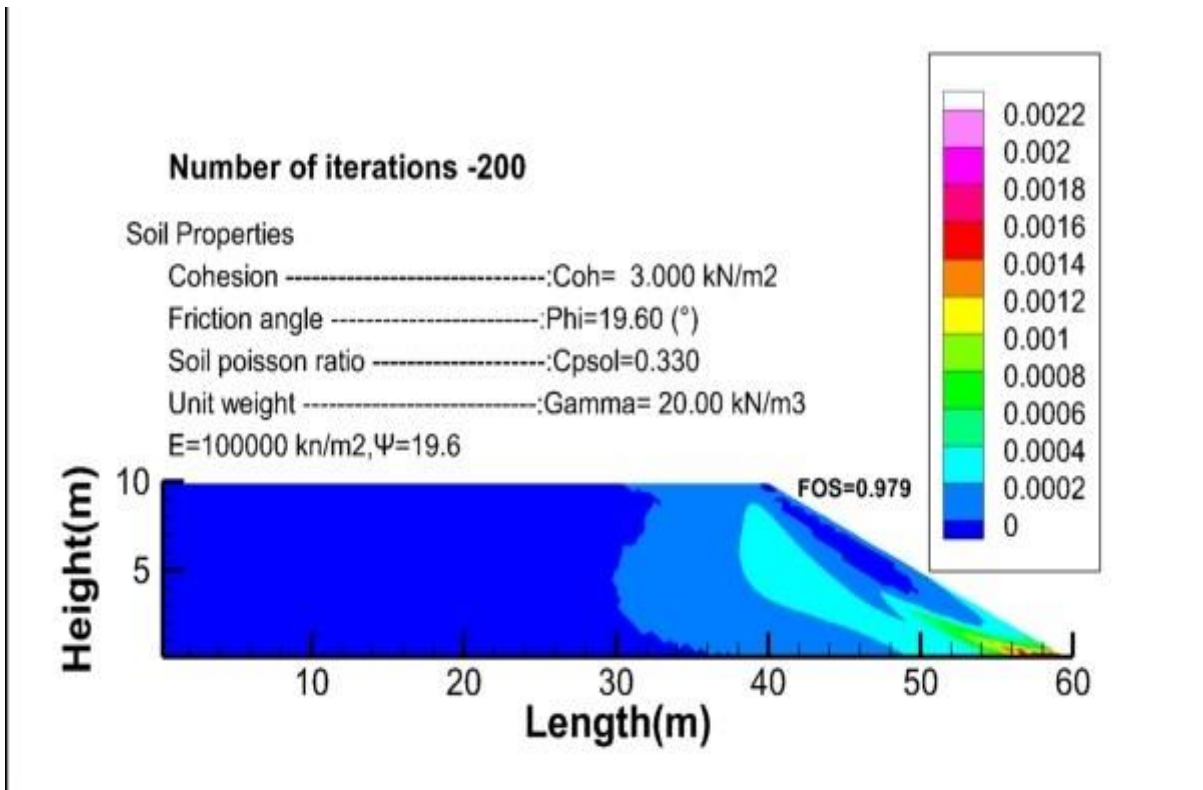


Figure 5.11 4 Strain contours corresponding to the step of failure for 200 iterations, without the foundation.

**c) Number of iterations 300**

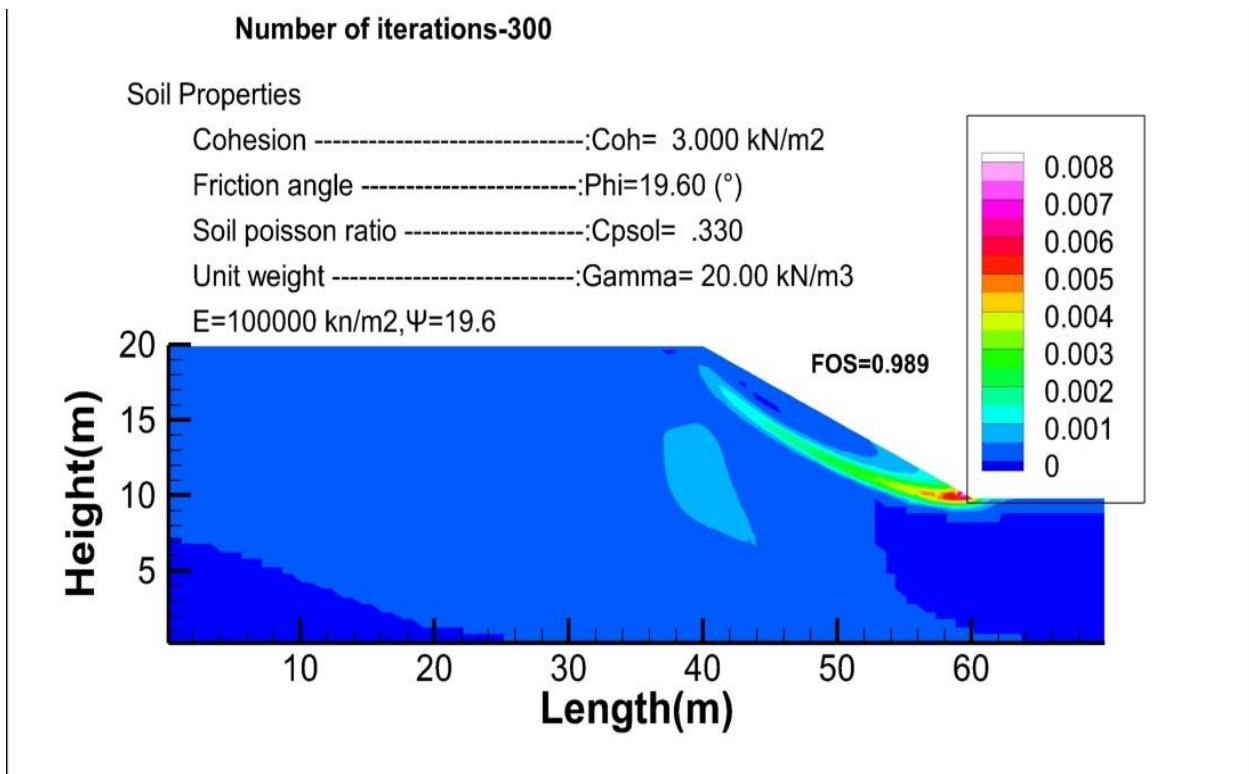


Figure 5.11 5 Strain contours corresponding to the step of failure for 300 iterations, with the foundation.

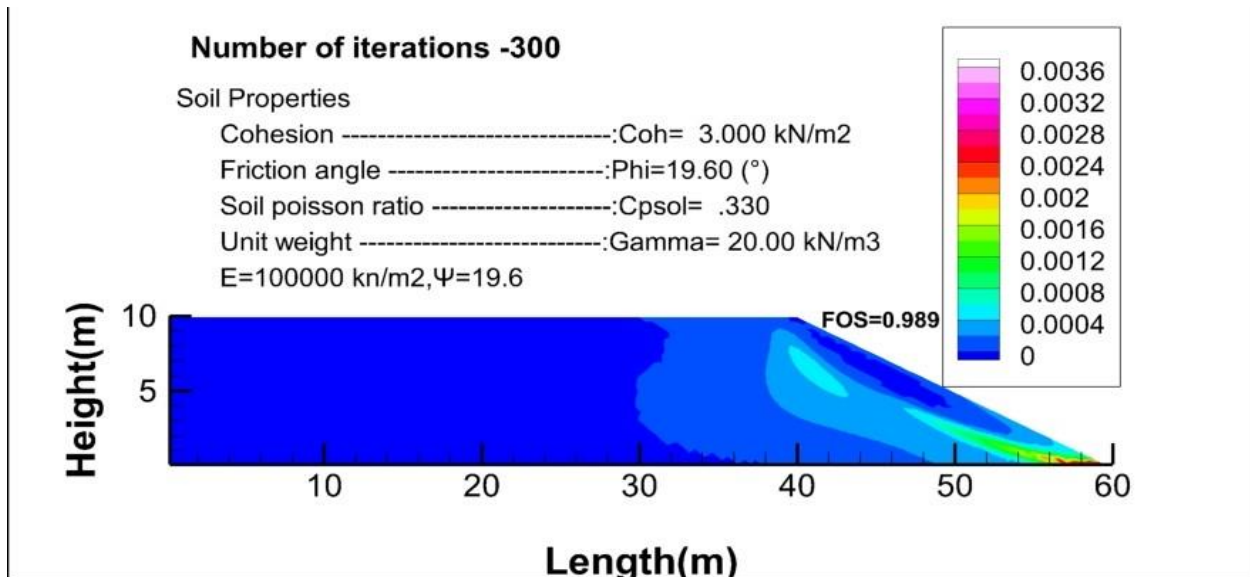


Figure 5.11 6 Strain contours corresponding to the step of failure for 300 iterations, without the foundation.

**d) Number of iterations 400**

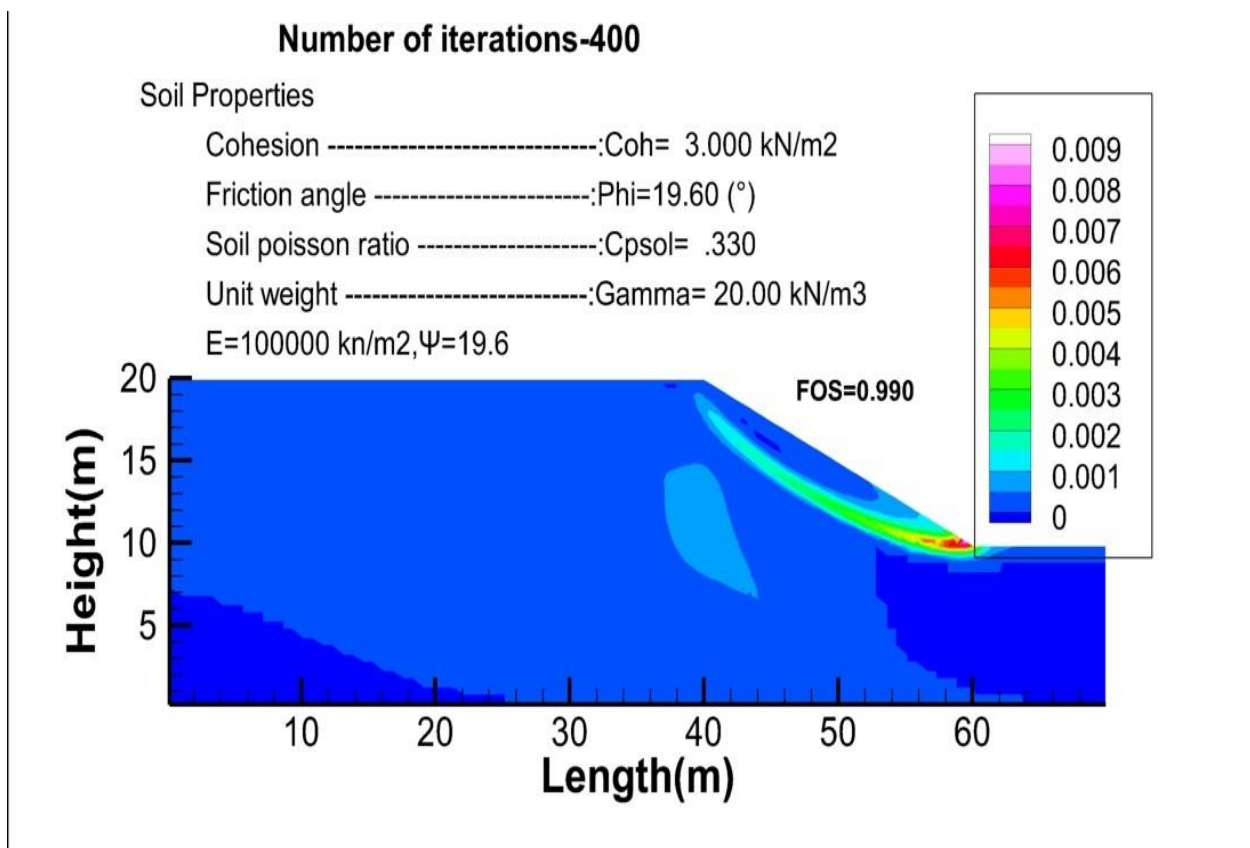


Figure 5.11 7 Strain contours corresponding to the step of failure for 400 iterations, with the foundation.

At this stage we can clearly see the slide line being addressed forward to the crest, where when reach the condition for the convergence will be met, following the factor of safety we can see is still underestimated only will be acceptable when all convergence is reached.

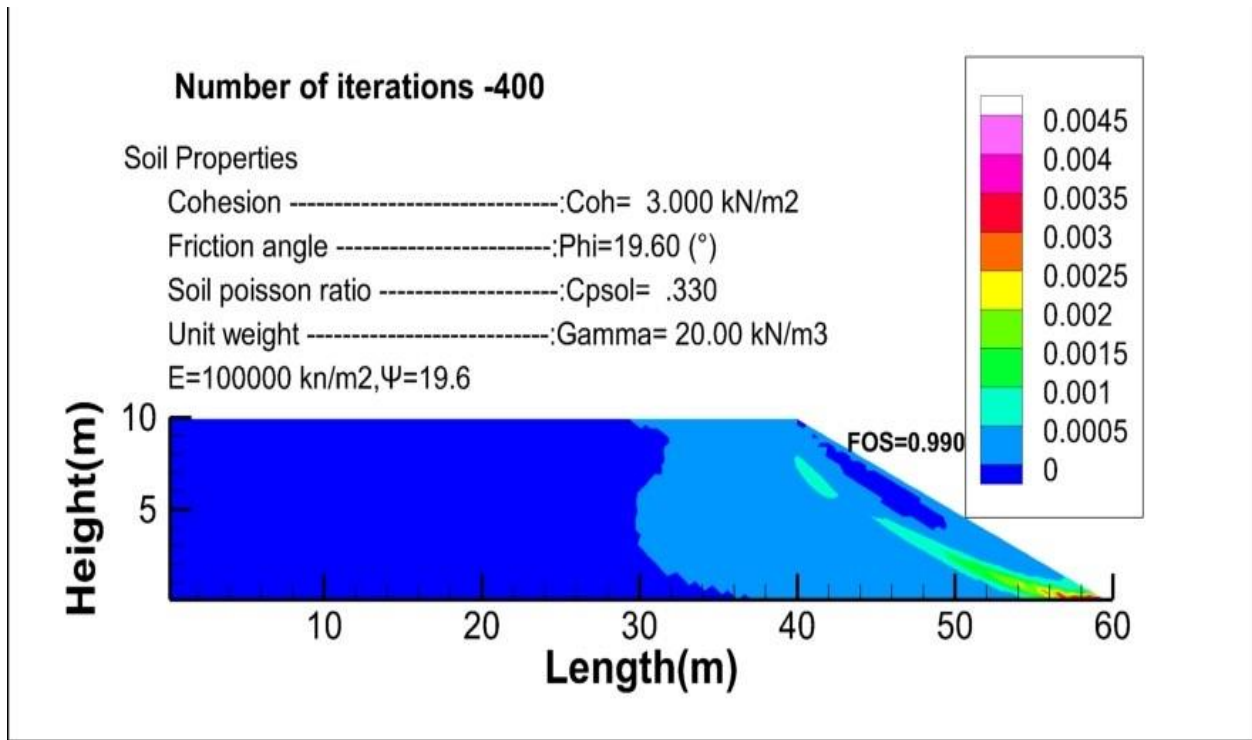


Figure 5.11 8 Strain contours corresponding to the step of failure for 400 iterations, without the foundation.

**e) Number of iterations 500**

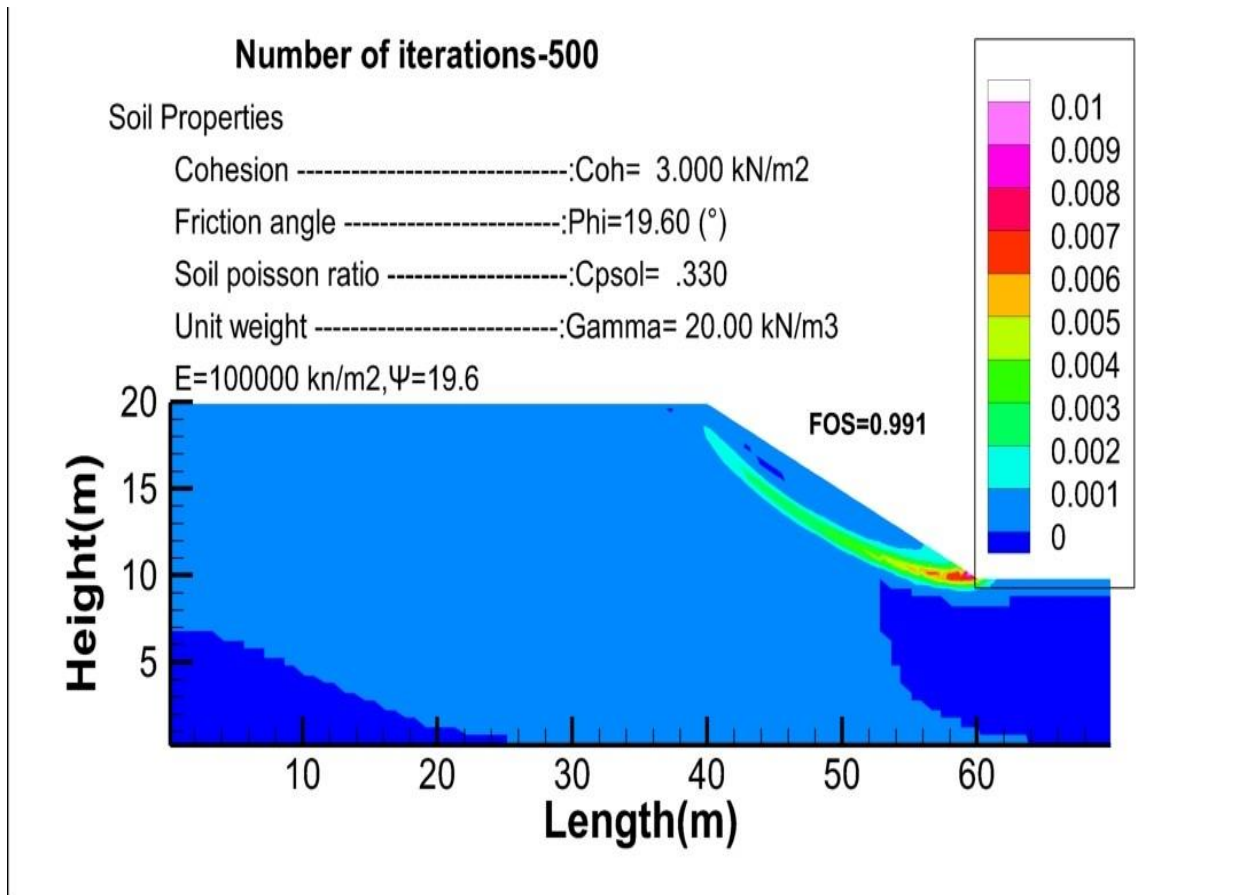


Figure 5.11 9 Strain contours corresponding to the step of failure for 500 iterations, with the foundation

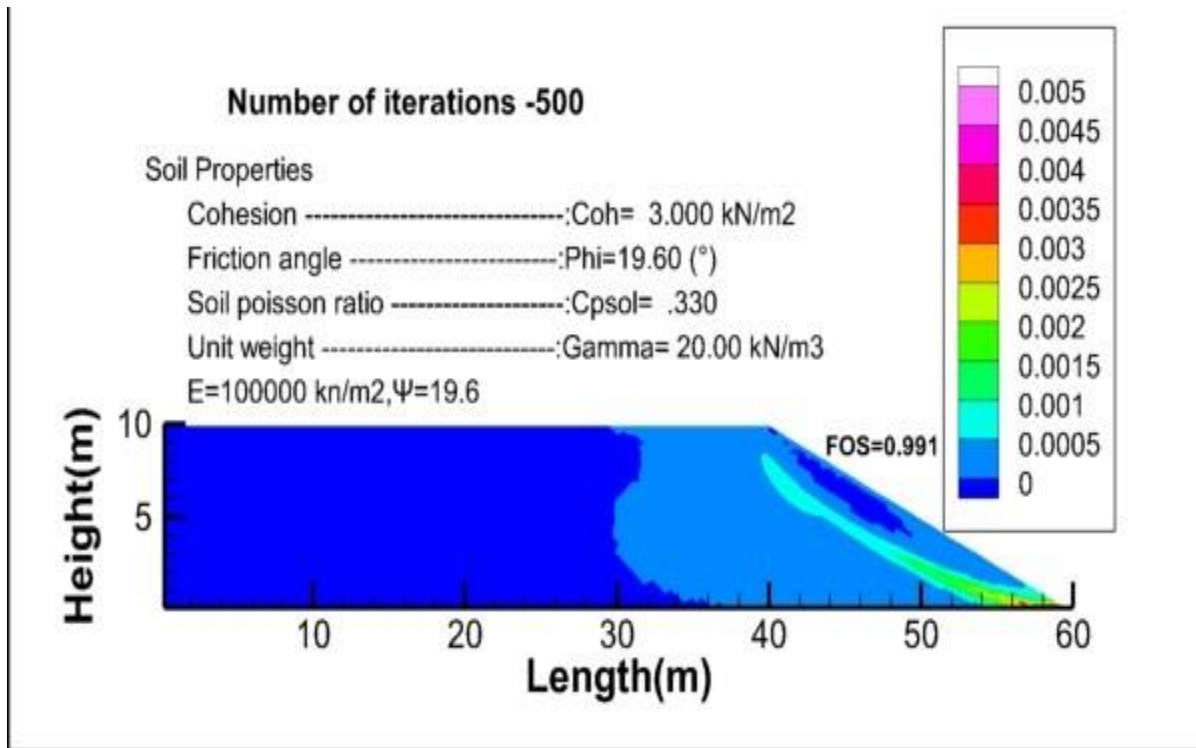


Figure 5.11 10 Strain contours corresponding to the step of failure for 500 iterations, without the foundation

**f) Number of iterations**

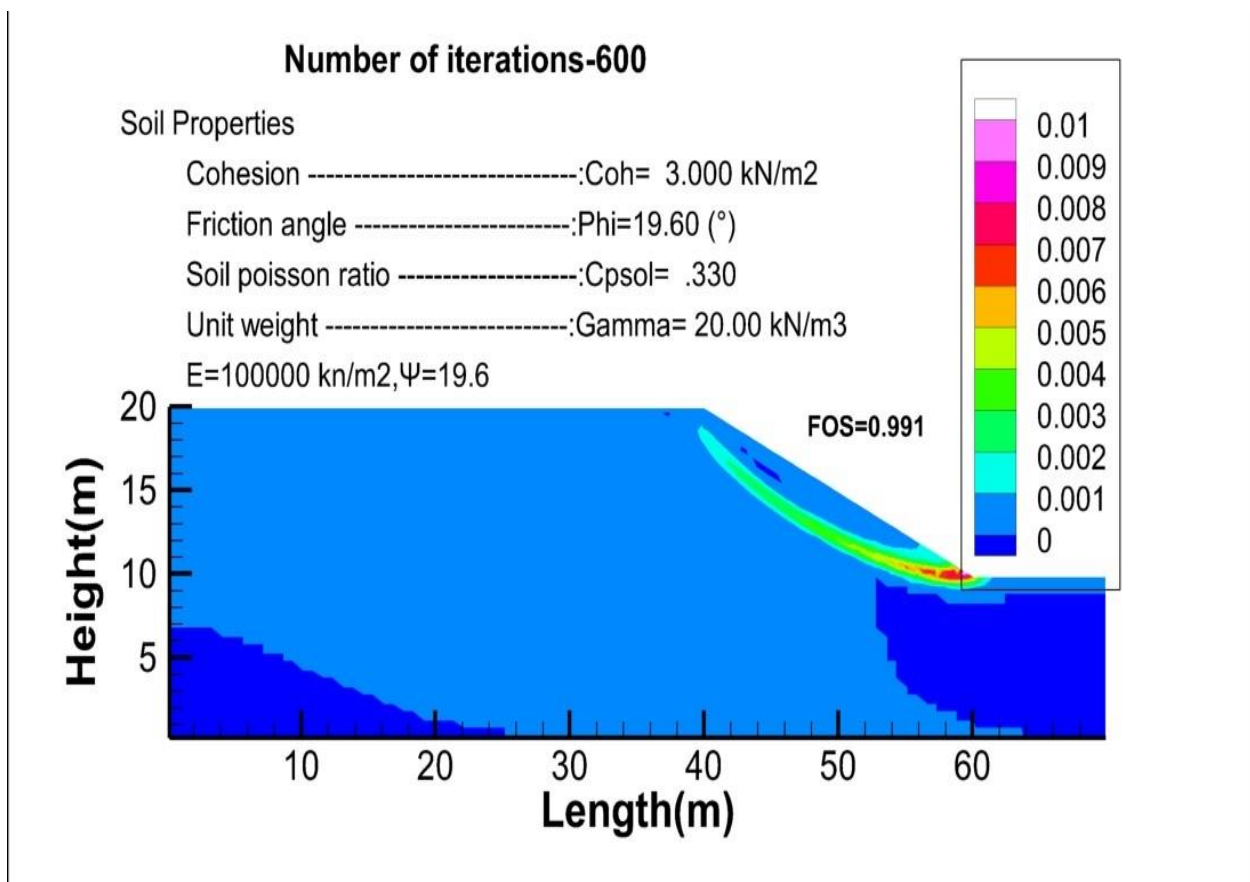


Figure 5.11 11 Strain contours corresponding to the step of failure for 600 iterations, with the foundation

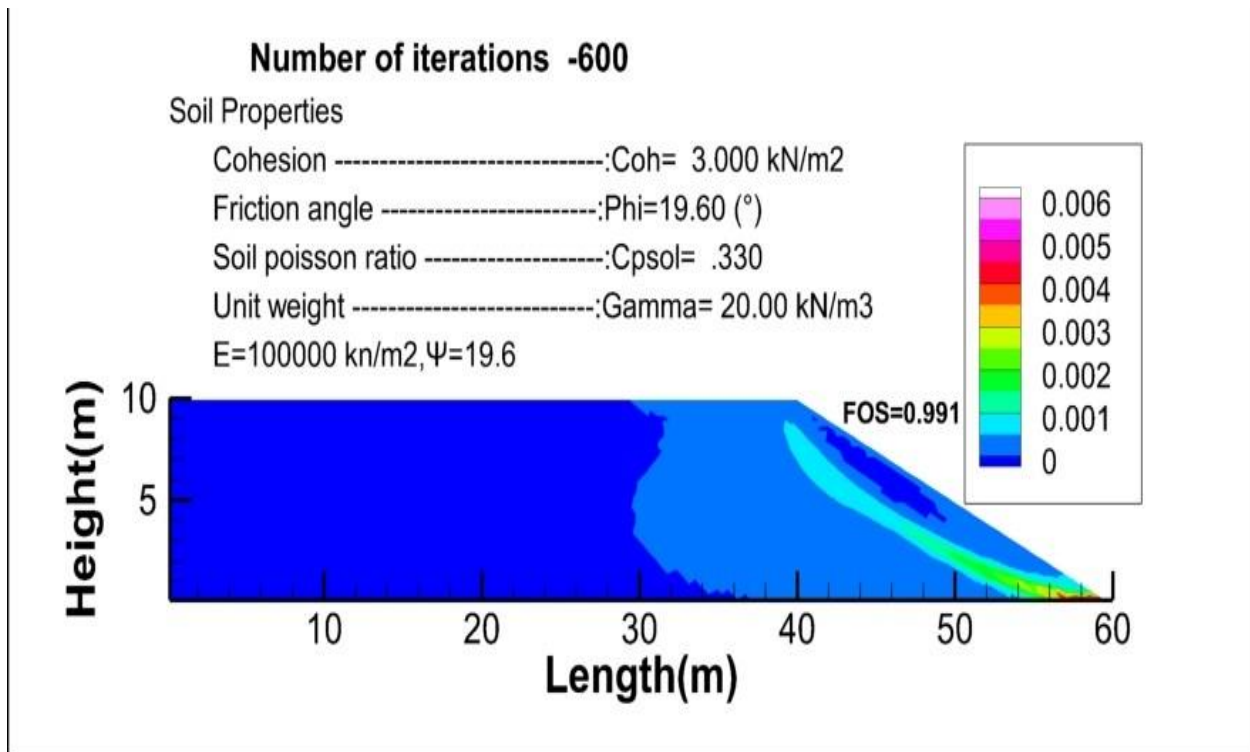


Figure 5.11 12 Strain contours corresponding to the step of failure for 600 iterations, without the foundation

**g) Number of iterations 700**

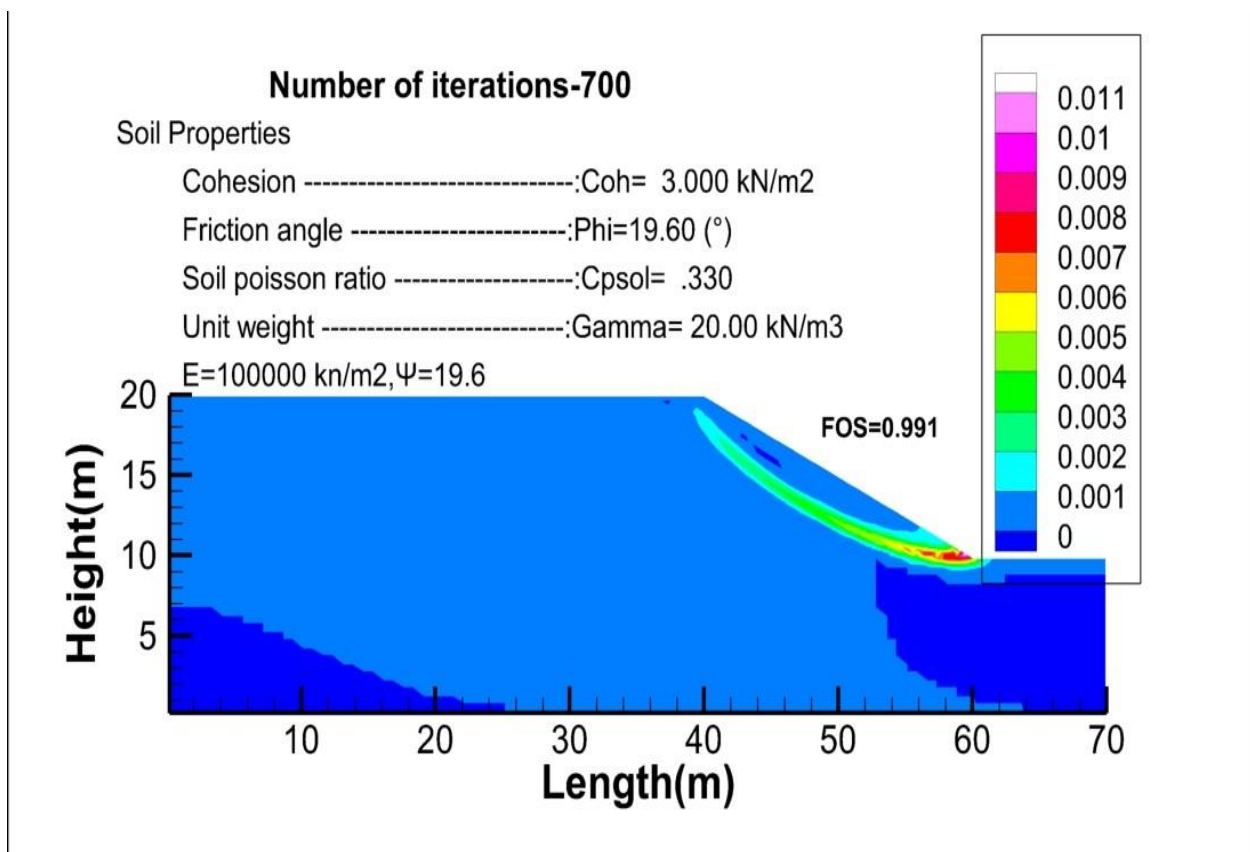


Figure 5.11 13 Strain contours corresponding to the step of failure for 700 iterations, with the foundation.

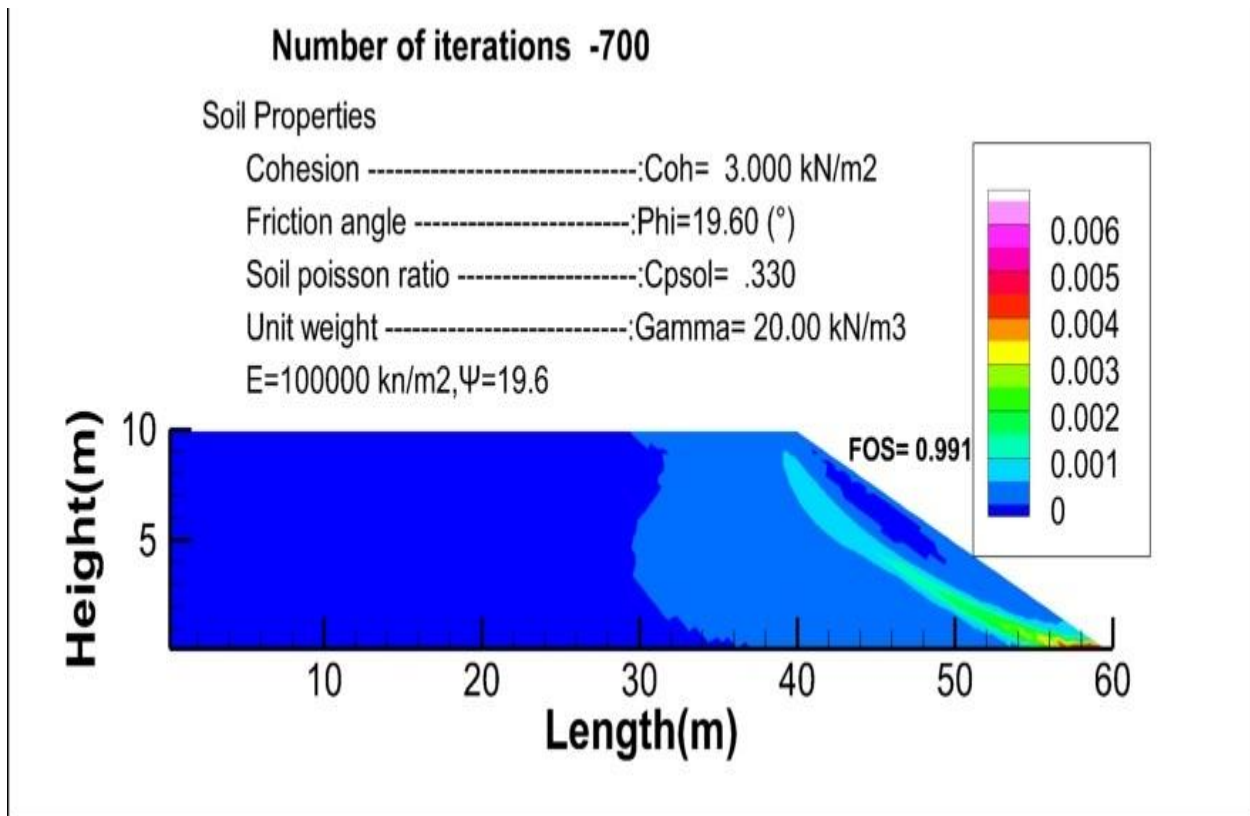


Figure 5.11 14 Strain contours corresponding to the step of failure for 700 iterations, without the foundation

**h) Number of iterations 800**

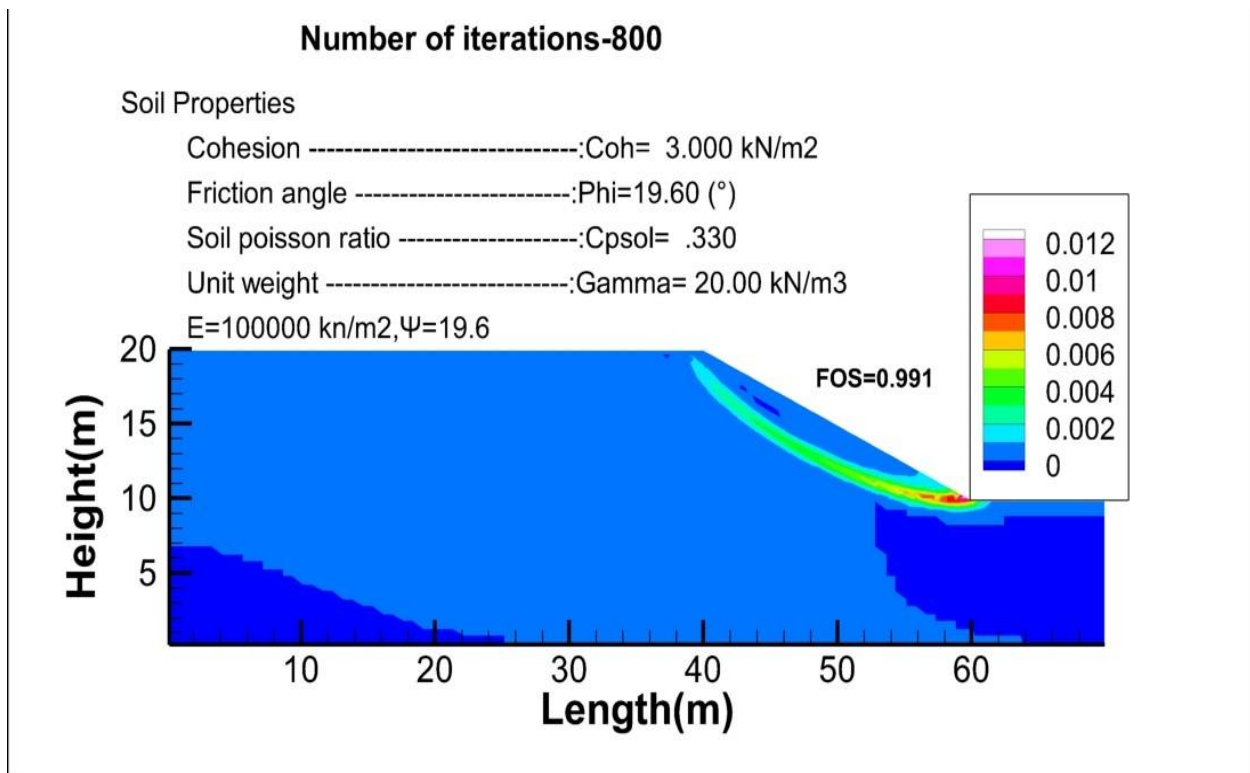


Figure 5.11 15 Strain contours corresponding to the step of failure for 700 iterations, with the foundation

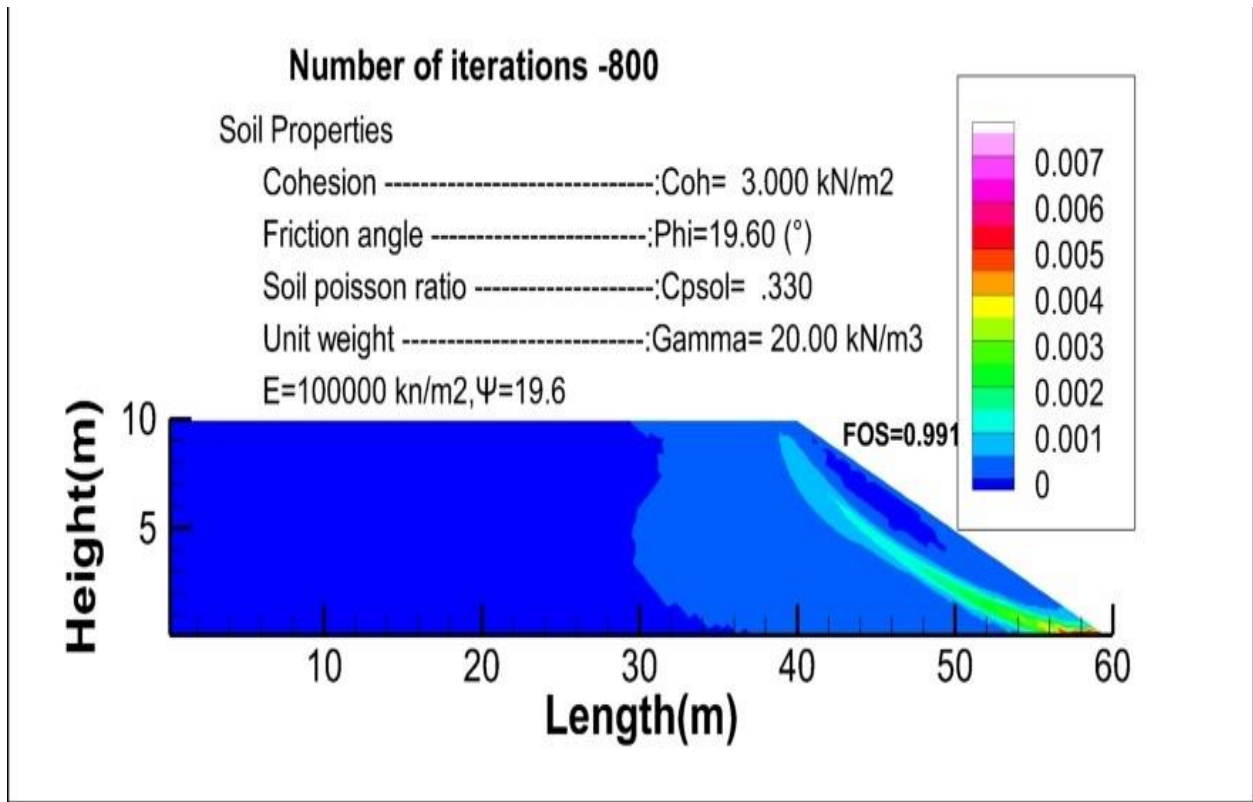


Figure 5.11 16 Strain contours corresponding to the step of failure for 800 iterations, without the foundation

**i) Number of iterations 900**

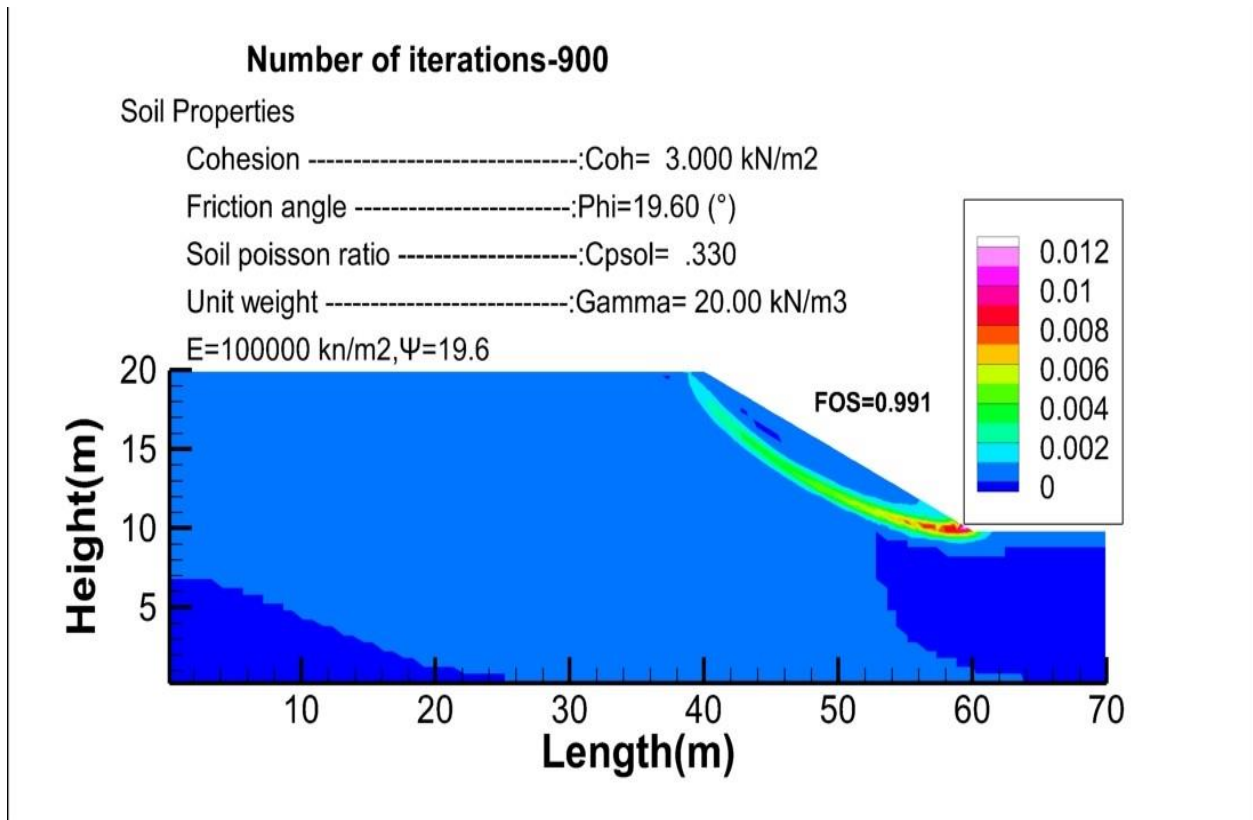


Figure 5.11 17 Strain contours corresponding to the step of failure for 900 iterations, with the foundation



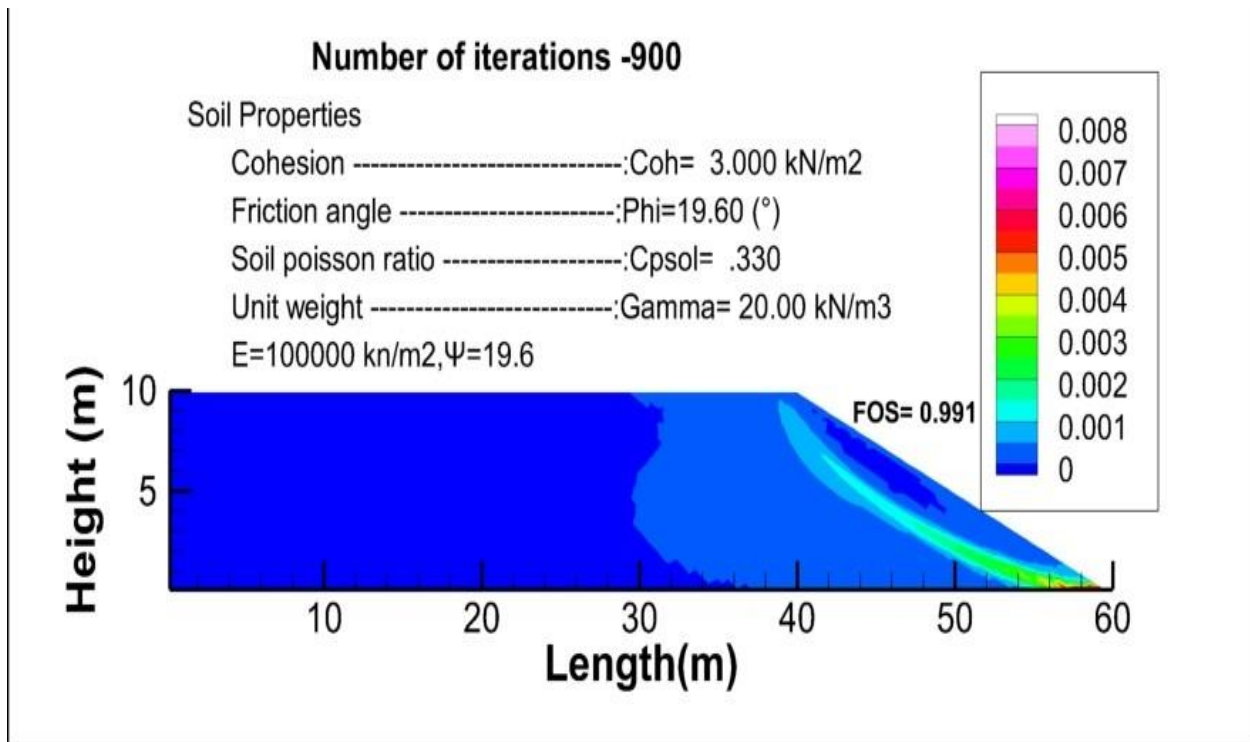


Figure 5.11 18 Strain contours corresponding to the step of failure for 900 iterations, without the foundation.

j) Number of iterations 1000

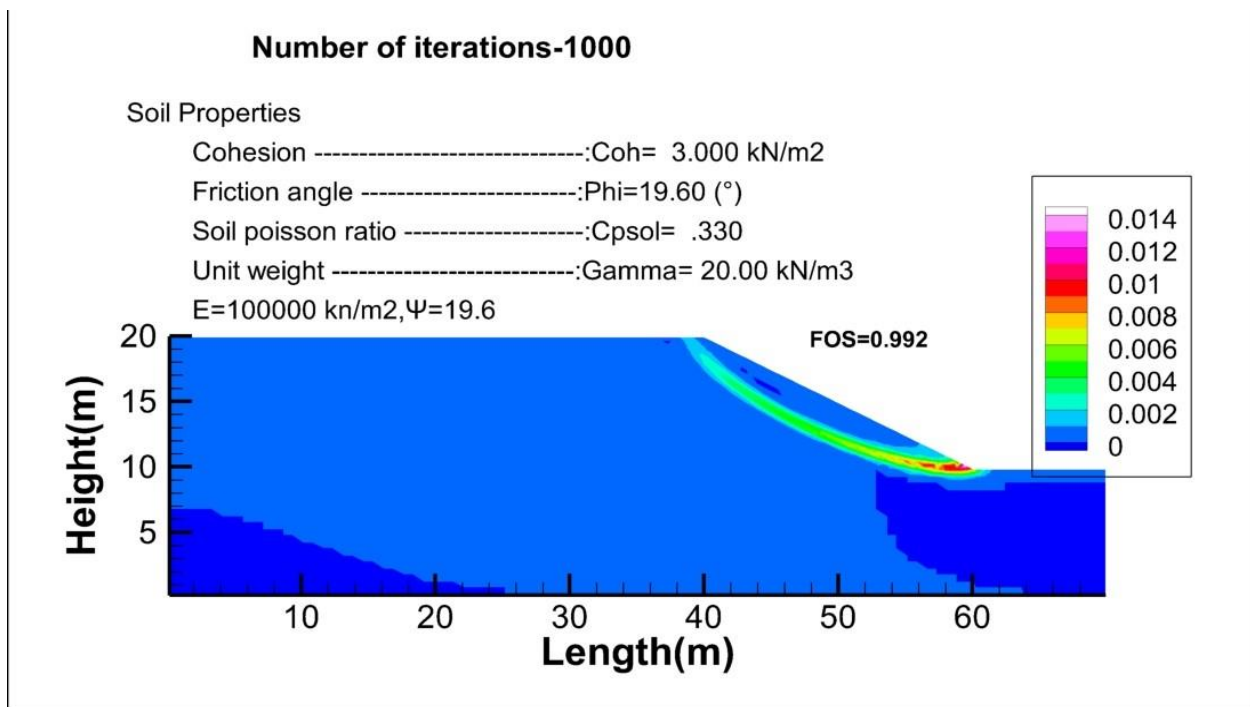


Figure 5.11 19 Strain contours corresponding to the step of failure for 1000 iterations, with the foundation.

At 1000 iteration the convergence was reached and the factor of safety is acceptable and even with further increasing of the iteration number any change will be verified because at this stage the failure process has started. So at this point no need to go further increasing the number of iteration.

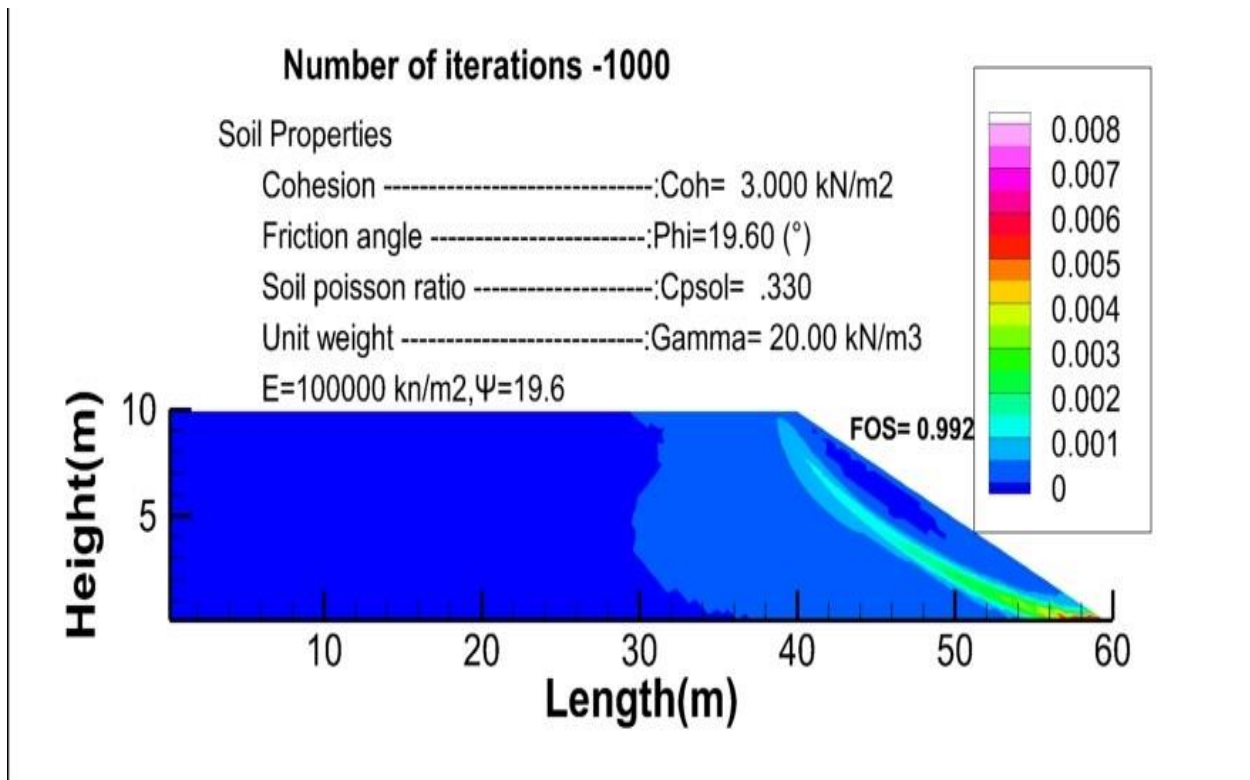


Figure 5.11 20Strain contours corresponding to the step of failure for 1000 iterations, without the foundation.

**k) Number of iterations 1100**

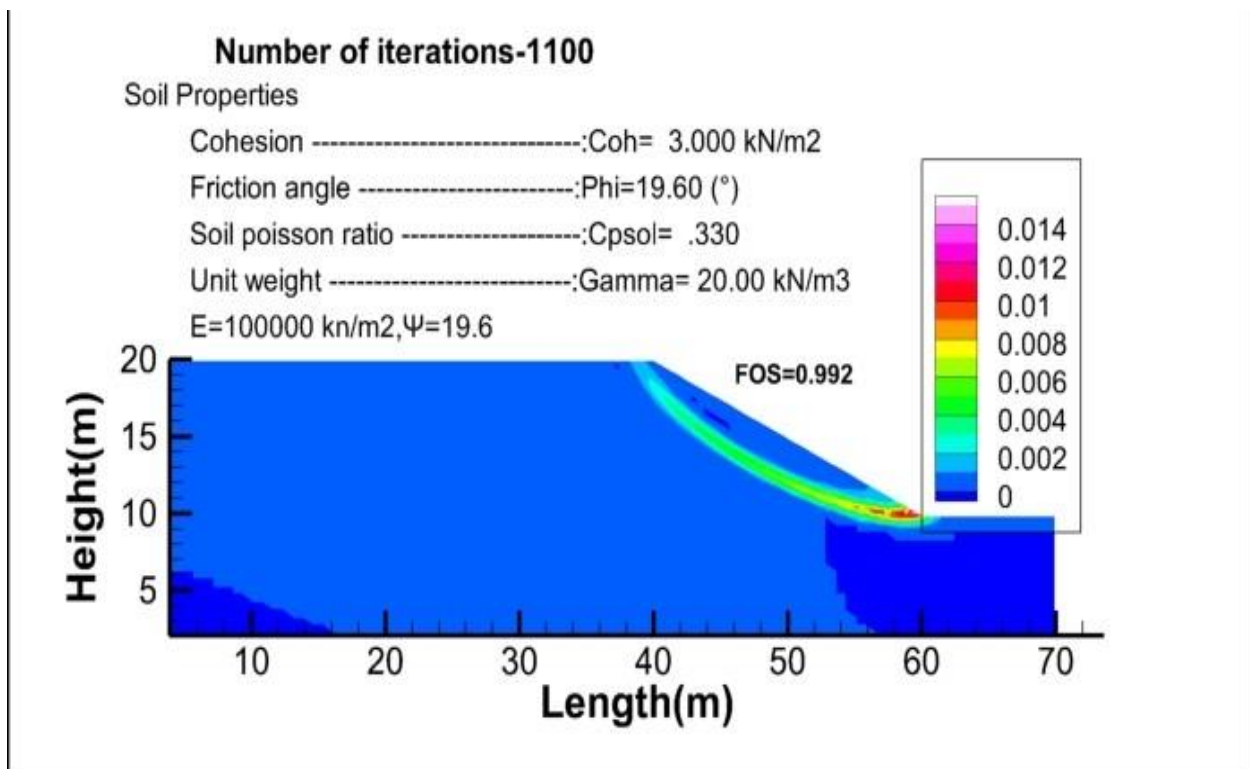


Figure 5.11 21 Strain contours corresponding to the step of failure for 1100 iterations, with the foundation

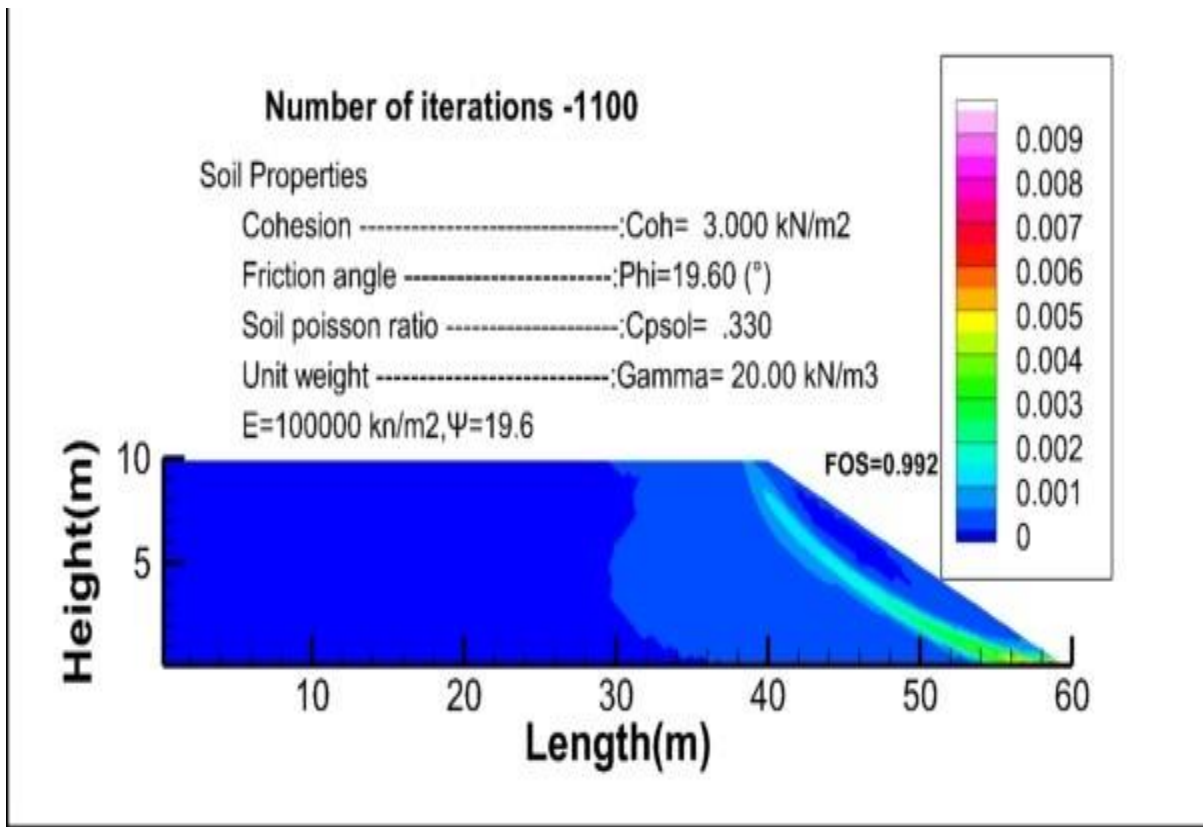


Figure 5.11 22 Strain contours corresponding to the step of failure for 1100 iterations, without the foundation

**1) Number of iteration 1200**

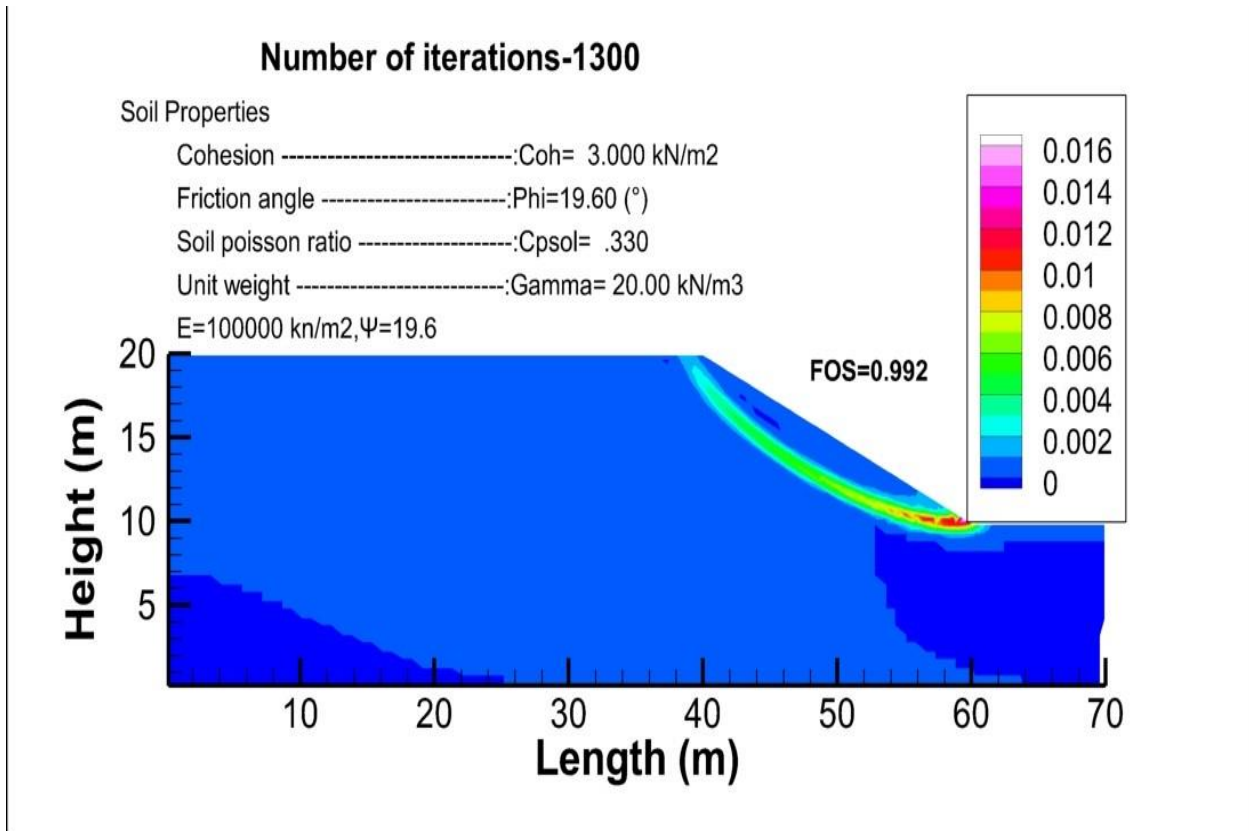
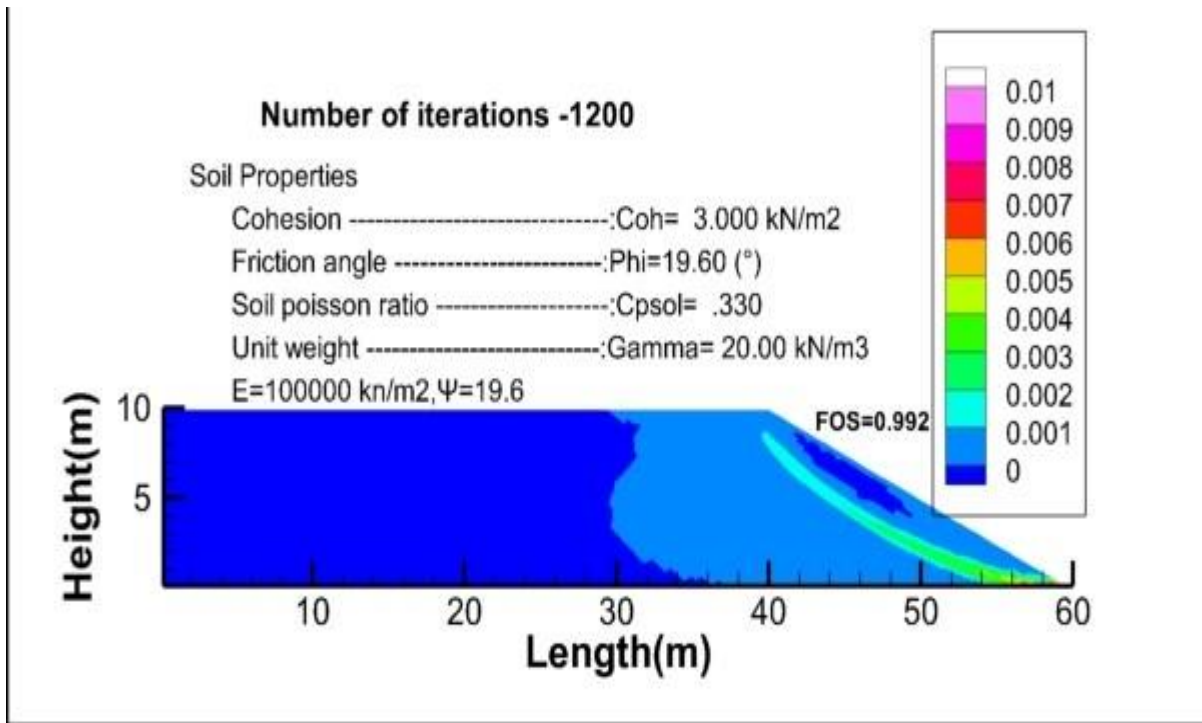


Figure 5.11 23 Strain contours corresponding to the step of failure for 1200 iterations, with the foundation



fig

Figure 5.11 24 Strain contours corresponding to the step of failure for 1200 iterations, without the foundation.

**m) Number of iterations 1300**

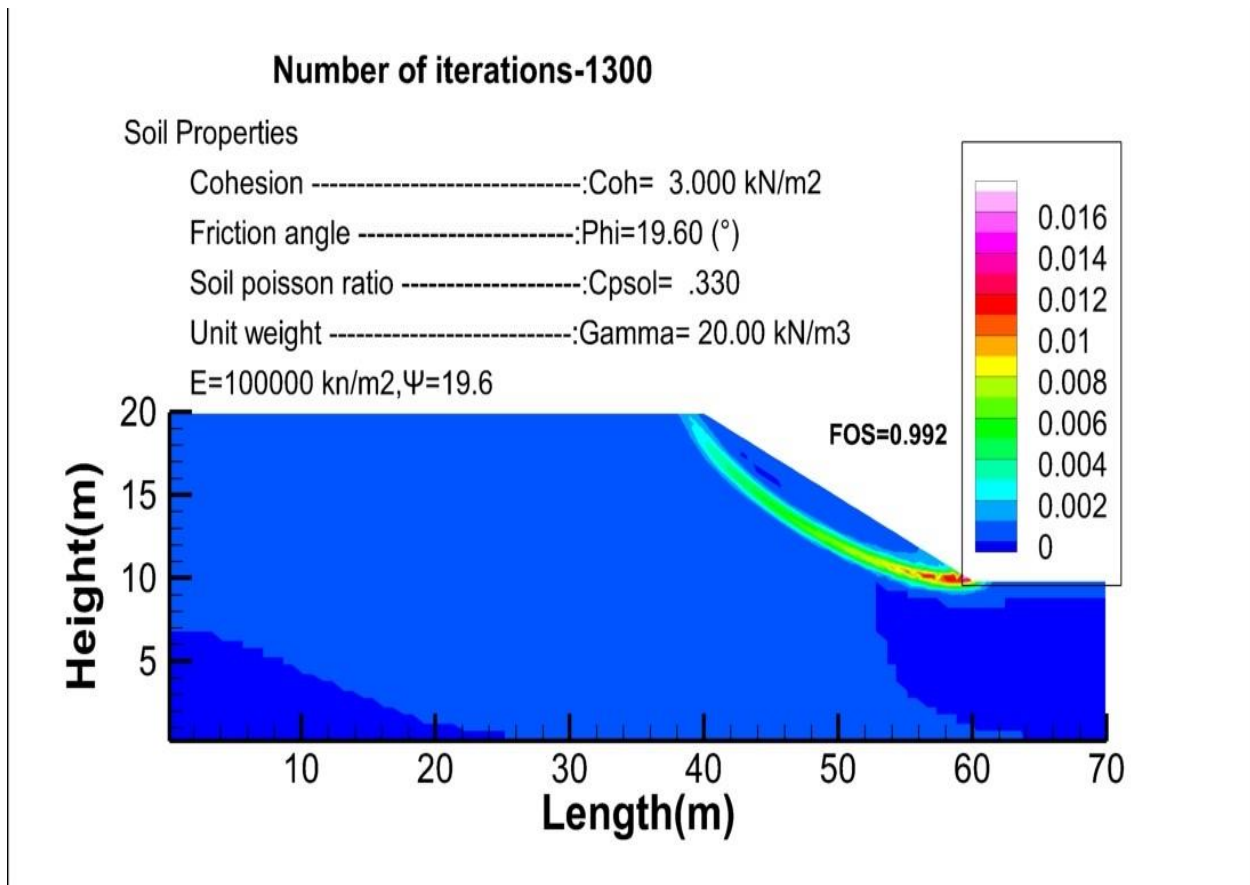


Figure 5.11 25 Strain contours corresponding to the step of failure for 1300 iterations, with the foundation.

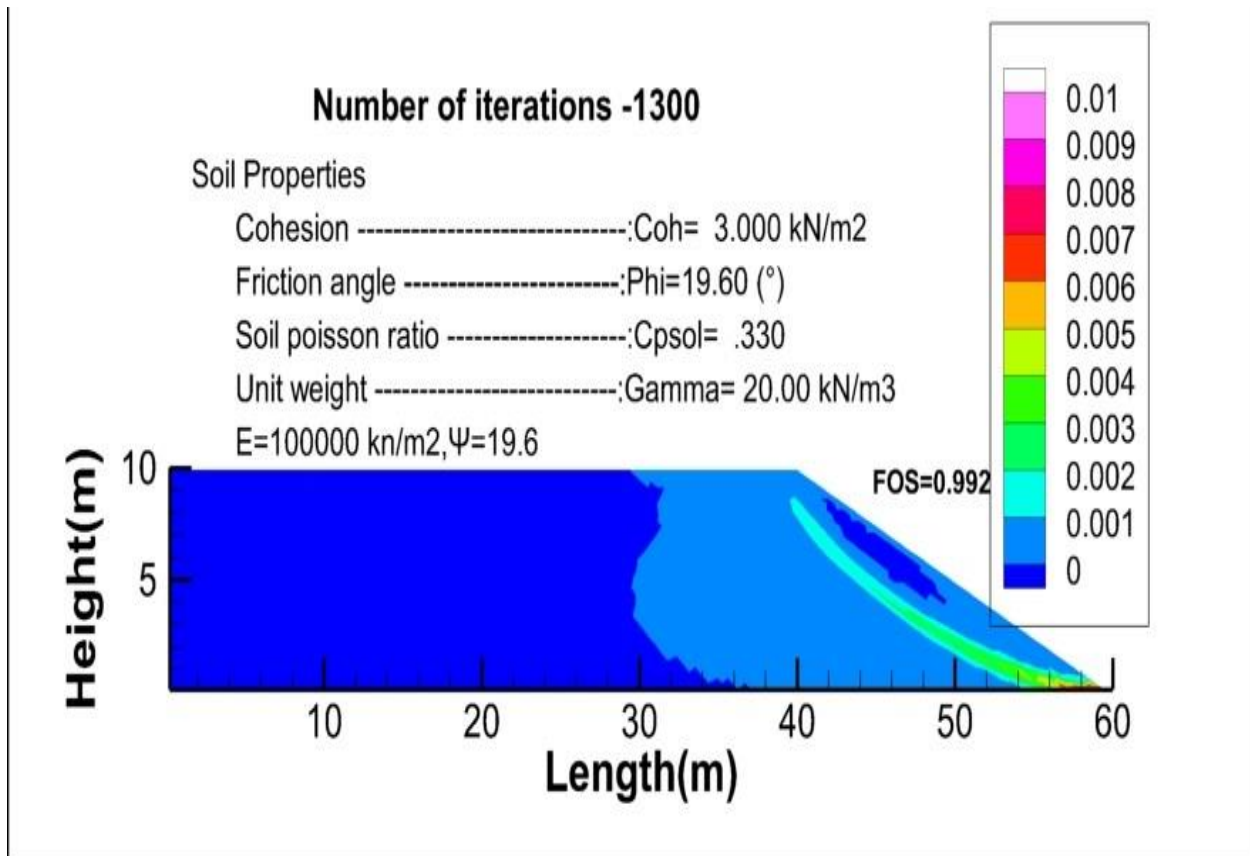


Figure 5.11 26 Strain contours corresponding to the step of failure for 1300 iterations, without the foundation.

**n) Number of iterations 1400**

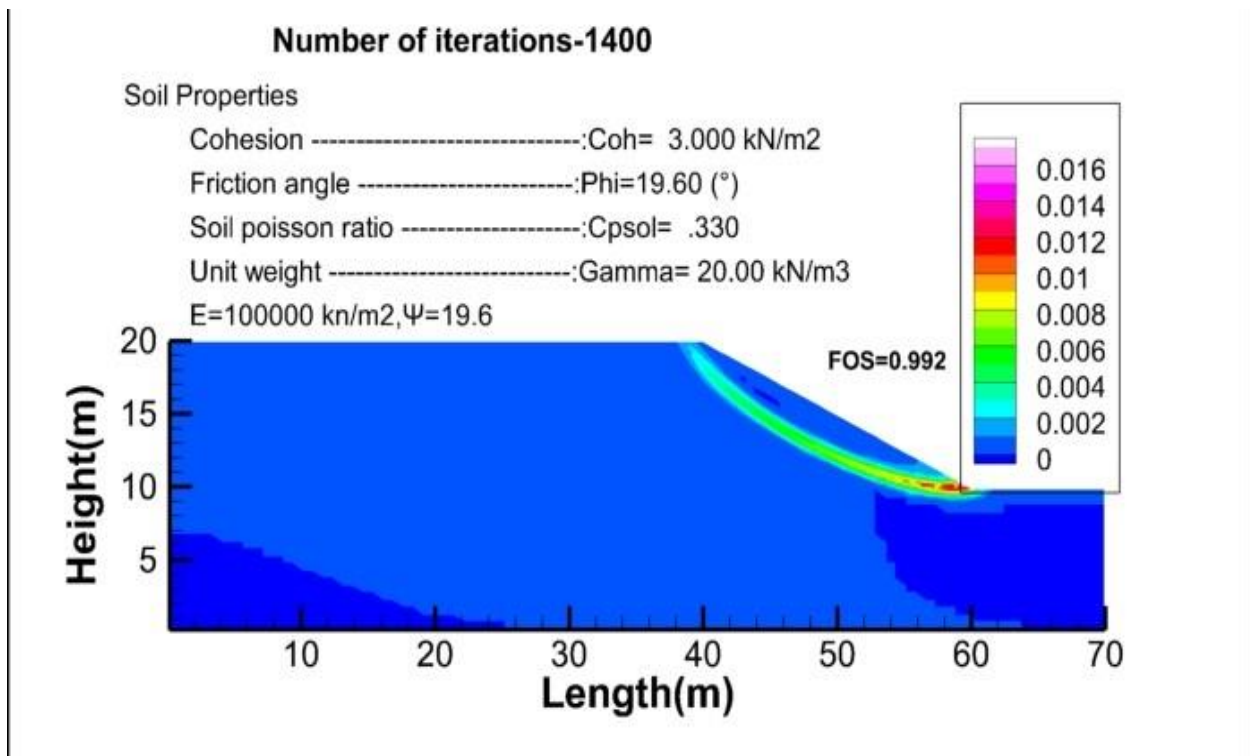


Figure 5.11 27 Strain contours corresponding to the step of failure for 1400 iterations, with the foundation.

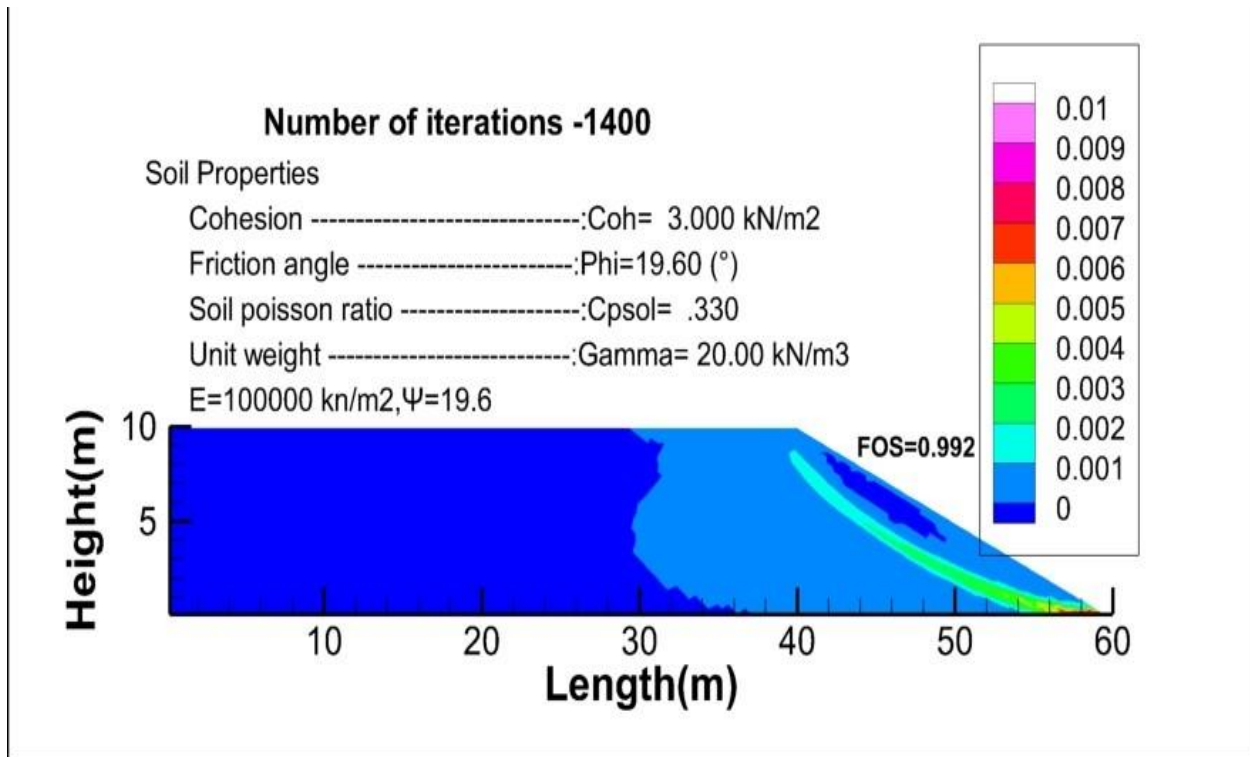


Figure 5.11 28 Strain contours corresponding to the step of failure for 1400 iterations, without the foundation.

**o) Number of iterations 1500**

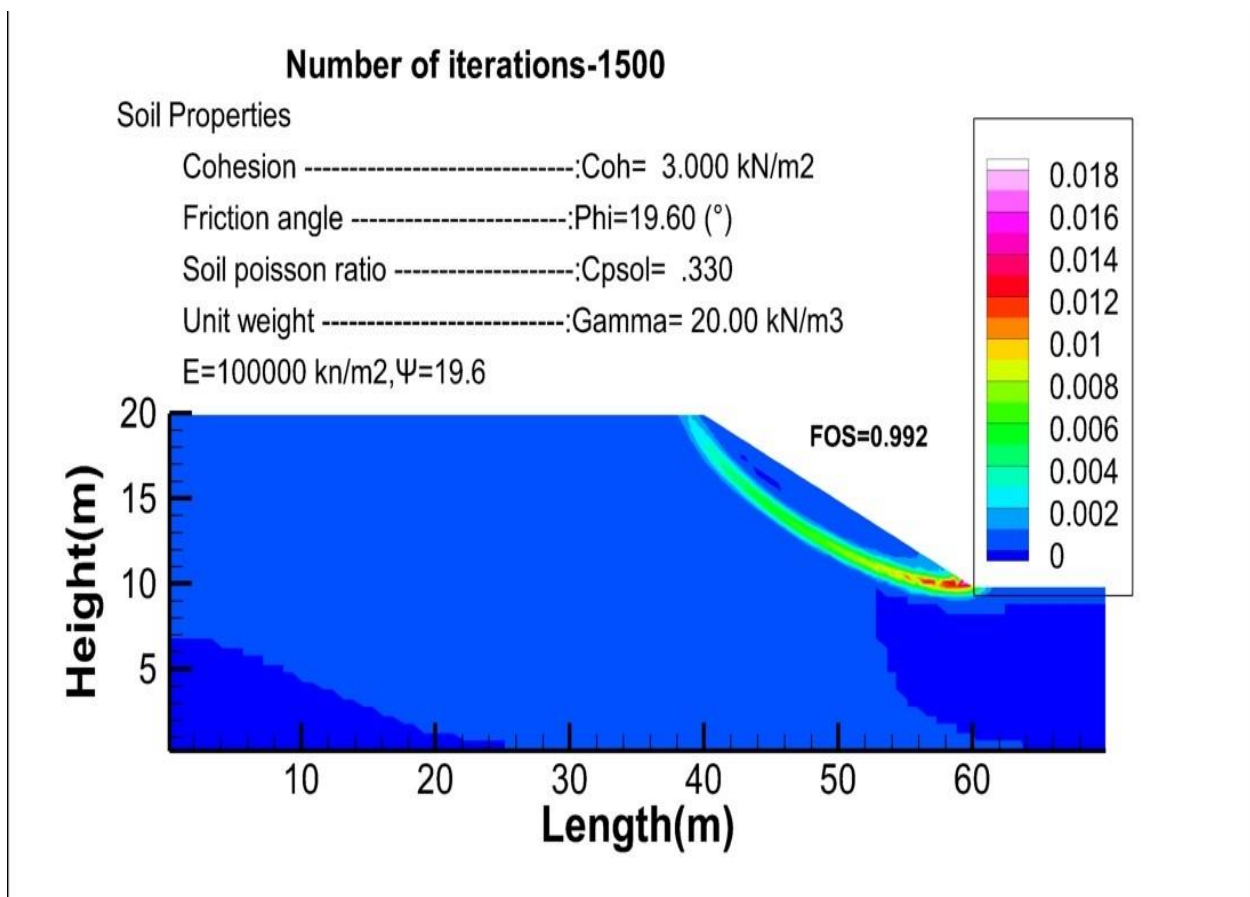


Figure 5.11 29 Strain contours corresponding to the step of failure for 1500 iterations, with the foundation.

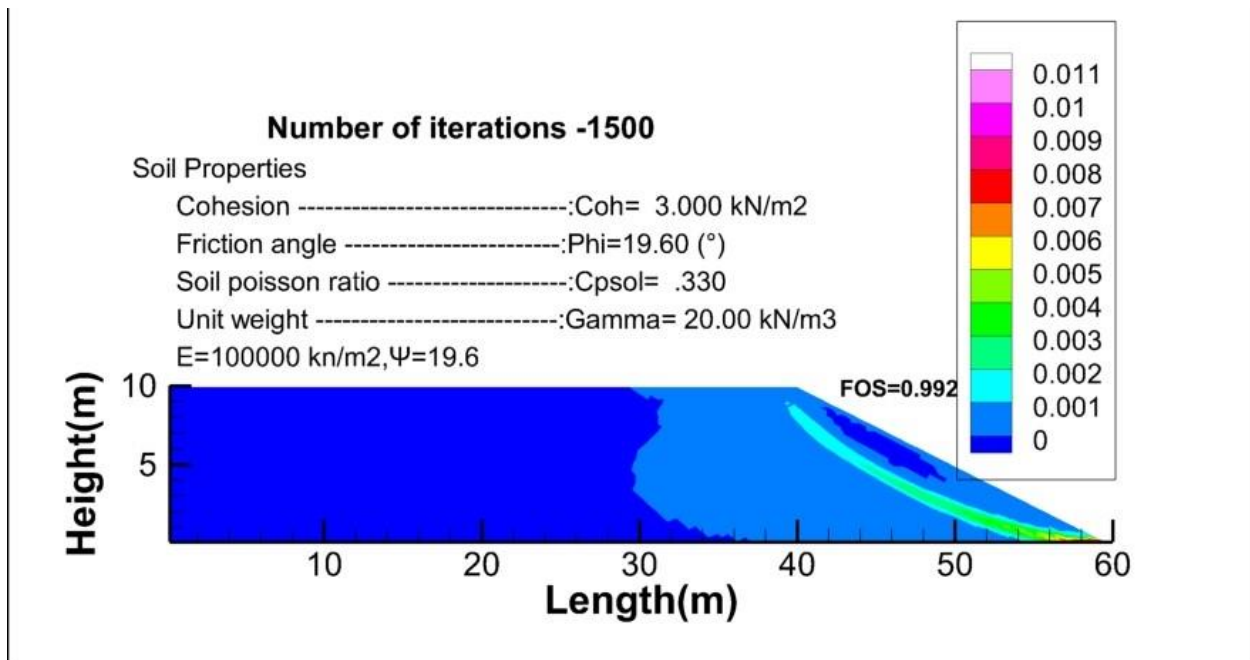


Figure 5.11 30 Strain contours corresponding to the step of failure for 1500 iterations, without the foundation.

As mention early any change is to be expected while when reached the convergence so after reaching the convergence the factor of safety and plasticity zones won't suffer any changes.

### 5.7.2. Non-Associated flow rule

Exactly the same behaviour from the associated flow rule is expected in the non-associated flow rule.

Table 5 2 4 Rapport of the Results of the effect of the Number of Iteration for FS of the 3 methods.

Iteracions	BS	MP	SDIM
100			0.914
200			0.924
300			0.928
400			0.929
500			0.931
600			0.933
700			0.936
800	0.989	0.984	0.938
900			0.938
1000			0.938
1100			0.938
1200			0.938
1300			0.940
1400			0.940
1500			0.940

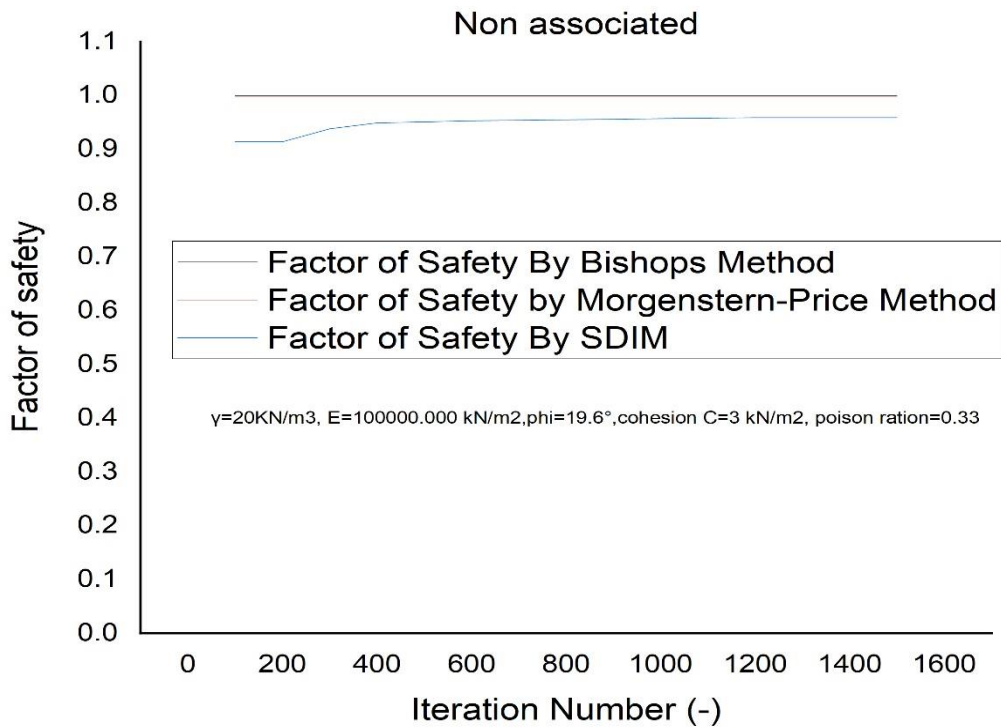


Figure 5.11 31 Iteration Number for the slope without foundation, **non-associated**

**a) Number of Iterations 100**

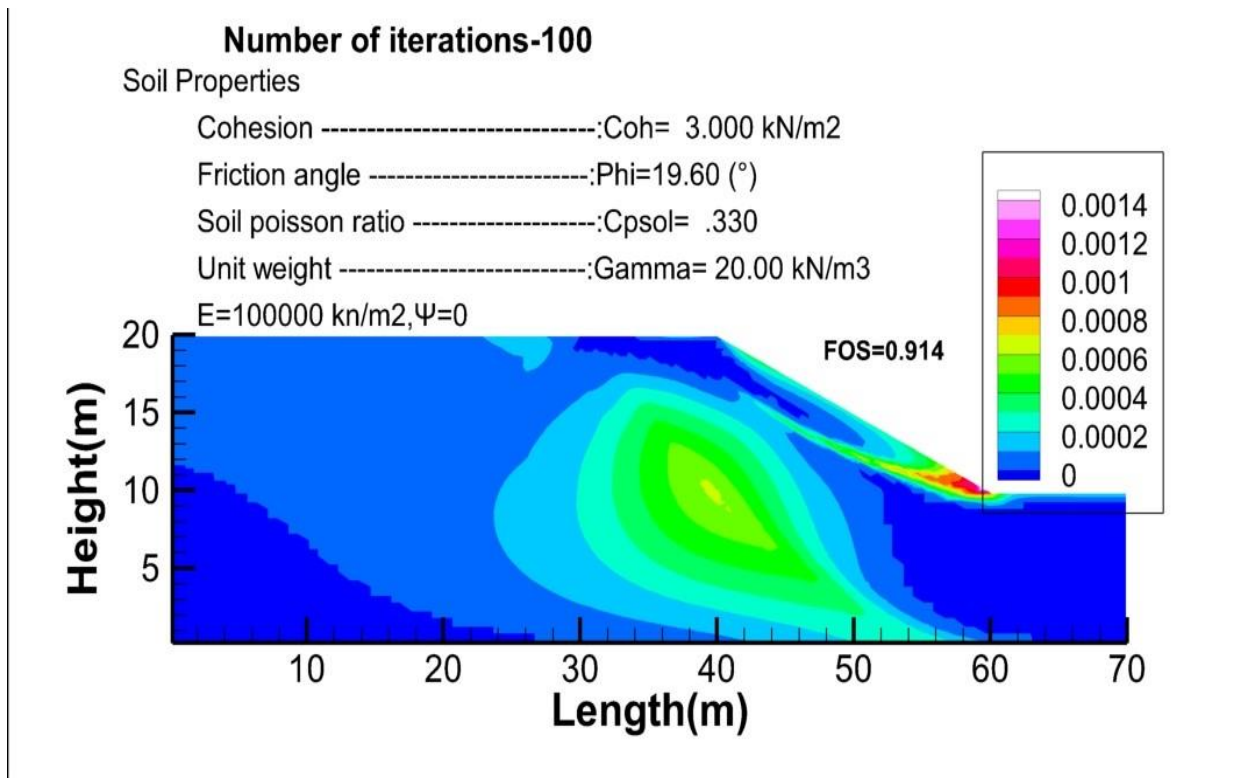


Figure 5.11 32 Strain contours corresponding to the step of failure for 100 iterations, with the foundation



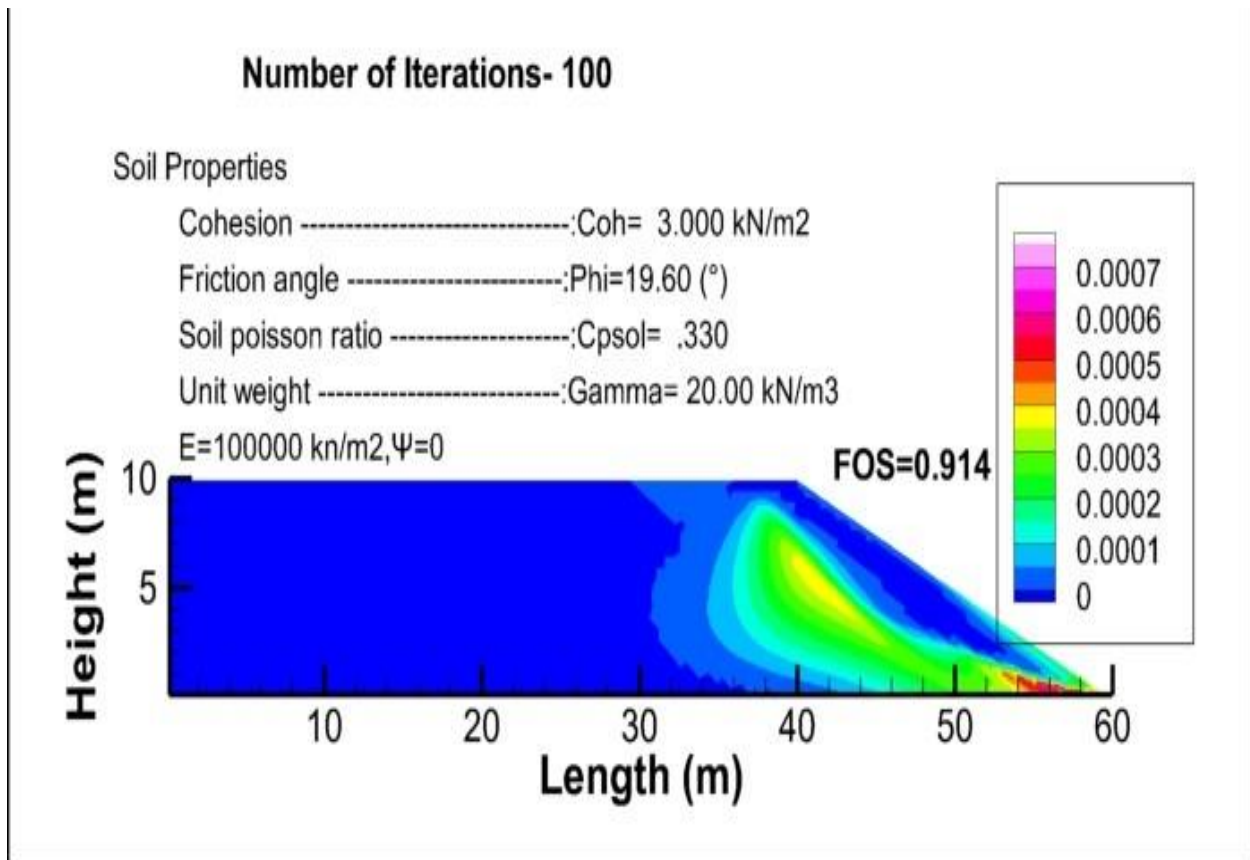


Figure 5.11 33 Strain contours corresponding to the step of failure for 100 iterations, without the foundation

**b) Number of iterations 200**

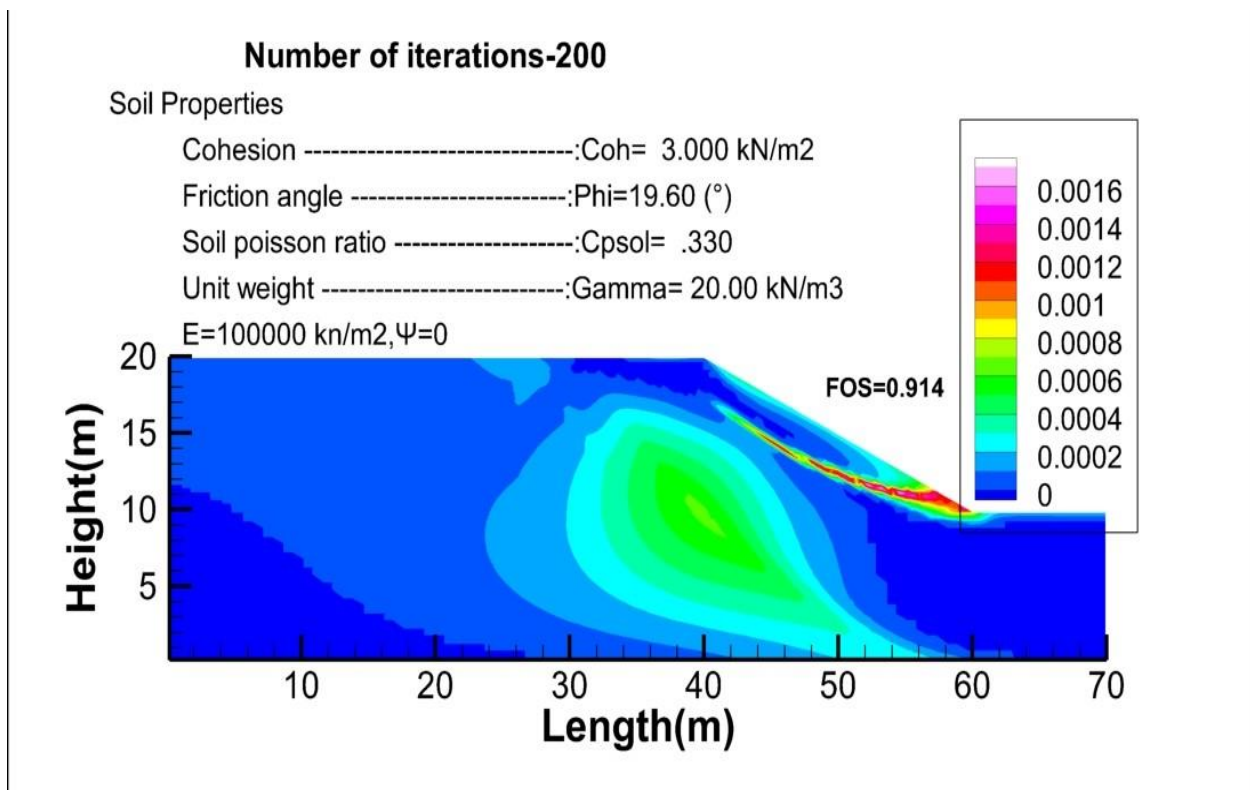


Figure 5.11 34 Strain contours corresponding to the step of failure for 200 iterations, with the foundation

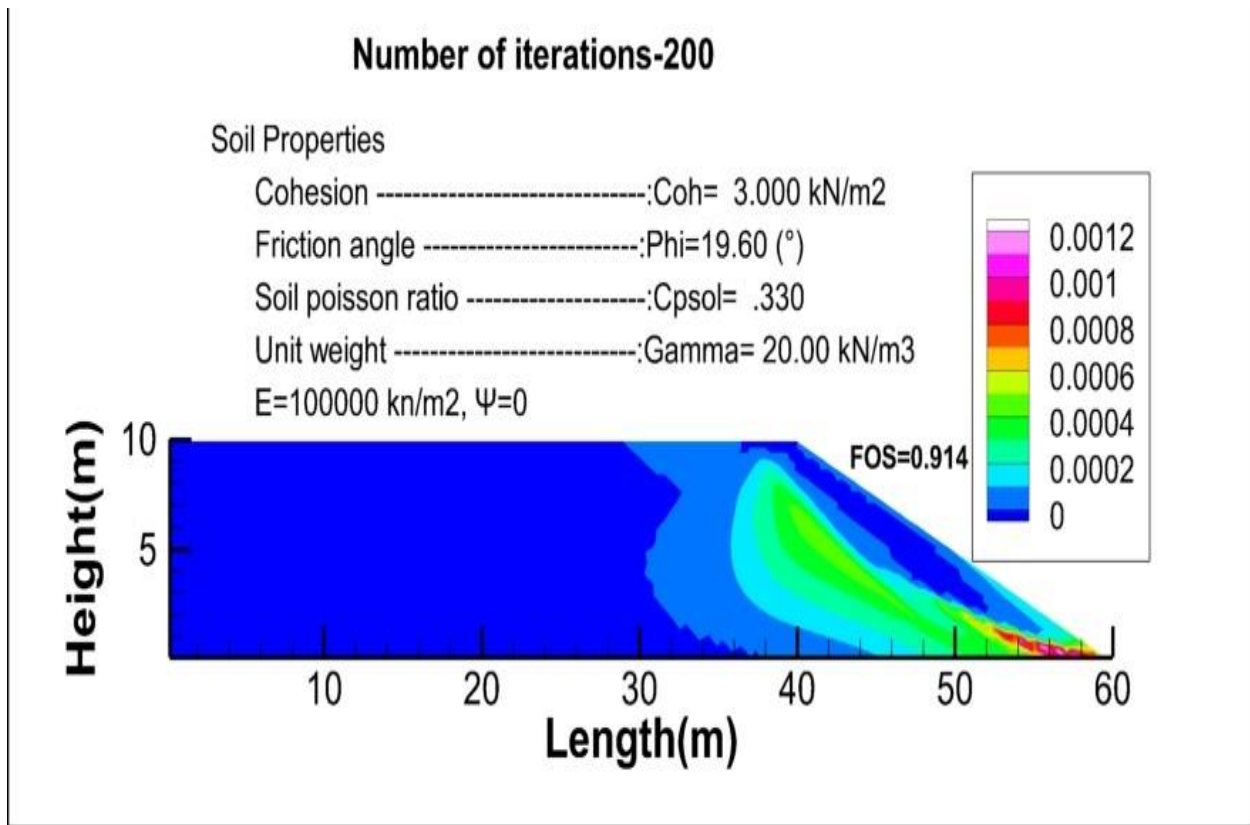


Figure 5.11 35 Strain contours corresponding to the step of failure for 200 iterations, without the foundation.

### c) Number of iterations 300

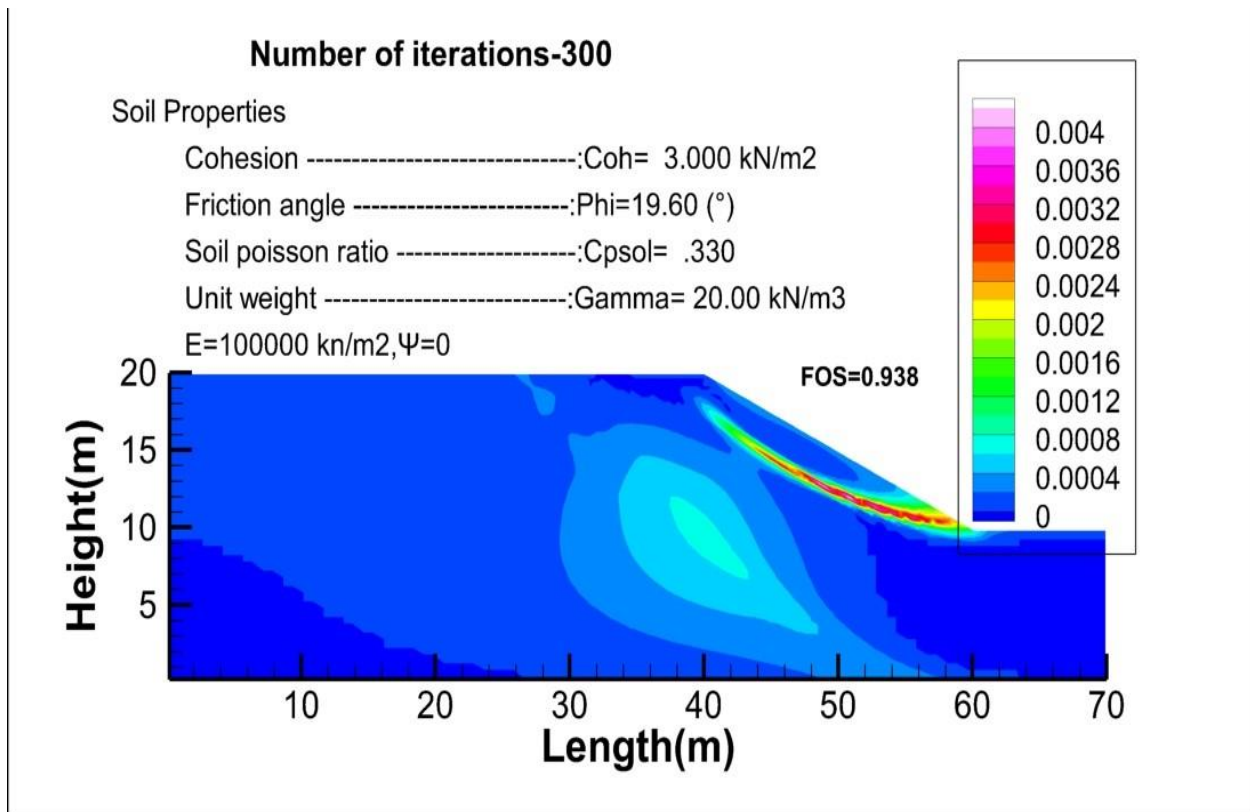


Figure 5.11 36 Strain contours corresponding to the step of failure for 300 iterations, with the foundation

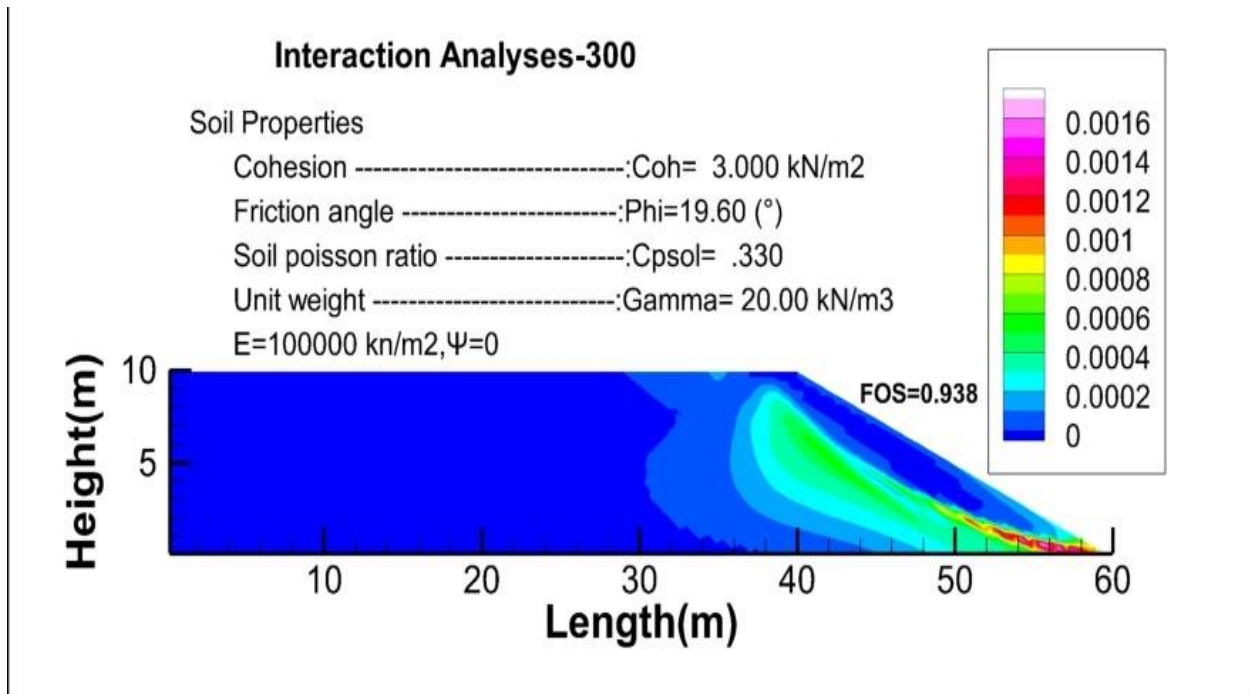


Figure 5.11 37 Strain contours corresponding to the step of failure for 300 iterations, without the foundation.

**d) Number of iterations**

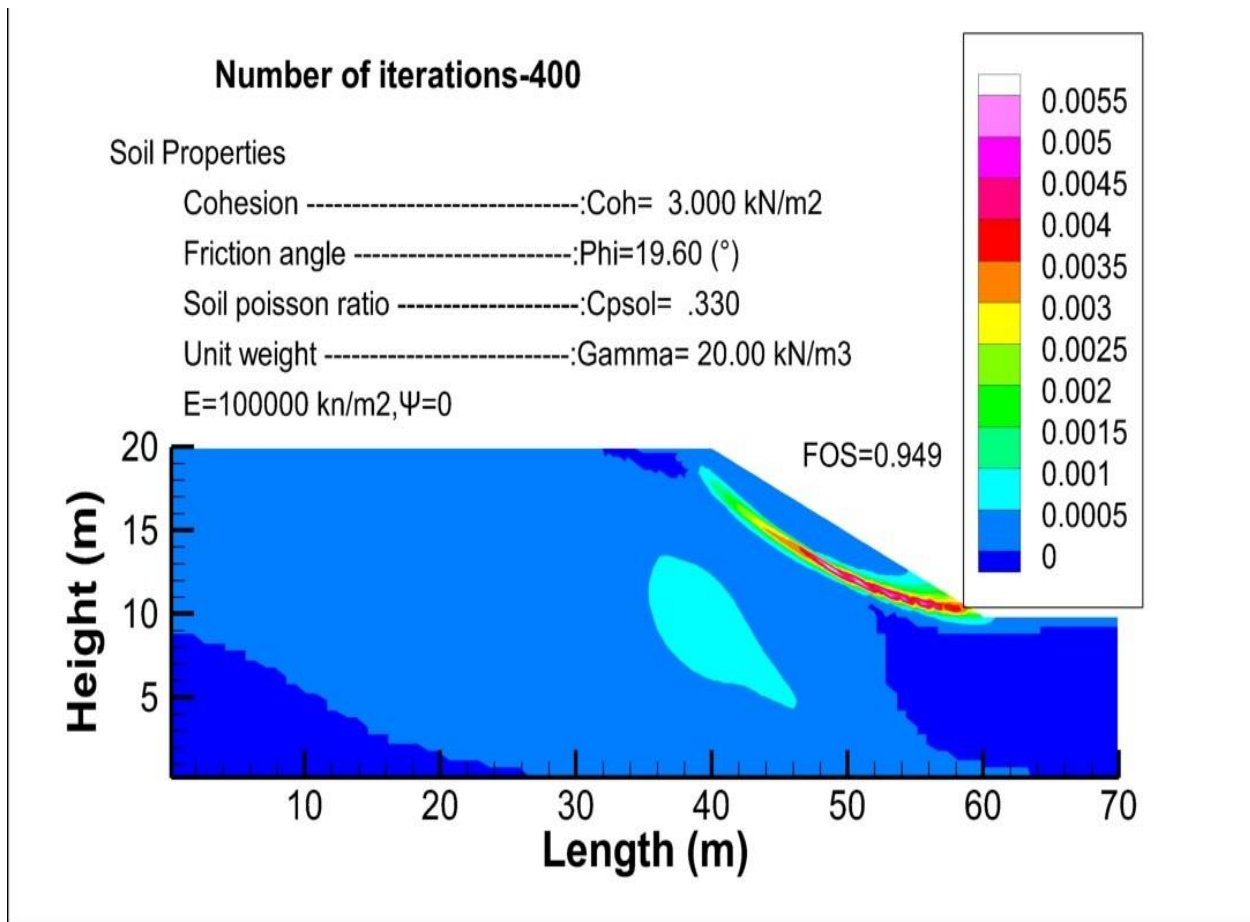


Figure 5.11 38 Strain contours corresponding to the step of failure for 400 iterations, with the foundation.

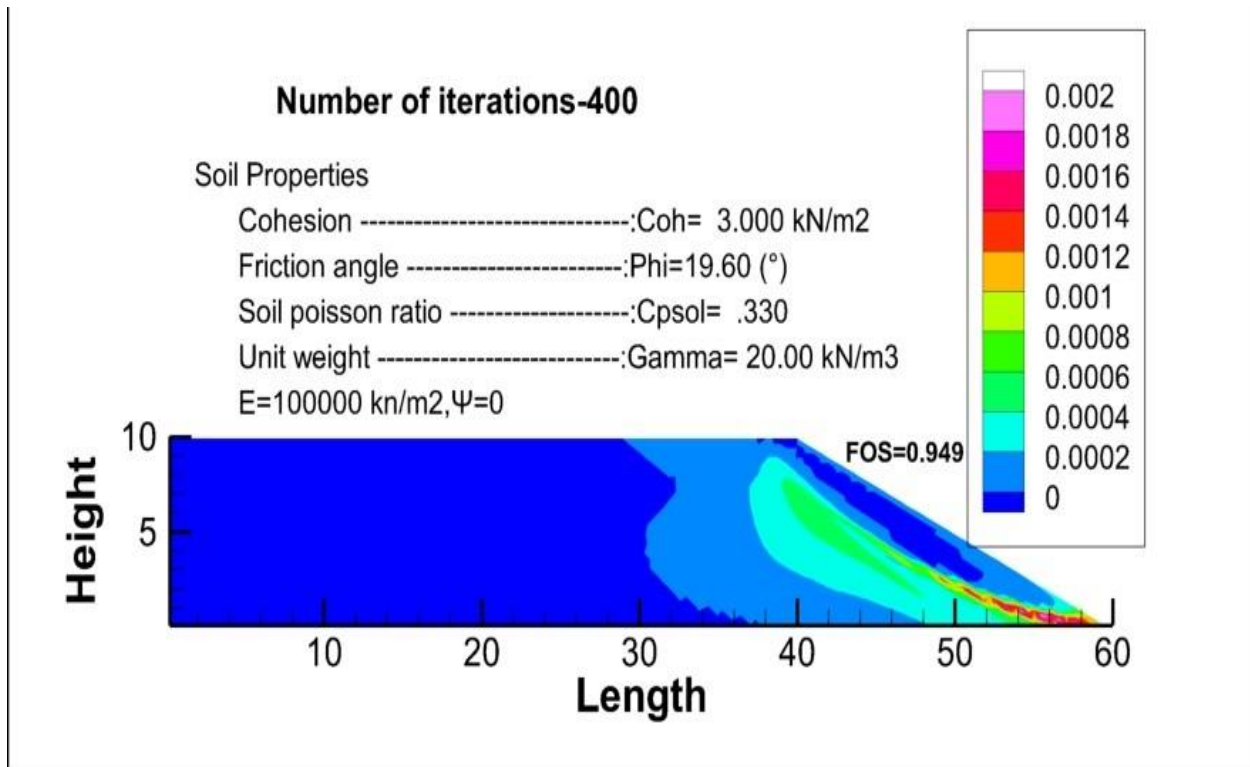


Figure 5.11 39 Strain contours corresponding to the step of failure for 400 iterations, without the foundation

**e) Number of iterations 500**

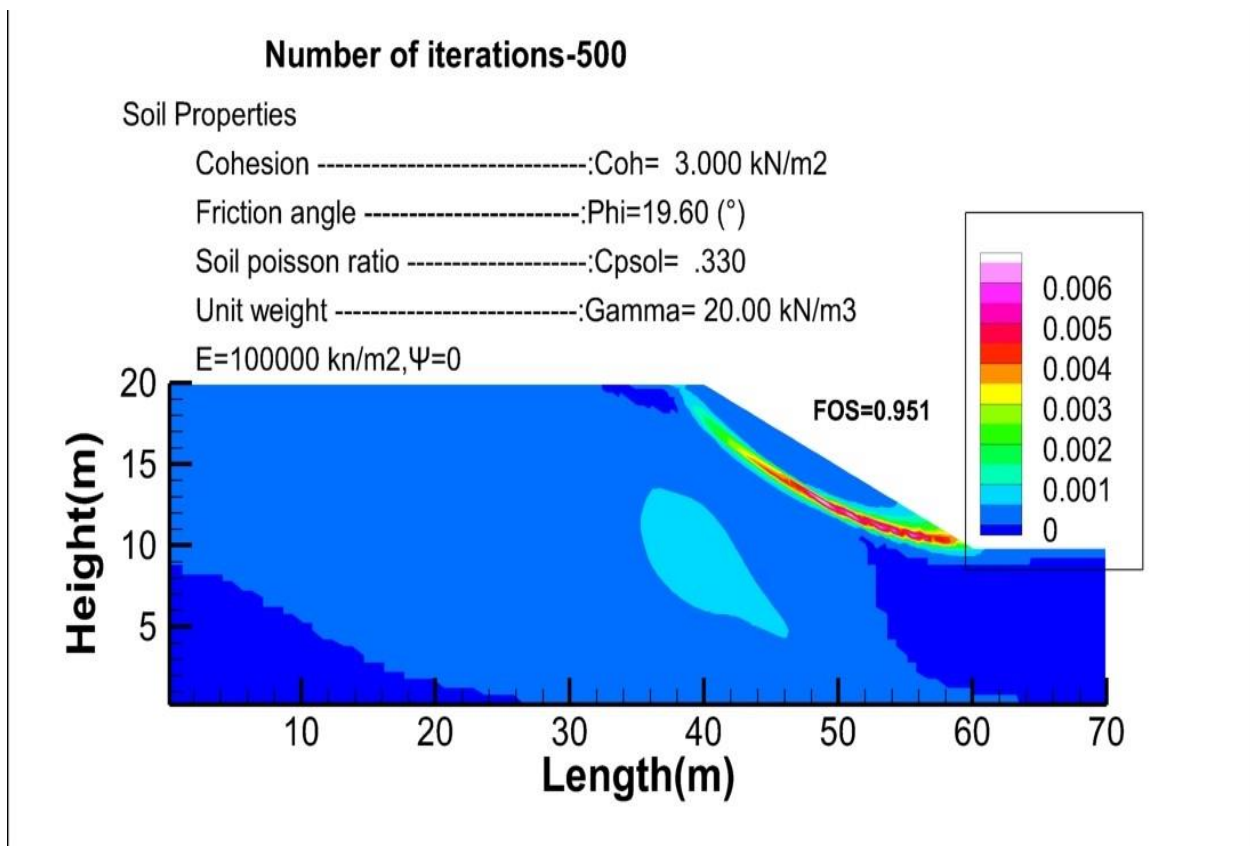


Figure 5.11 40 Strain contours corresponding to the step of failure for 500 iterations, with the foundation

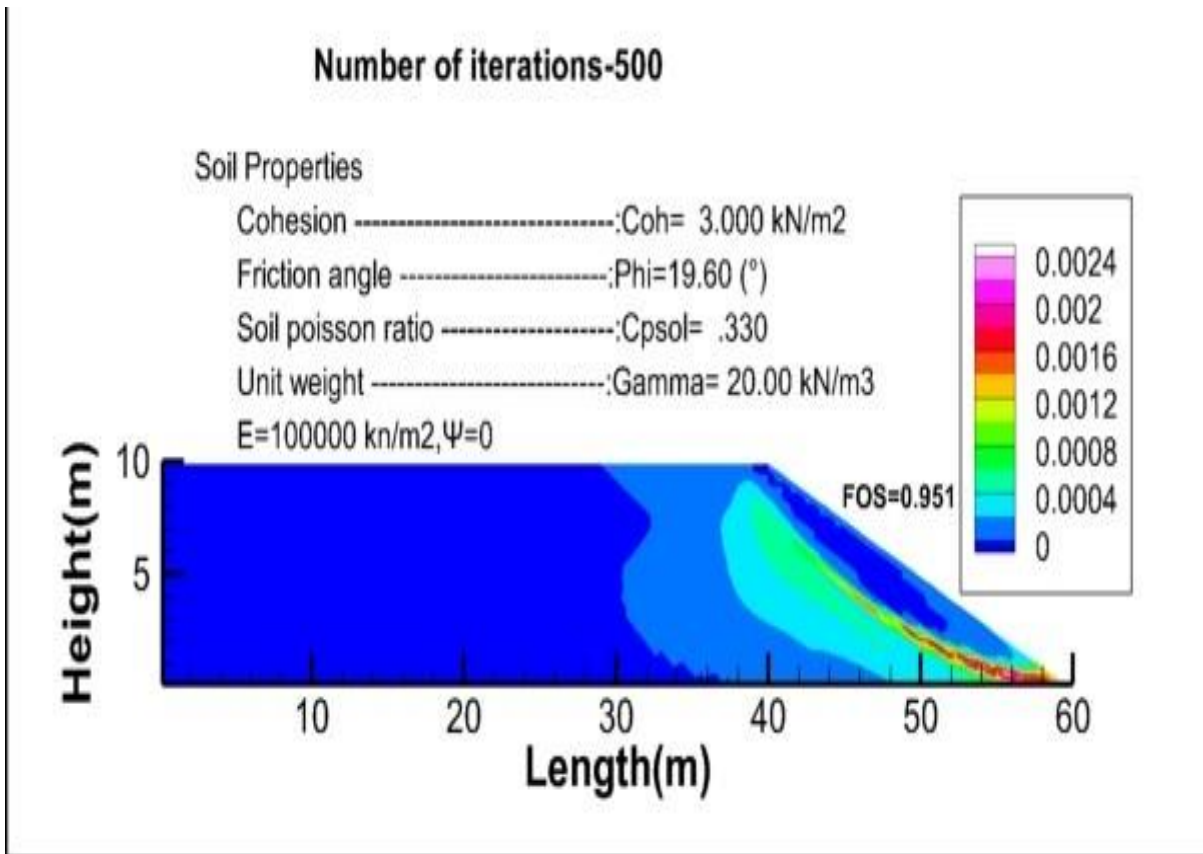


Figure 5.11 41 Strain contours corresponding to the step of failure for 500 iterations, without the foundation

**f) Number of iterations 600**

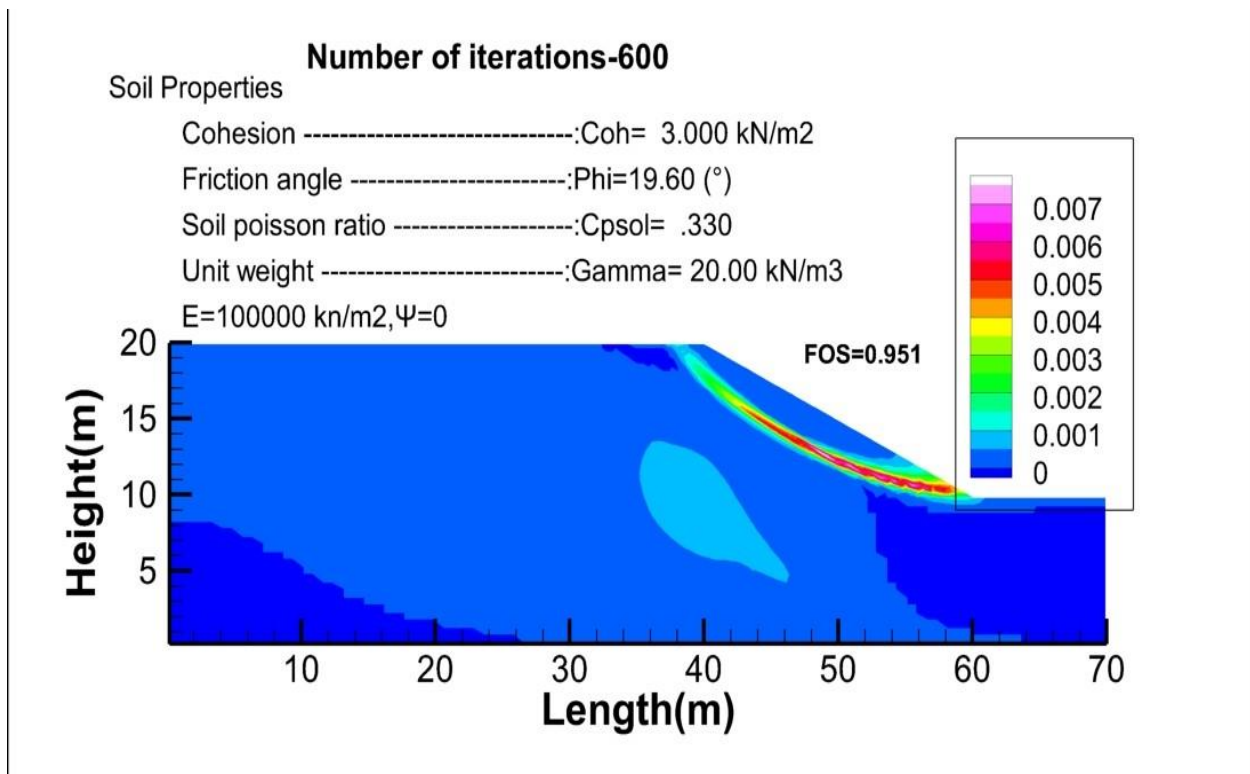


Figure 5.11 42 Strain contours corresponding to the step of failure for 600 iterations, with the foundation

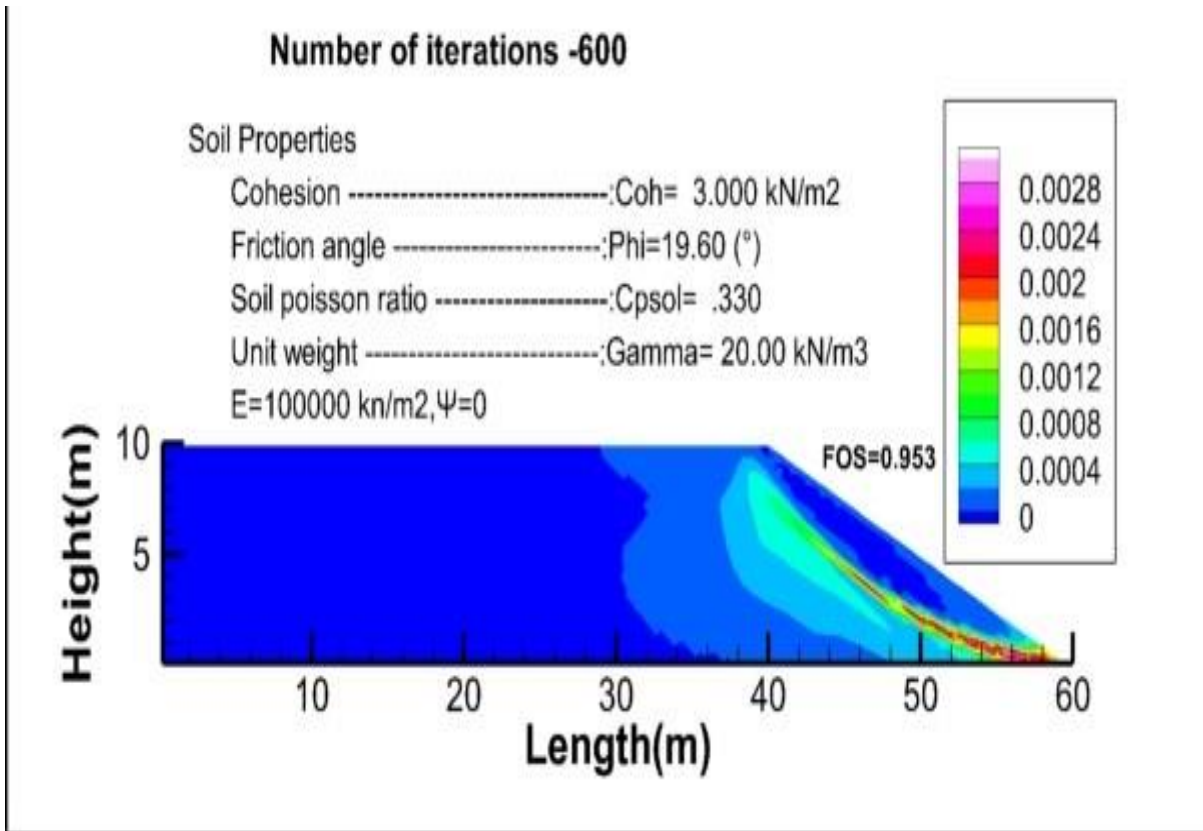


Figure 5.11 43 Strain contours corresponding to the step of failure for 600 iterations, without the foundation

**g) Number of iterations 700**

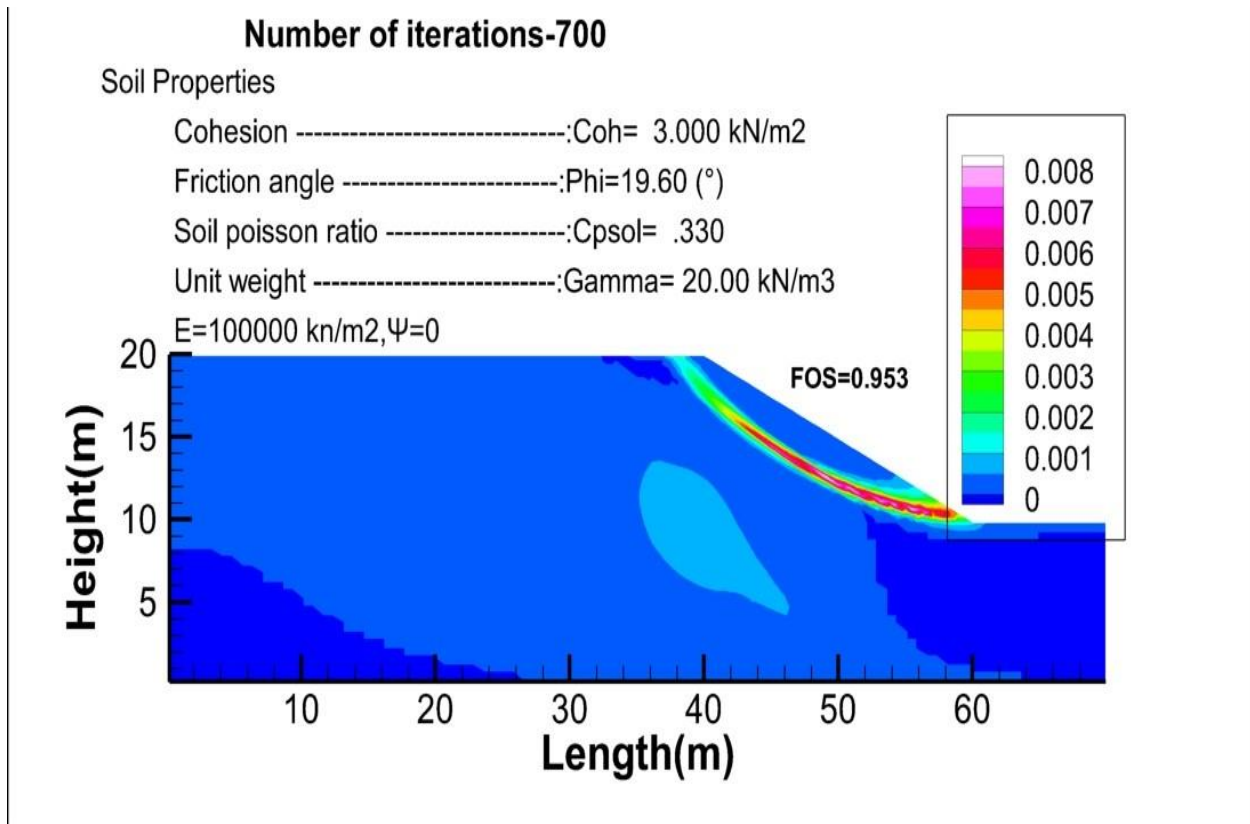


Figure 5.11 44 Strain contours corresponding to the step of failure for 700 iterations, with the foundation

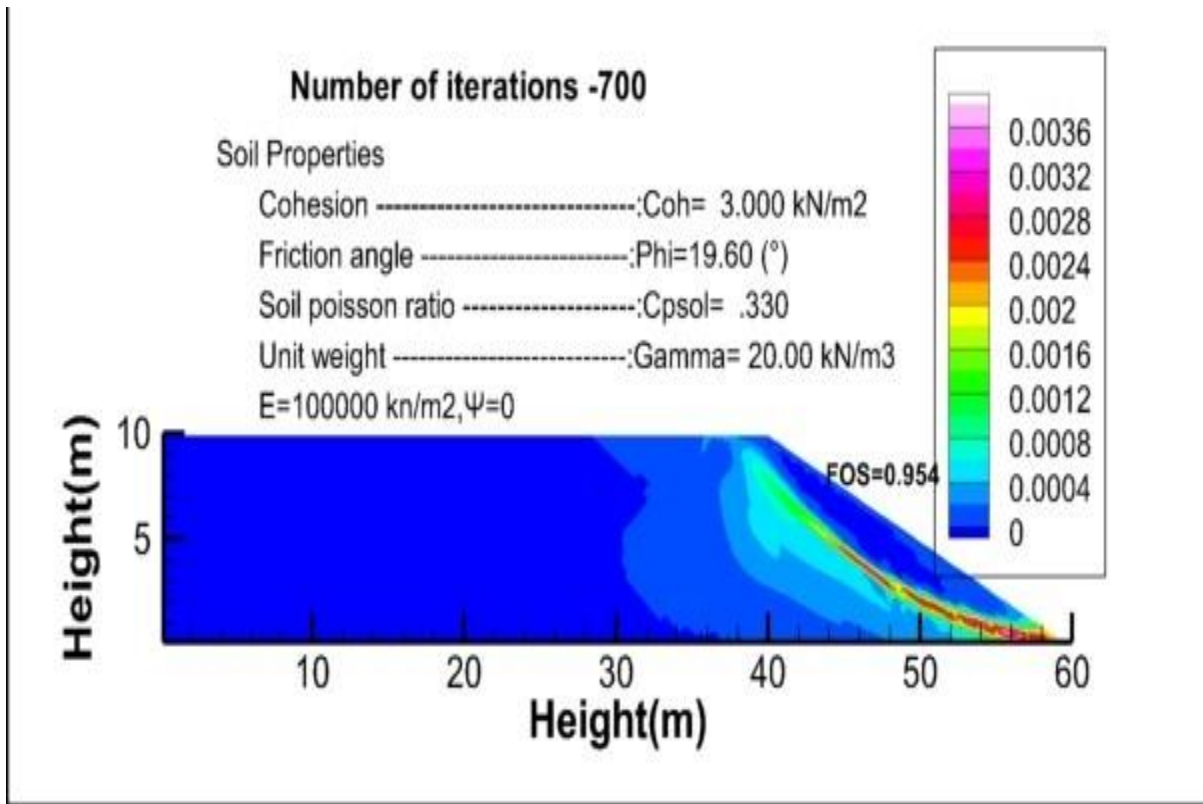


Figure 5.11 45 Strain contours corresponding to the step of failure for 700 iterations, without the foundation.

**h) Number of iterations 800**

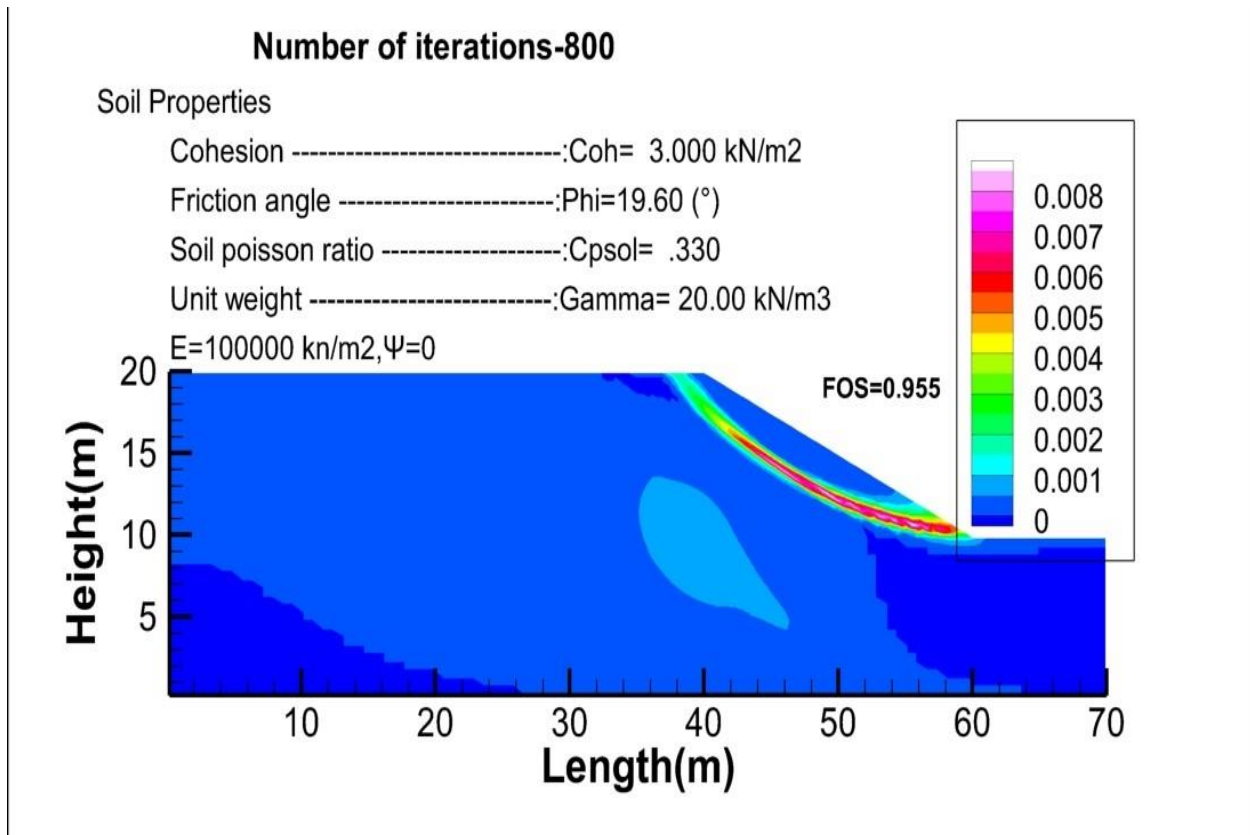


Figure 5.11 46 Strain contours corresponding to the step of failure for 800 iterations, with the foundation

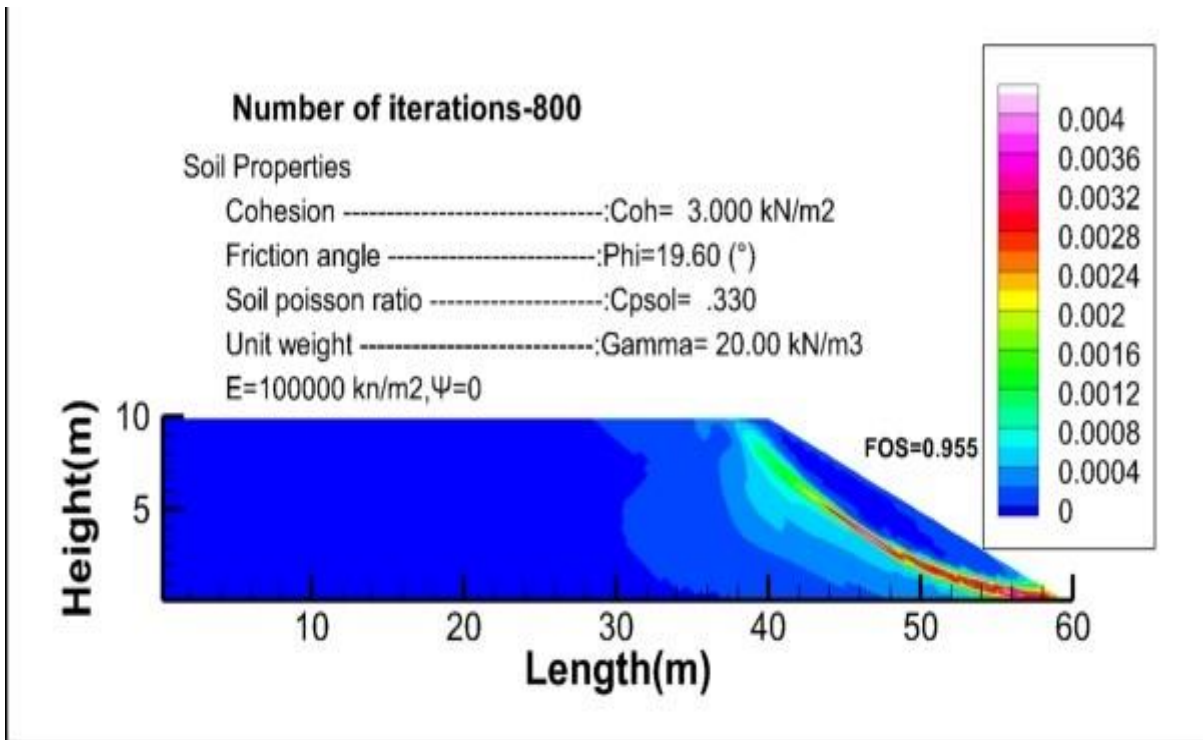


Figure 5.11 47 Strain contours corresponding to the step of failure for 800 iterations, without the foundation.

**i) Number of iterations 900**

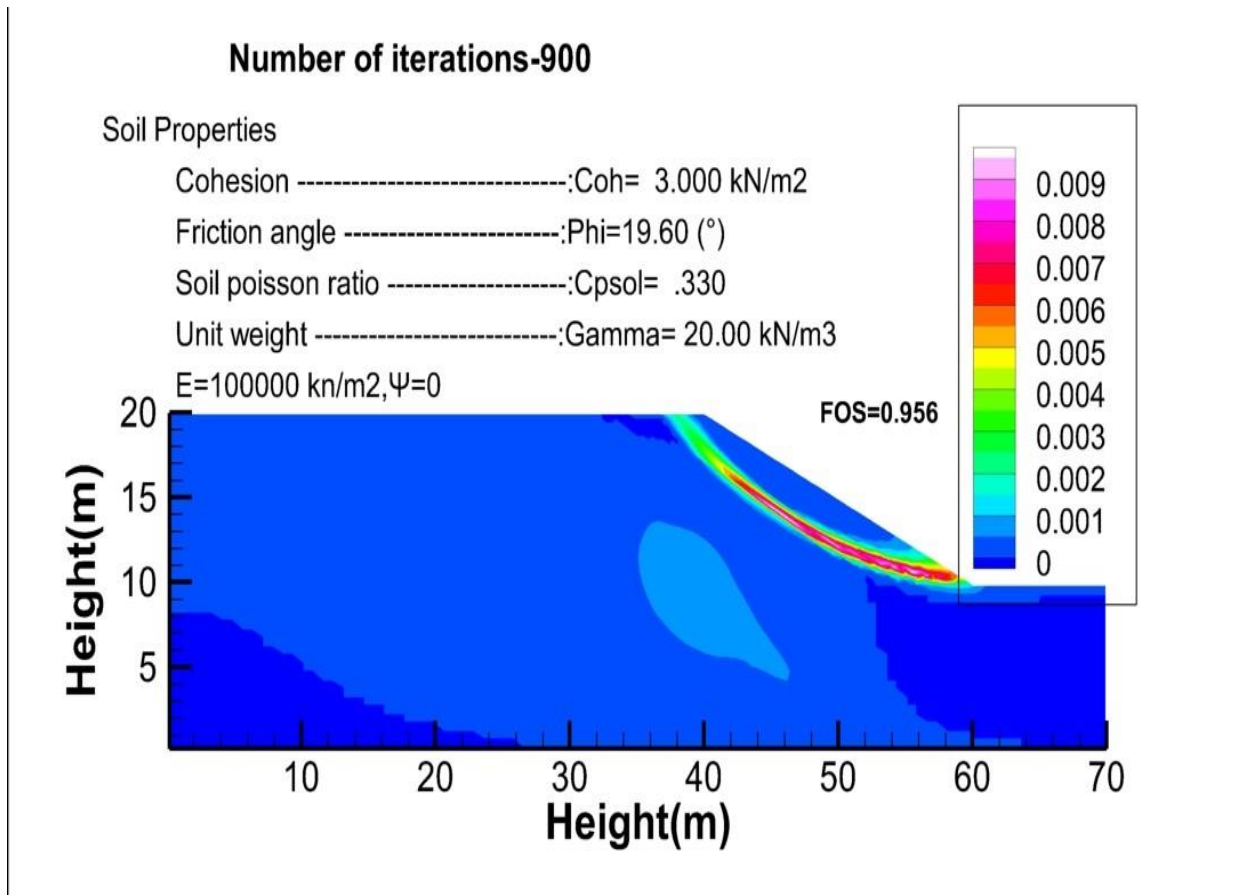


Figure 5.11 48 Strain contours corresponding to the step of failure for 900 iterations, with the foundation



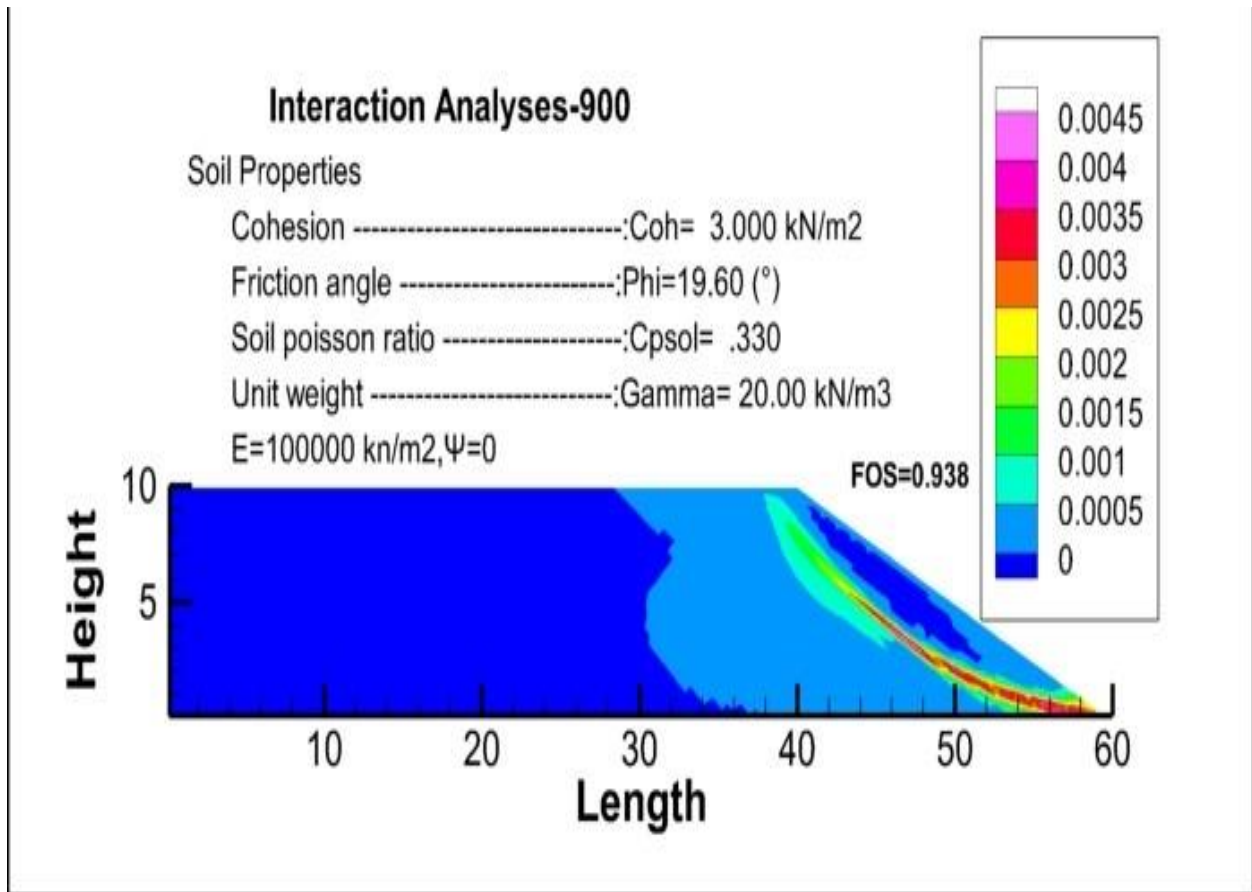


Figure 5.11 49 Strain contours corresponding to the step of failure for 900 iterations, without the foundation.

### j) Number of iterations 1000

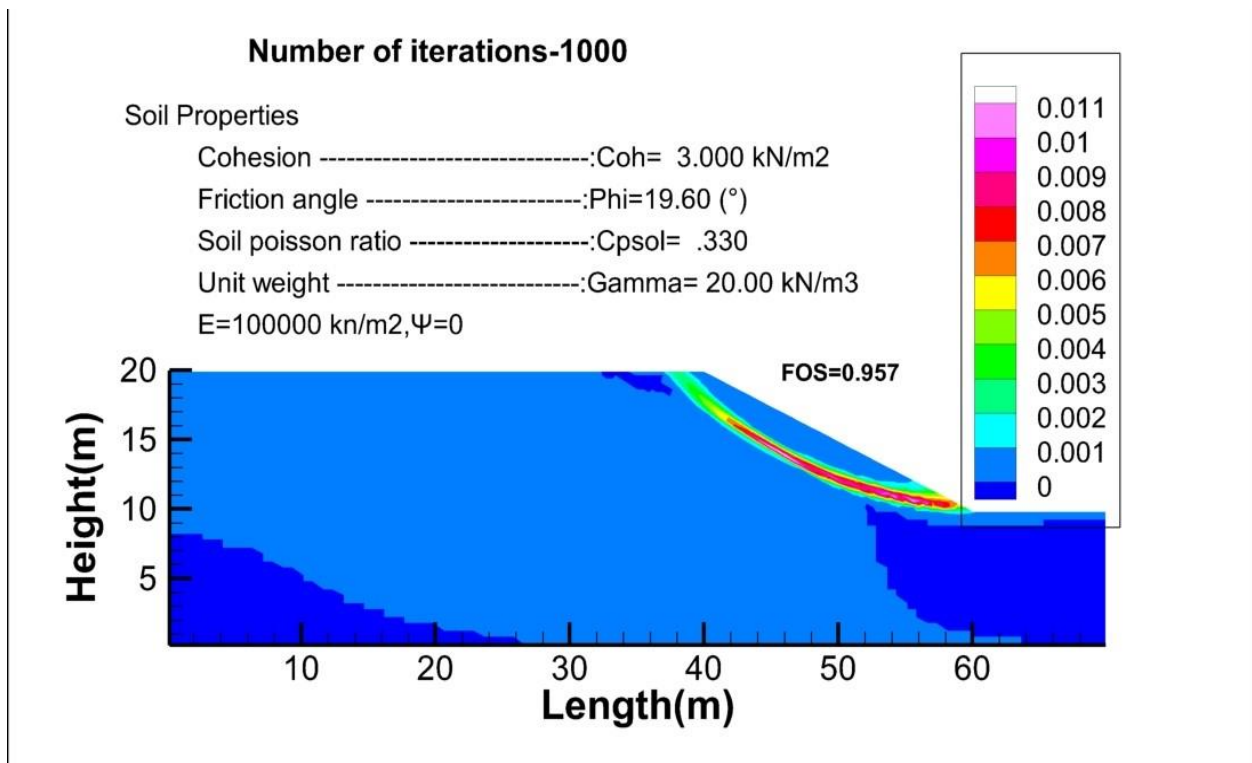


Figure 5.11 50 Strain contours corresponding to the step of failure for 1000 iterations, with the foundation

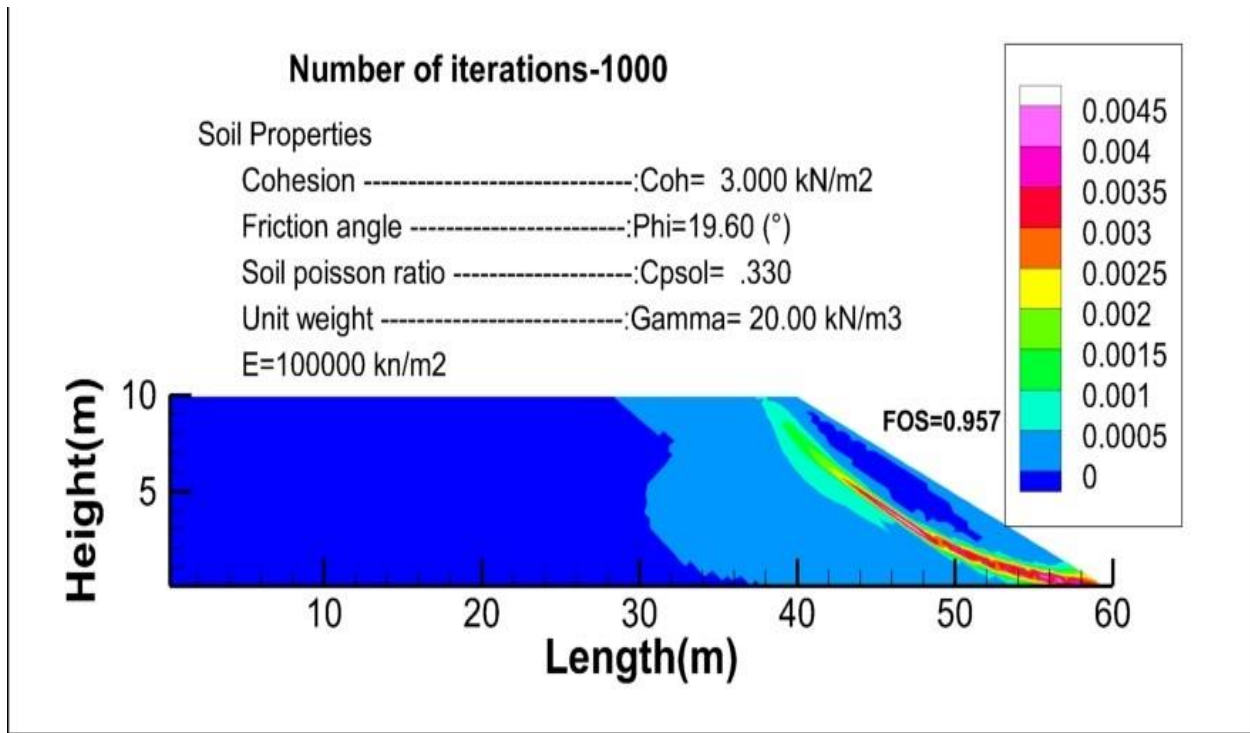


Figure 5.11 51 Strain contours corresponding to the step of failure for 1000 iterations, without the foundation.

**k) Number of iterations 1100**

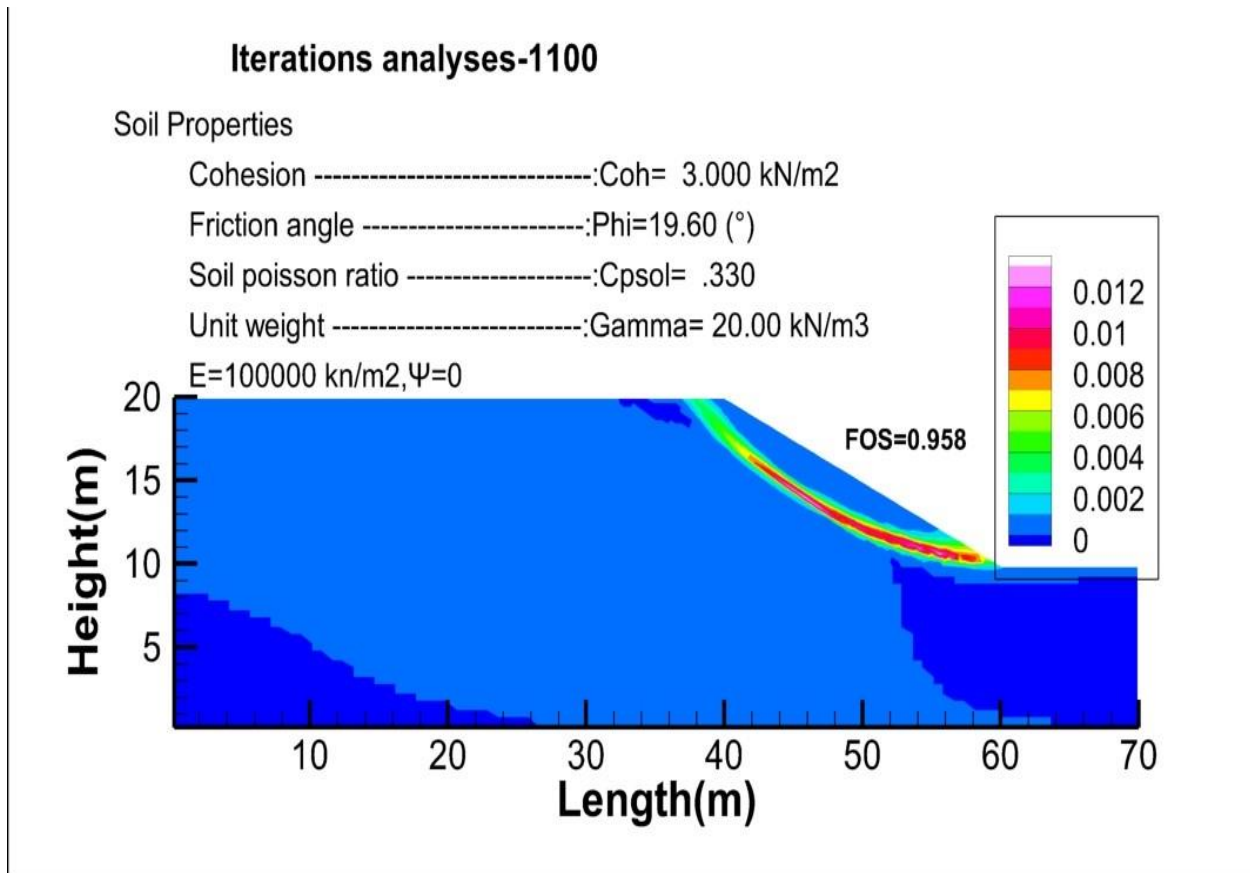


Figure 5.11 52 Strain contours corresponding to the step of failure for 1100 iterations, with the foundation

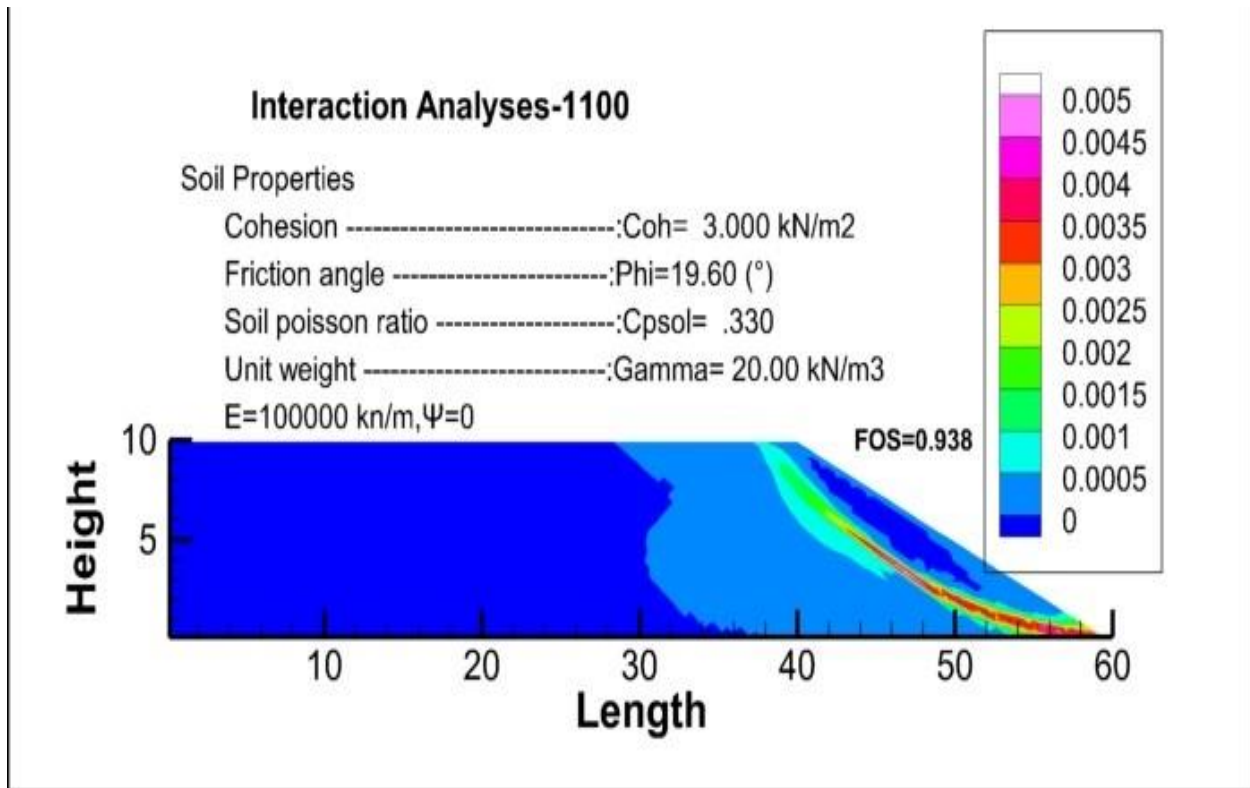


Figure 5.11 53 Strain contours corresponding to the step of failure for 1100 iterations, without the foundation

**1) Number of iterations 1200**

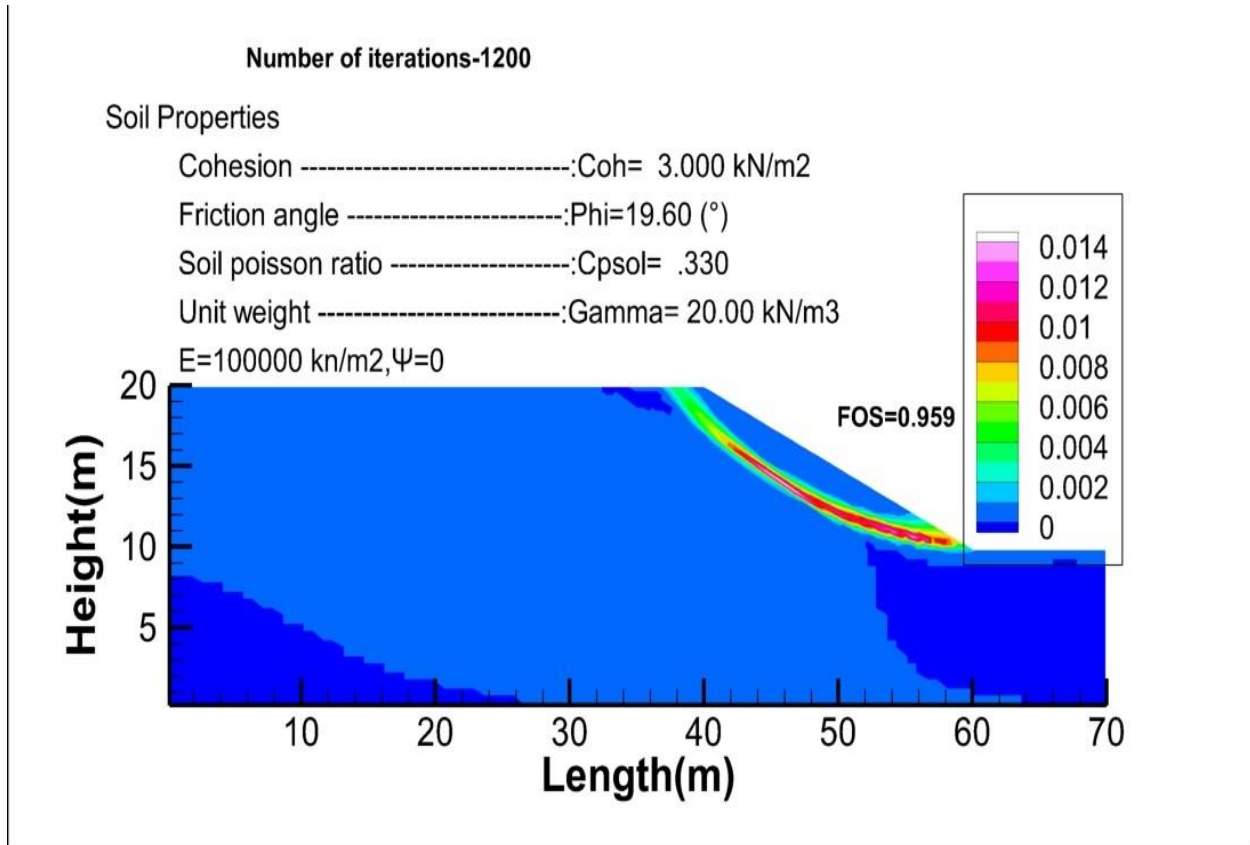


Figure 5.11 54 Strain contours corresponding to the step of failure for 1200 iterations, with the foundation

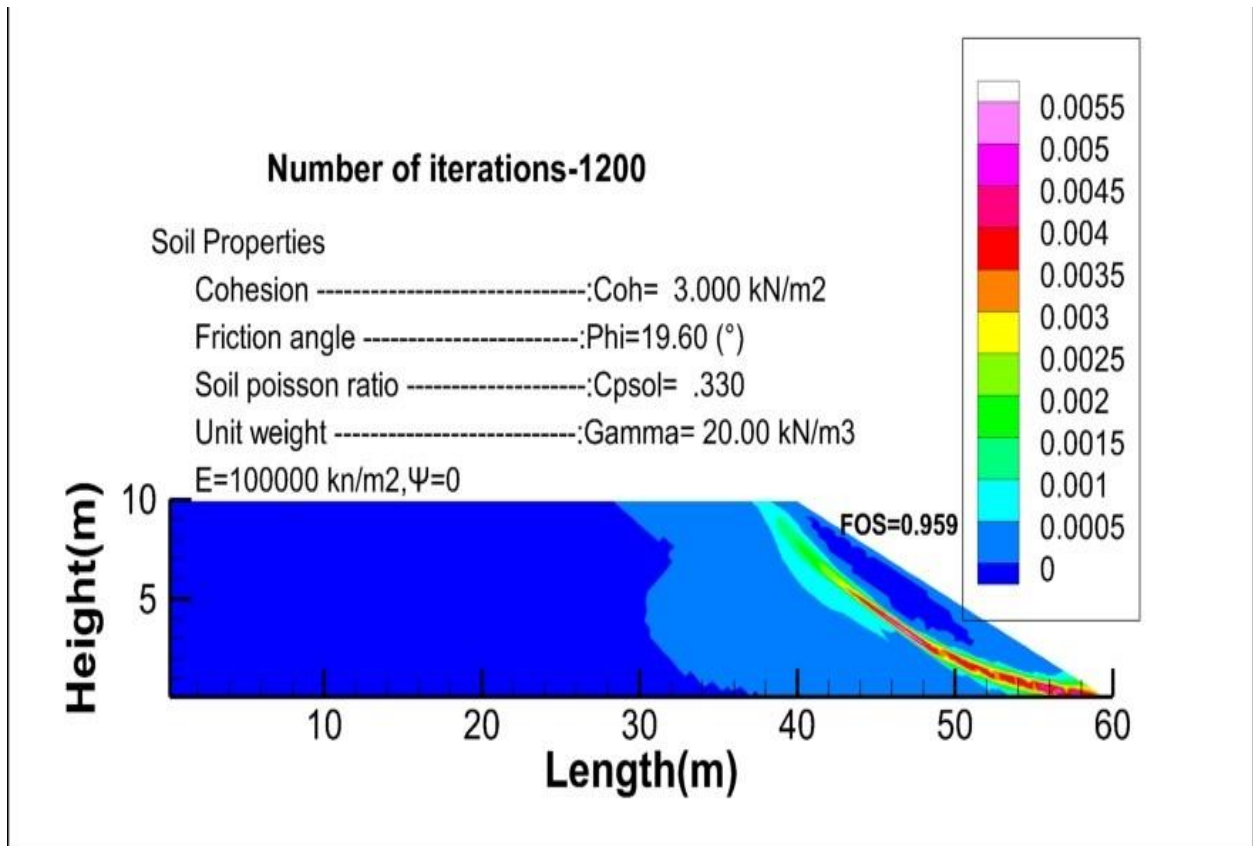


Figure 5.11 55 Strain contours corresponding to the step of failure for 1200 iterations, without the foundation

**m) Number of iterations 1300**

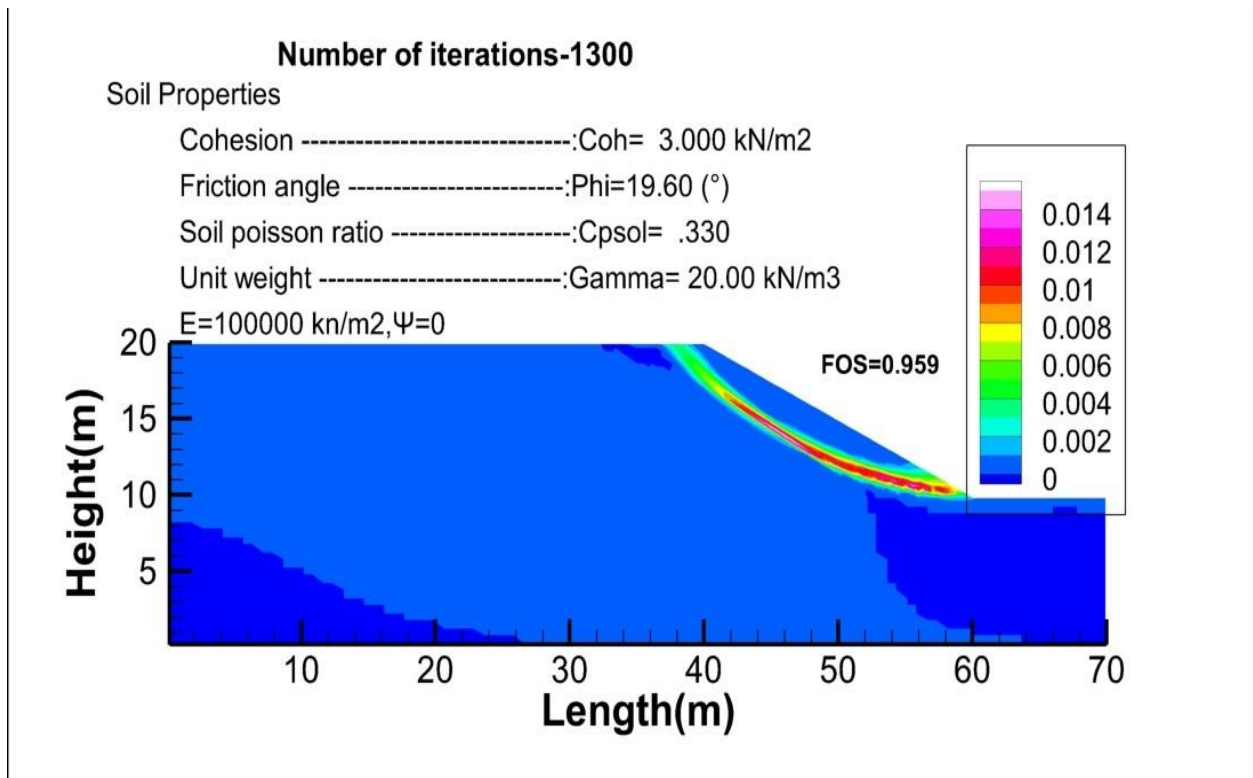


Figure 5.11 56 Strain contours corresponding to the step of failure for 1300 iterations, with the foundation.

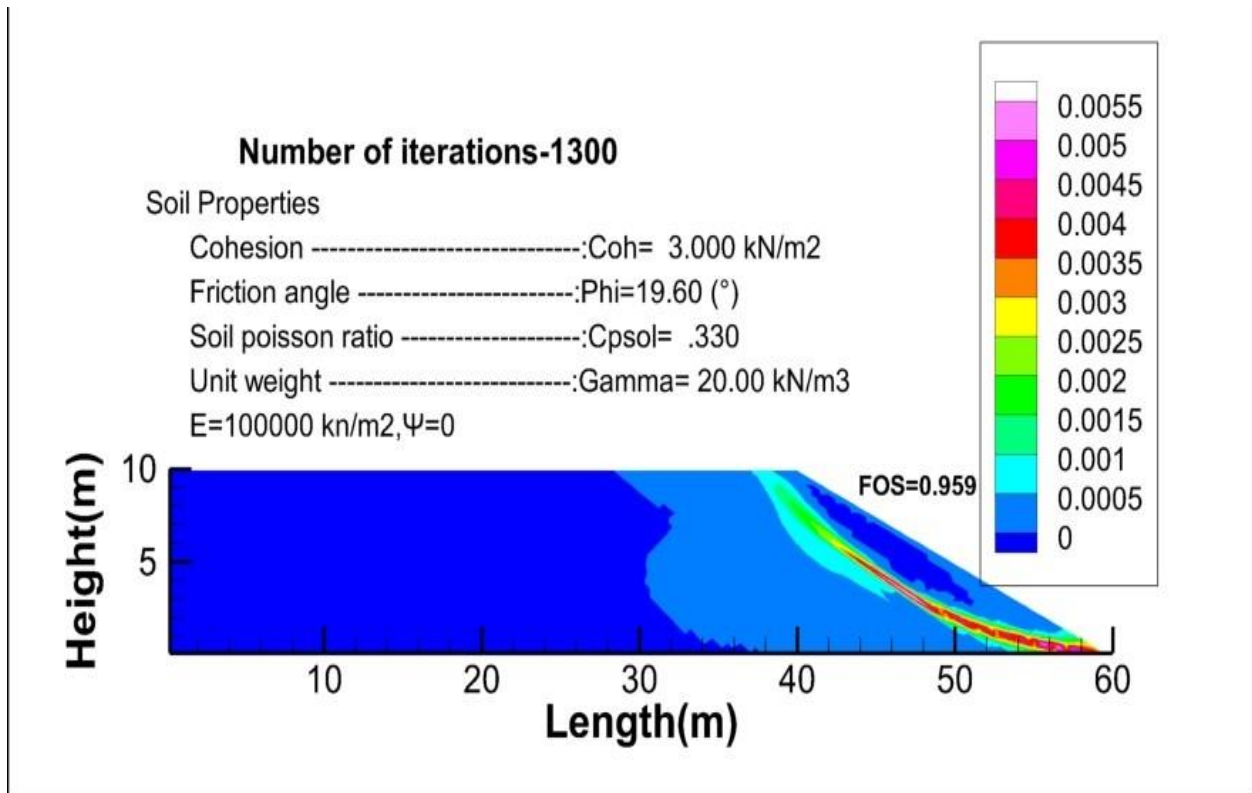


Figure 5.11 57 Strain contours corresponding to the step of failure for 1300 iterations, without the foundation

**n) Number of iterations 1400**

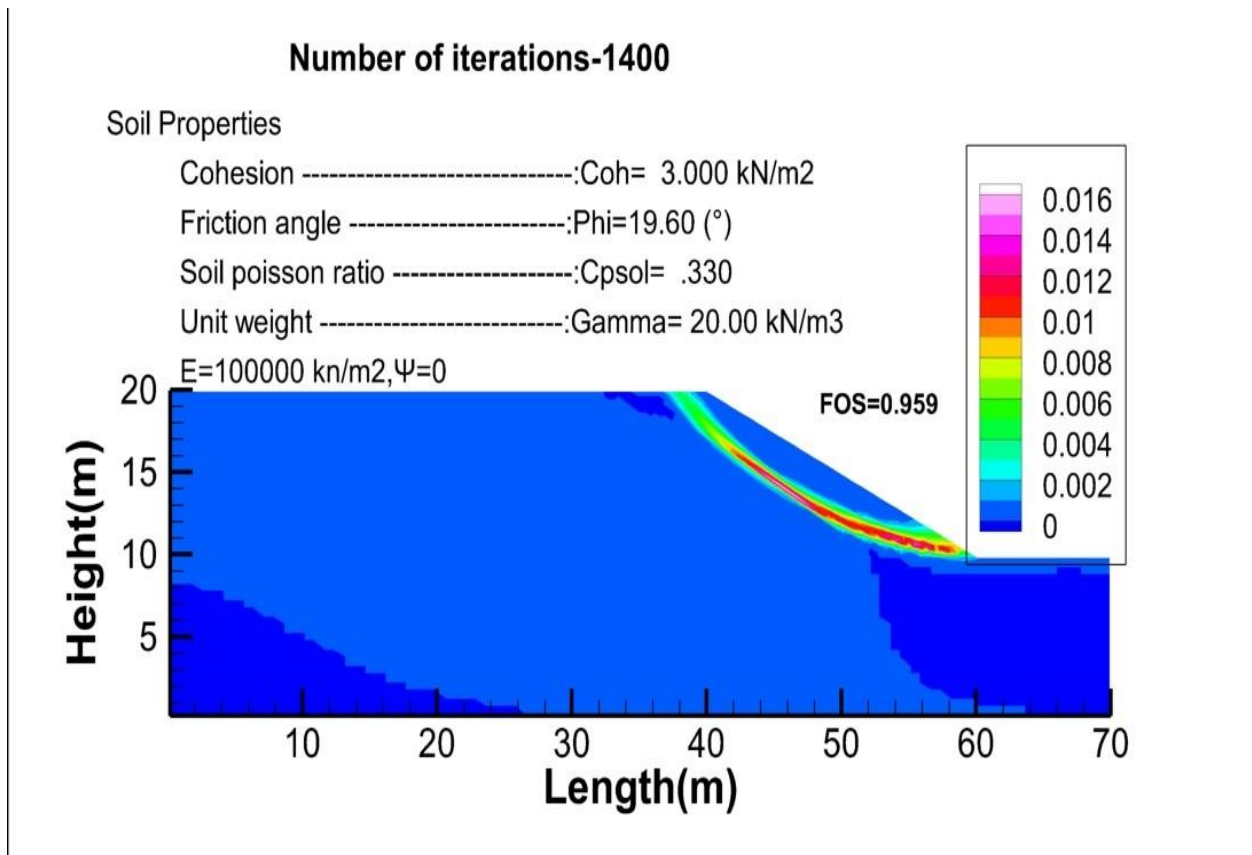


Figure 5.11 58 Strain contours corresponding to the step of failure for 1400 iterations, with the foundation.

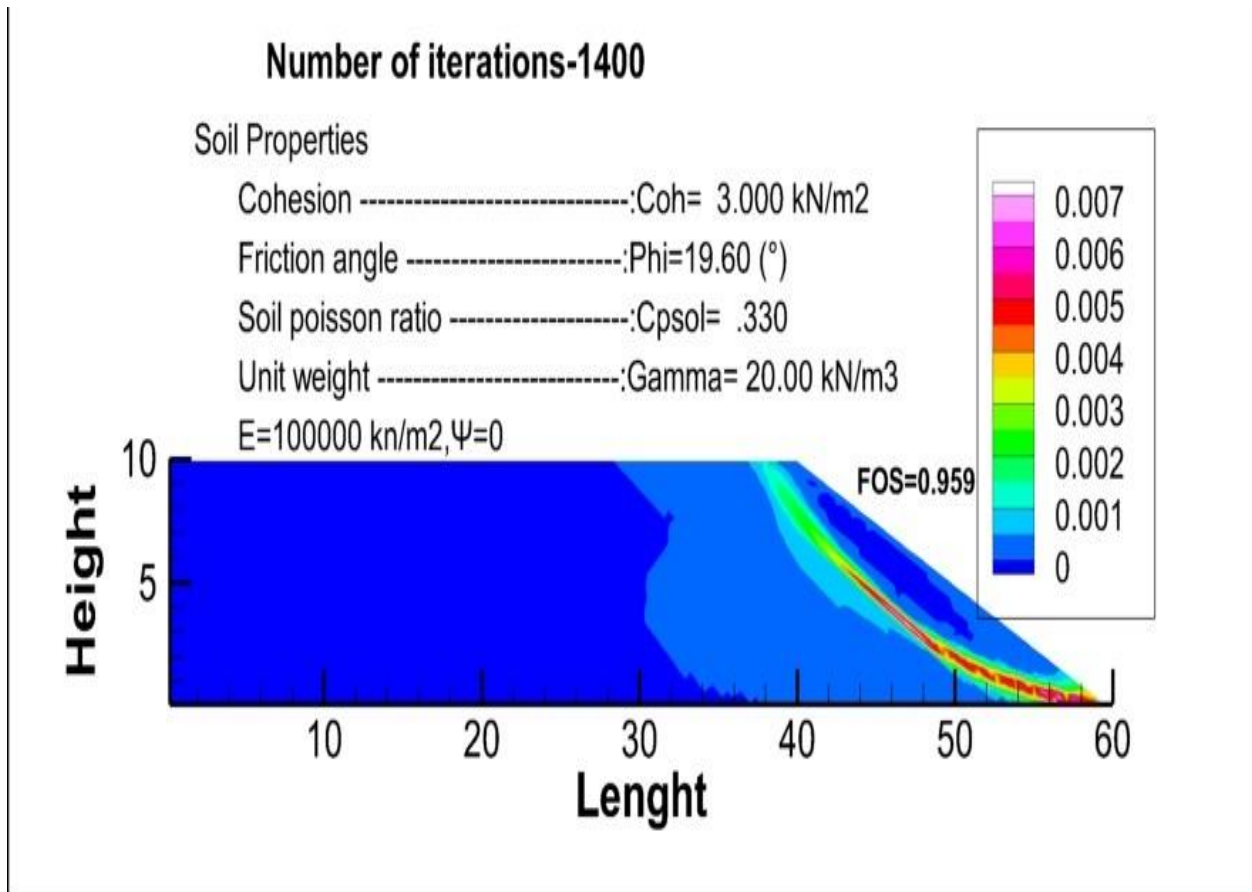


Figure 5.11 59 Strain contours corresponding to the step of failure for 1400 iterations, without the foundation

**o) Number of iterations 1500**

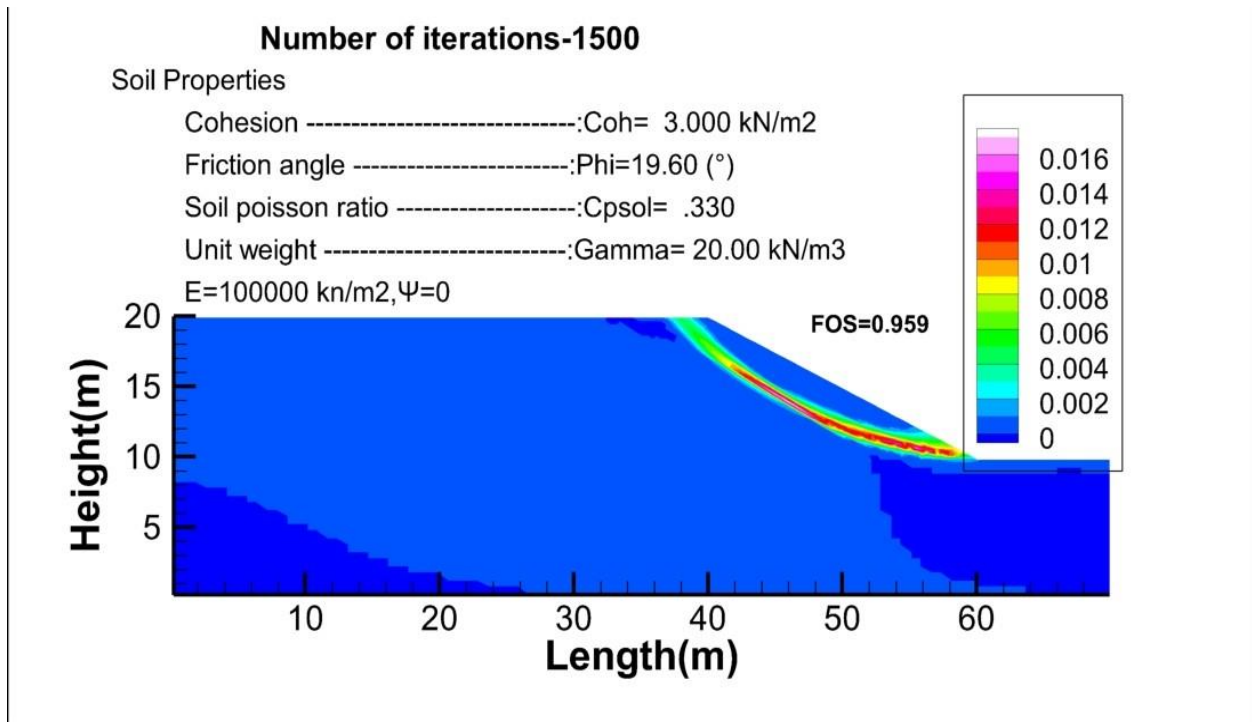


Figure 5.11 60 Strain contours corresponding to the step of failure for 1500 iterations, with the foundation.

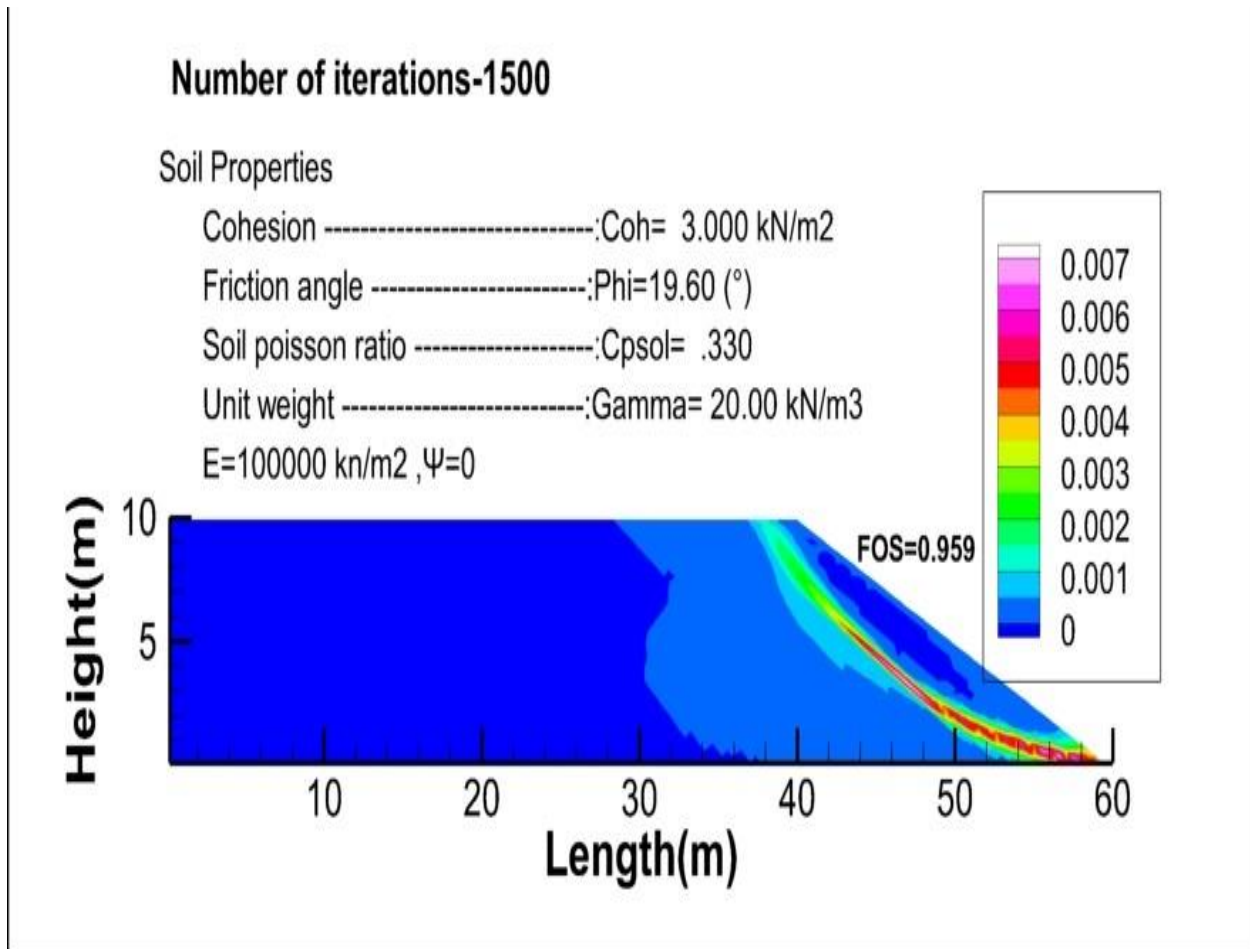


Figure 5.11 61 Strain contours corresponding to the step of failure for 1500 iterations, without the foundation.

Here we clearly see that the deformations are more netted and almost reached the crest due to the lack of the resistance since we assumed that  $\psi = 0$ .

## 5.8. Deformation Parametric

### 5.8.1. Young's Modulus Analyses

#### Associated flow rule.

Table 5 2 5 Results of Evaluation of the young's Modulus variation. Associated.

E	BS	MP	SDIM
1000	0.999	0.997	0.992
5000			
10000			
50000			
100000			

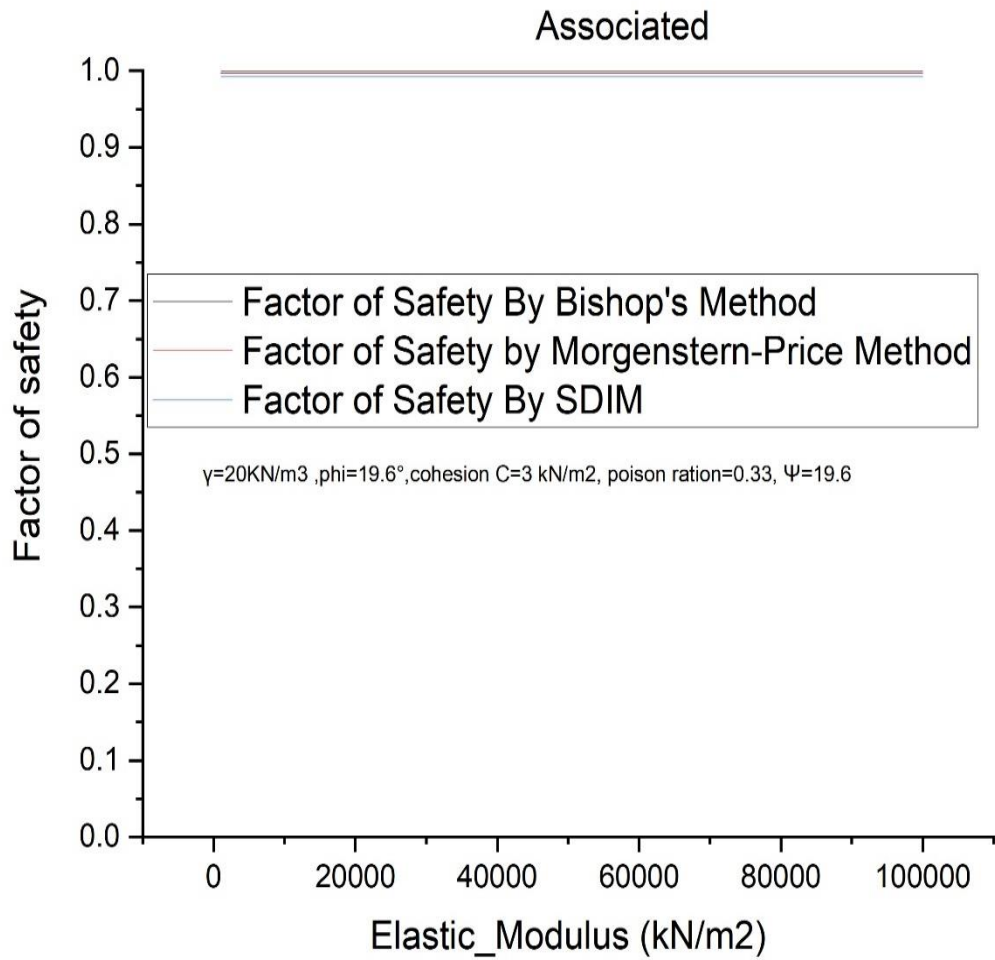


Figure 5.11 62 Evaluation of the young's Modulus variation. Associated

### 5.8.2. Associated flow rule

Table 5 2 6 Results of Evaluation of the young's Modulus variation. Associated

E	BS	MP	SDIM
1000	0.989	0.984	0.986
5000			
10000			
50000			
100000			



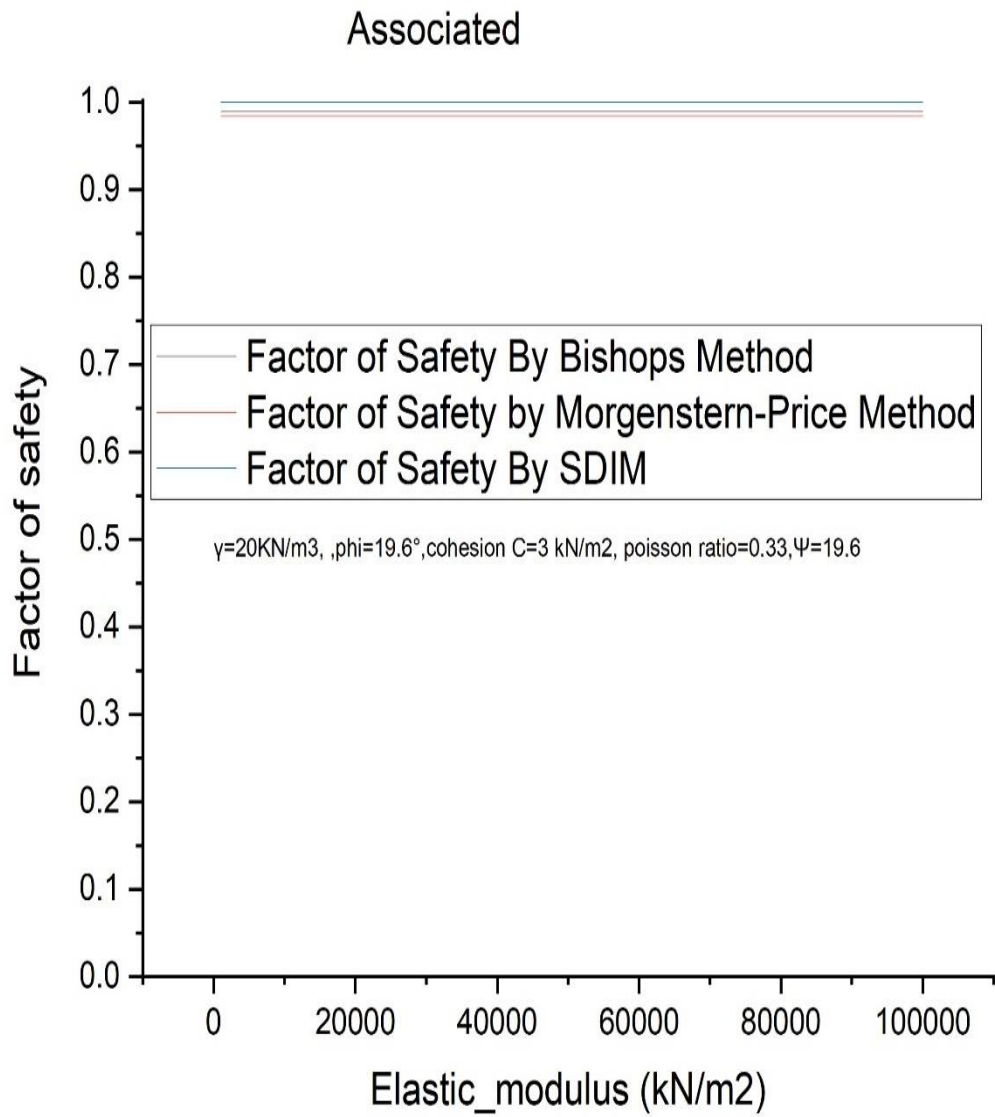


Figure 5.11 63. Evaluation of the young's Modulus variation. Associated

Clearly shown that the Young Modulus has no effects at all on the calculation. So the factor of safety gotten from SDIM are very close from LEM.

The plastic strain counters are expected to be the same through all the process of increasing this parameter.

a) Young's Modulus  $E=1000 \text{ kN/m}^2$

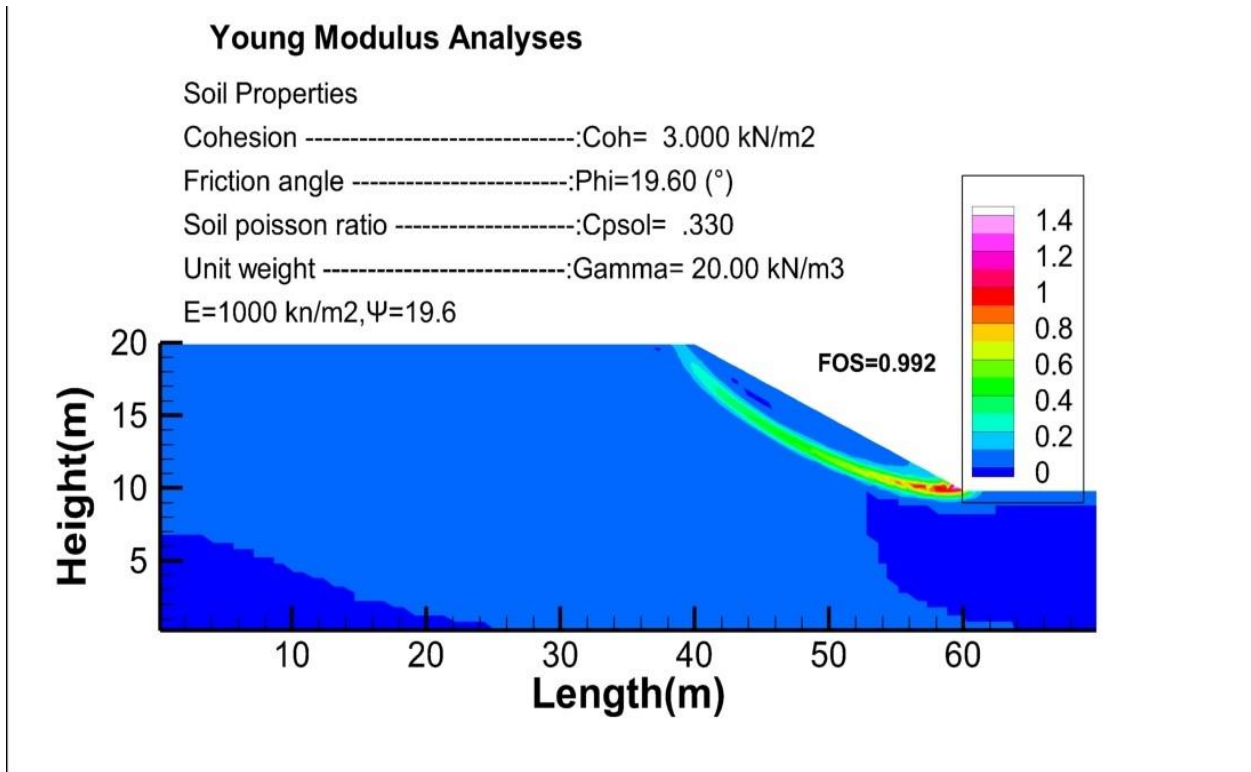


Figure 5.11 64 Strain contours corresponding to the step of failure for  $E=1000 \text{ kN/m}^2$ , with the foundation.

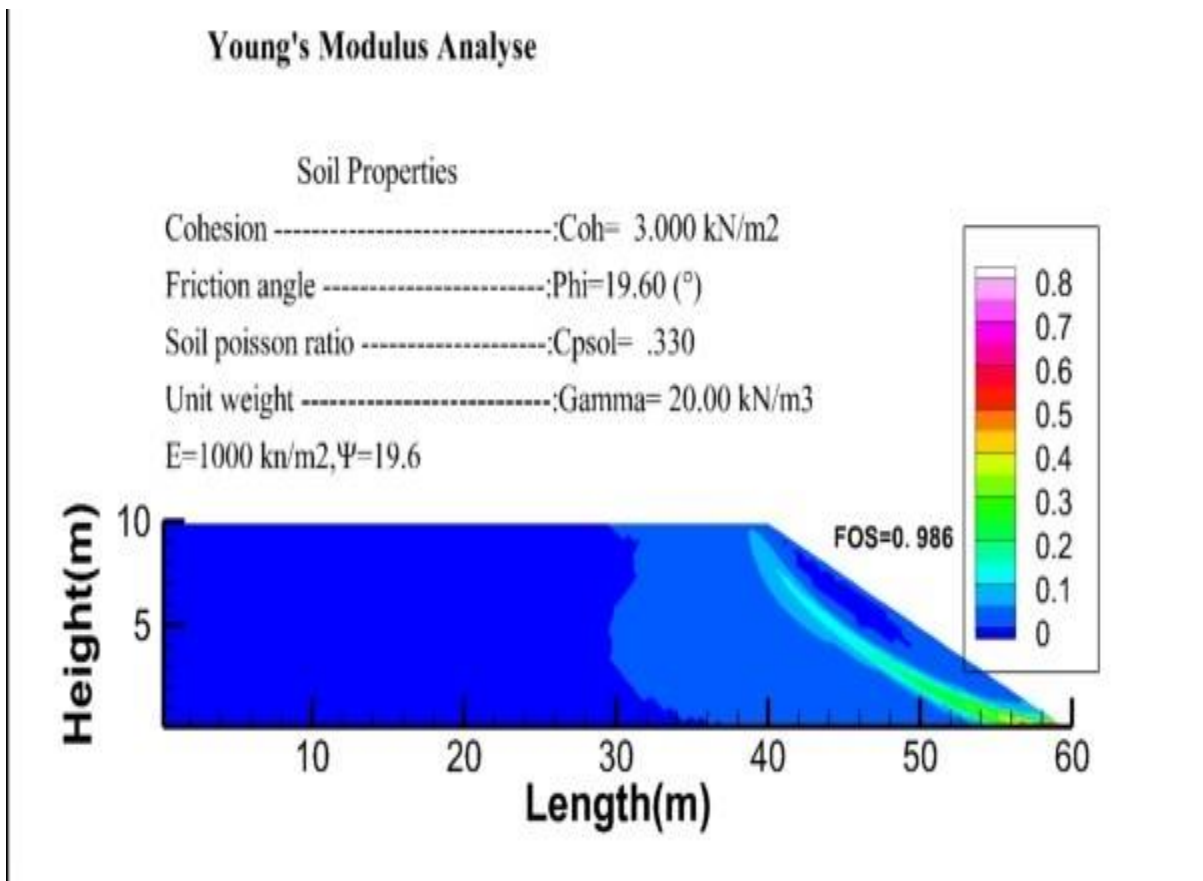


Figure 5.11 65 Strain contours corresponding to the step of failure for  $E=1000 \text{ kN/m}^2$ , without the foundation.

**b) Young's Modulus  $E=5000\text{kN/m}^2$**

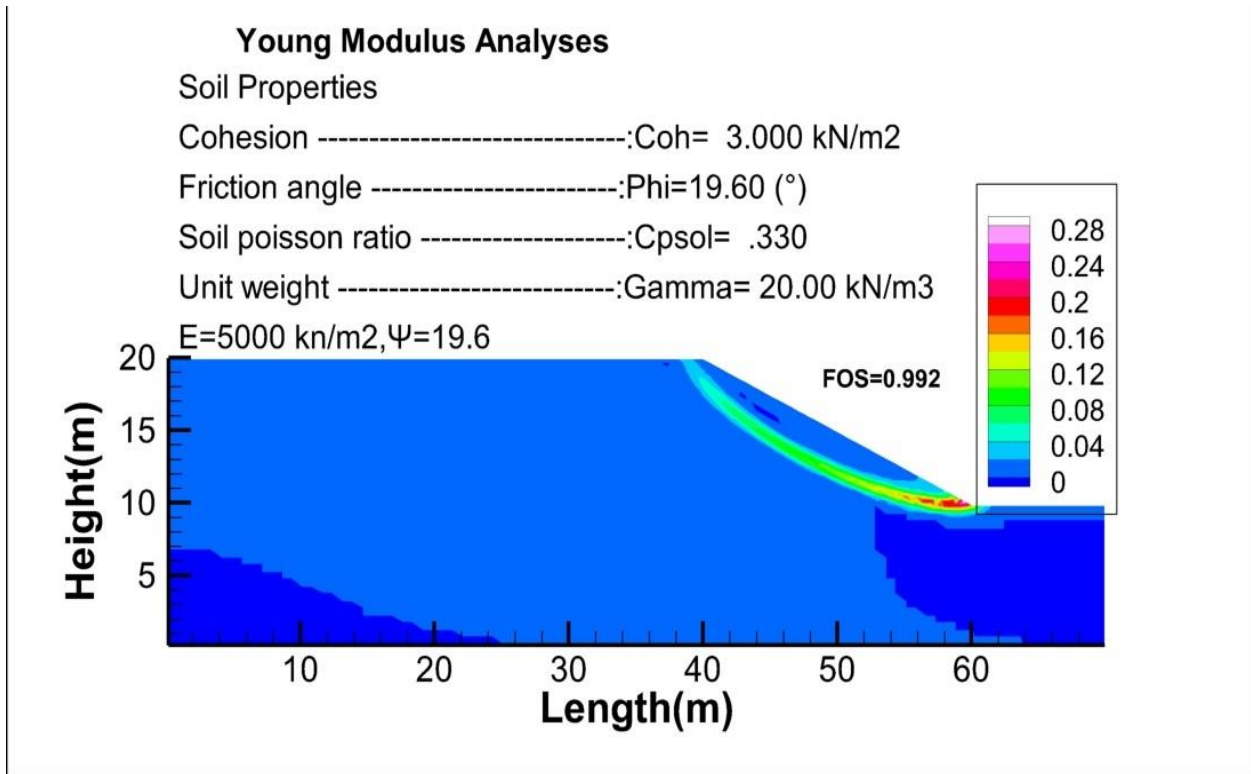


Figure 5.11 66 Strain contours corresponding to the step of failure for  $E=5000\text{ kN/m}^2$ , with the foundation

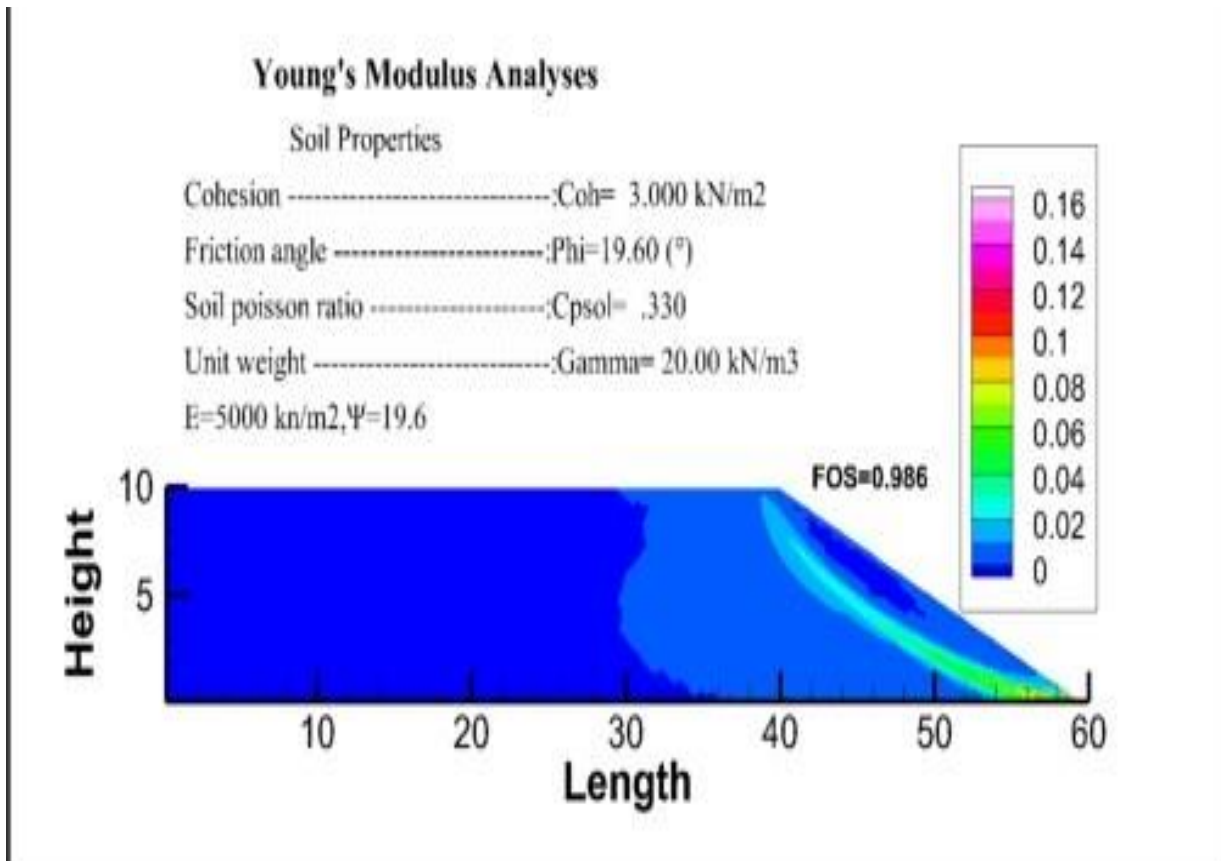


Figure 5.11 67 Strain contours corresponding to the step of failure for  $E=5000\text{ kN/m}^2$ , without the foundation.

c) Young's Modulus  $E=10000\text{kn/m}^2$

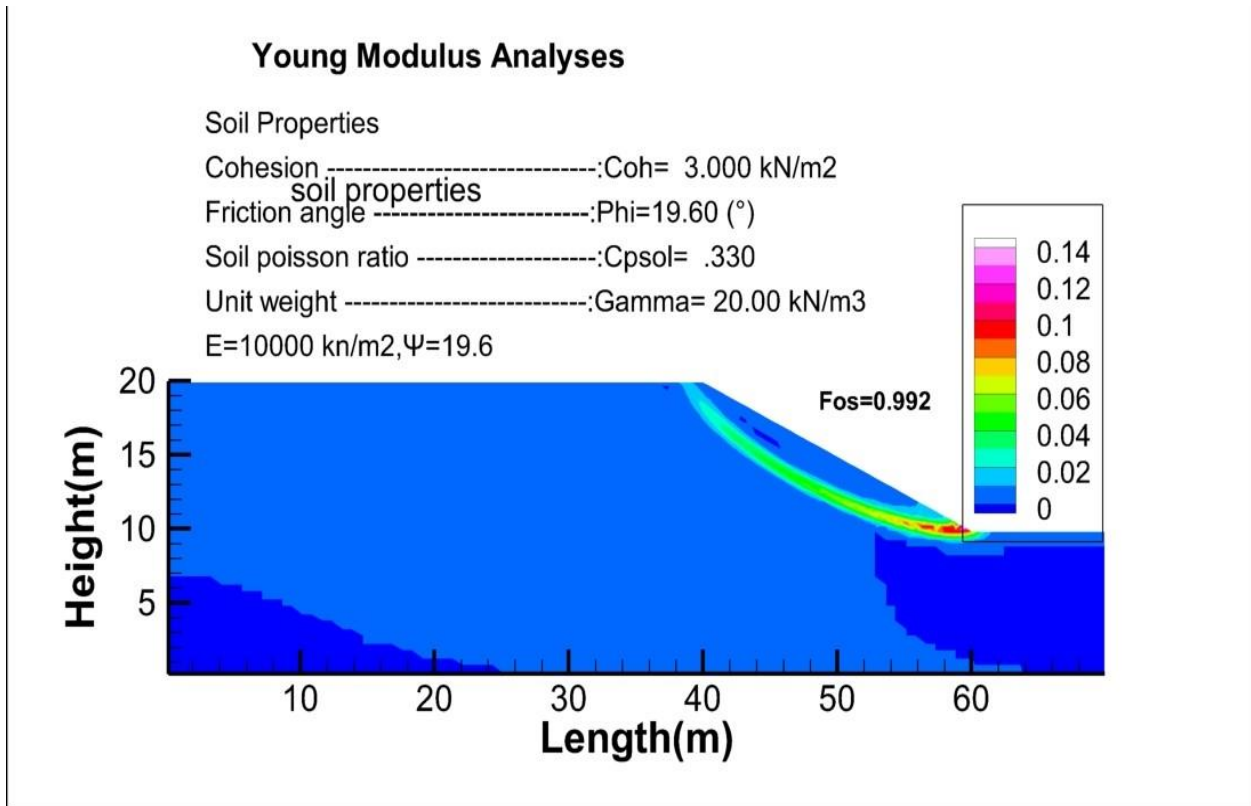


Figure 5.11 68 Strain contours corresponding to the step of failure for  $E=1000\text{ kN/m}^2$ , with the foundation.

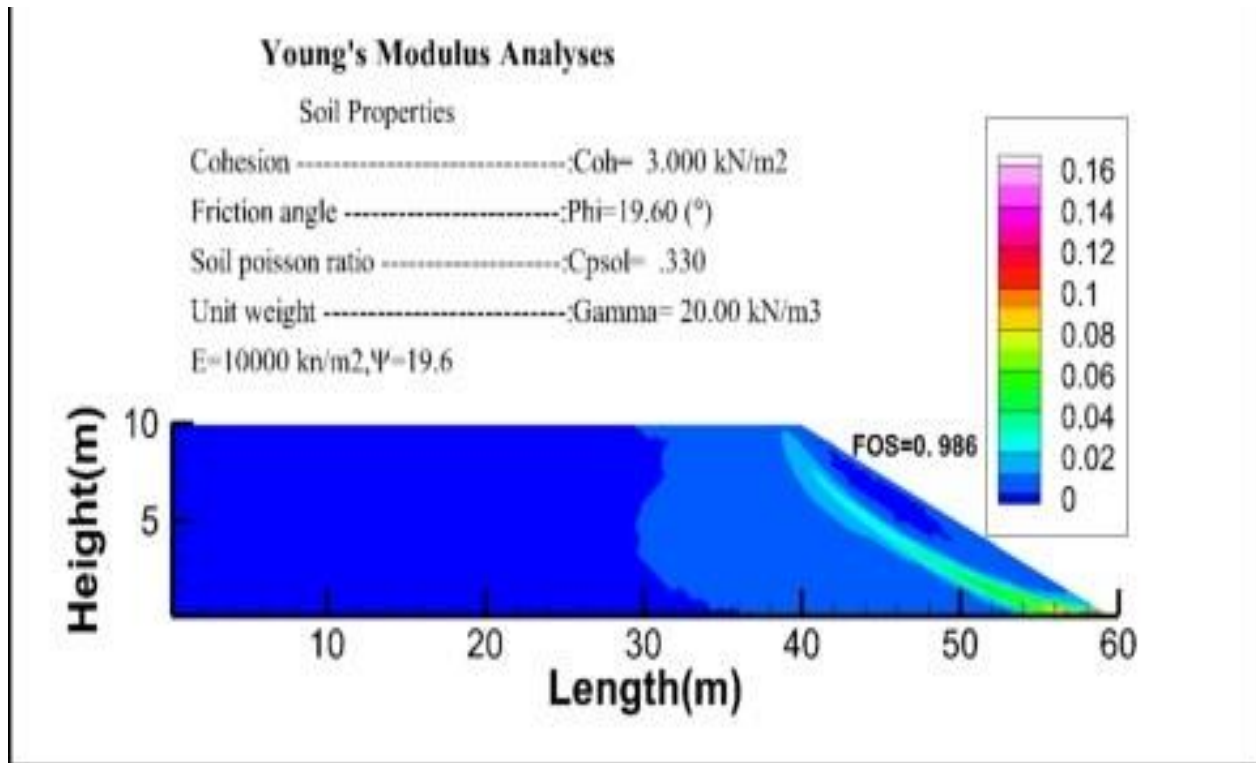


Figure 5.11 69 Strain contours corresponding to the step of failure for  $E=10000\text{ kN/m}^2$ , without the foundation.

d) Young's Modulus  $E=100000\text{KN/m}^2$

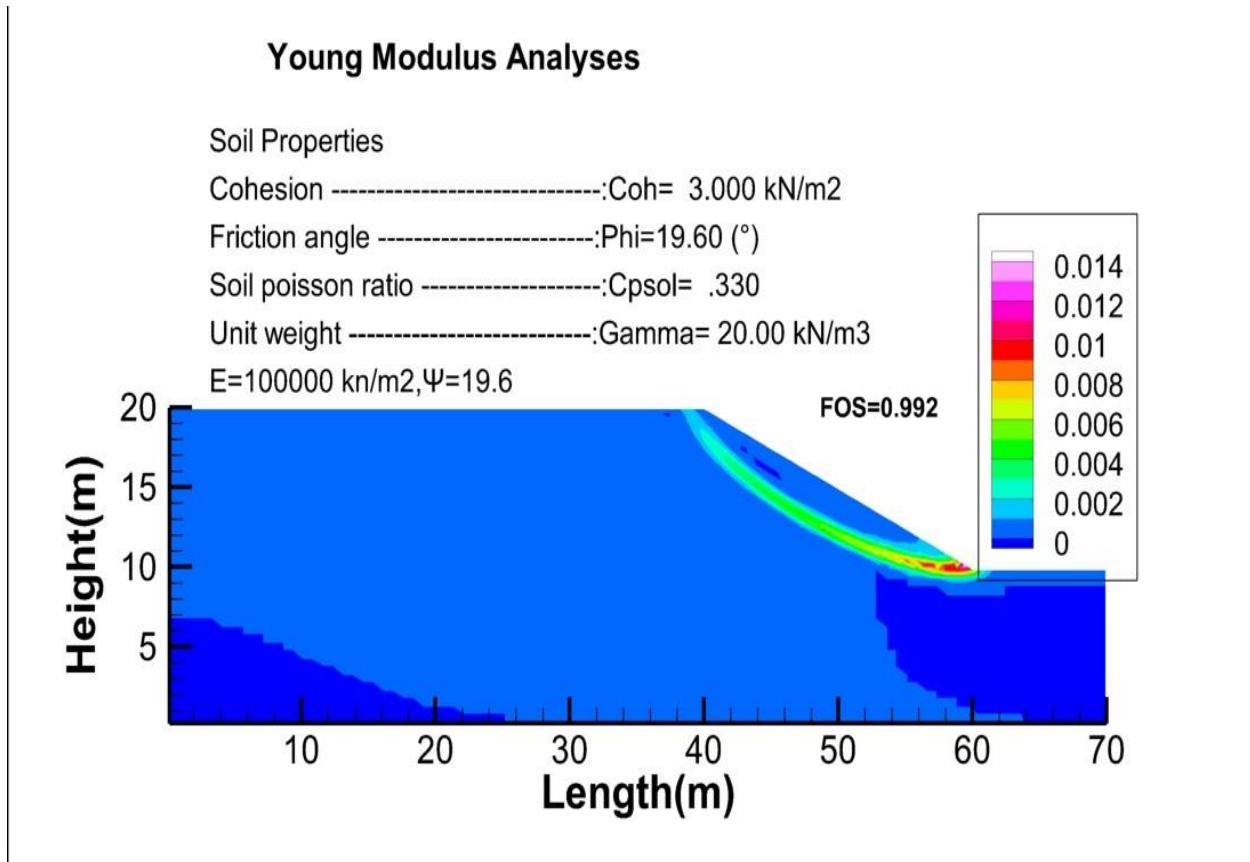


Figure 5.11 70 Strain contours corresponding to the step of failure for  $E=100000\text{ kN/m}^2$ , with the foundation

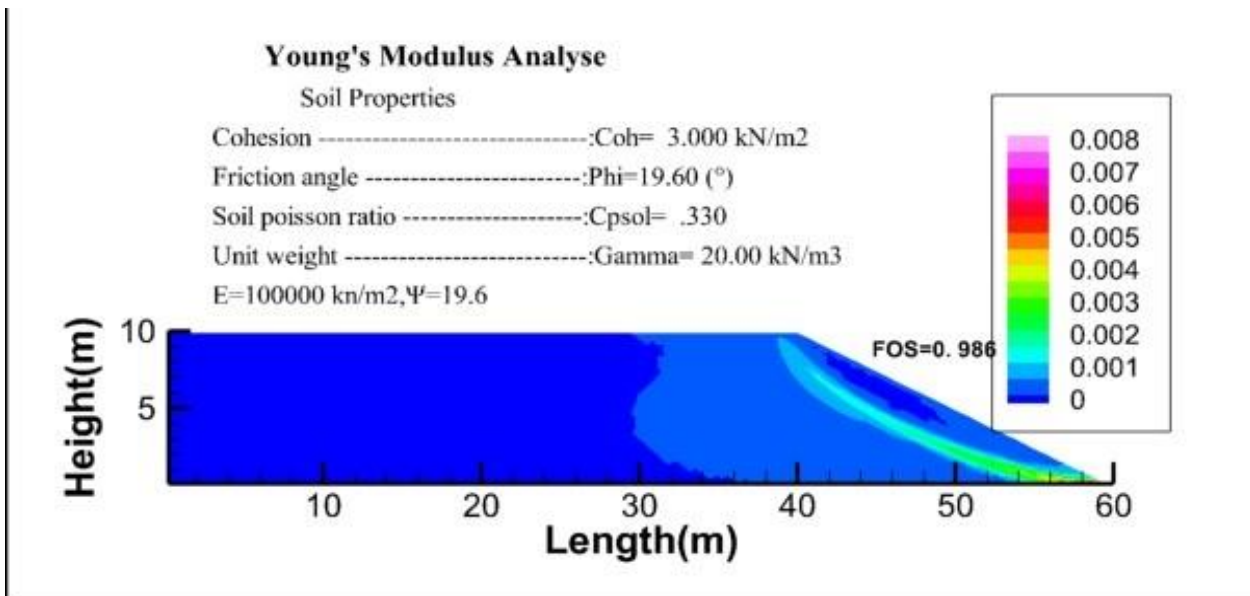


Figure 5.11 71 Strain contours corresponding to the step of failure for  $E=1000\text{ kN/m}^2$ , without the foundation.

Any change of behaviour is to be expected because the Young Modulus has no influence in the calculation so any value of Young Modulus is valid.

### 5.8.3. Non-Associate flow rule.

Table 5 2 7 Results of Evaluation of the young's Modulus variation. Non-associated

E	BS	MP	SDIM
1000	0.999	0.997	0.957
5000			
10000			
50000			
100000			

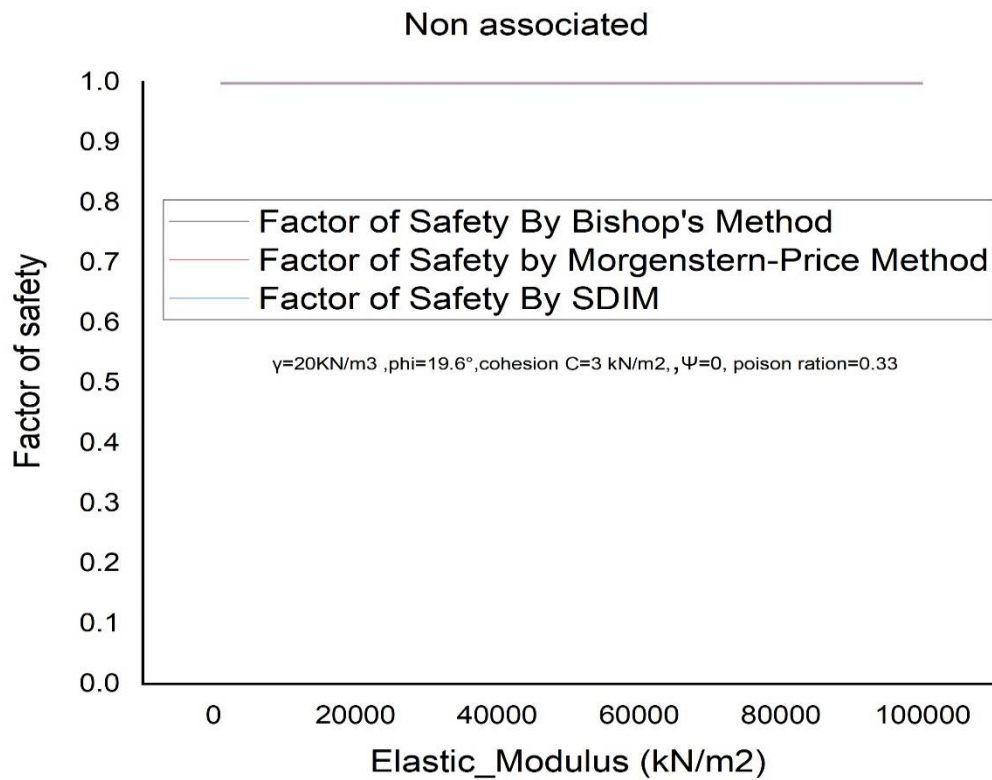


Figure 5.11 72 Evaluation of the young's Modulus variation. Non-associated

### 5.8.4. Non associated flow rule.

Table 5 2 8 Results of Evaluation of the young's Modulus variation. Non-associated

E	BS	MP	SDIM
1000	0.989	0.984	0.938
5000			
10000			
50000			
100000			

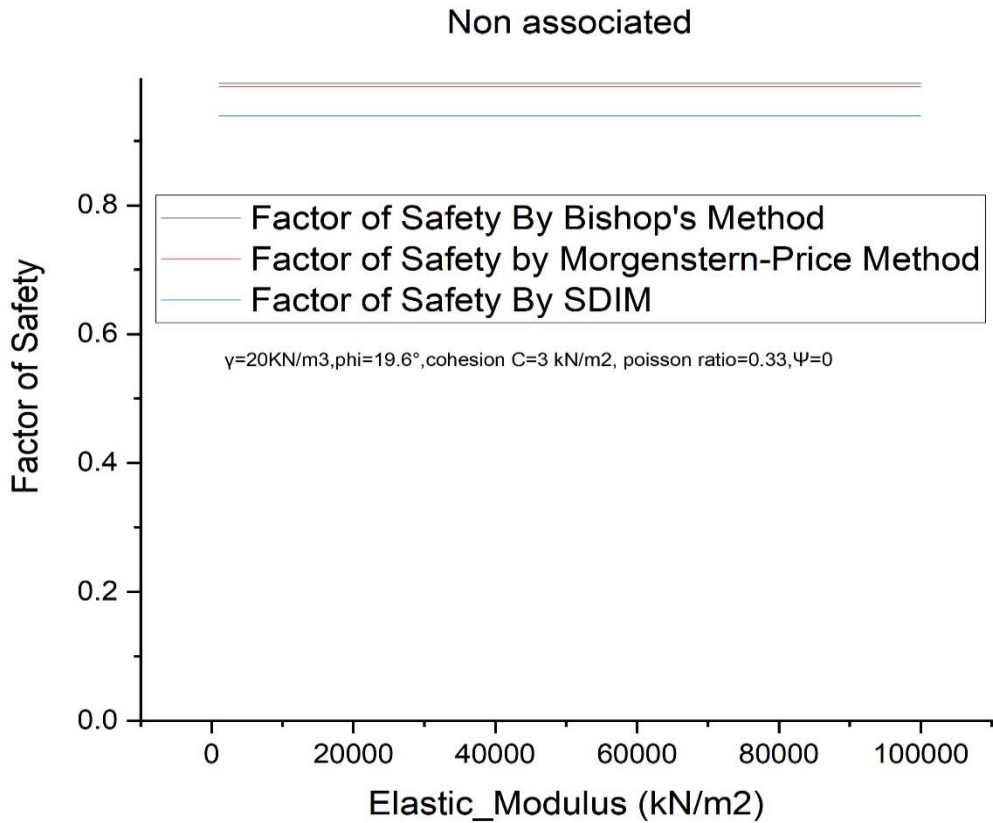


Figure 5.11 73 Evaluation of the young's Modulus variation. Non-associated

**a) Young's Modulus E=1000kN/m<sup>2</sup>**

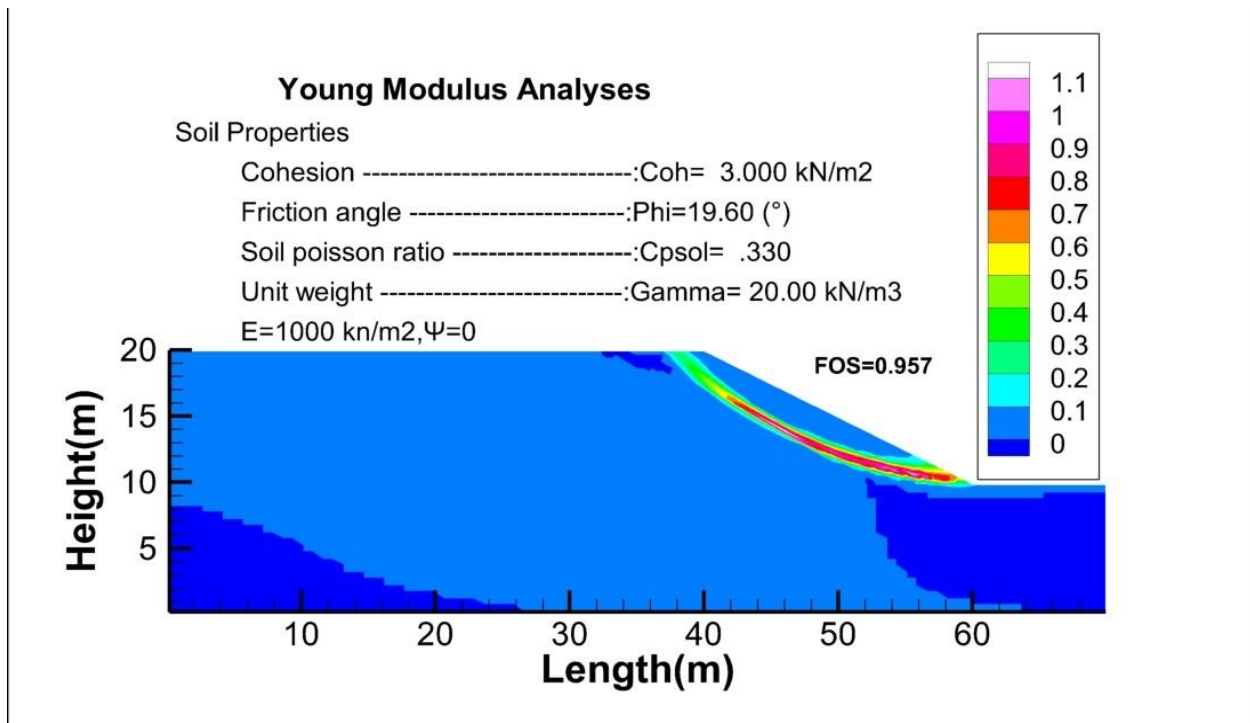


Figure 5.11 74 Strain contours corresponding to the step of failure for E=1000kN/m<sup>2</sup>, with the foundation

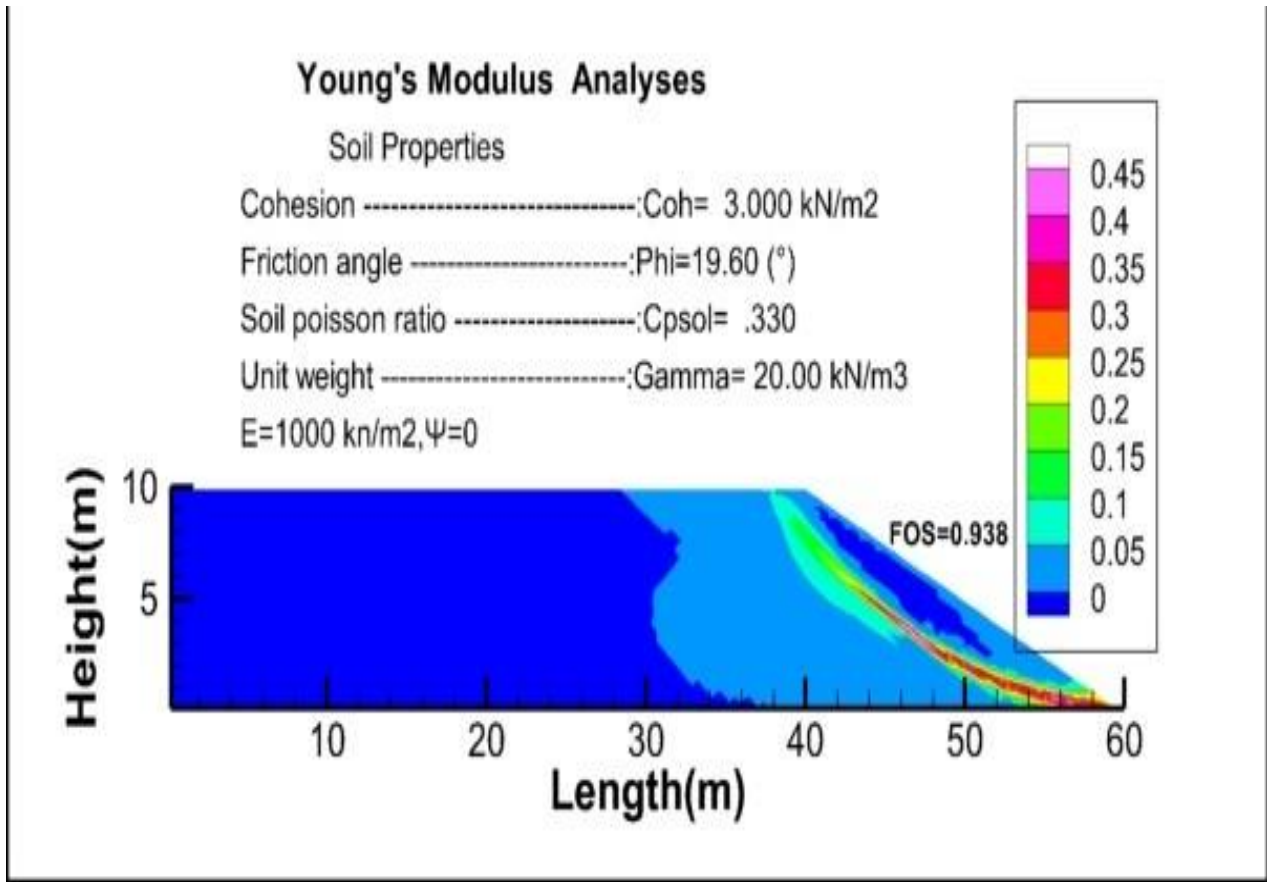


Figure 5.11 75 Strain contours corresponding to the step of failure for E=1000 kN/m<sup>2</sup>, without the foundation.

**b) Young's Modulus E=5000kN/m<sup>2</sup>**

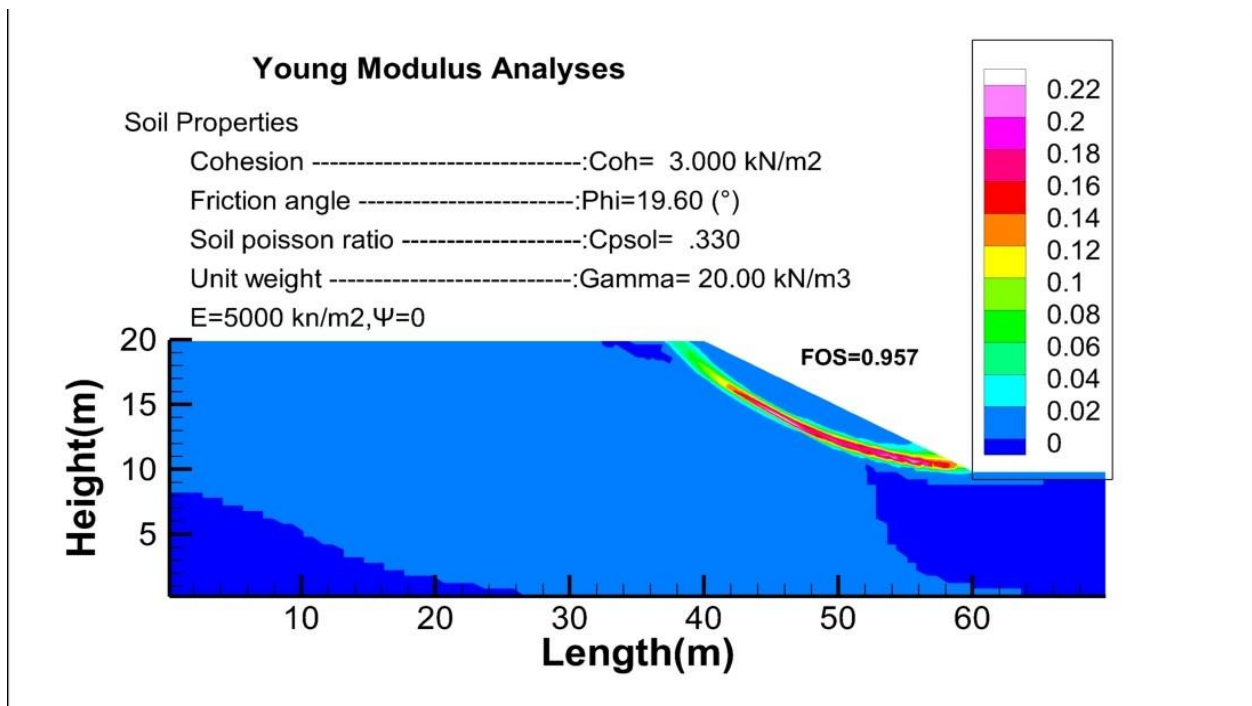


Figure 5.11 76 Strain contours corresponding to the step of failure for E=5000 kN/m<sup>2</sup>, with the foundation.



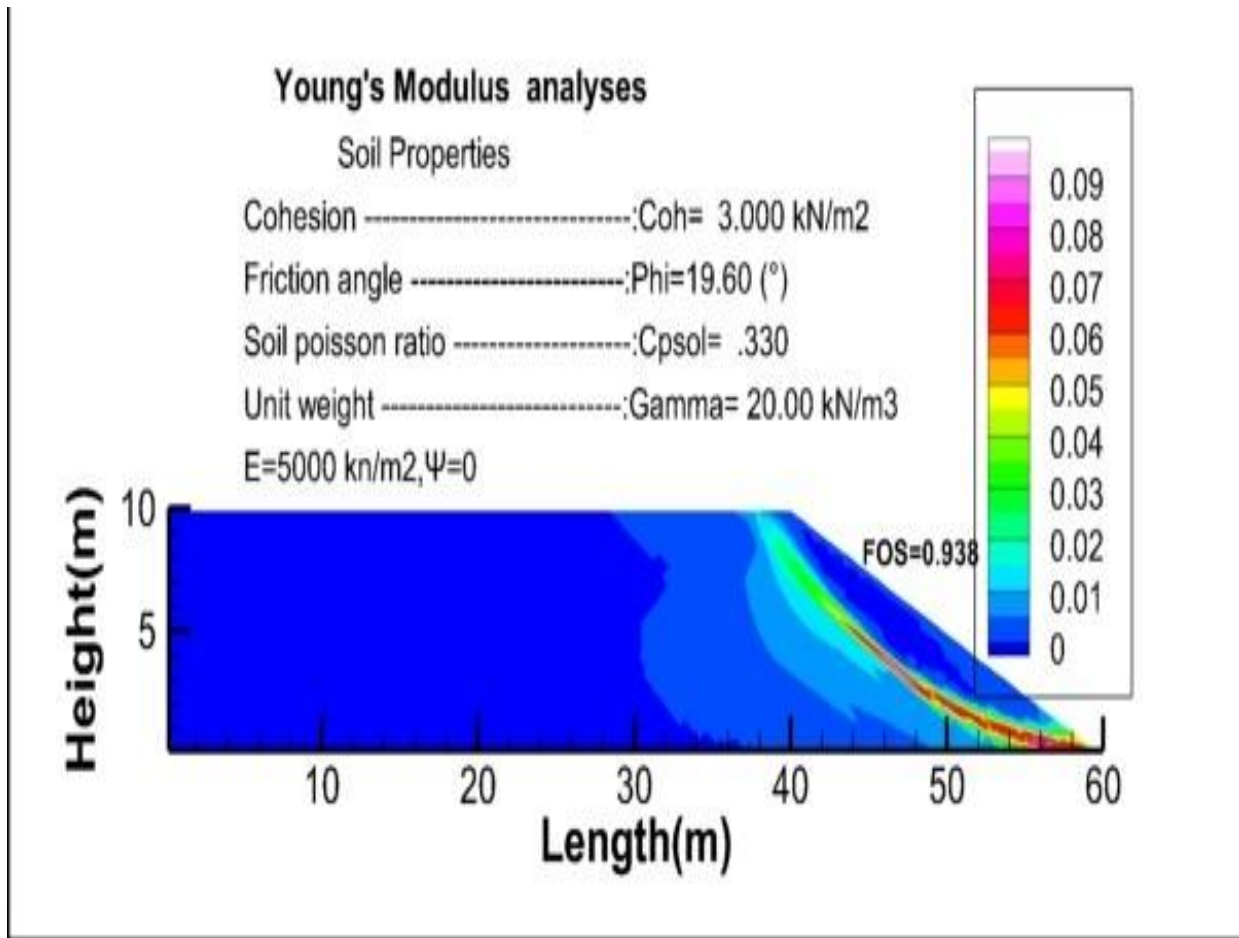


Figure 5.11 77 Strain contours corresponding to the step of failure for E=5000 kN/m<sup>2</sup>, without the foundation.

**c) Young's Modulus E=10000kn/m<sup>2</sup>**

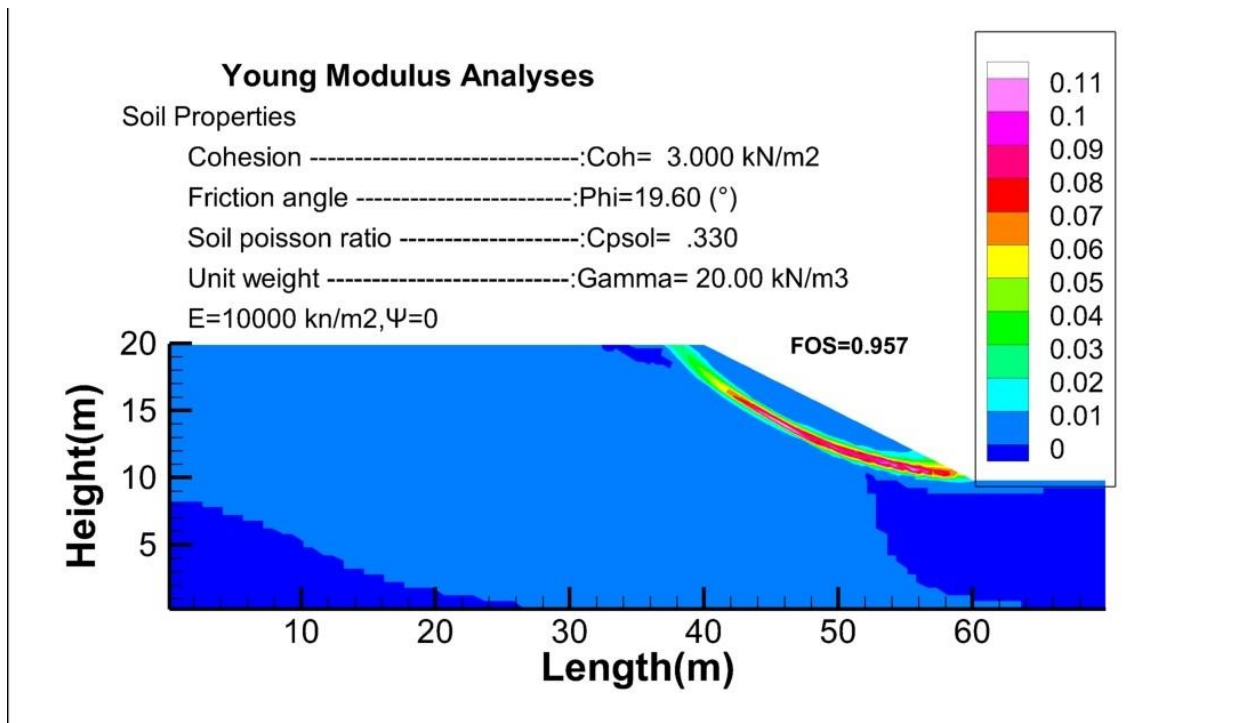


Figure 5.11 78 Strain contours corresponding to the step of failure for E=10000 kN/m<sup>2</sup>, with the foundation.

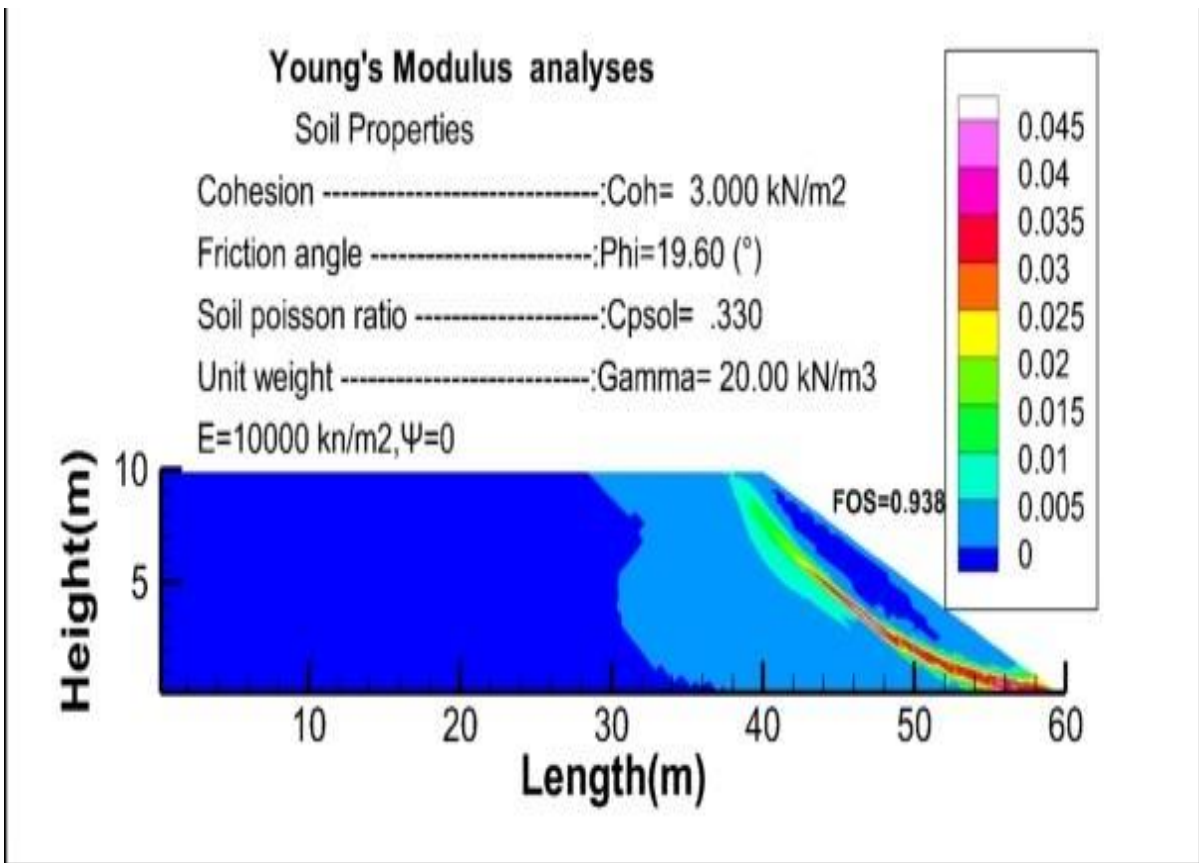


Figure 5.11 79 Strain contours corresponding to the step of failure for E=10000 kN/m<sup>2</sup>, without the foundation.

**d) Young's Modulus E=100000kn/m<sup>2</sup>**

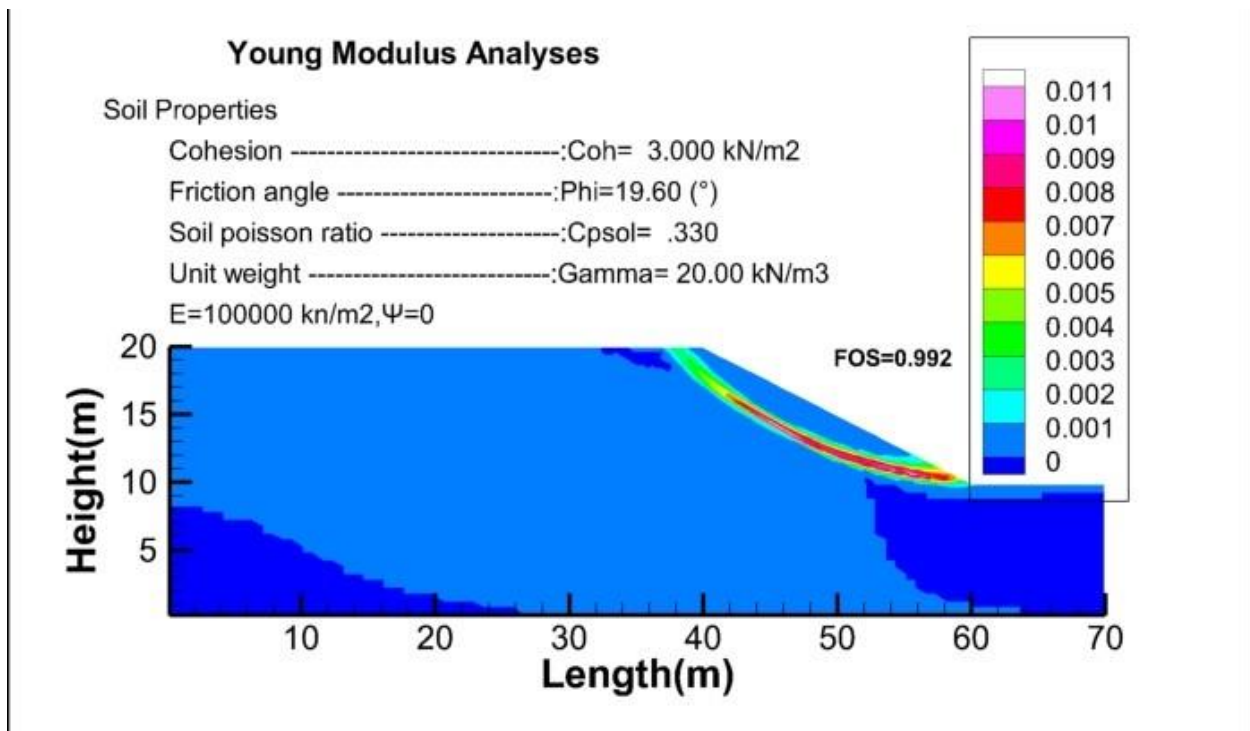


Figure 5.11 80 Strain contours corresponding to the step of failure for E=100000 kN/m<sup>2</sup>, with the foundation.

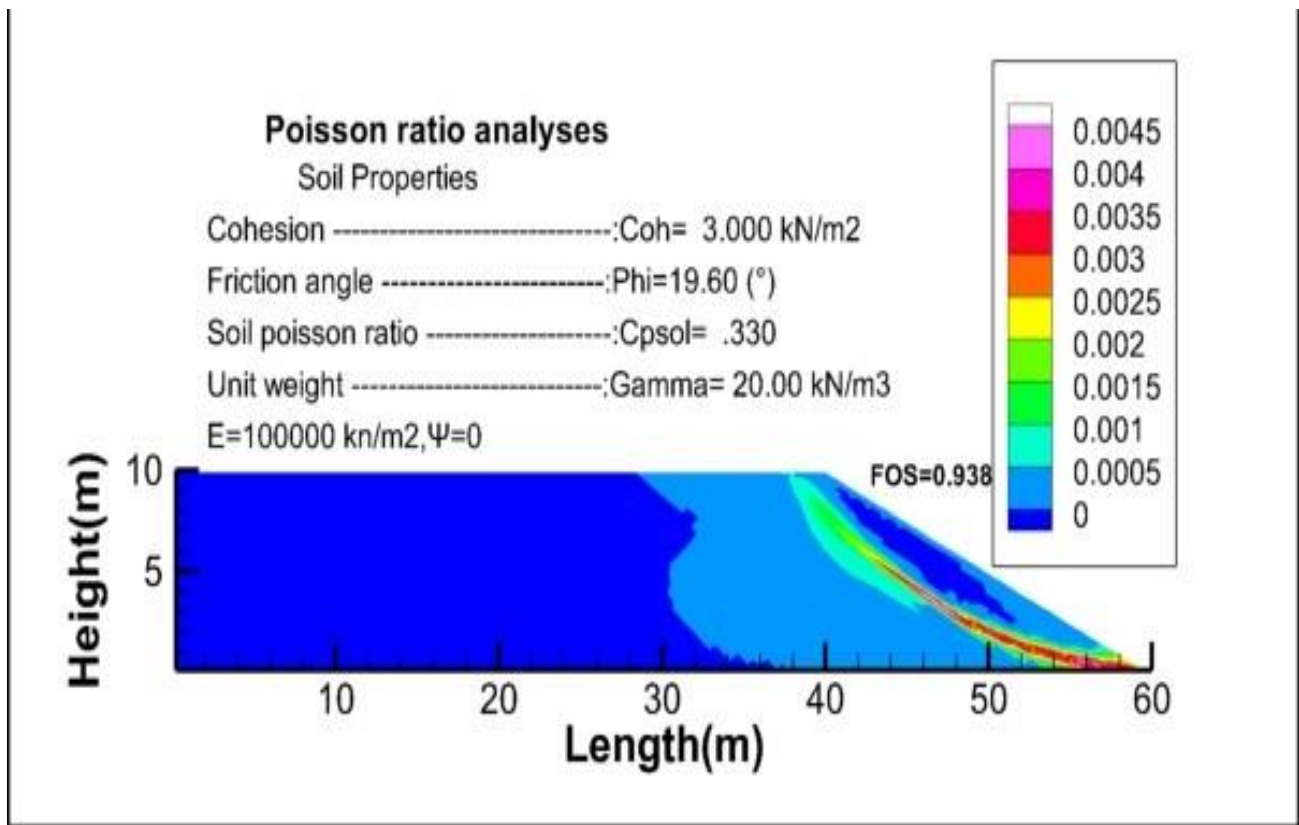


Figure 5.11 81 Strain contours corresponding to the step of failure for  $E=100000 \text{ kN/m}^2$ , without the foundation.

### 5.8.5. Poisson ratio Evaluation

#### 1.2 Analyse of Poisson ratio on slope with Foundation and without foundation

##### 1) Poisson ratio Analyses

#### 5.8.6. Associated flow rule.

Table 5 2 9 Results of Evaluation of the Poisson ratio variation. Associated

Poisson ratio	BS	MP	SDIM
0.1	0.999	0.997	0.994
0.15			0.993
0.20			0.992
0.25			0.992
0.30			0.992
0.35			0.992
0.40			0.991
0.45			0.991
0.49			0.991

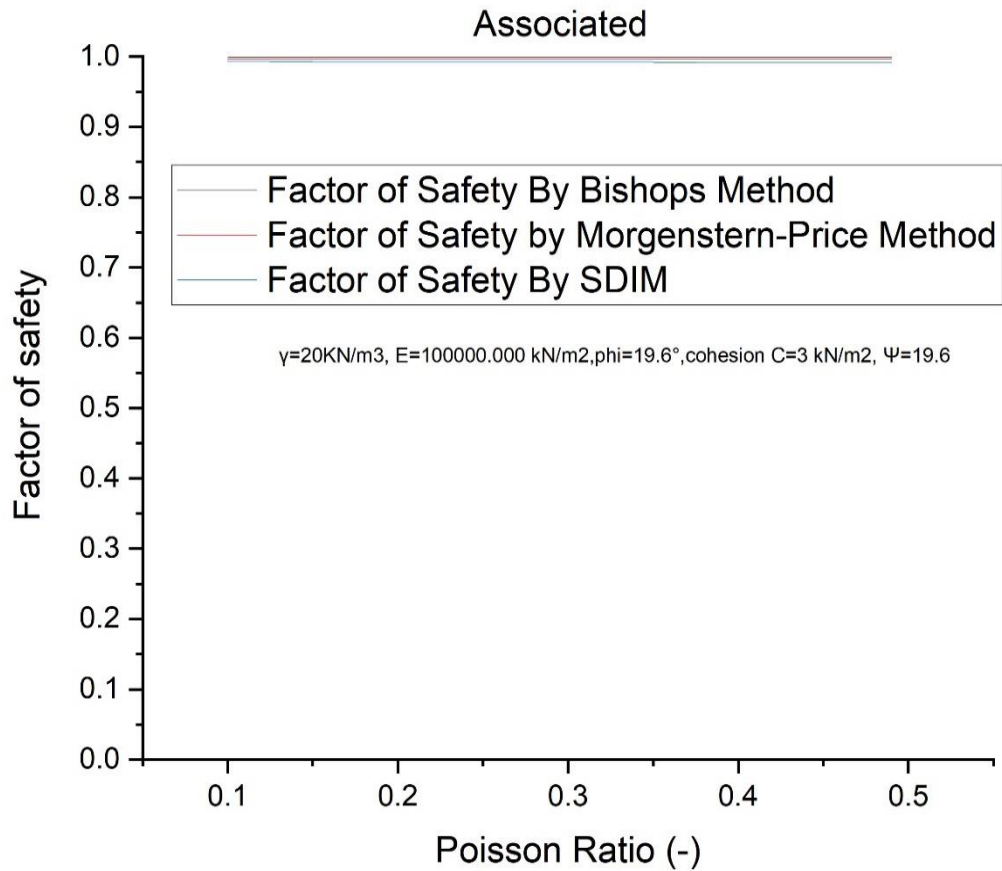


Figure 5.11 82 Evaluation of the Poisson ratio variation. Associated

### 5.8.7. Associated flow rule.

Table 5 2 10 Results of Evaluation of the Poisson ratio variation. Associated

Poisson Ratio	BS	MP	SDIM
0.1	0.989	0.984	0.984
0.15			0.985
0.20			0.985
0.25			0.985
0.30			0.986
0.35			0.987
0.40			0.987
0.45			0.988
0.49			0.992

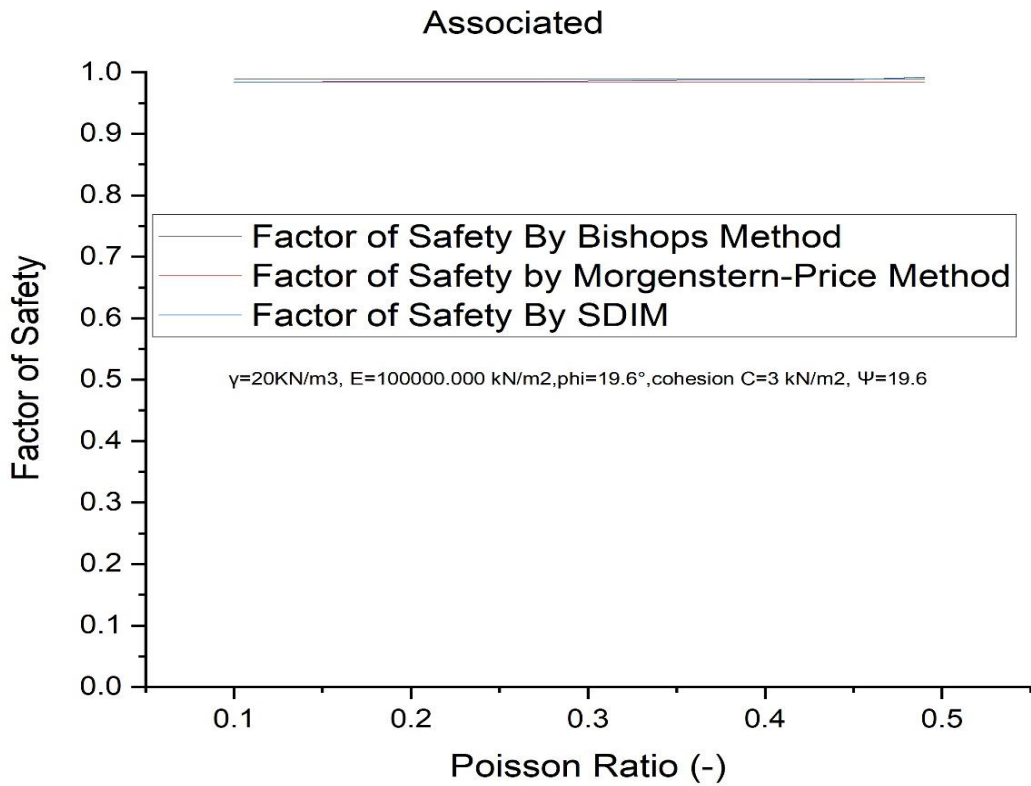


Figure 5.11 83 Evaluation of the Poisson ratio variation. Associated.

Poisson ratio has a small effect on the calculation since the results of the factor of safety from SDIM are very close form LEM. This parameter should be careful treated since it must obey the plasticity condition by regarding the factor of safety is harder to detect this effects it's only visible by regarding the plastic counters.

#### a) Poisson Ratio 0.10

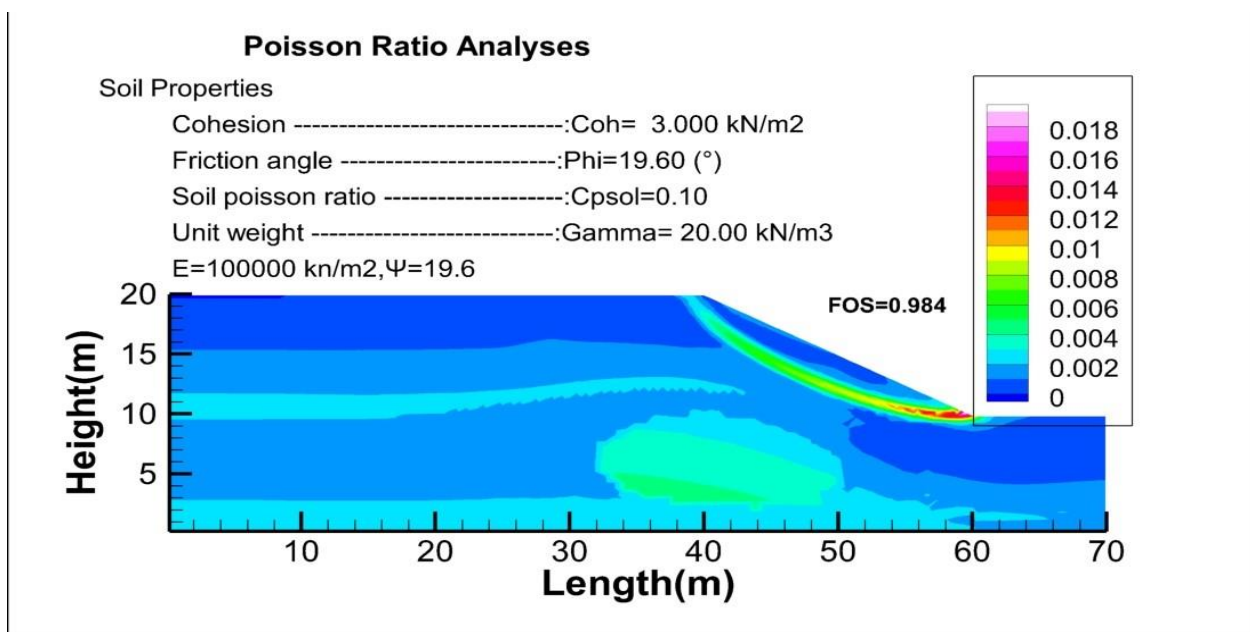


Figure 5.11 84 Strain contours corresponding to the step of failure for  $v=0.10$ , with the foundation.

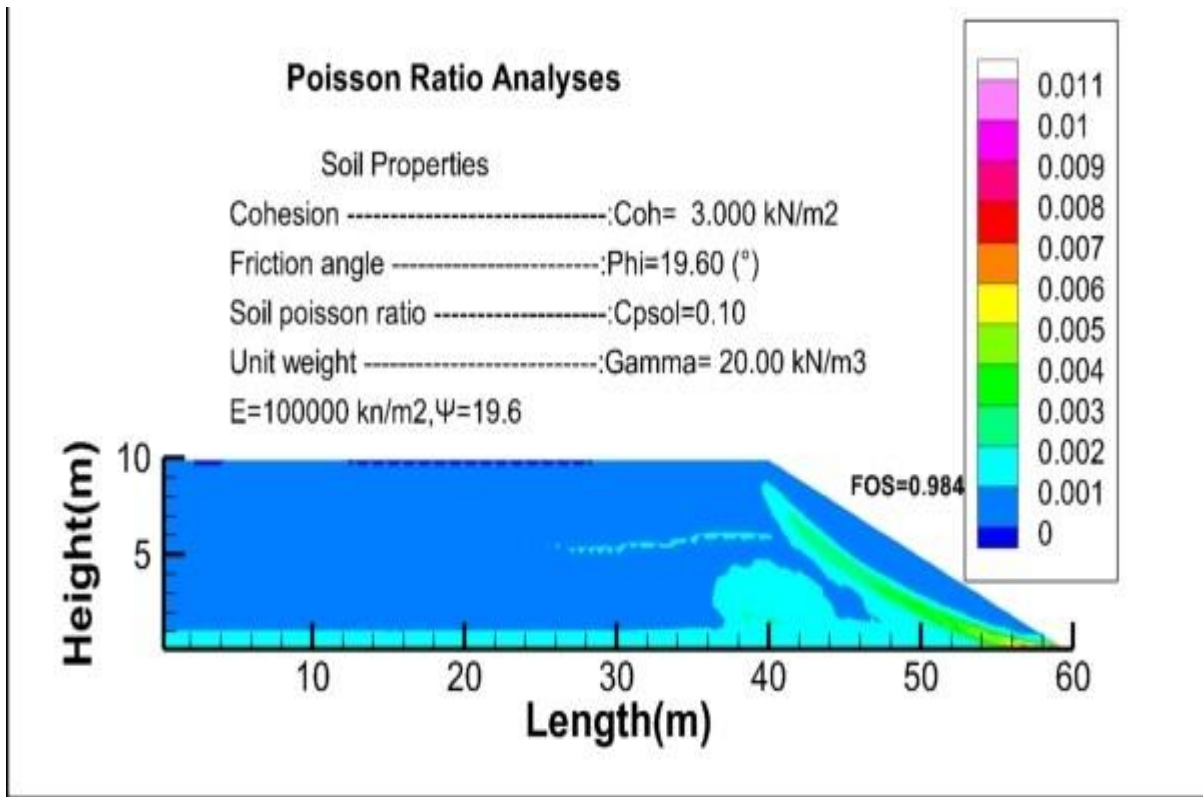


Figure 5.11 85 Strain contours corresponding to the step of failure for  $\nu=0.10$ , without the foundation

### b) Poisson Ratio 0.15

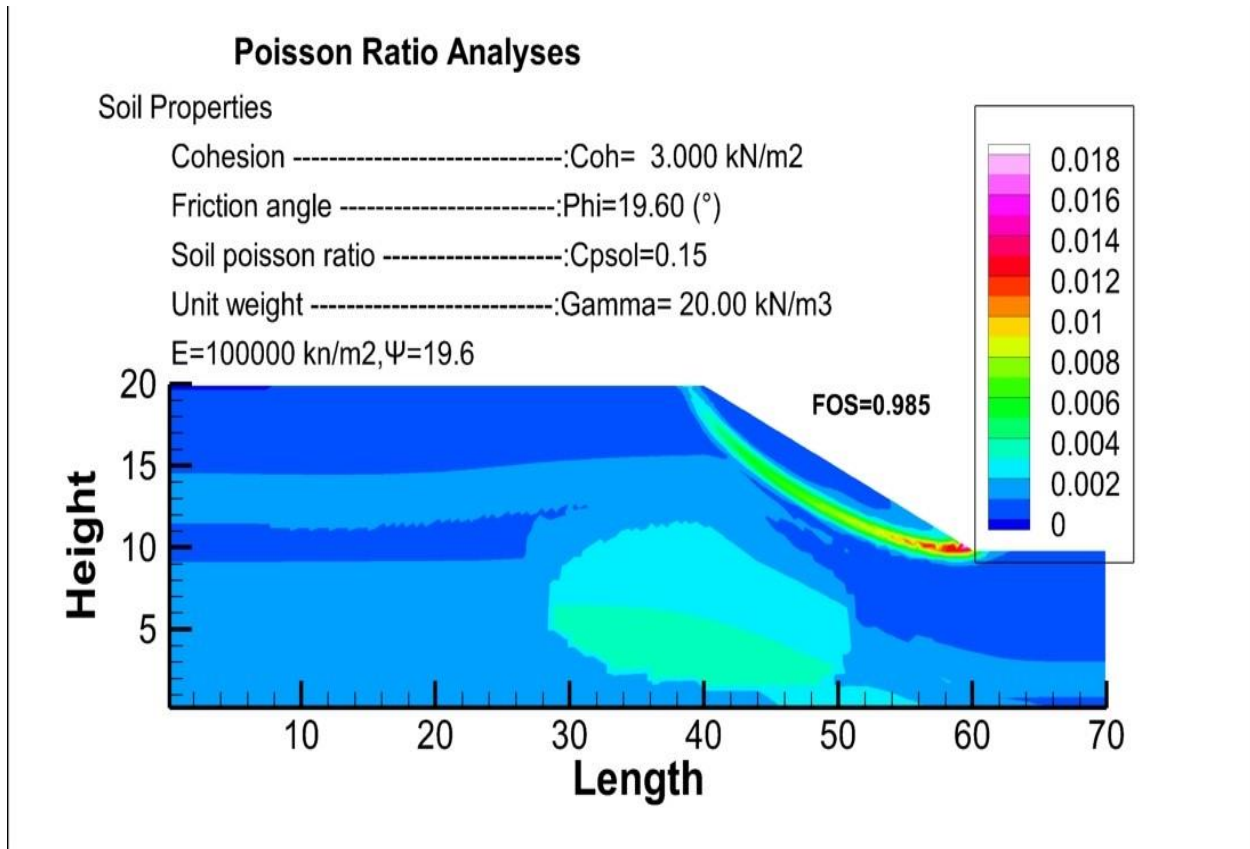


Figure 5.11 86 Strain contours corresponding to the step of failure for  $\nu=0.15$ , with the foundation.

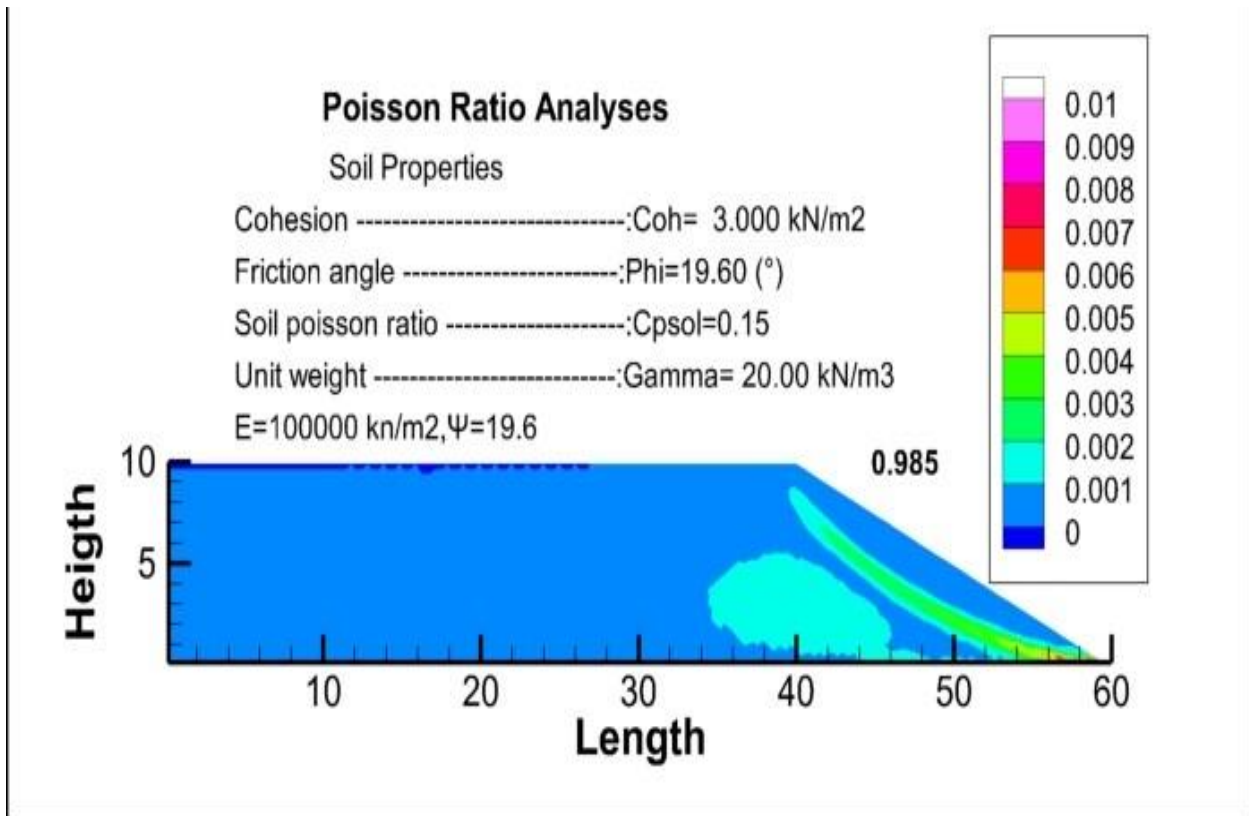


Figure 5.11 87 Strain contours corresponding to the step of failure for  $v=0.10$ , without the foundation.

**c) Poisson Ratio 0.20**

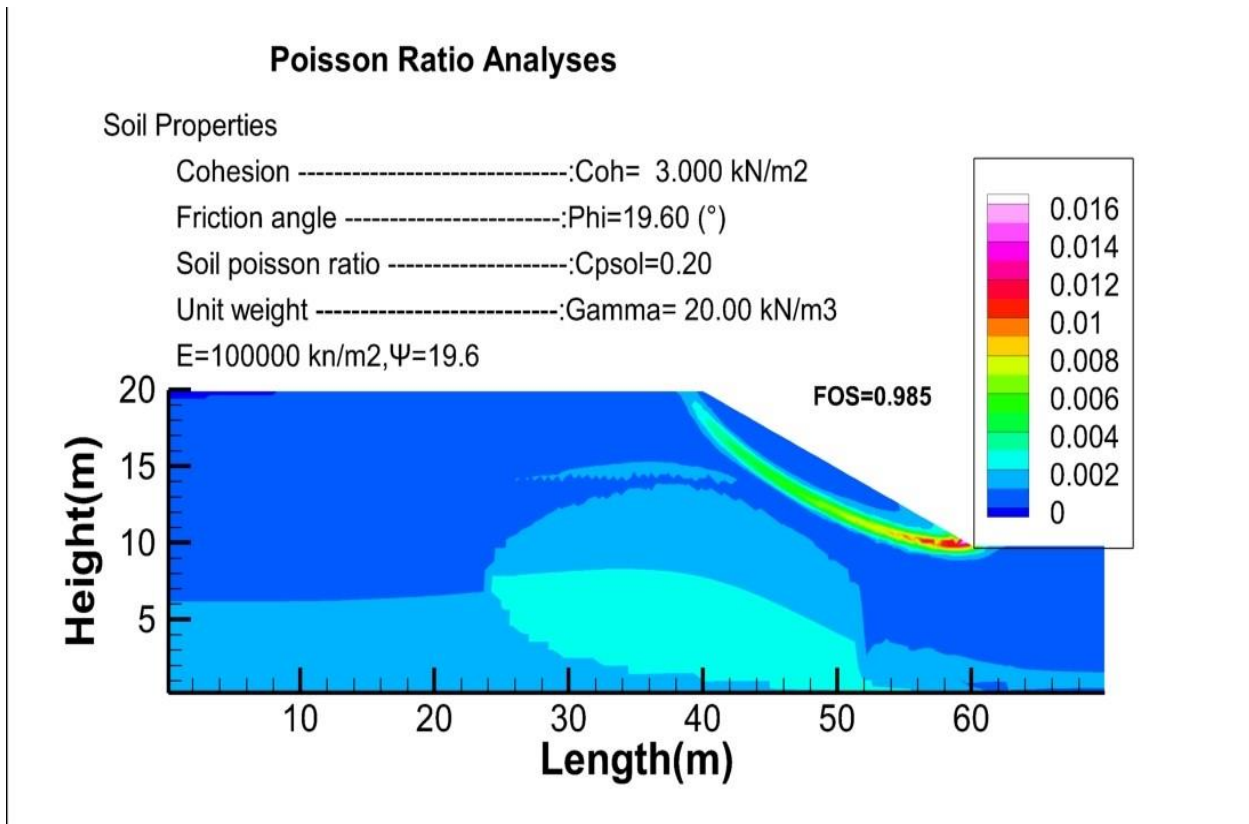


Figure 5.11 88 Strain contours corresponding to the step of failure for  $v=0.20$ , with the foundation

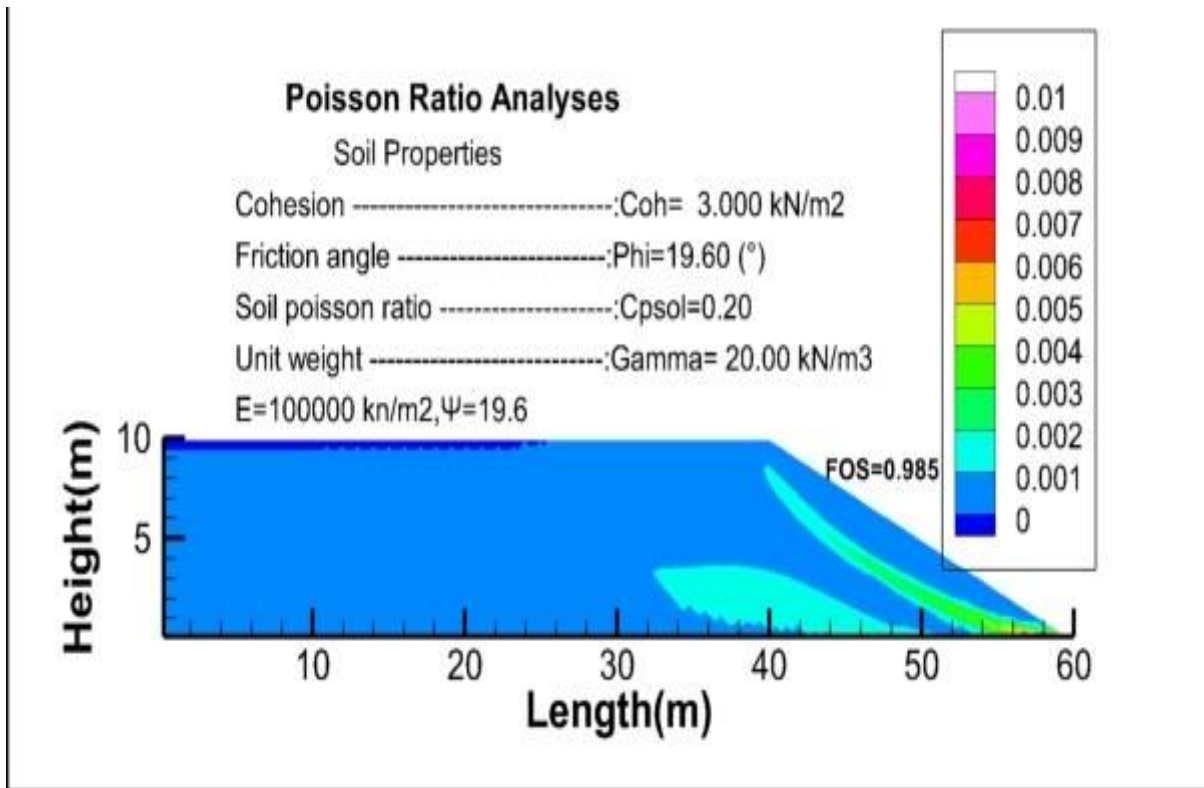


Figure 5.11 89 Strain contours corresponding to the step of failure for  $\nu=0.20$ , without the foundation.

**d) Poisson Ratio 0.25**

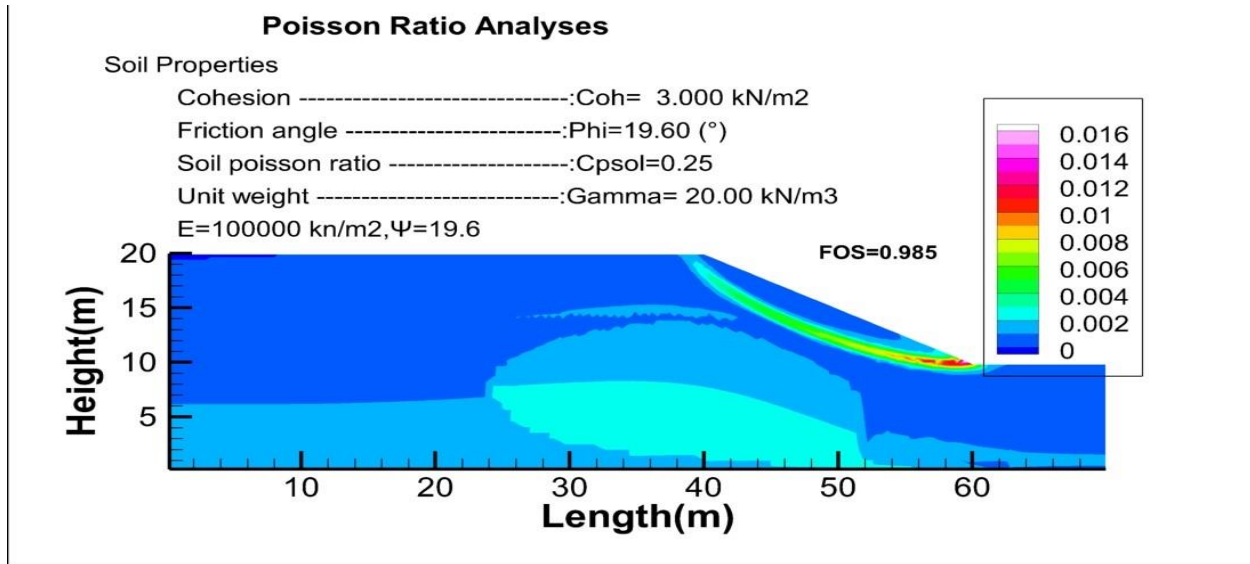


Figure 5.11 90 Strain contours corresponding to the step of failure for  $\nu=0.25$ , with the foundation.

So from the 0.10 Poisson Ratio we can see that the yield counters are abnormal or we can say the appearance of parasite zones or the spurious zones due to the non-respected conditions, in such case the poisson ratio is expected to be greater than 0.32 in other to attain good results so further increasing is needed to reaches valid factor of safety.



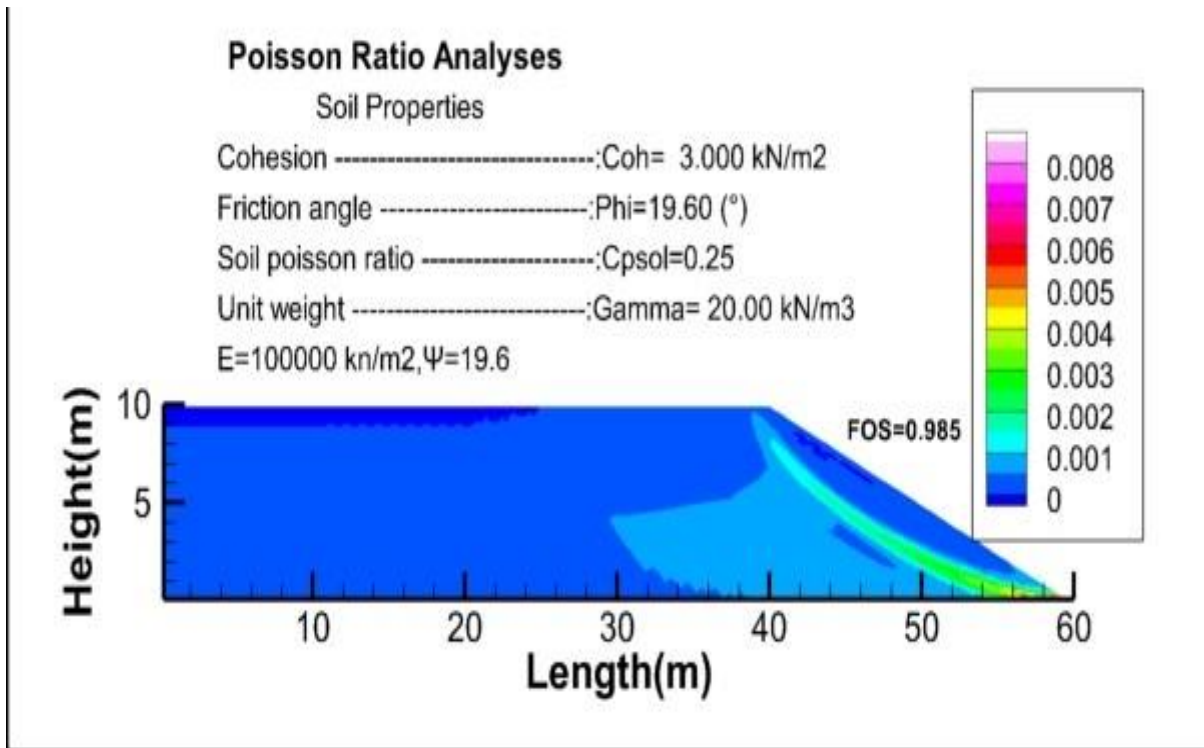


Figure 5.11 91 Strain contours corresponding to the step of failure for  $v=0.25$ , without the foundation

**e) Poisson Ratio 0.30**

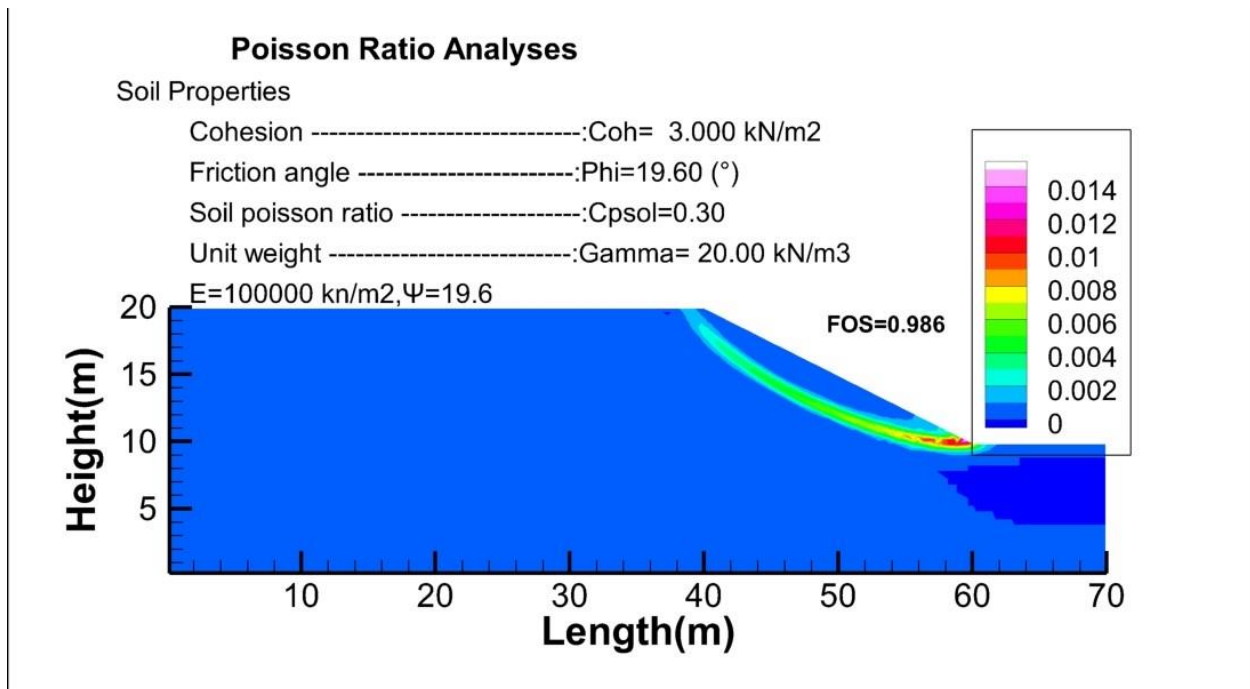


Figure 5.11 92 Strain contours corresponding to the step of failure for  $v=0.30$ , without the foundation

in this stages of increasing the Poison ratio we clear see the disappearance of the parasite zones and appearance of plastic zones because the condition is met and this factor of safety are valid to use since they both closer form each other even with further increasing not a big change is encountered.

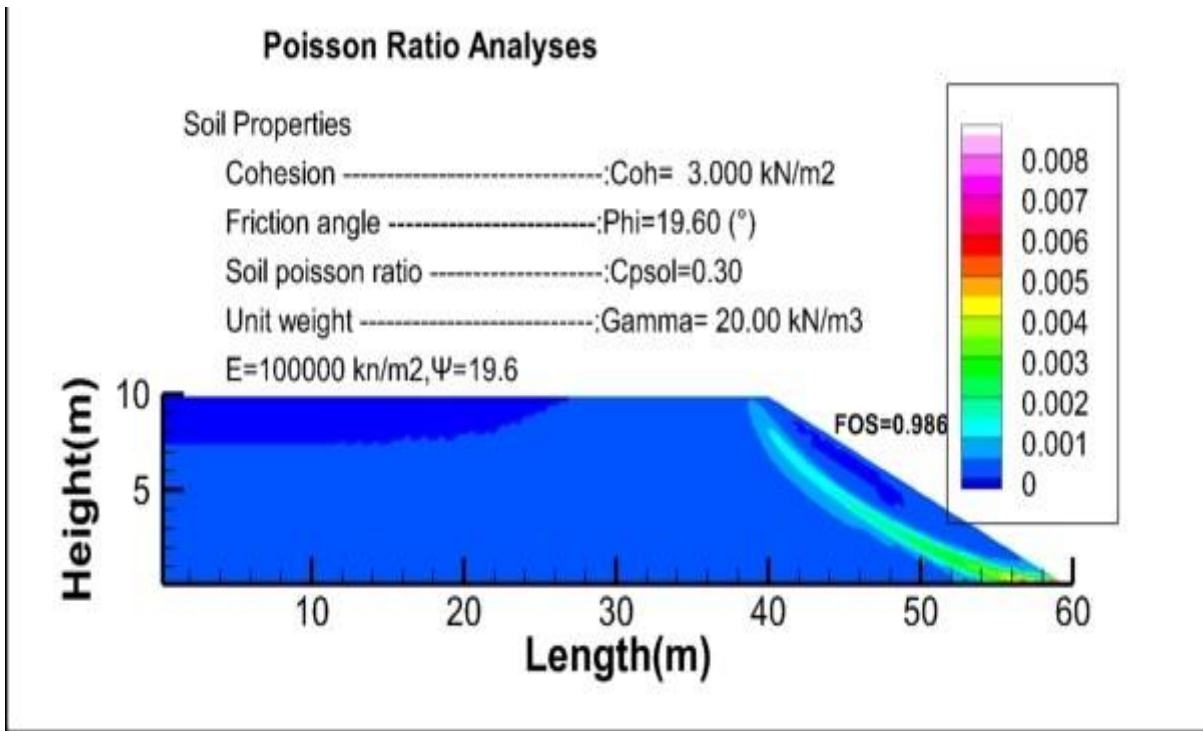


Figure 5.11 93 Strain contours corresponding to the step of failure for  $\nu=0.30$ , without the foundation.

**f) Poisson Ratio 0.35**

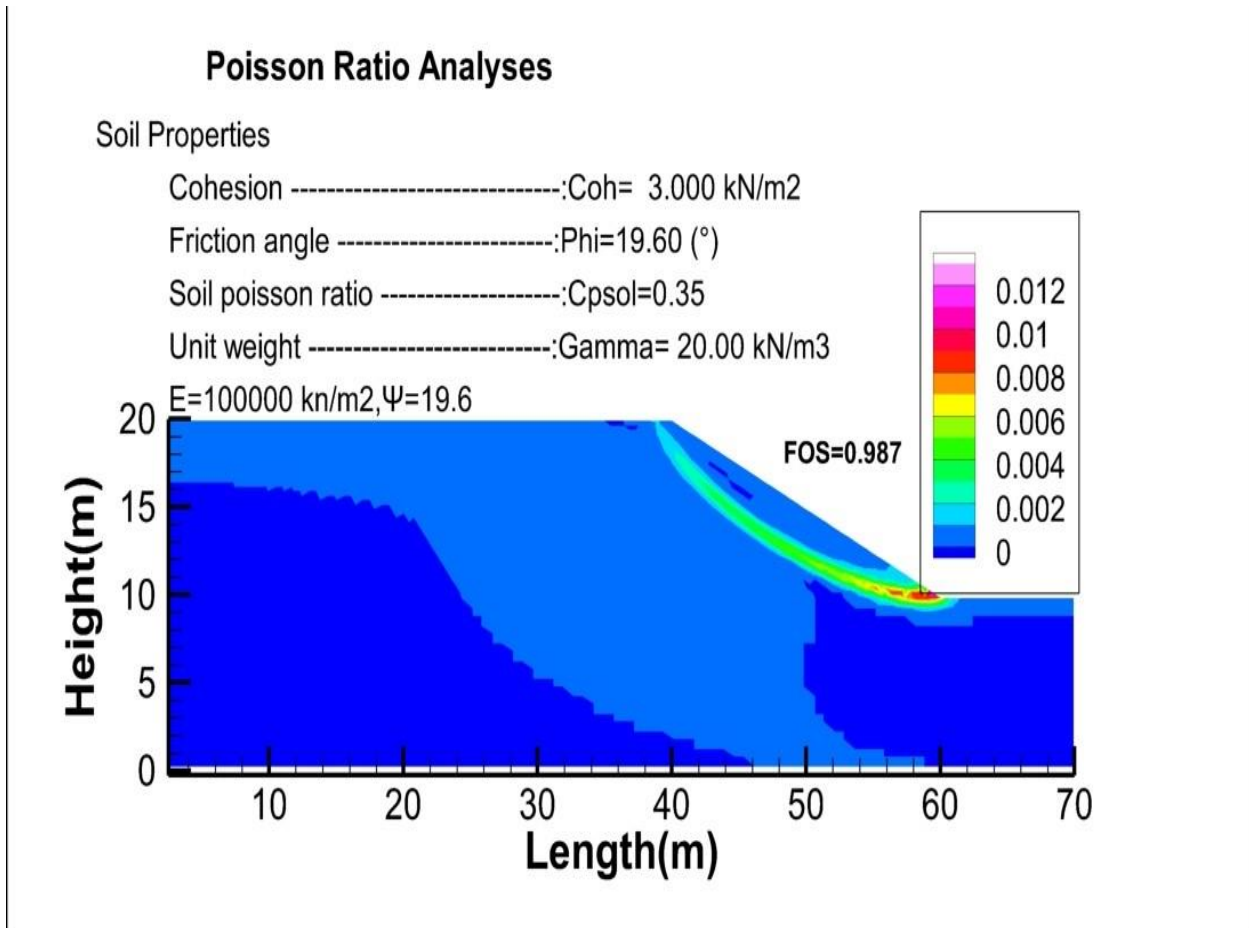


Figure 5.11 94 Strain contours corresponding to the step of failure for  $\nu=0.35$ , with the foundation.

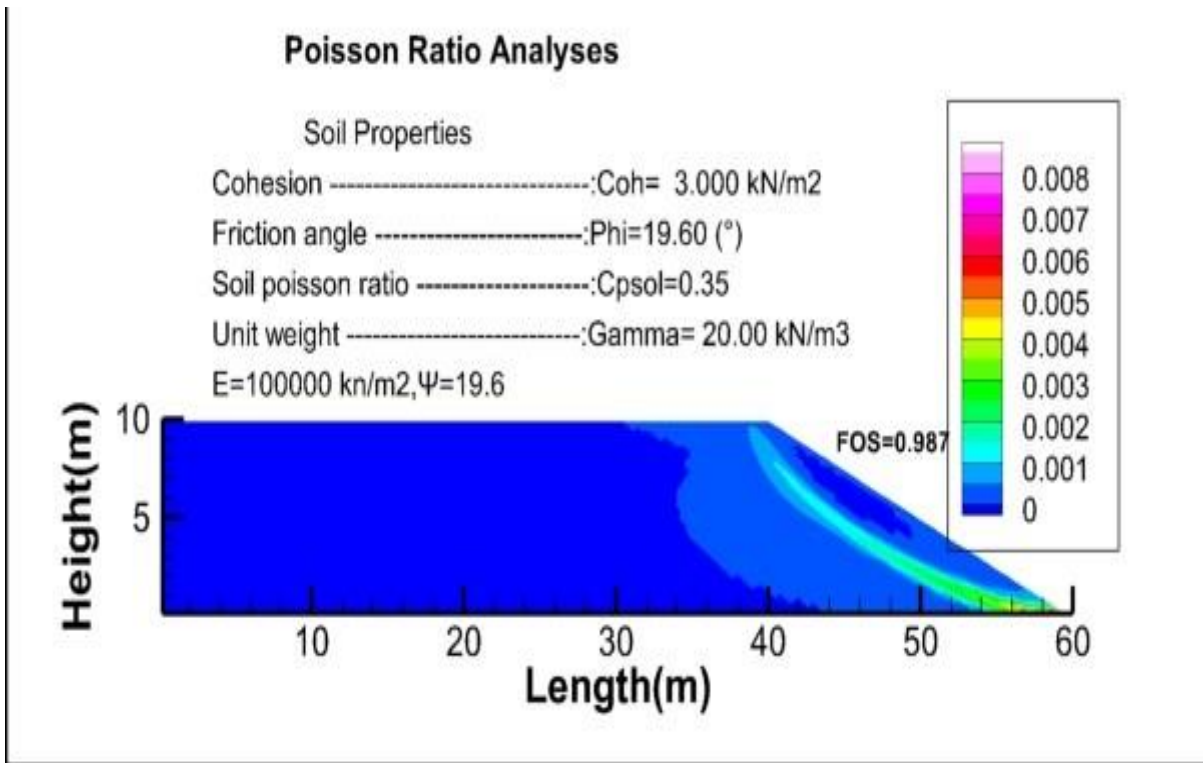


Figure 5.11 95 Strain contours corresponding to the step of failure for  $\nu=0.35$ , without the foundation.

**g) Poisson Ratio 0.40**

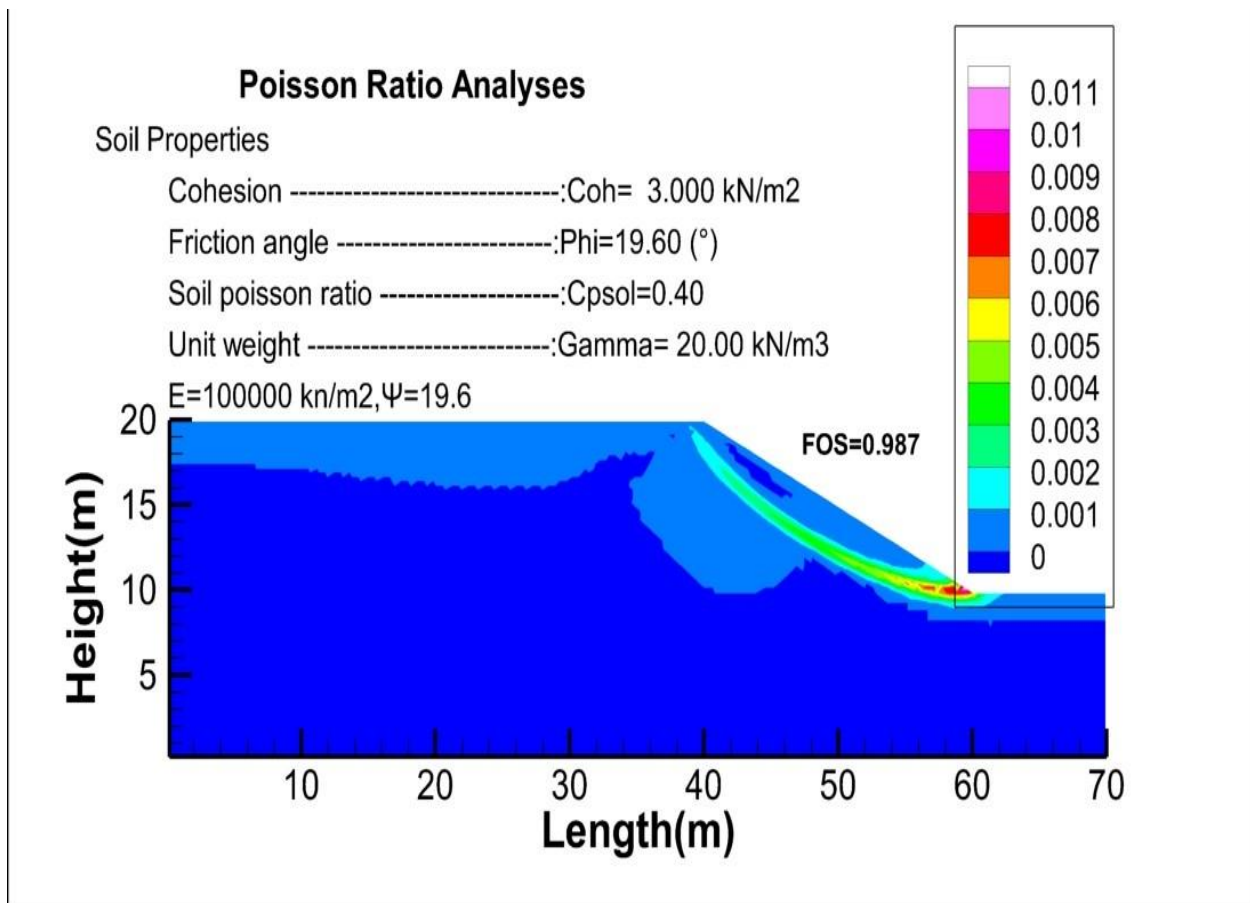


Figure 5.11 96 Strain contours corresponding to the step of failure for  $\nu=0.40$ , with the foundation.

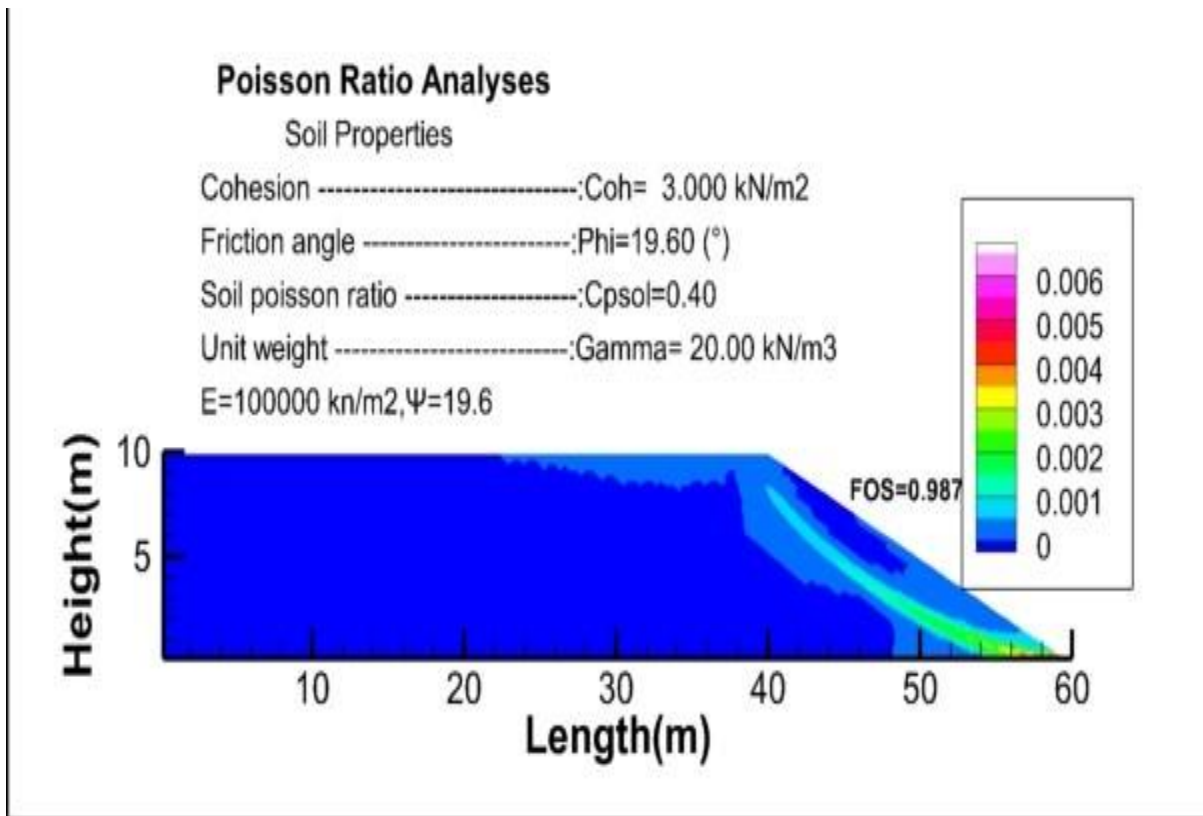


Figure 5.11 97 Strain contours corresponding to the step of failure for  $\nu=0.40$ , without the foundation.

**h) Poisson Ratio 0.45**

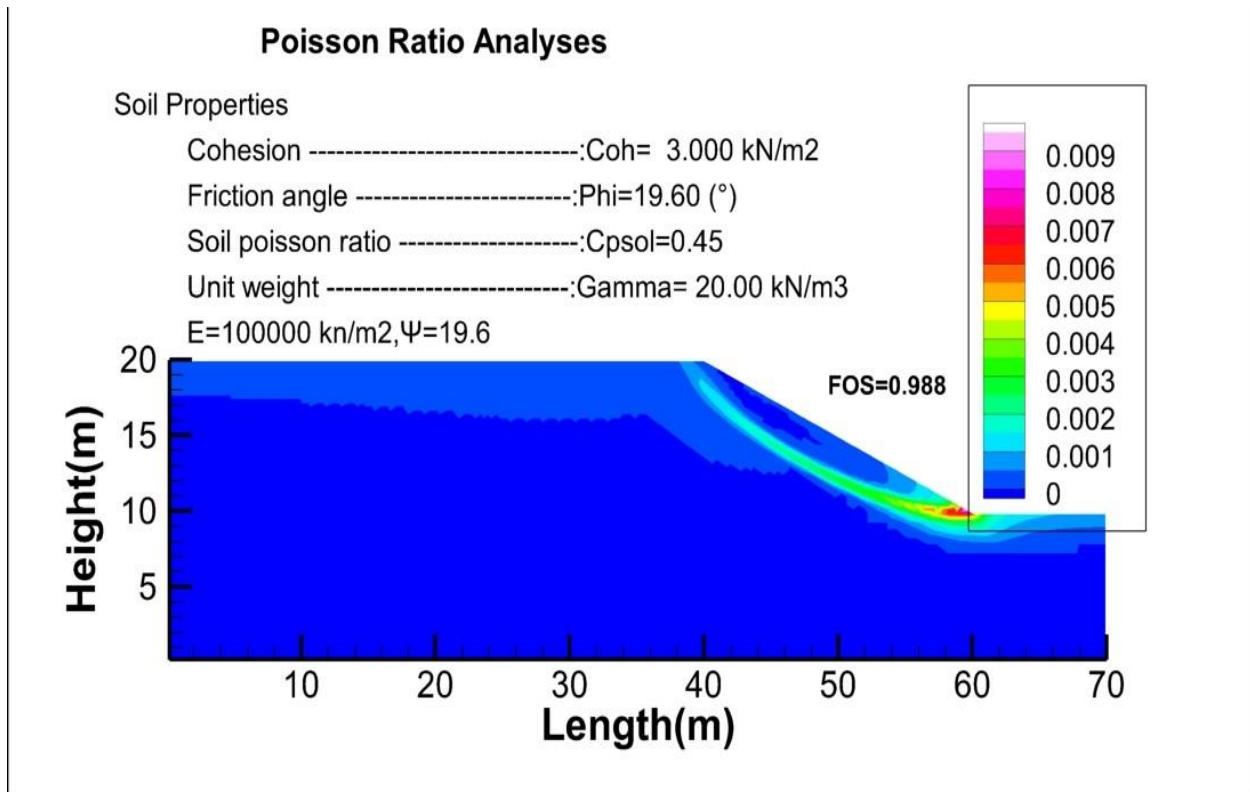


Figure 5.11 98 Strain contours corresponding to the step of failure for  $\nu=0.45$ , without the foundation

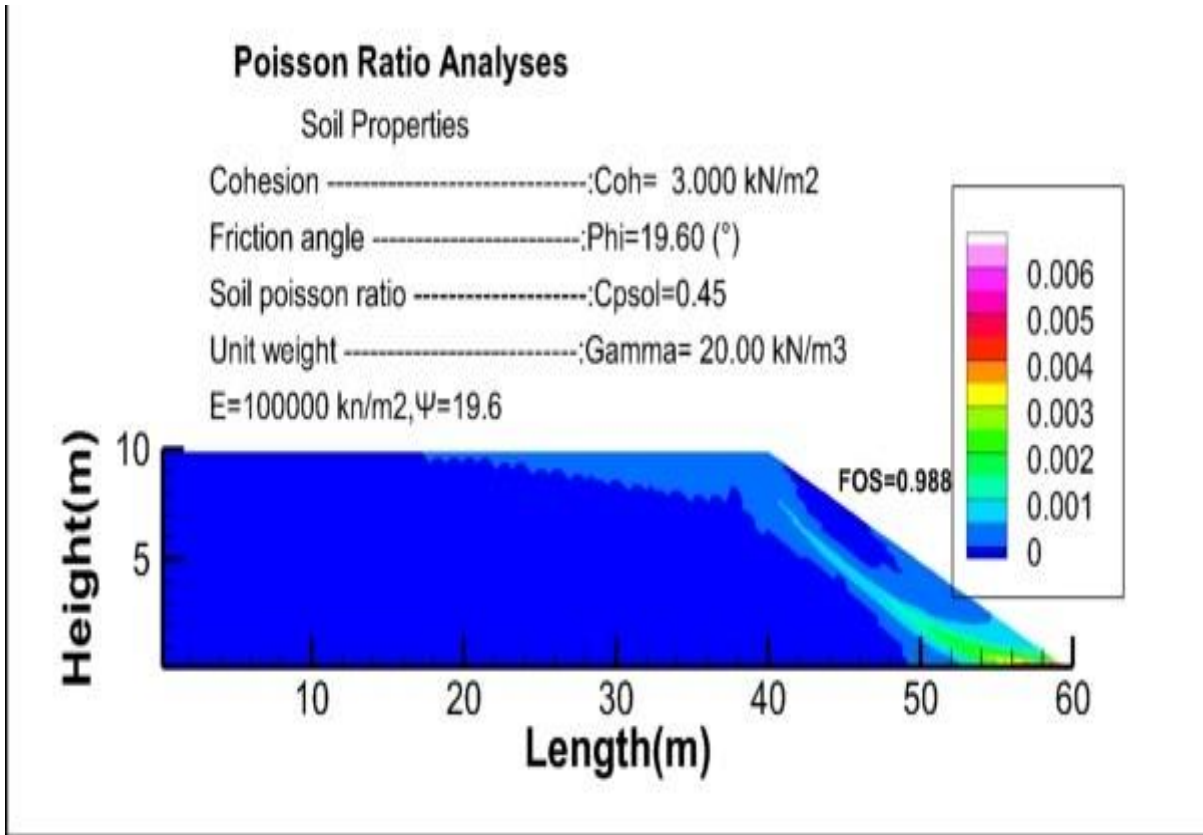


Figure 5.11 99 Strain contours corresponding to the step of failure for  $\nu=0.45$ , with the foundation

**i) Poisson Ratio 0.49**

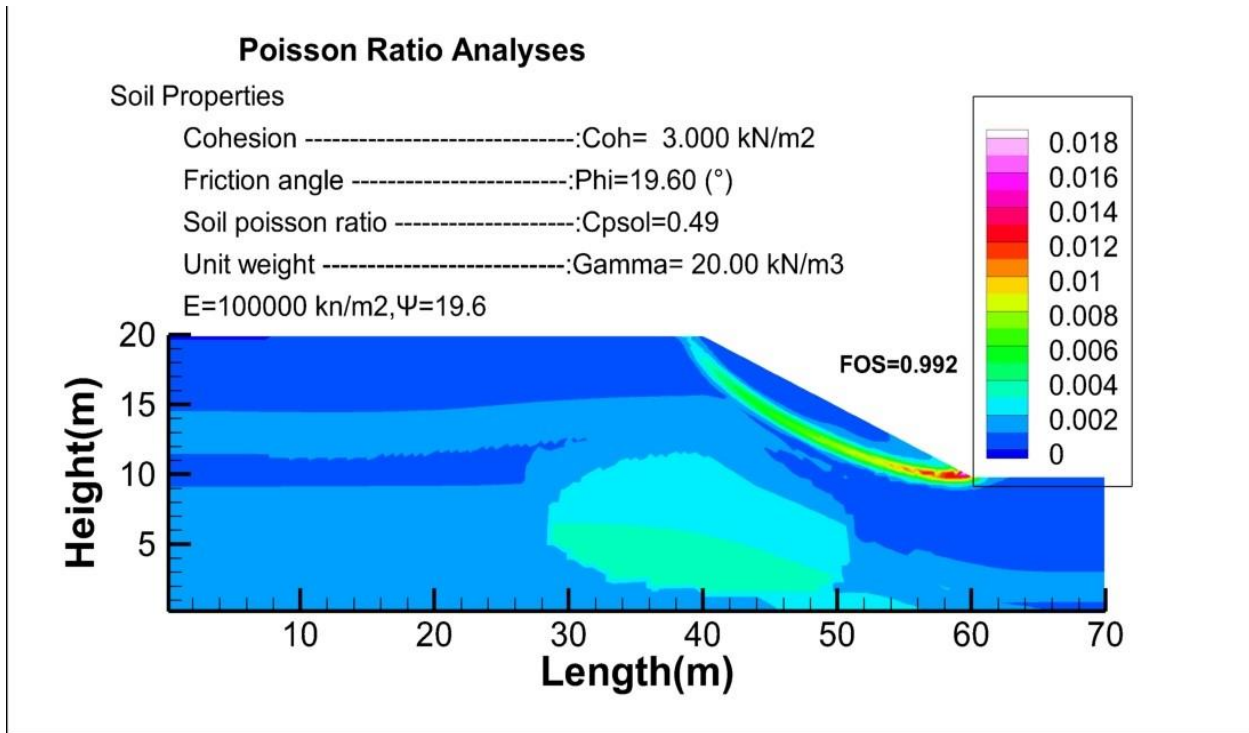


Figure 5.11 100 Strain contours corresponding to the step of failure for  $\nu=0.49$ , with the foundation

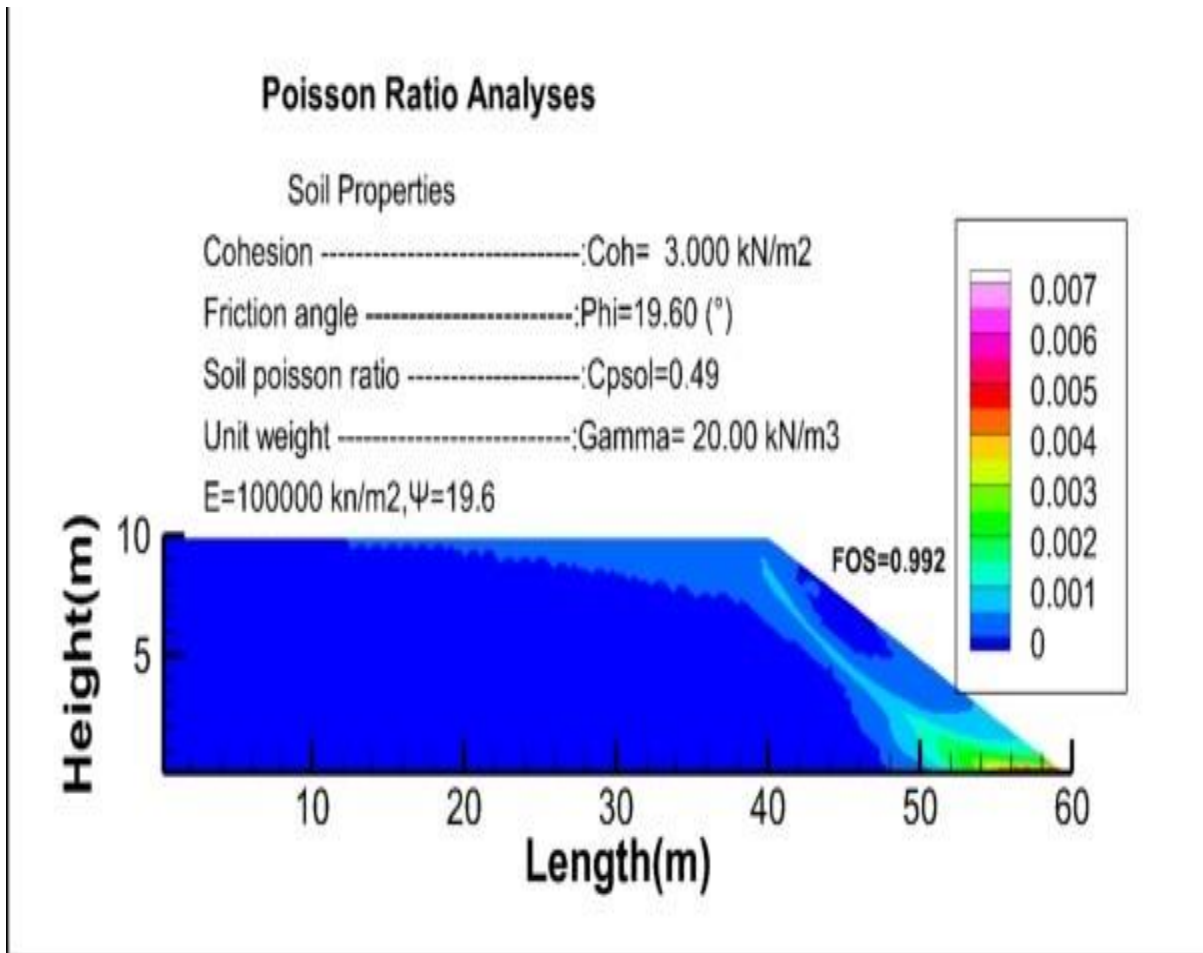


Figure 5.11 101 Strain contours corresponding to the step of failure for  $\nu=0.49$ , without the foundation

### 5.8.8. Non associated flow rule

Same behaviour described above is to be expected when the assumption is  $\psi=0$ .

Table 5 2 11 Results of Evaluation of the Poisson ratio variation. Non-Associated

Poisson ratio	BS	MP	SDIM
0.1	0.999	0.997	0.961
0.15			0.962
0.20			0.962
0.25			0.964
0.30			0.956
0.35			0.957
0.40			0.957
0.45			0.954
0.49			0.950

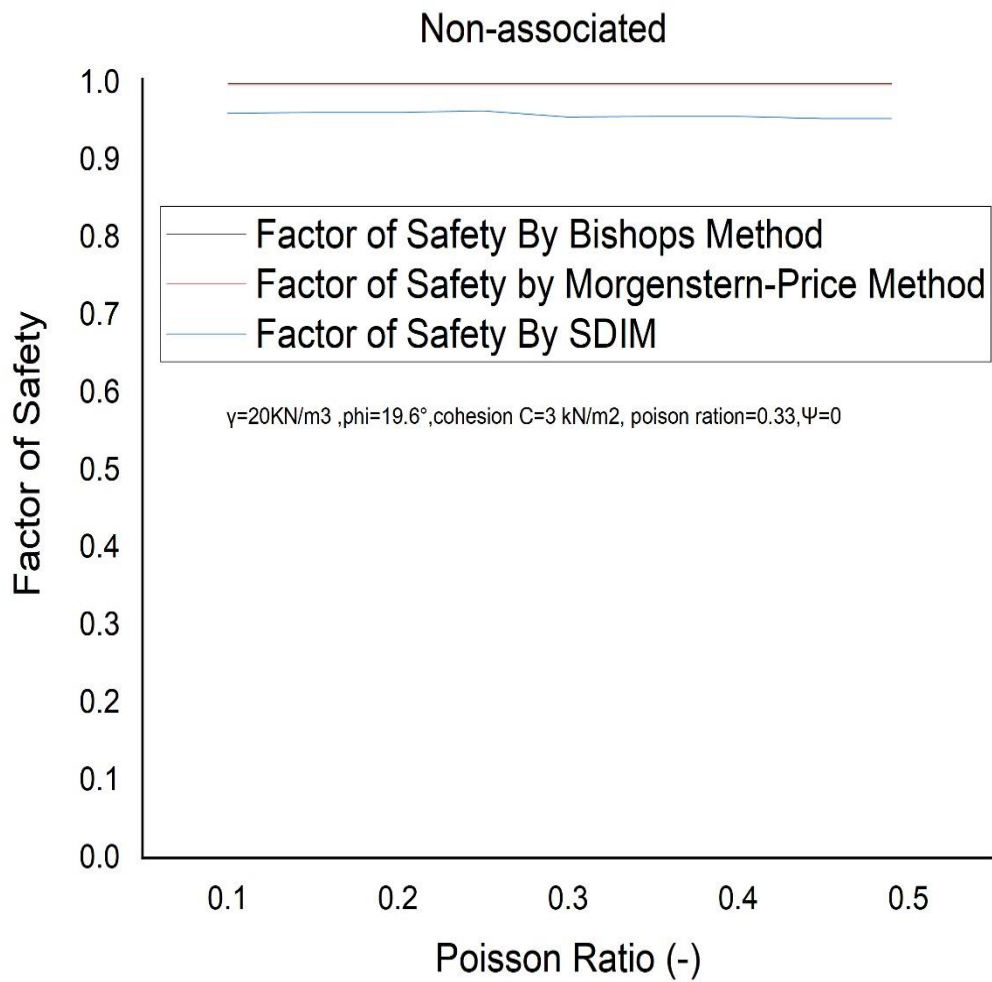


Figure 5.11 102 Evaluation of the Poisson ratio variation. Non-Associated

### Non-Associated flow rule

Table 5 2 12 Results of Evaluation of the Poisson ratio variation. Non-Associated

Poisson Ratio	BS	MP	SDIM
0.1	0.989	0.984	0.929
0.15			0.929
0.20			0.935
0.25			0.935
0.30			0.937
0.35			0.940
0.40			0.940
0.45			0.968
0.49			0.979

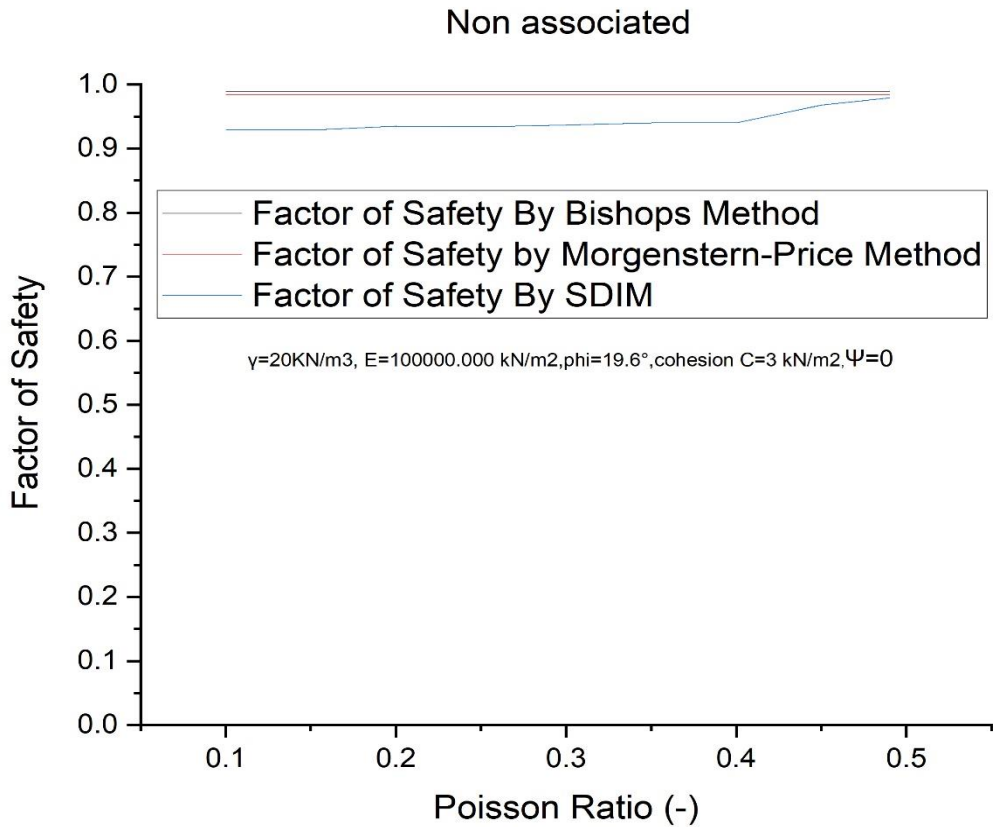


Figure 5.11 103 Evaluation of the Poisson ratio variation. Non-Associated

**a) Poisson Ratio 0.10**

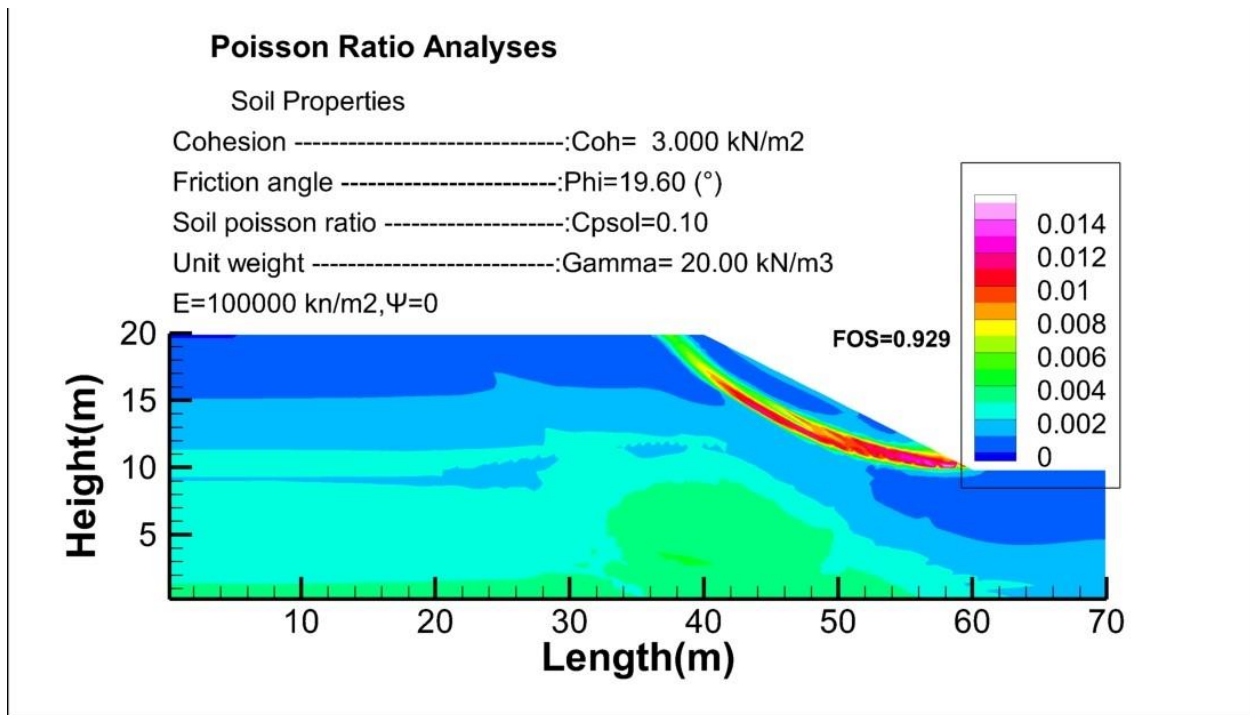


Figure 5.11 104 Strain contours corresponding to the step of failure for  $v=0.10$  , with the foundation



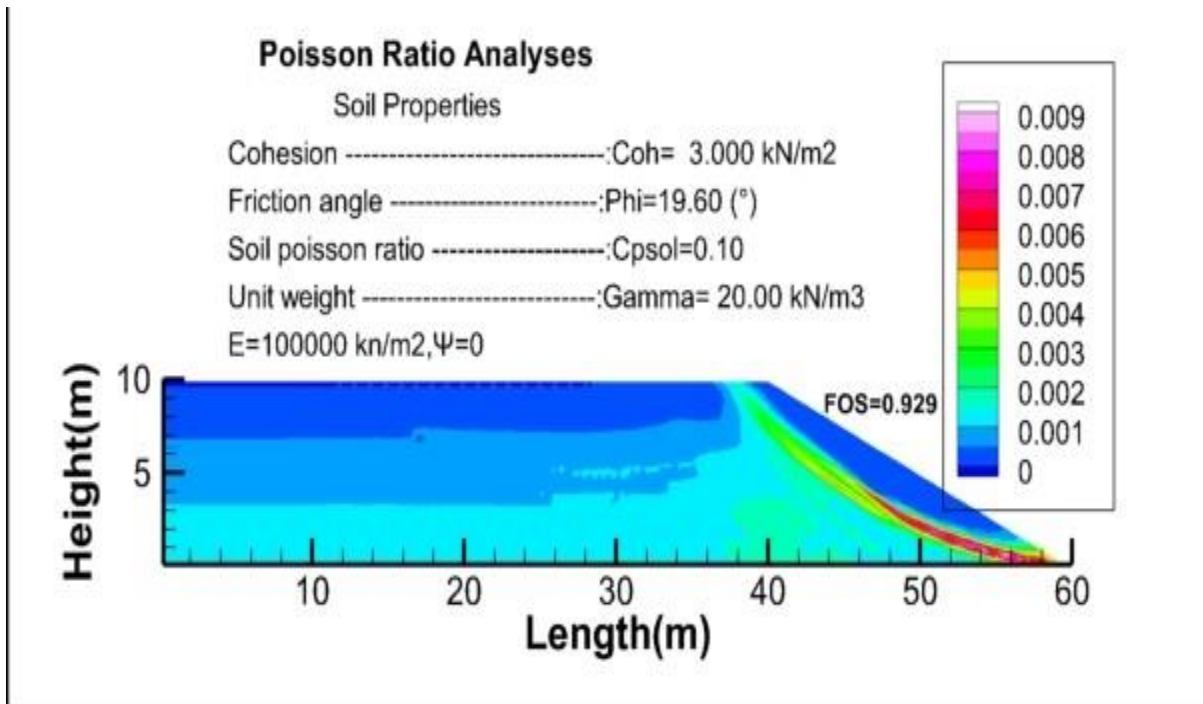


Figure 5.11 105 Strain contours corresponding to the step of failure for  $\nu=0.10$ , without the foundation.

**b) Poisson Ratio 0.15**

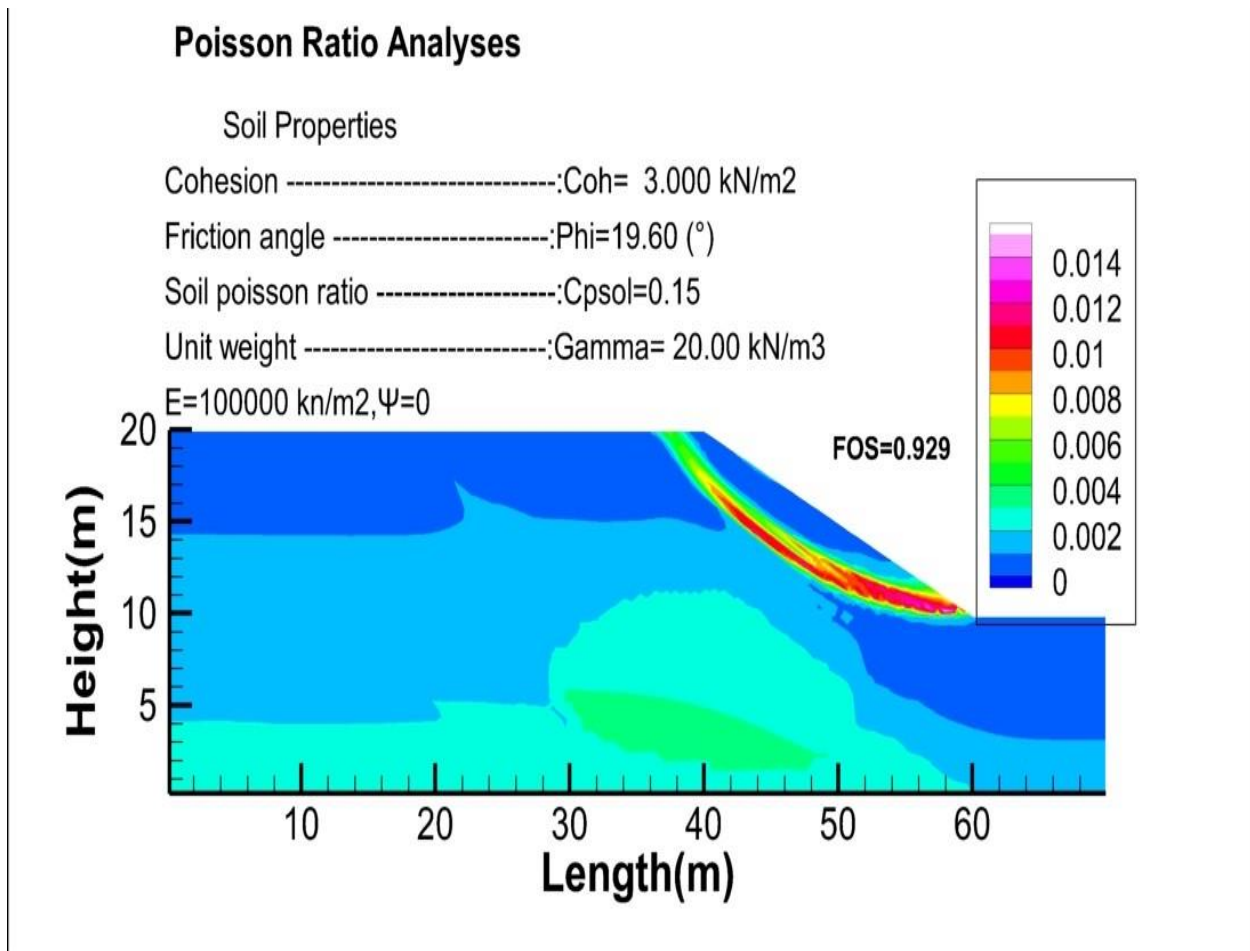


Figure 5.11 106 Strain contours corresponding to the step of failure for  $\nu=0.15$ , with the foundation

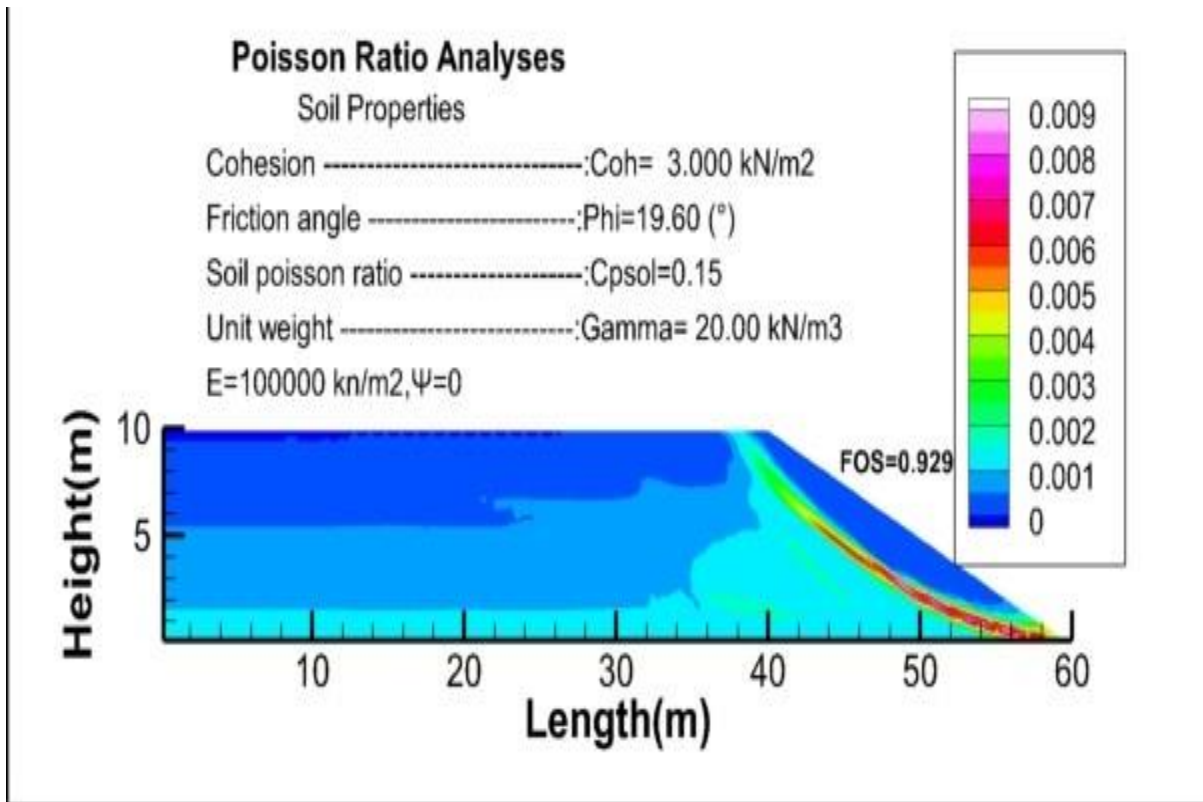


Figure 5.11 107 Strain contours corresponding to the step of failure for  $\nu=0.15$ , without the foundation.

### c) Poisson ratio 0.20

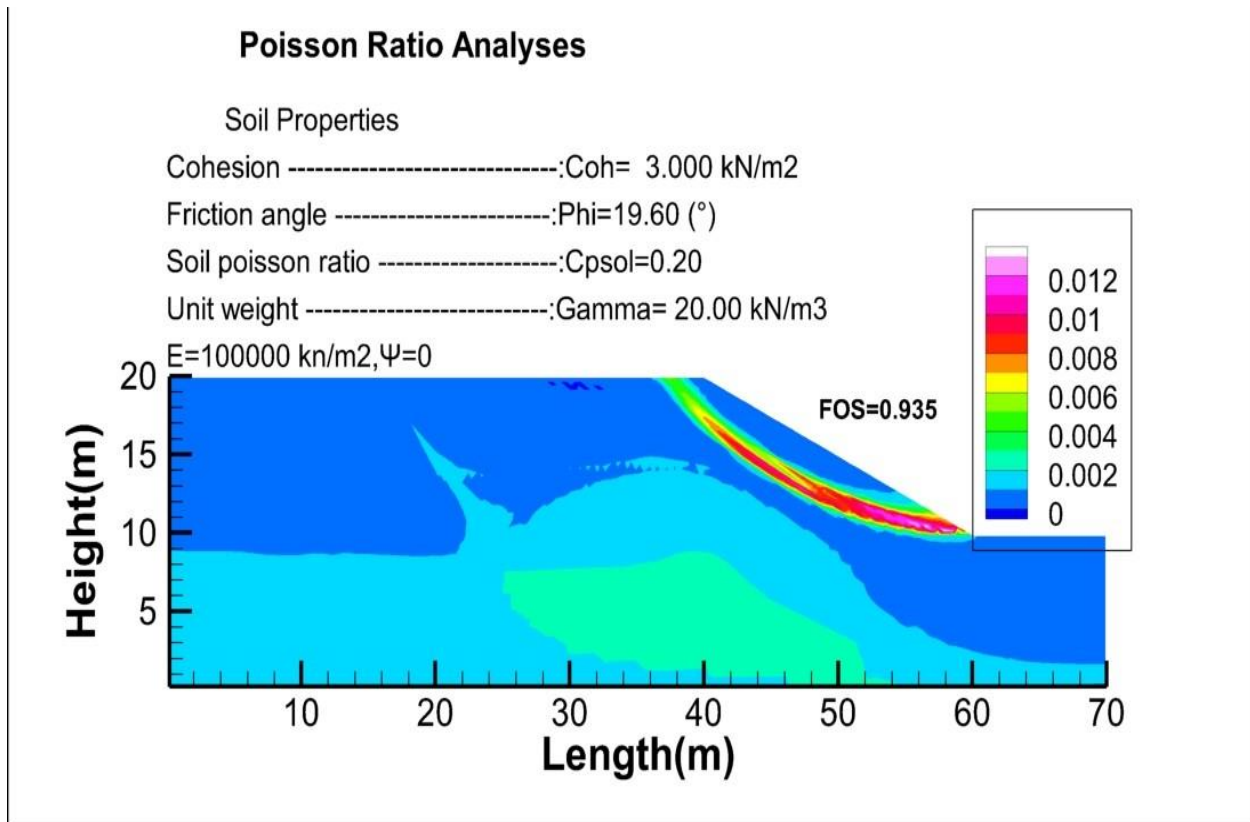


Figure 5.11 108 Strain contours corresponding to the step of failure for  $\nu=0.20$ , with the foundation

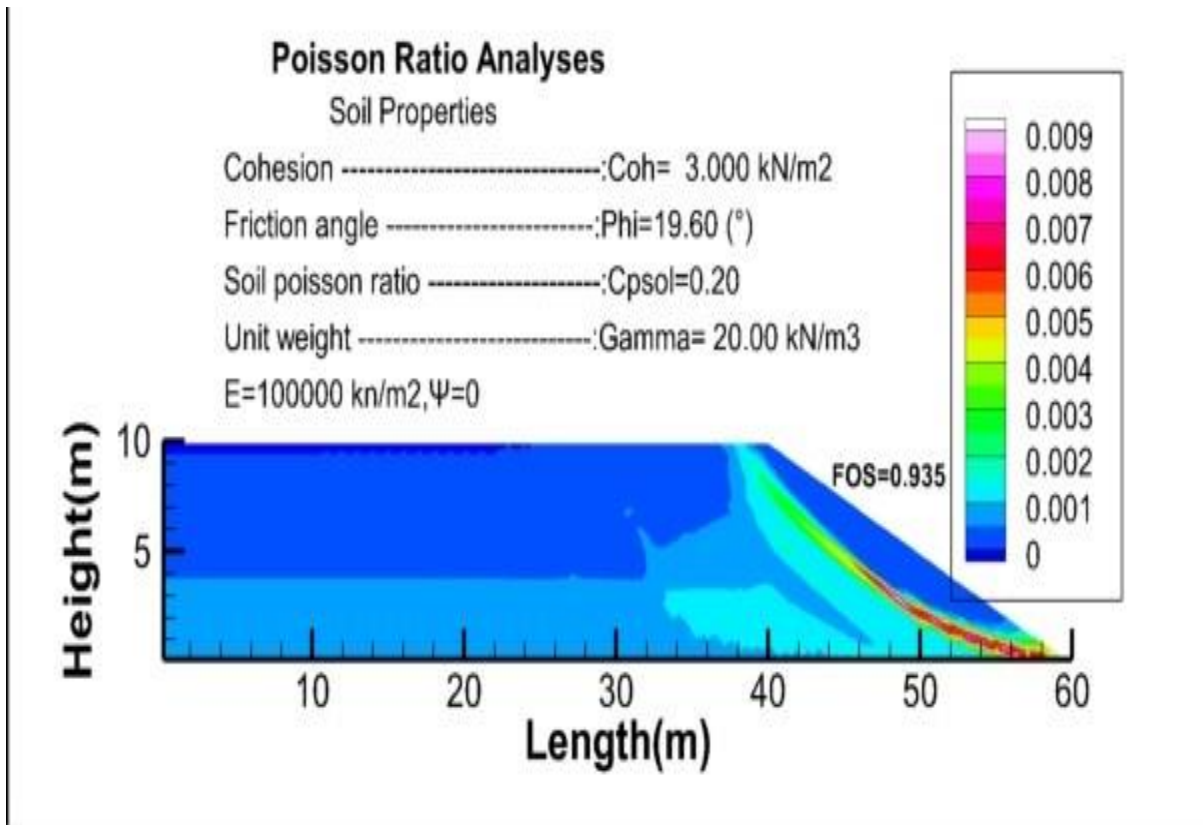


Figure 5.11 109 Strain contours corresponding to the step of failure for  $\nu=0.20$ , without the foundation.

#### d) Poisson Ratio 0.25

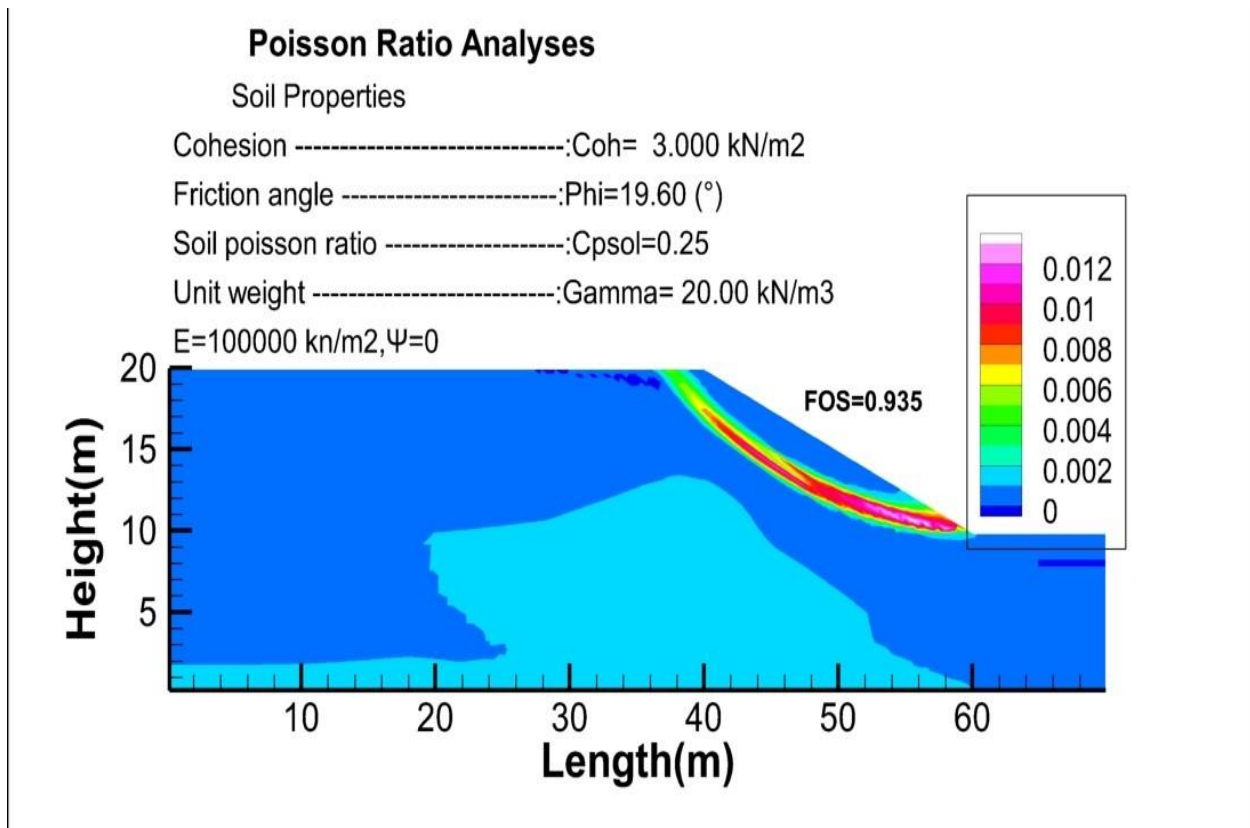


Figure 5.11 110 Strain contours corresponding to the step of failure for  $\nu=0.25$ , with the foundation.

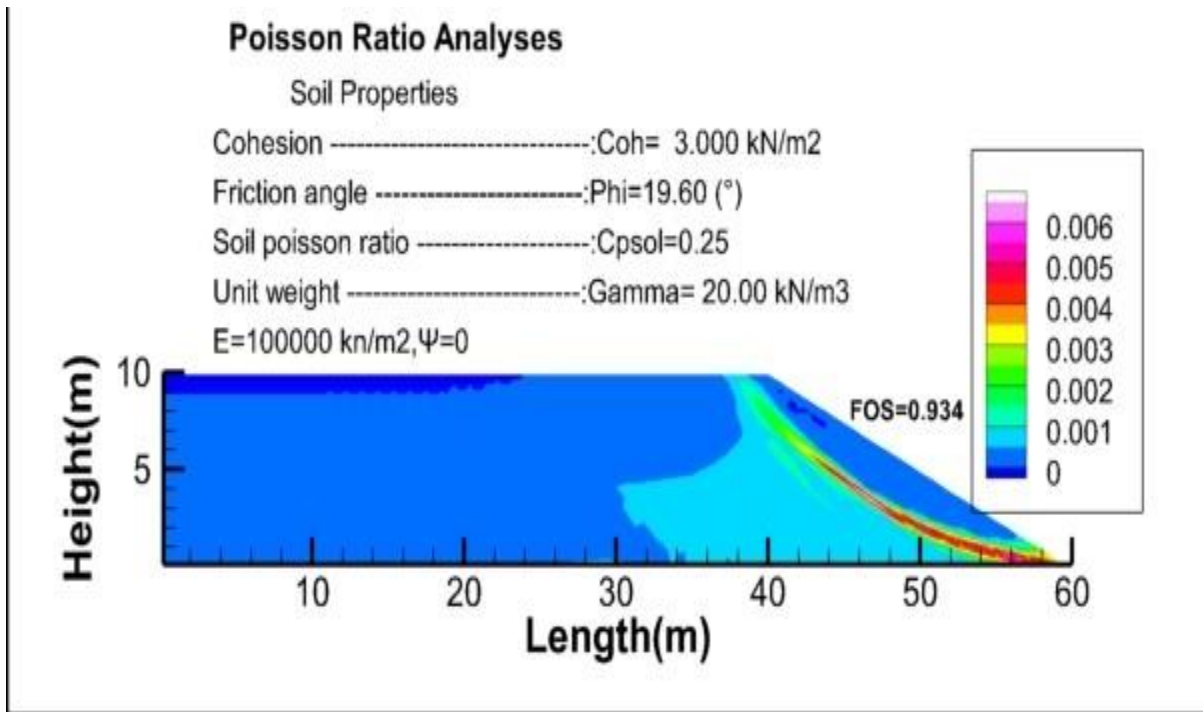


Figure 5.11 111 Strain contours corresponding to the step of failure for  $v=0.25$ , without the foundation.

e) **Poisson ratio 0.30**

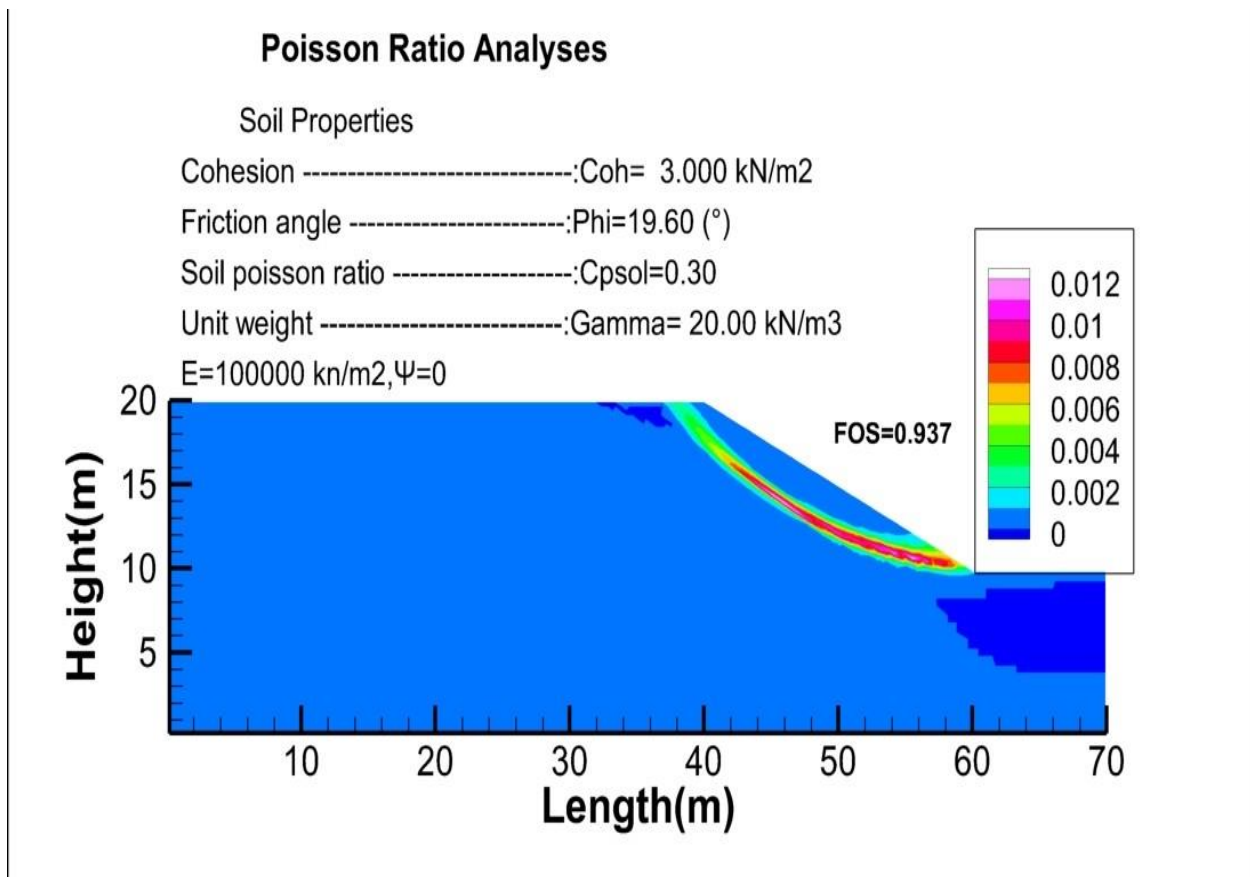


Figure 5.11 112 Strain contours corresponding to the step of failure for  $v=0.30$ , with the foundation

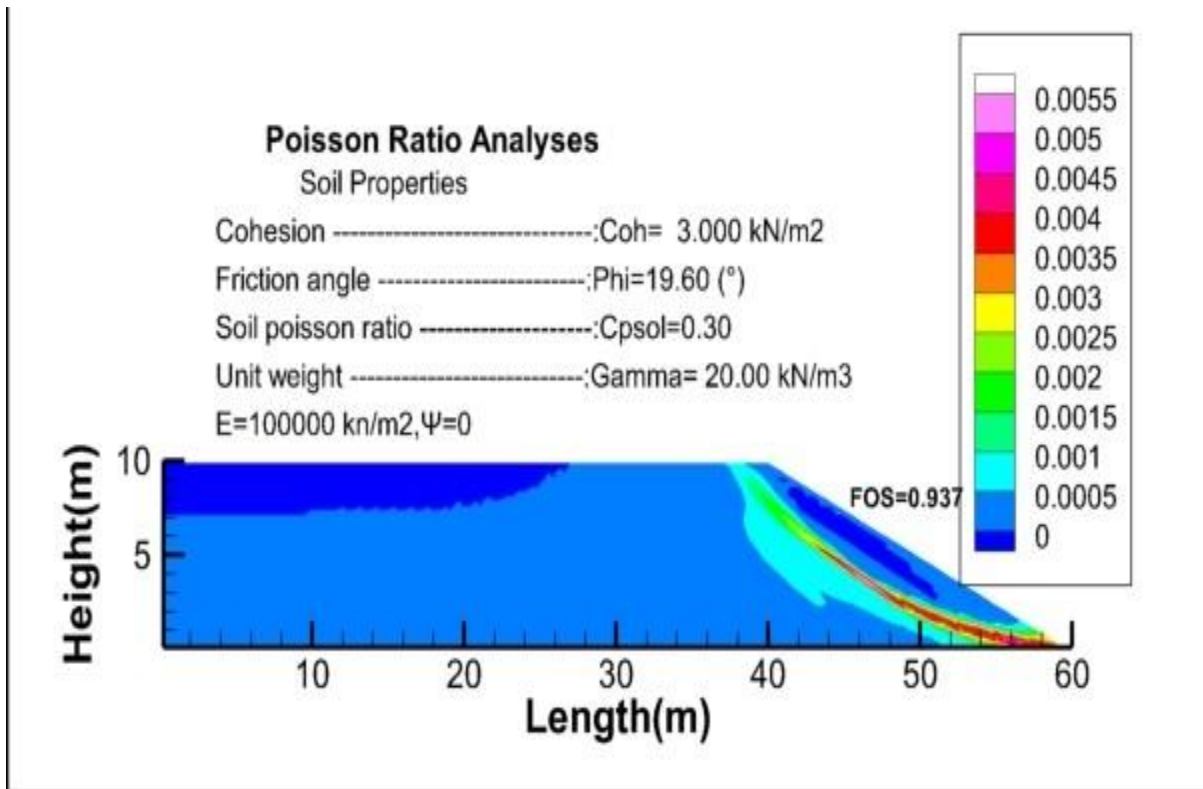


Figure 5.11 113 Strain contours corresponding to the step of failure for  $v=0.30$ , without the foundation.

**f) Poisson Ratio 0.35**

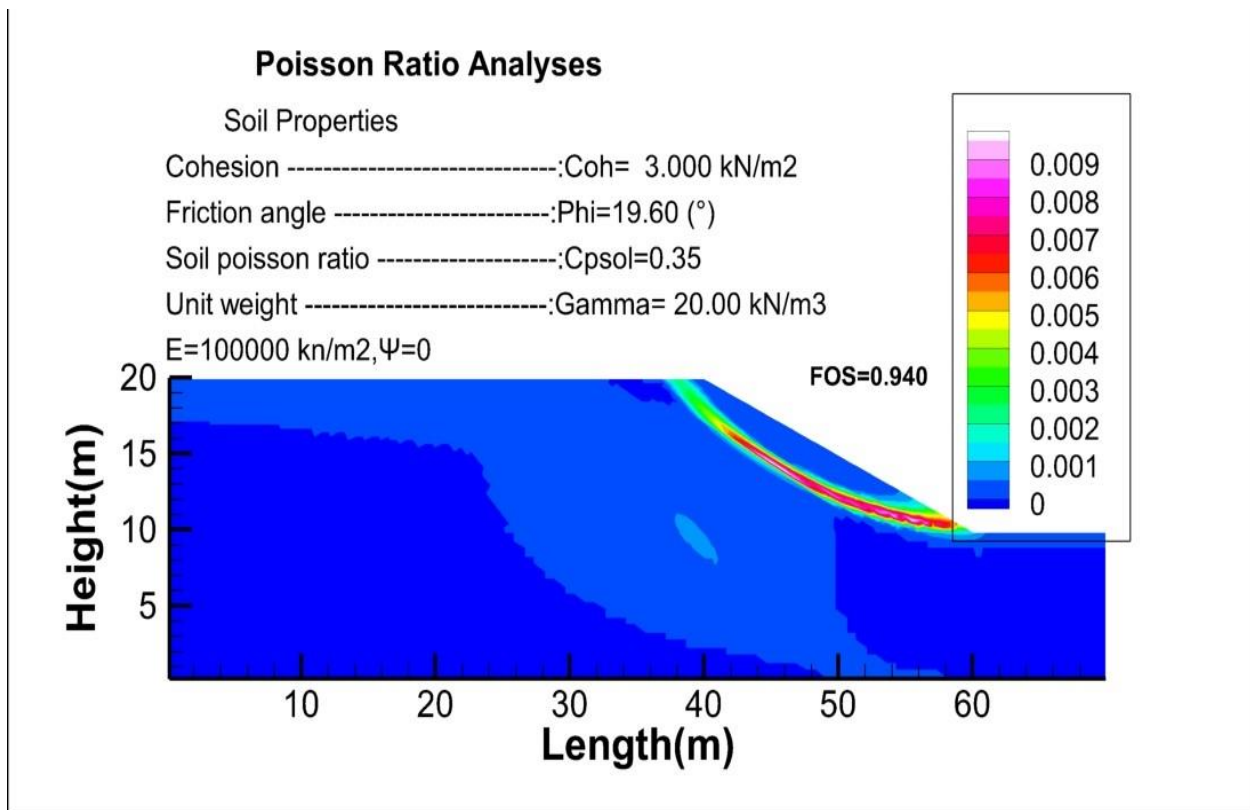


Figure 5.11 114 Strain contours corresponding to the step of failure for  $v=0.35$ , with the foundation

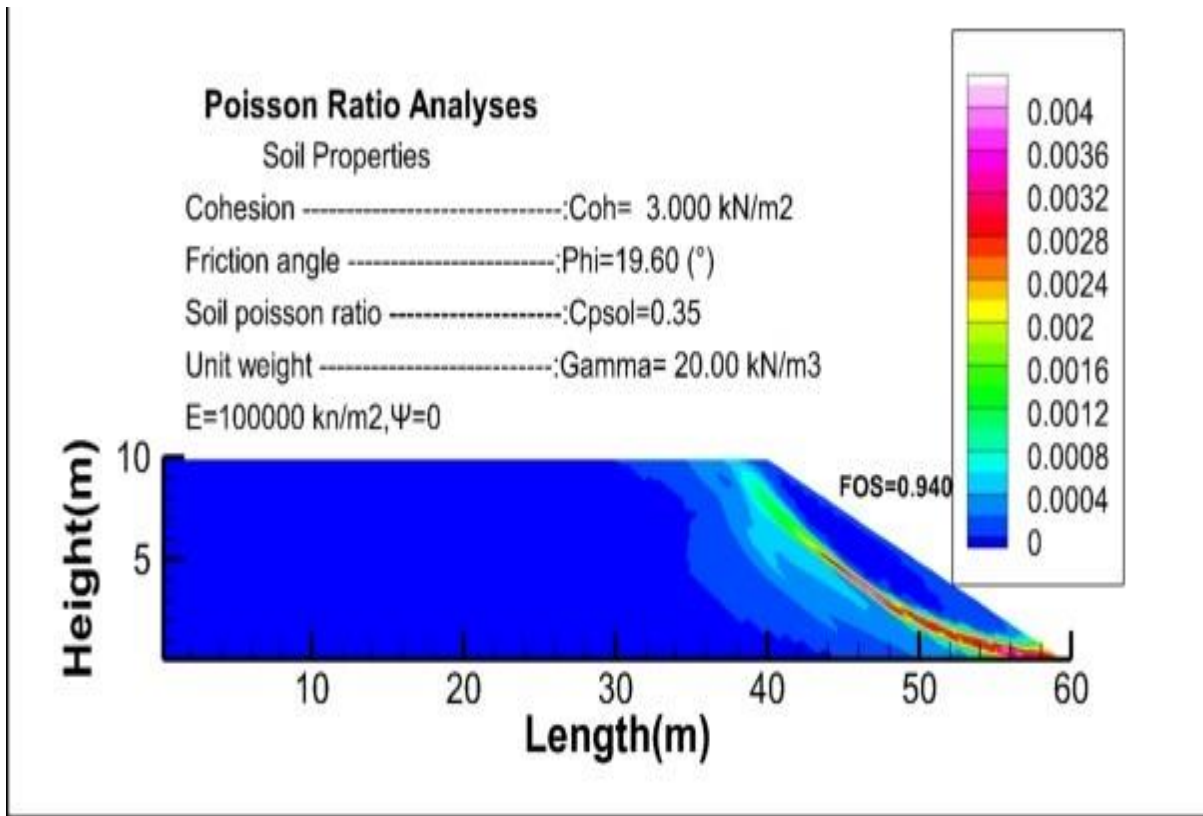


Figure 5.11 115 Strain contours corresponding to the step of failure for  $v=0.35$ , without the foundation.

**g) Poisson Ratio 0.40**

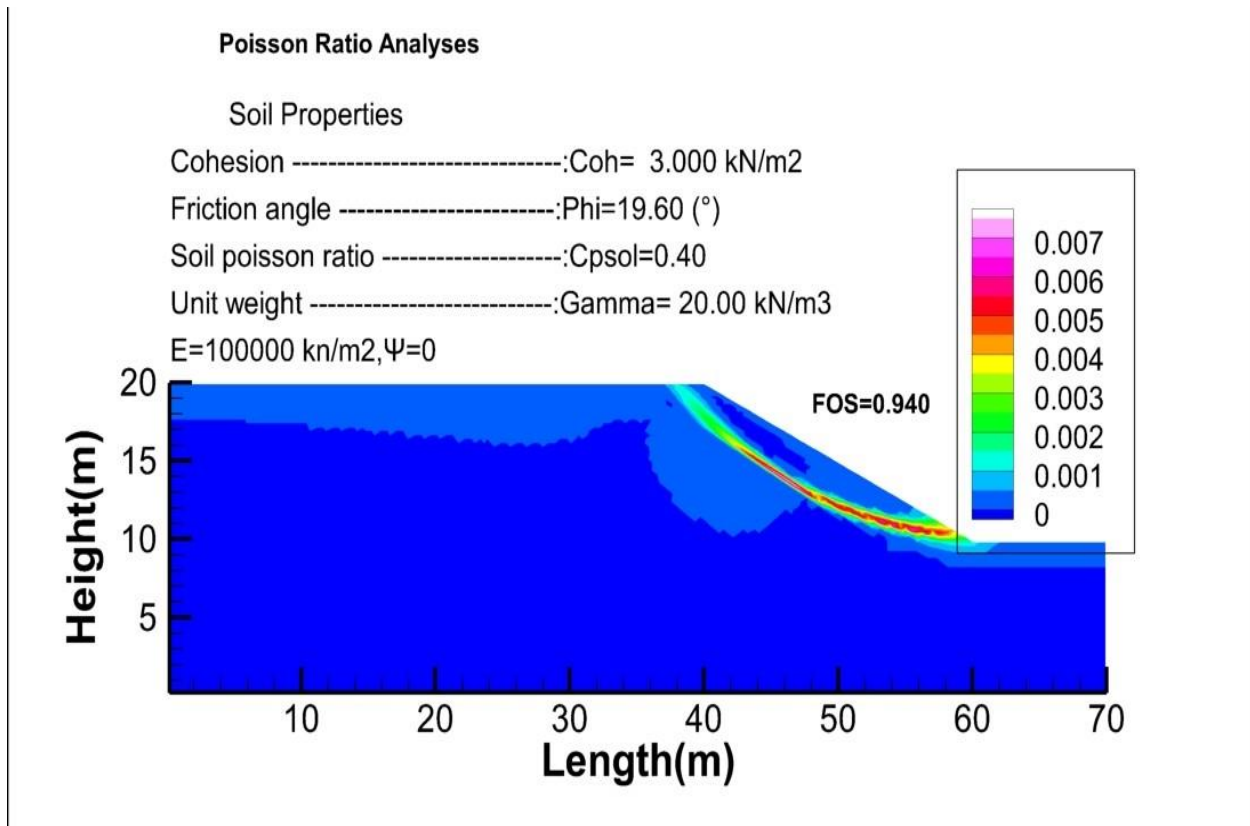


Figure 5.11 116 Strain contours corresponding to the step of failure for  $v=0.40$ , with the foundation.

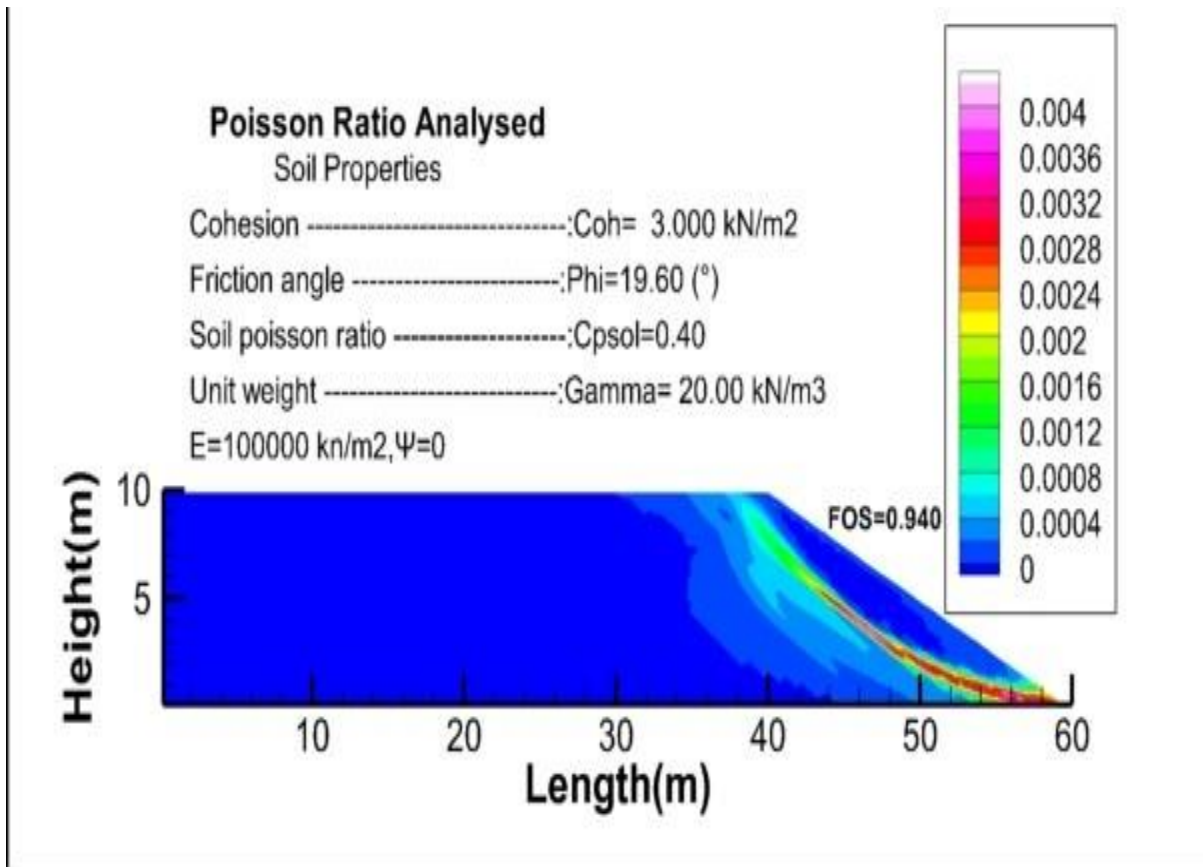


Figure 5.11 117 Strain contours corresponding to the step of failure for  $\nu=0.40$ , without the foundation.

#### h) Poisson Ratio 0.45

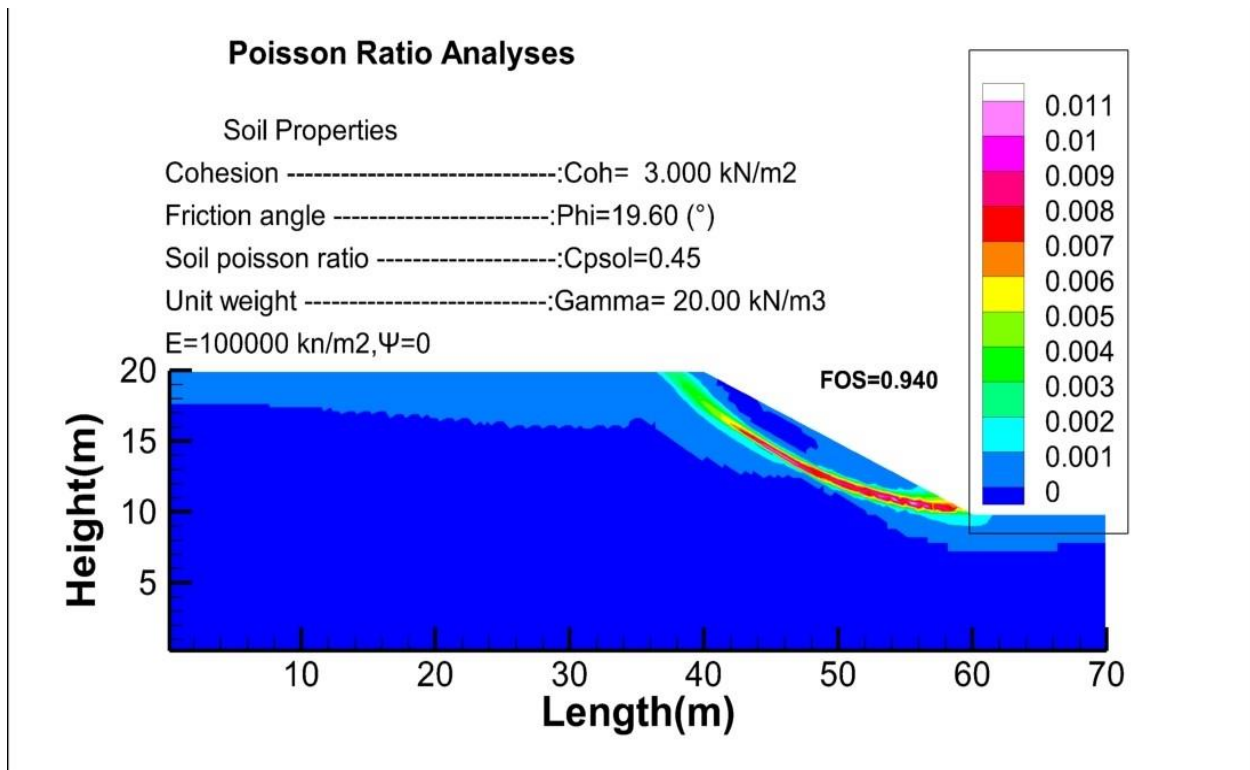


Figure 5.11 118 Strain contours corresponding to the step of failure for  $\nu=0.45$ , with the foundation.

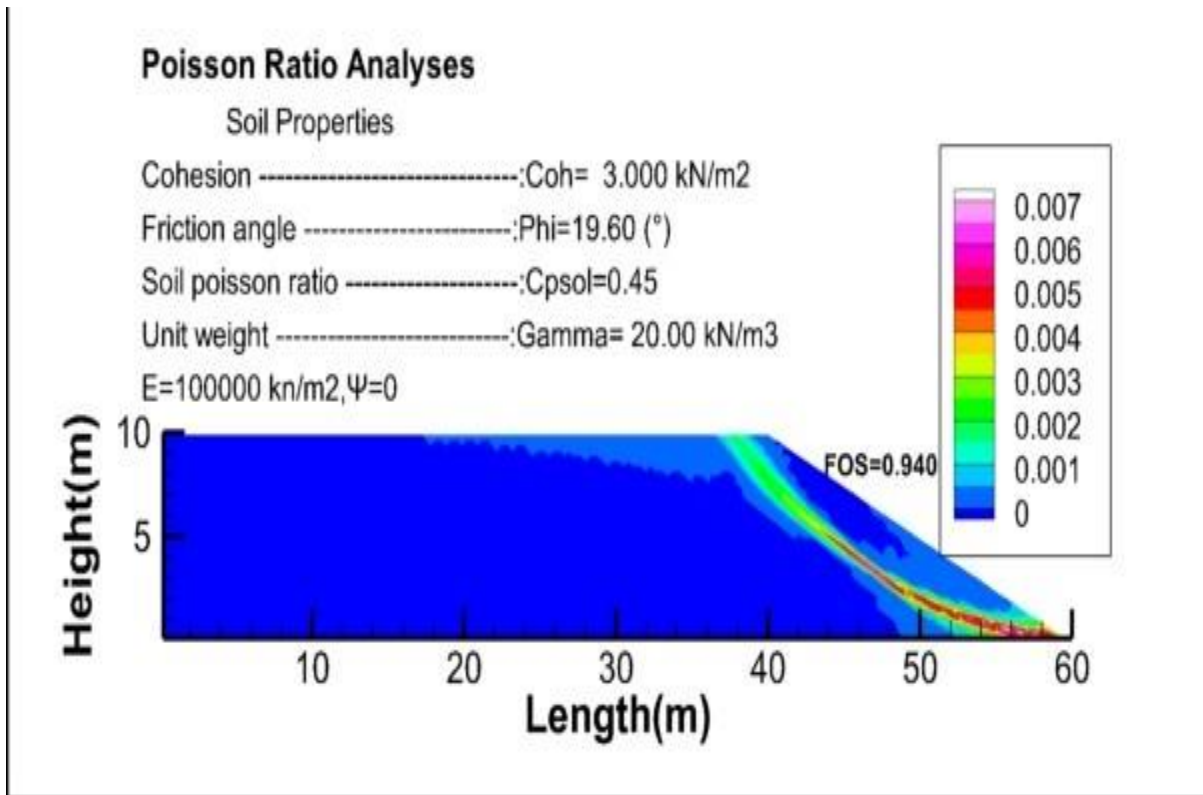


Figure 5.11 119 Strain contours corresponding to the step of failure for  $\nu=0.45$ , without the foundation.

#### i) Poisson Ratio 0.49

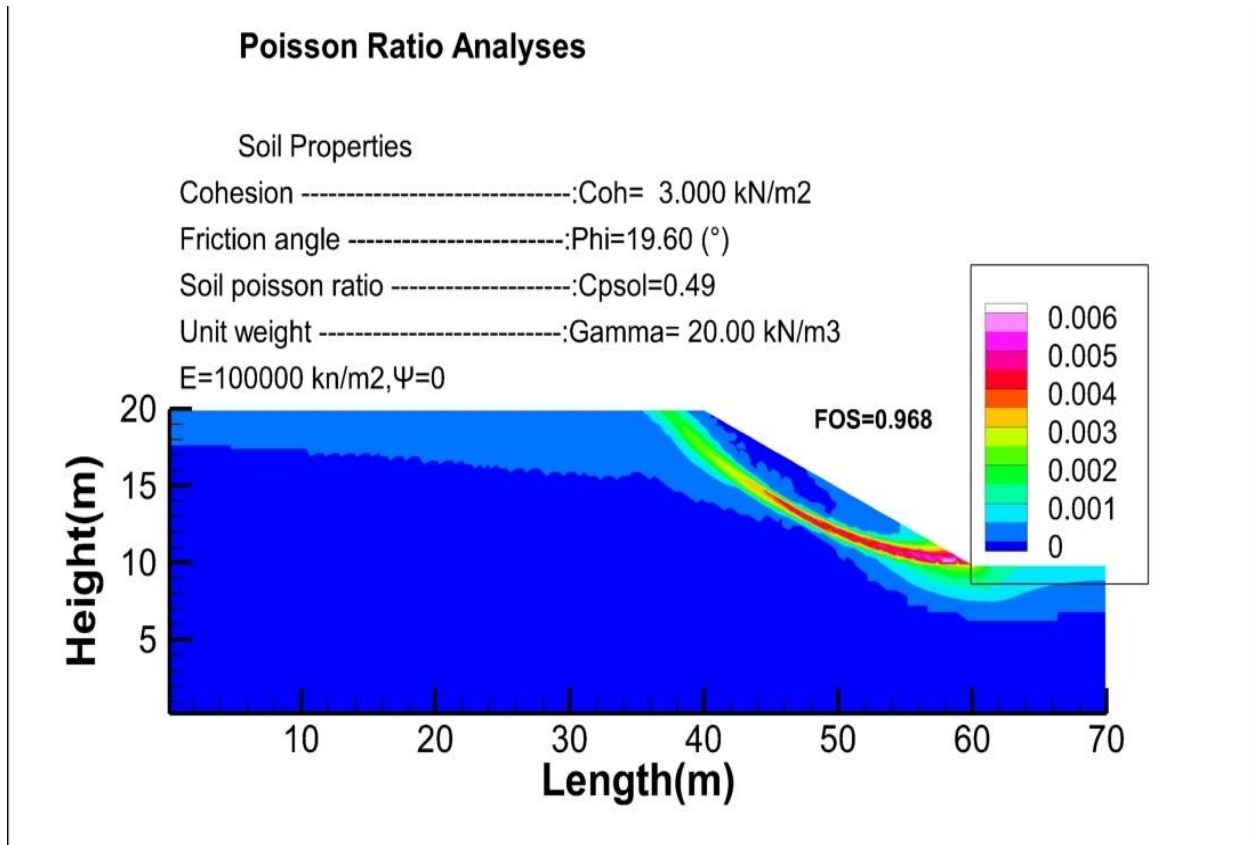


Figure 5.11 120 Strain contours corresponding to the step of failure for  $\nu=0.49$ , with the foundation



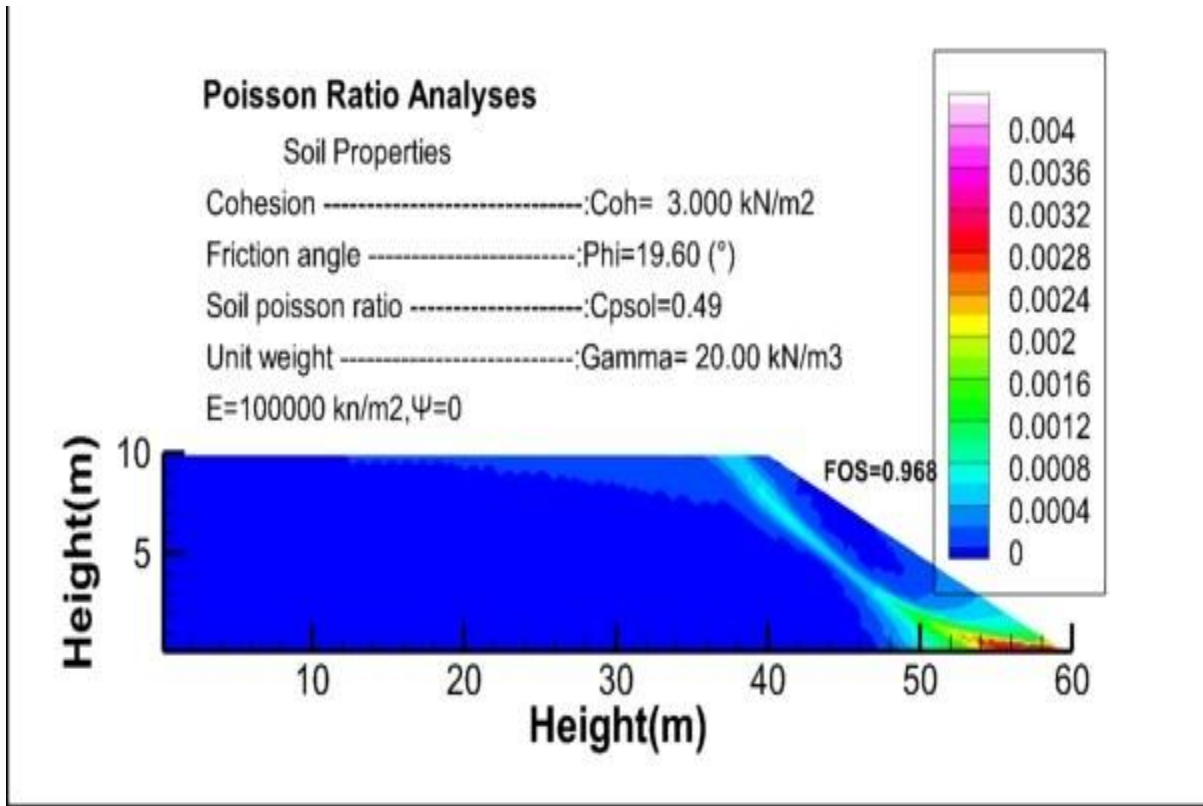


Figure 5.11 121 Strain contours corresponding to the step of failure for  $\nu=0.49$ , without the foundation.

## 5.9. Number of Finite elements without foundation

In this section we looking to understand how the number of finite elements can affect the factor of safety.

### 5.9.1. Associated flow rule

Number of elements	BS	MP	SDIM
225	0.989	0.984	0.996
325			0.996
670			0.989
1500			0.985

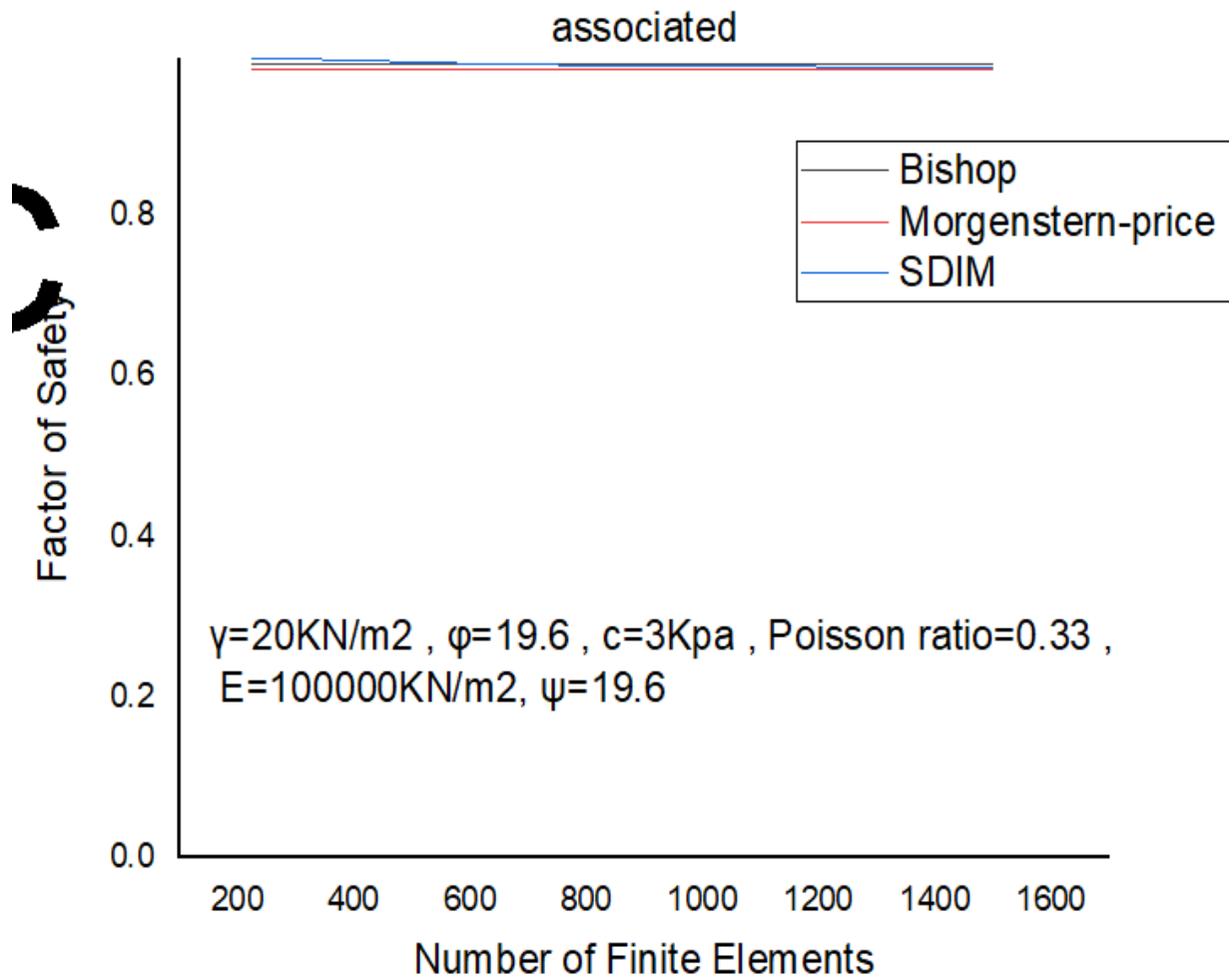


Figure 5.11 122 Evaluation of the Finite elements variation. Associated

### 5.9.2. Associated flow rule with foundation.

Number of elements	BS	MP	SDIM
225	0.989	0.984	1.008
325			1.001
670			0.996
1500			0.992

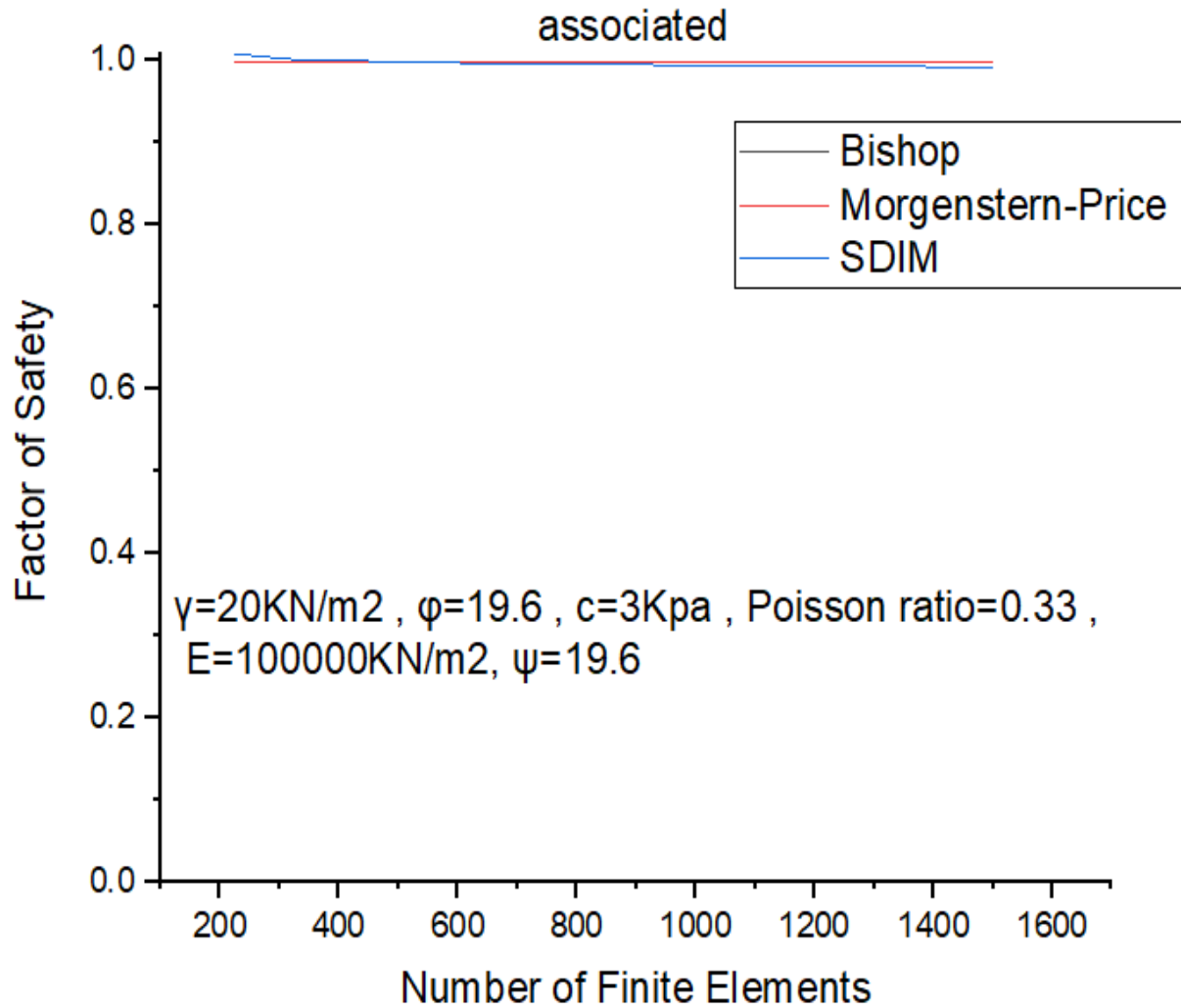


Figure 5.11 124 Evaluation of the Finite elements variation. Associated

We see that while the number of finite elements are lower the value of the factor of safety is overestimated, is important to put the correct or enough number of finite elements in order to get good values of the factor of safety that we accurately represented the state of the case of study.

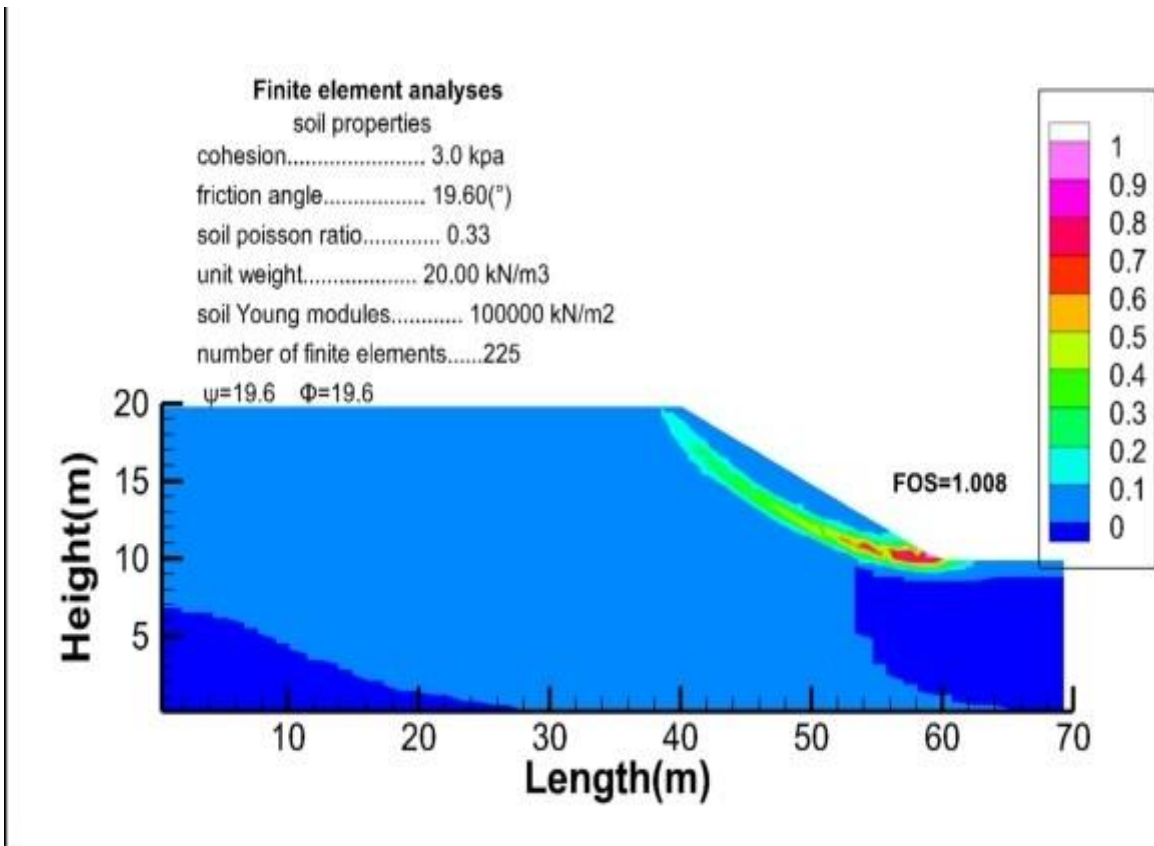


Figure 5.11 125 Strain contours corresponding to the step of failure for FE=225, with the foundation.

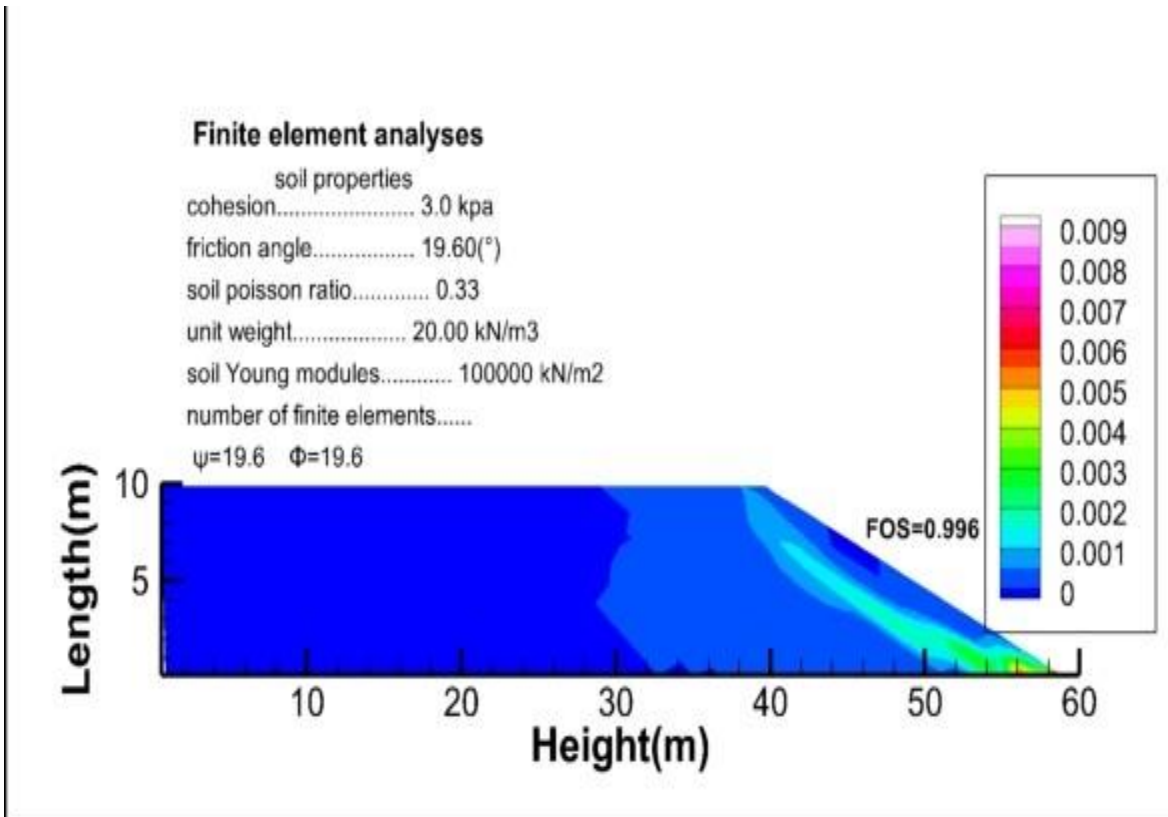


Figure 5.11 126 Strain contours corresponding to the step of failure for FE=225, without the foundation.

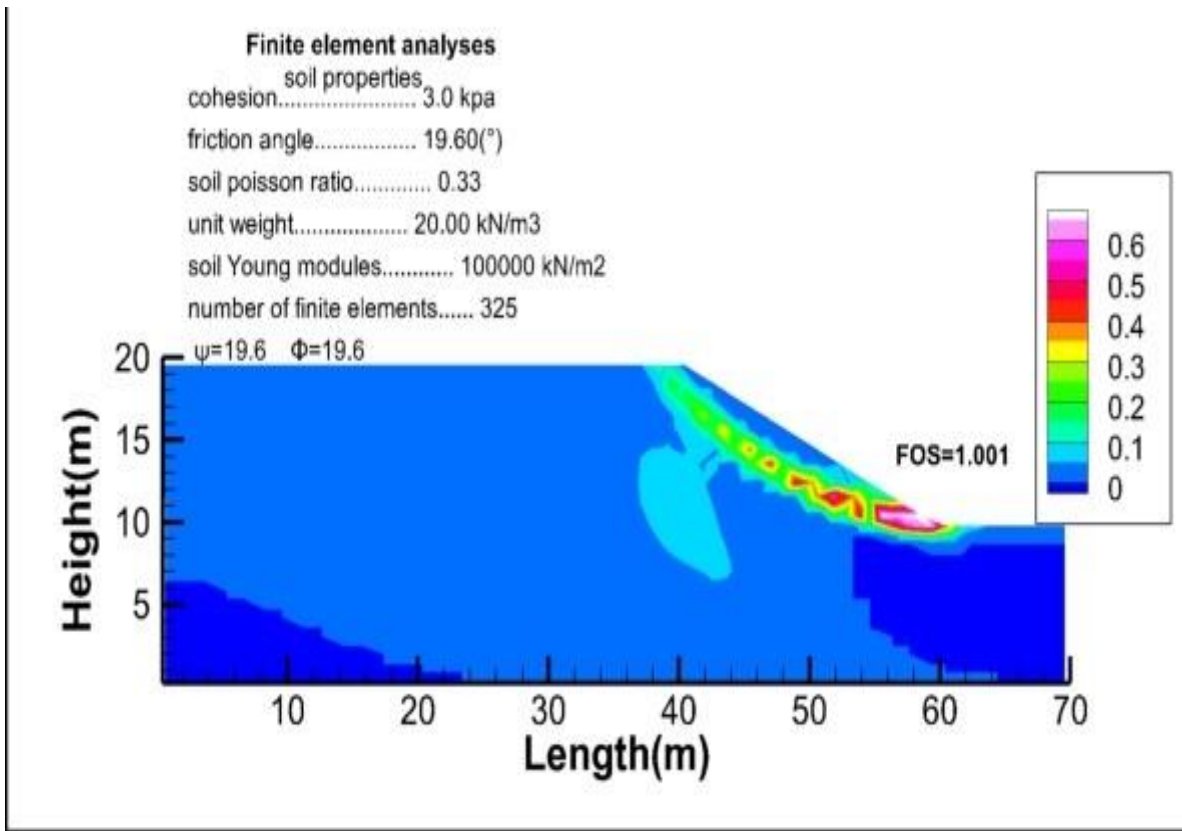


Figure 5.11 127 Strain contours corresponding to the step of failure for FE=325, with the foundation.

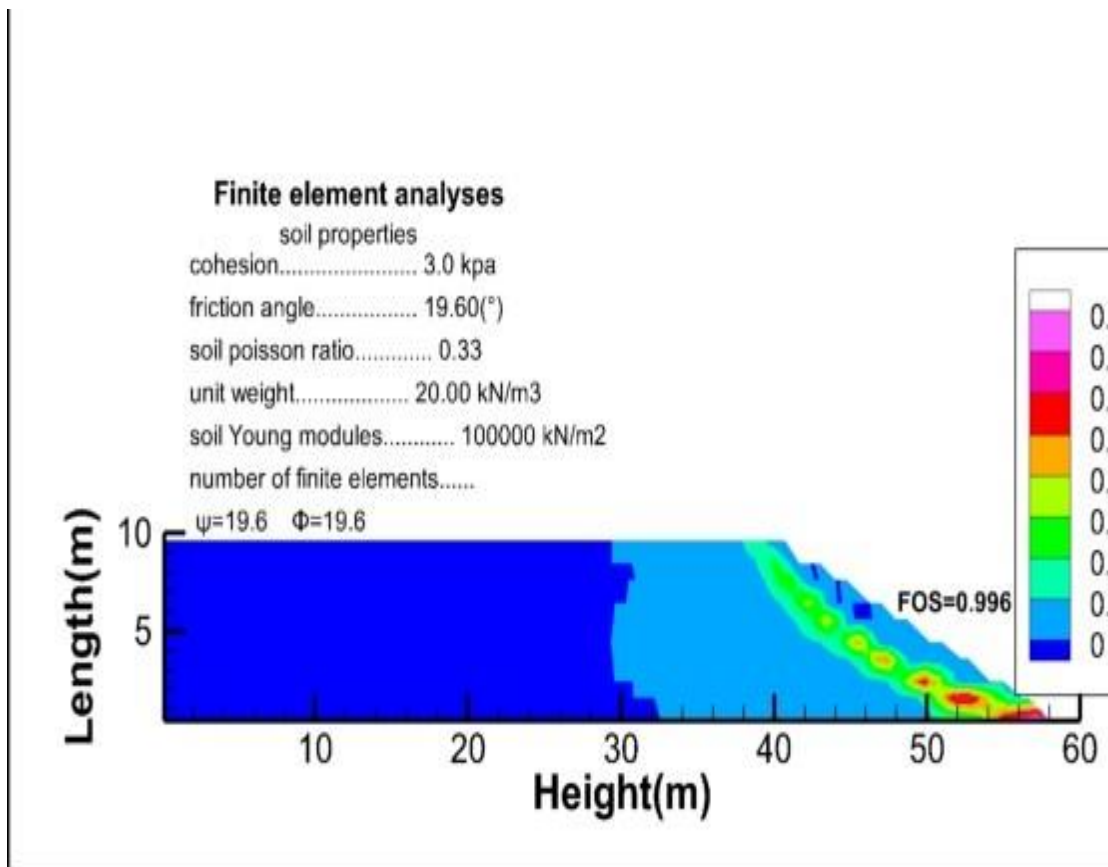


Figure 5.11 128 Strain contours corresponding to the step of failure for FE=325, without the foundation.

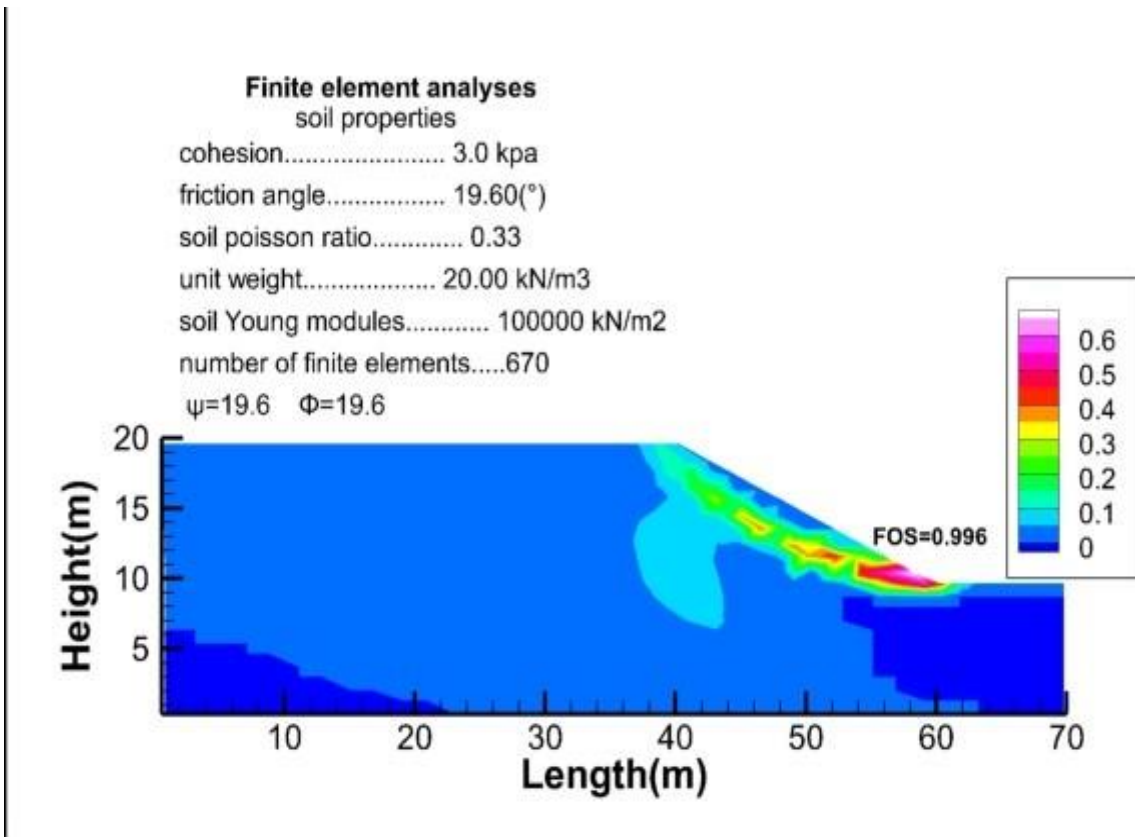


Figure 5.11 129 Strain contours corresponding to the step of failure for FE=670, with the foundation.

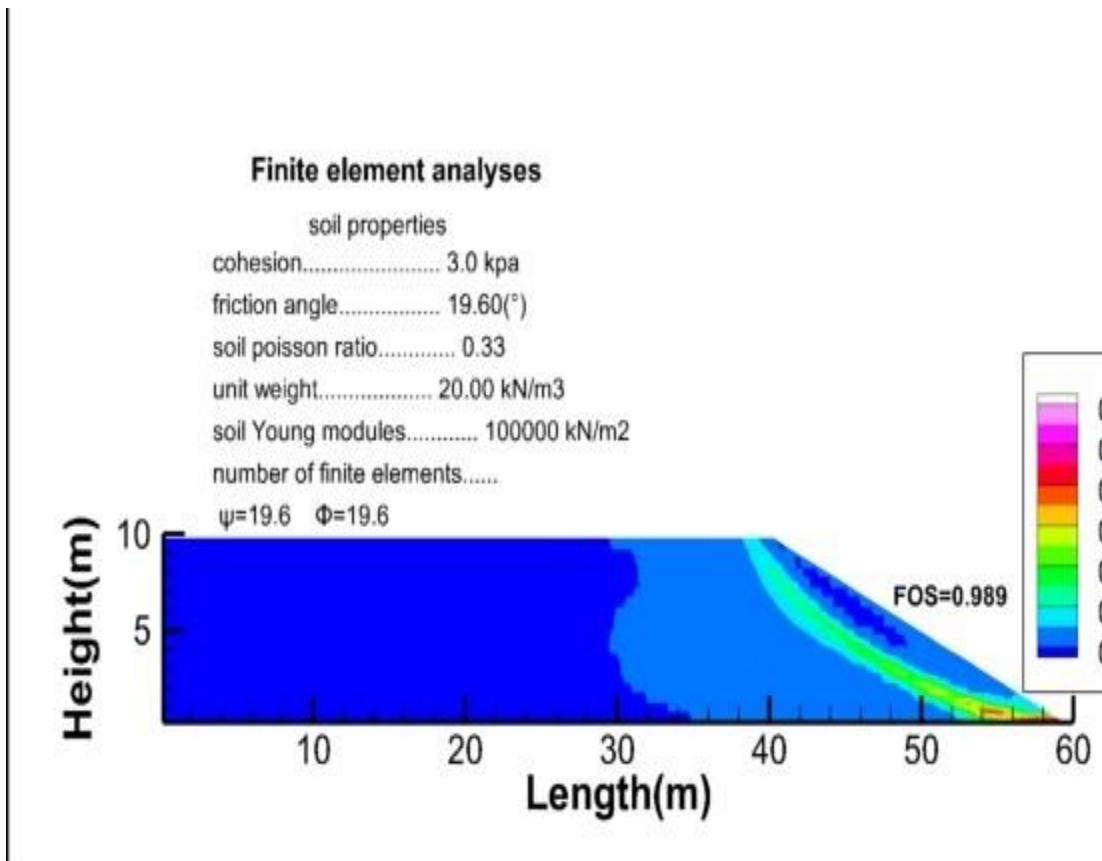


Figure 5.11 130 Strain contours corresponding to the step of failure for FE=670 , without the foundation.

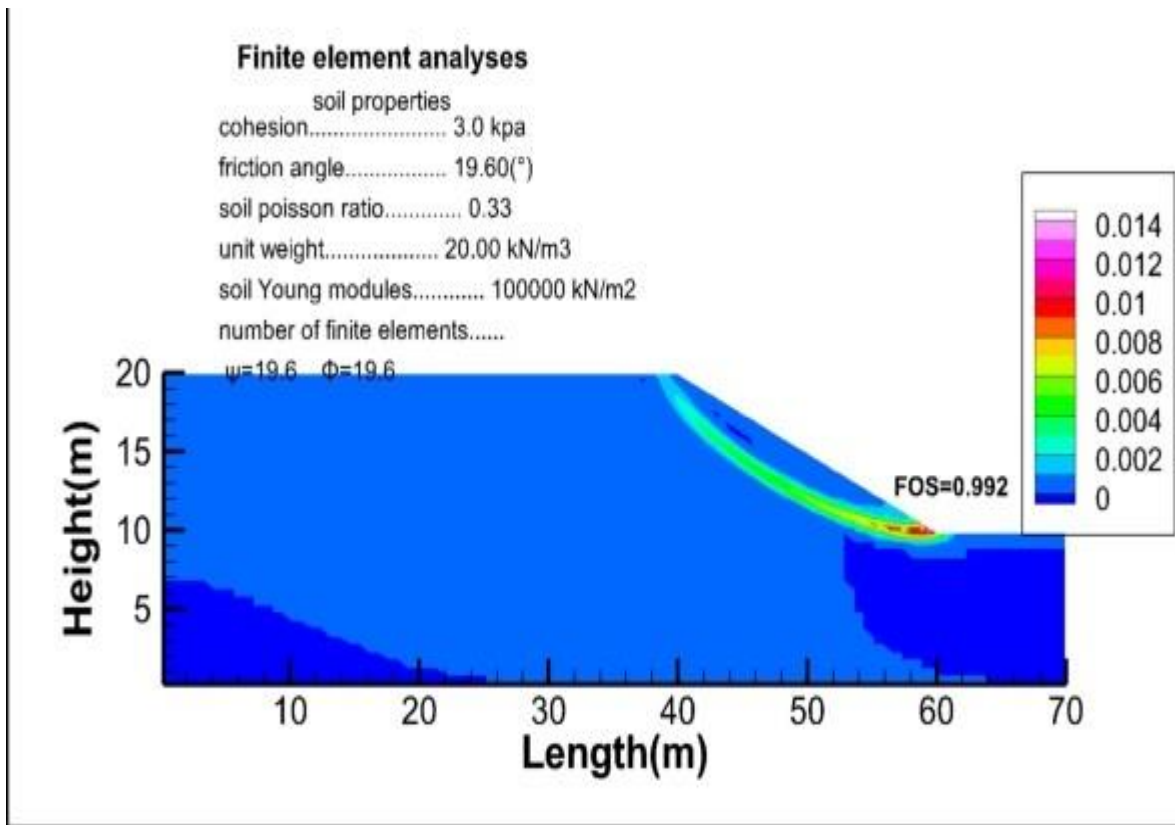


Figure 5.11 131 Strain contours corresponding to the step of failure for FE=150, with the foundation.

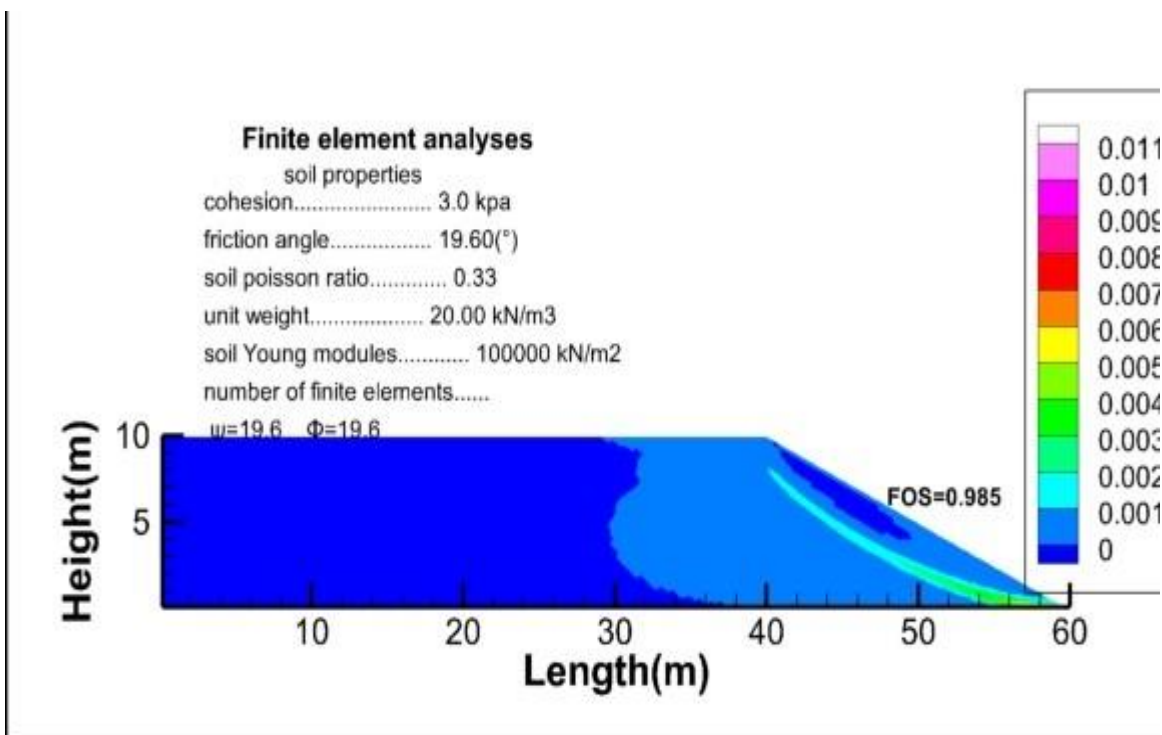


Figure 5.11 132 Strain contours corresponding to the step of failure for FE=1500 , without the foundation.

Higher is the number of finite elements better and lower is the factor of safety is to mention that the program accept for the slope a total of 1000 number finite elements and for the foundation 1000 is the max. So meeting

this requirements we can consider the study accurately of course regarding the good input of all data need for analysing.

### 5.9.3. Non-associated without foundation

Number of elements	BS	MP	SDIM
225	0.989	0.984	0.958
325	0.989	0.984	0.951
670	0.989	0.984	0.937
1500	0.989	0.984	0.935

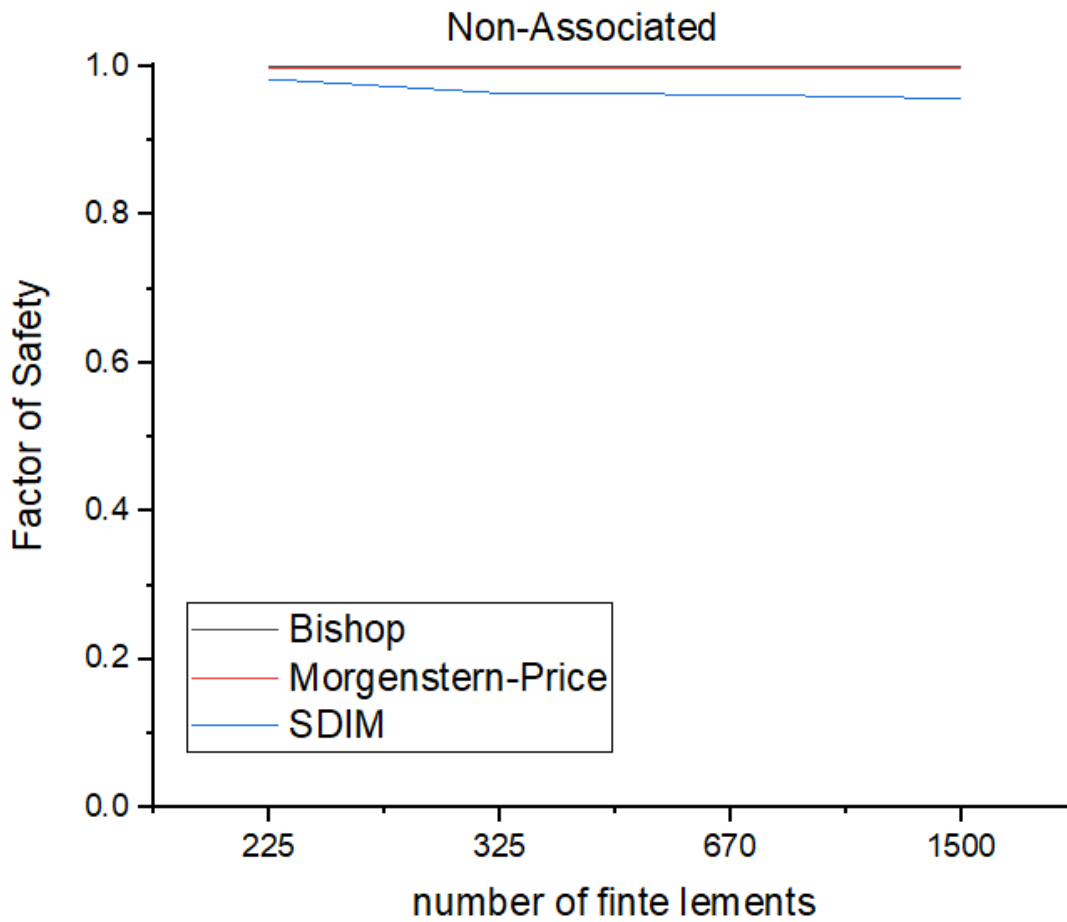


Figure 5.11 123 Evaluation of the Finite elements variation. Non-Associated

### 5.9.4. Non-Associated without foundation

Number of elements	BS	MP	SDIM
225	0.989	0.984	0.958
325			0.951
670			0.997
1500			0.935



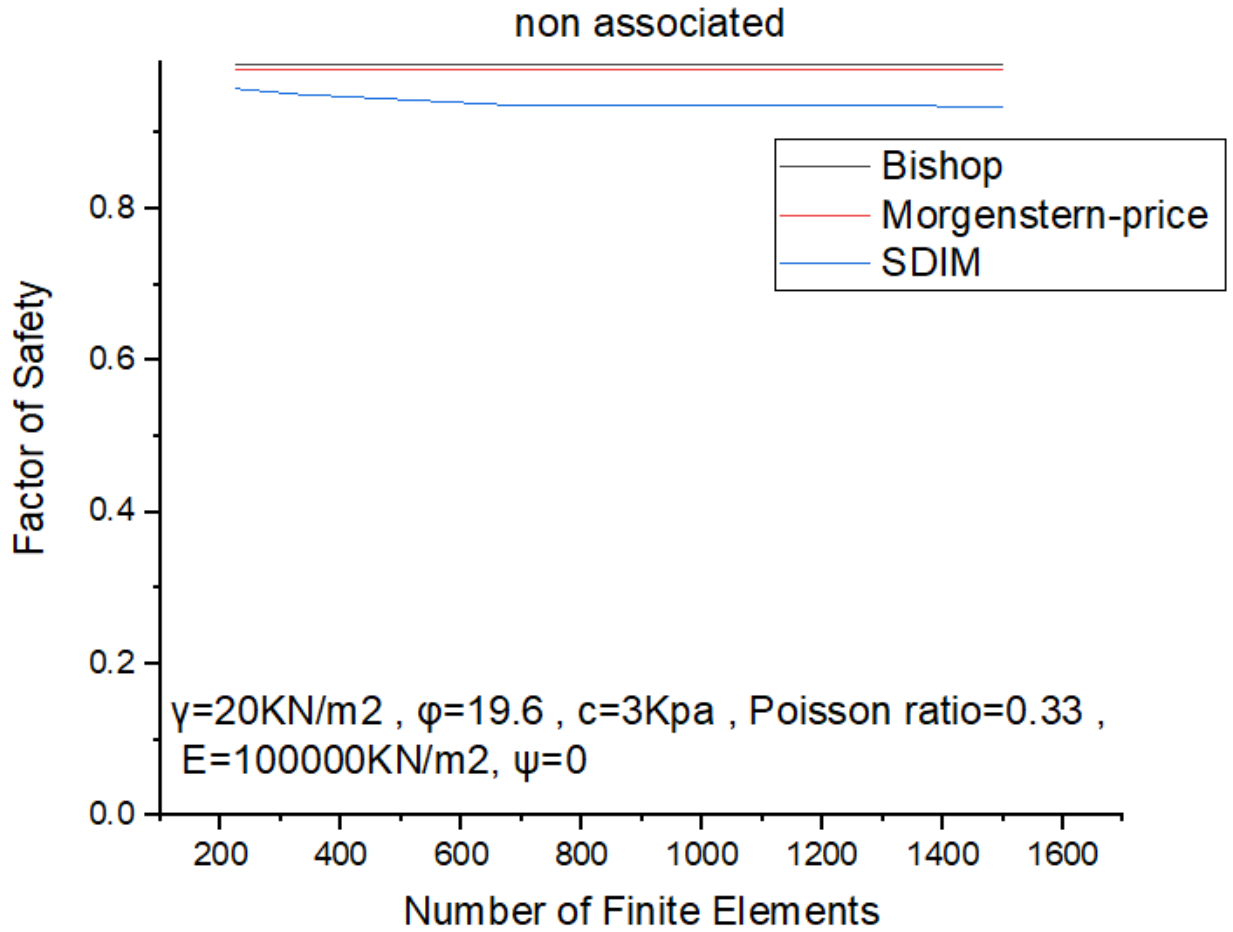


Figure 5.11 134 Evaluation of the Finite elements variation. Associated

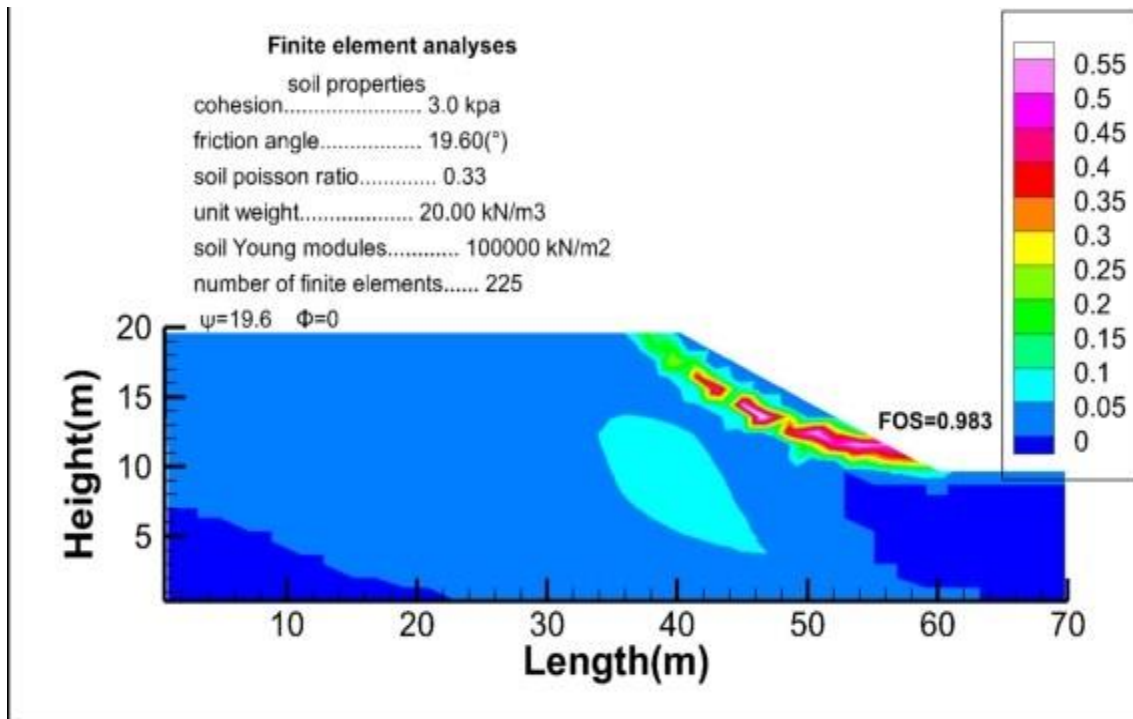


Figure 5.11 135 Strain contours corresponding to the step of failure for FE=225, with the foundation.

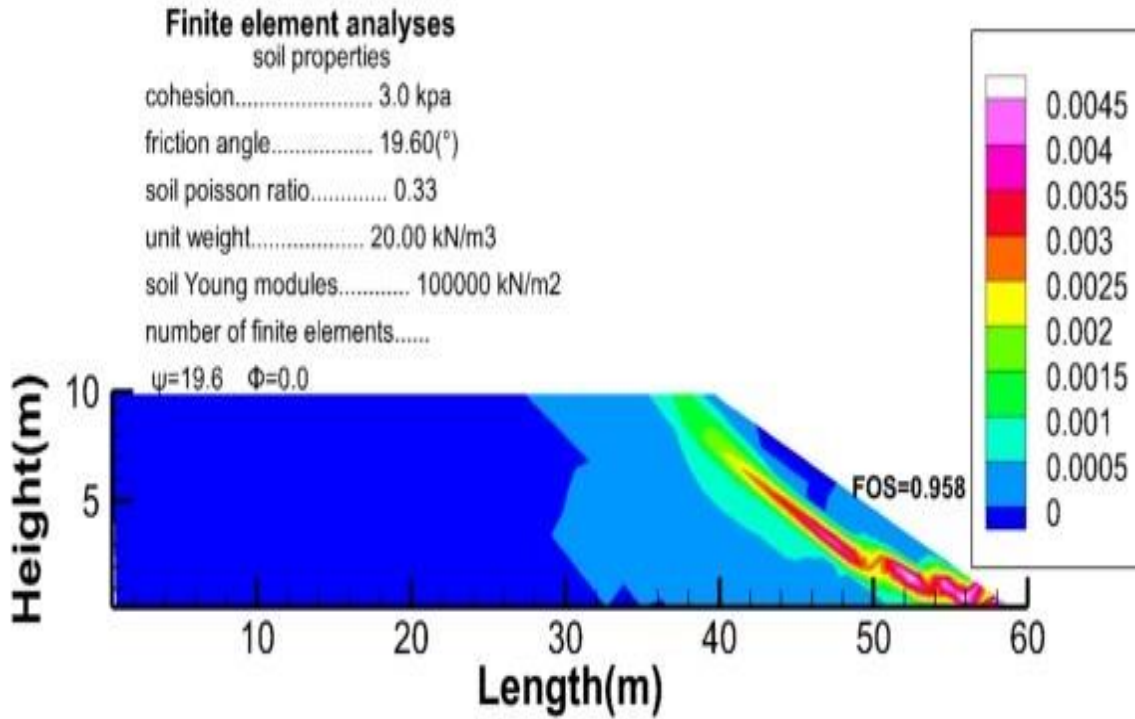


Figure 5.11 136 Strain contours corresponding to the step of failure for FE=225, without the foundation.

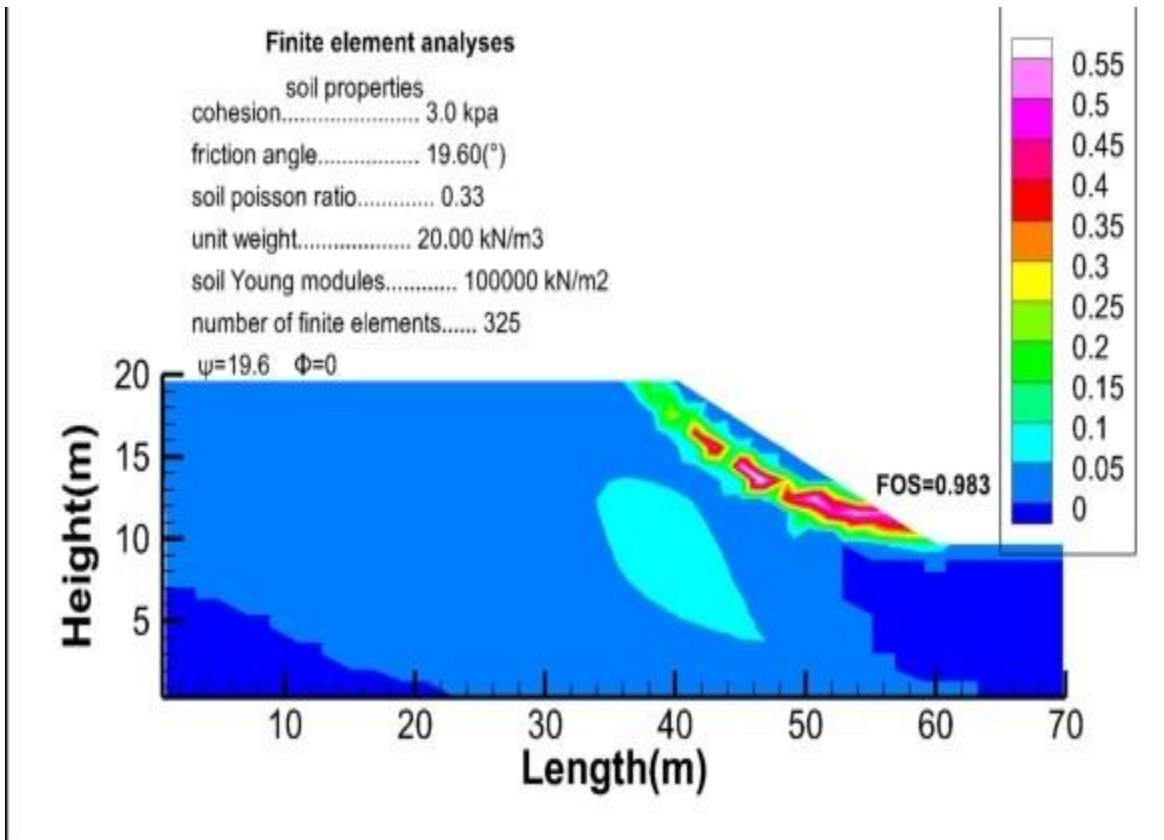


Figure 5.11 137 Strain contours corresponding to the step of failure for FE=325, with the foundation.

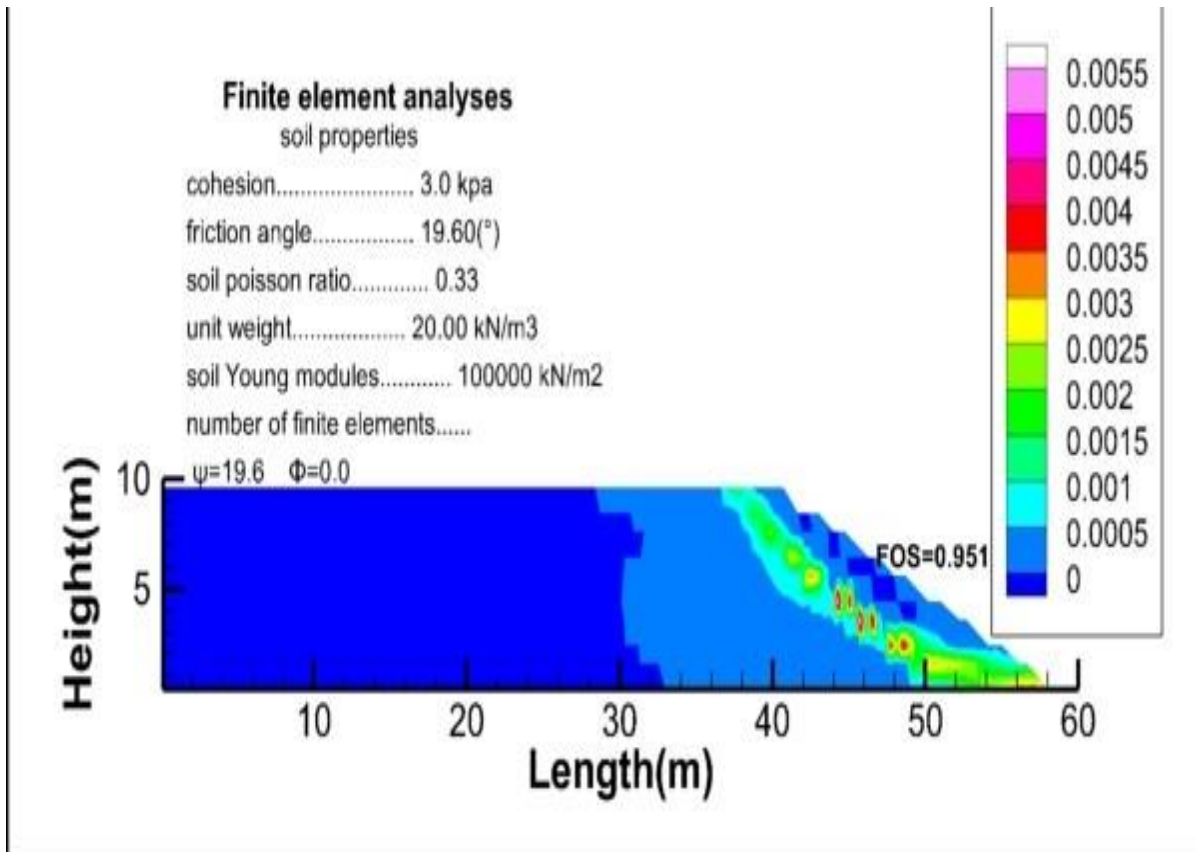


Figure 5.11 138 Strain contours corresponding to the step of failure for FE=325 , without the foundation.

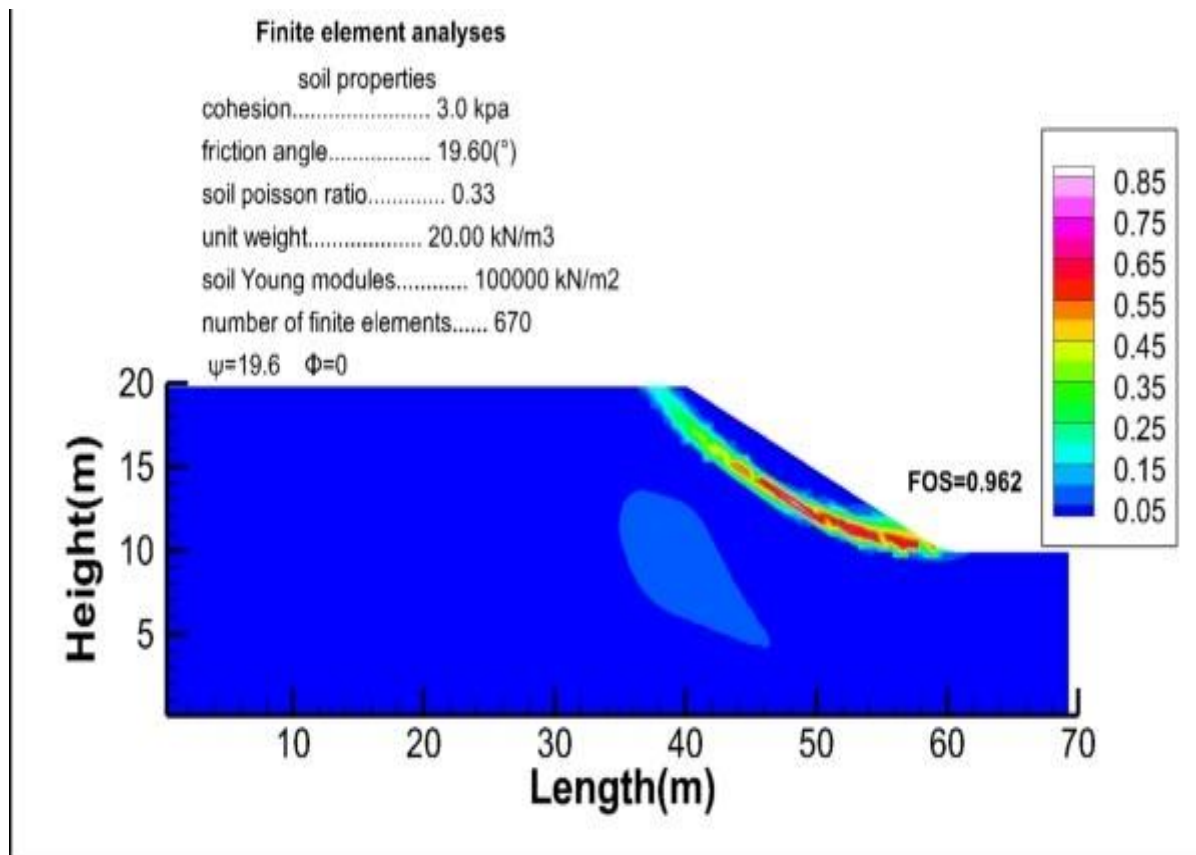


Figure 5.11 139 Strain contours corresponding to the step of failure for FE=670, with the foundation.

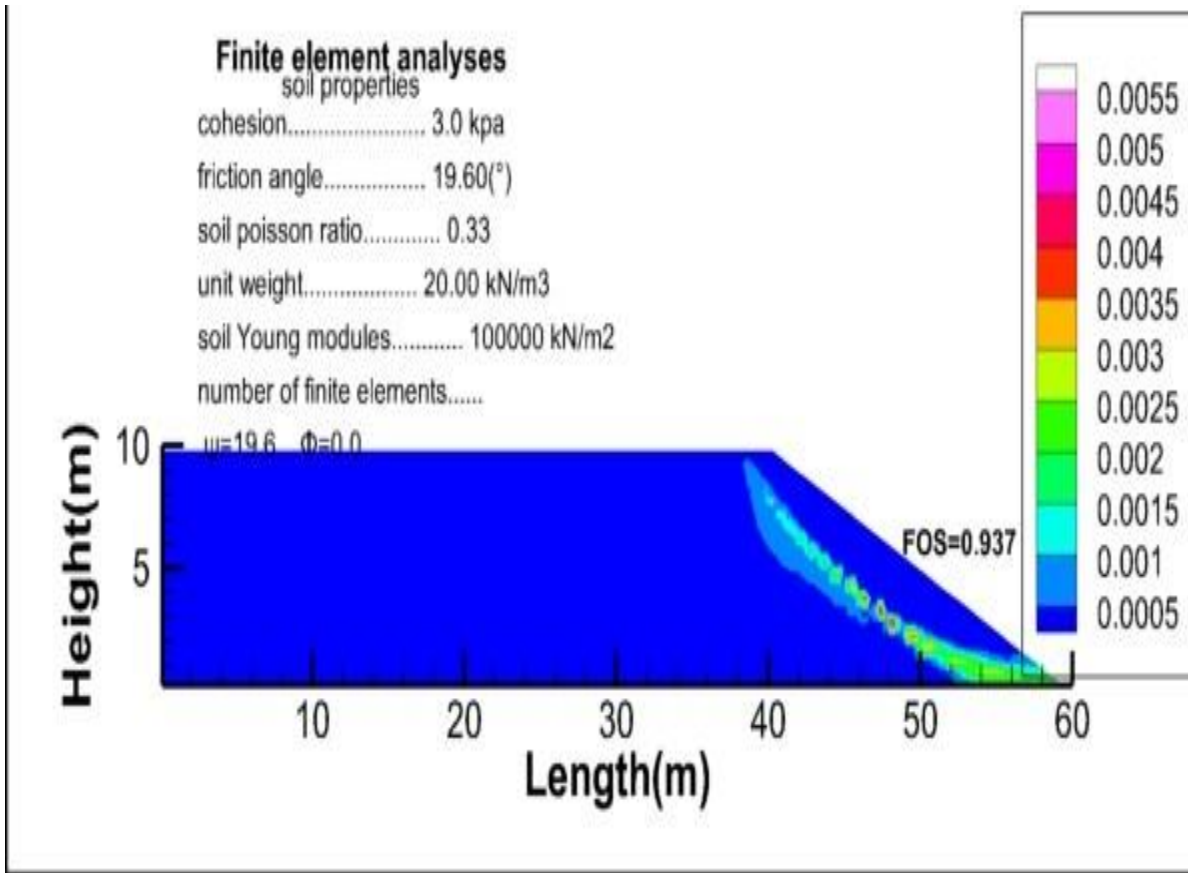


Figure 5.11 140 Strain contours corresponding to the step of failure for FE=670 , without the foundation.

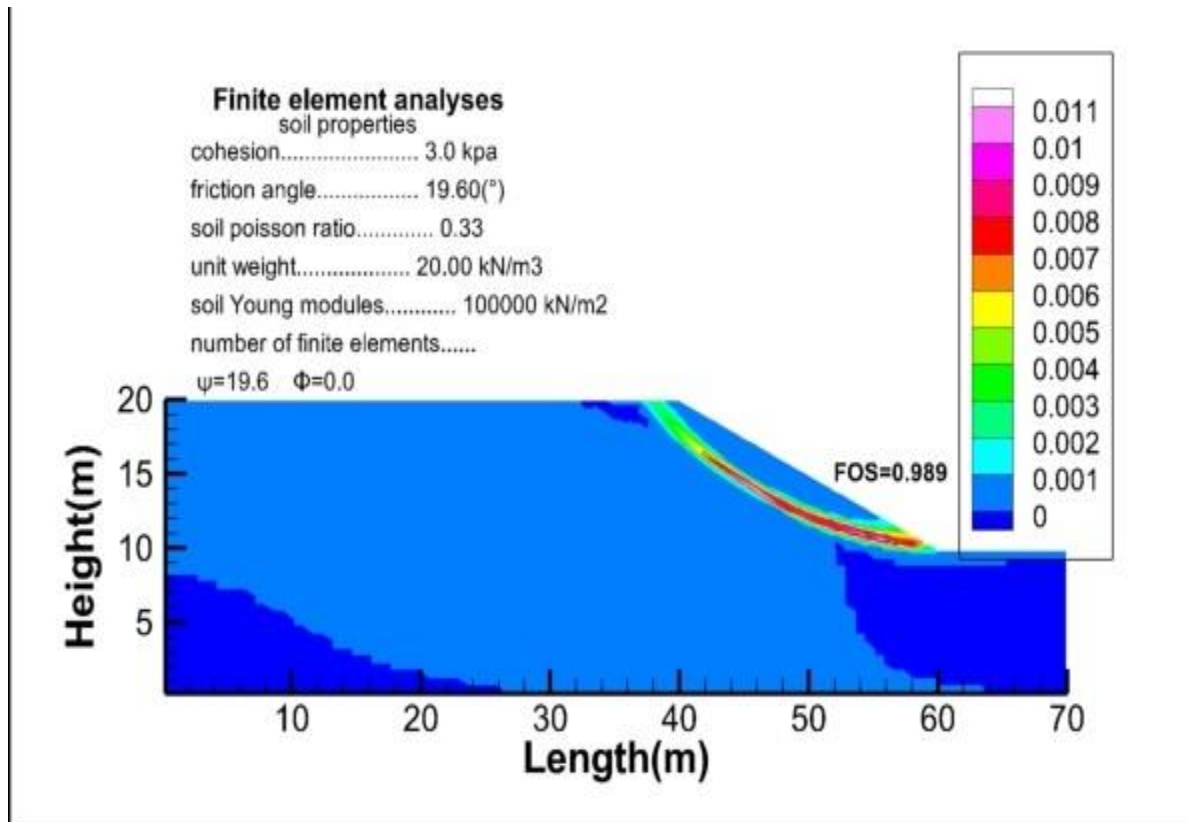


Figure 5.11 141 Strain contours corresponding to the step of failure for FE=1500, with the foundation.

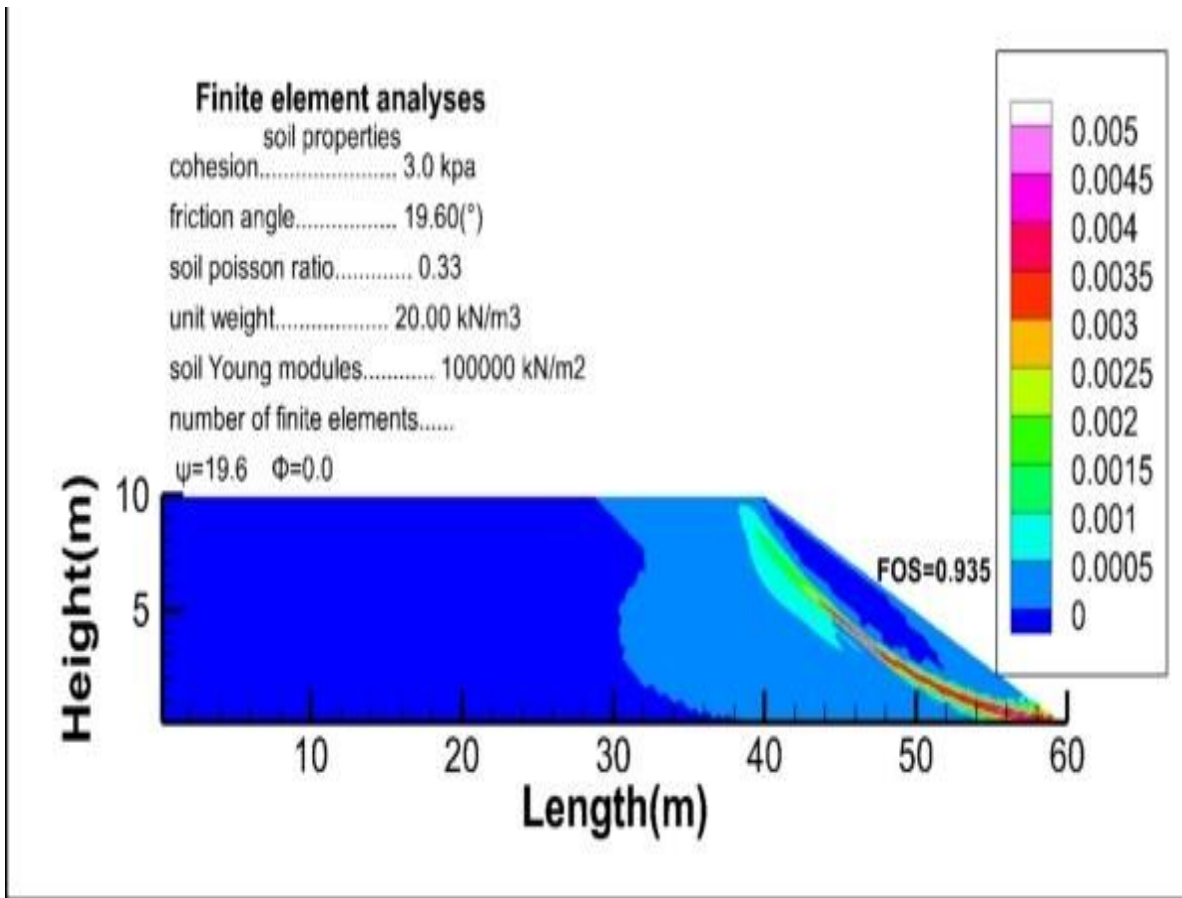


Figure 5.11 142 Strain contours corresponding to the step of failure for FE=1500, without the foundation.

As noticed in other study analyses when the assumption is  $\psi=0$  the lack of resistance gives a strong deformation line that suggest that.

## Conclusion

The slide is a software in general uses the assumption of associated flow rule, by this we conducted the calculation by association and non-association flow rule, when non-associated the results from SDIM were little far from those from SLIDE because SDIM gives the designer the control of this parameters and to put up the value closed to those from LEM we add up the angle  $\Psi$  on the profile meaning that the association is archived and the results got close because the resistance increasing.

At the first section we tested the number of iteration to check the effects of this calculation parameter and we could conclude by this study that the number of iterations have a big influence on the analyses and should careful be treated in order to get good and rigorous results by this method and the good use of the program will be the key to have an accurate analysis.

One of the interesting things that we found in the program SDIM we realised that the slip surface it gives automatically after calculating the factor of security.

The second section we performed a teste where we teste out the effects of the Young Modulus parameter and end conclude that this parameters actually has no influence on the analysis and any value for this is valid to get good and accurate results with this method.

At the third section we workout with the Poison ratio where we come across with a phenomena of the parasite appearance when the plasticity condition is not meted and to solve this problem further increasing of this value had to be made in order to attain good results and accurate factor of safety and plastic strain counter.

By the end we tested out the effects of the finite elements number in which we could conclude that this has a big effect in the analysis since when this value are lower we get overestimated factor of safety and after a further increasing we were able to get satisfied value of factor of safety and accurate results were obtain.

## Conclusion

In this work, we reviewed SDIM and S<sup>4</sup>DINA created by our supervisor Amar Bouzid, which tends to improve the research work that have been conducted over the past years on the subject of slope stability analysis, this method provides a rigorous and accurate factor safety that tends to value the existing soil parameters in a given land. We tested this method in this project, and we found good results and with whom this project is based. In this paper we provided comparative studies of already existing methods (LEM).

The capital importance of the stabilizations of earth slope have mobilized so many researchers into deep diving in this matter in order to come up with mathematical solutions to deal with such problems cause by this earth structures when not stabilized since in past and in nowadays this lead in various disaster that have cost a life of hundreds and economical losses so motivated by this factors the author conducted his research on this matter and come up with a new way of dealing with this problems, we are lucky to be part of the first one benchmarking this method into a such a paper and also working with the newer programme that solves this with efficacy. Many method were done by many authors that some were include in this project and by studying those method and picking two of them that are also used in geotechnical field practice and also academia we could compare this methods performance side to side with this newer method SDIM that showed a very consistence results in comparison with those methods SRM. The finite elements programme S<sup>4</sup>DINA that gives a very accurate results and more precise calculations that leads in a better predictions of the slope failure. As mentioned early SDIM It consists of progressively increasing a factor called Mohr's circle expansion factor until the slope failure is reached, borrowing thus, the reverse path of the SRM which consists of reducing the soil strength parameters. As the slope failure is said to occur when the iterative process fails to converge within the prescribed range of the maximum number of iterations. This method gives the designer or the geotechnical engineer the possibility of conducted the calculations using real in situs parametric and the ability to control the and visualize the contour lines of the plastic region that comes with a very accurate precision. Dealing with the finite elements programme S<sup>4</sup>DINA that have been created by the author of the method to illustrate and validate this method the designer gets to choose between a wide ranges of parametric that sectioned it the programme.

## References

1. **Benaissa, A** (2003) “*Glissement de terrains “édition- 2eme Edition, office des publications universitaires OPU. Edition : 1.05.4220, ISBN : 9961.0.0639.9, 95p.*”
2. **BISHOP, A. W. (1955).** “The Use of Slip Circle in the Stability Analysis of Earth Slopes,” *Geotechnique*, Vol. 5, No. 1, 7–17.
3. **BISHOP, A. W., and MORGENSTERN, N. R. (1960).** “Stability Coefficients for Earth Slopes,” *Geotechnique*, Vol. 10, No. 4, 129–147.
4. **Bouafia, A (2018)** « Conception et calcul des ouvrages géotechniques » Edition pages bleues. ISBN : 978-9947-34-133-9, 436p.
5. **Braja M Das**, Fundamentals of geotechnical engineering, third edition. ISBN-13: 978-0-495-29572-3.
6. **Cheng, Y.M., Lansivaara, T. and Wei, W.B., 2007.** Two-dimensional slope stability analysis by limit equilibrium and strength reduction methods. *Computers and Geotechnics*, 34, 137-150.
7. **Davis, E. H. (1968).** Theories of plasticity and failure of soil masses. In *Soil mechanics: selected topics.* (ed. I. K. Lee), pp. 341–354. New York, NY, USA: Elsevier.
8. **Djillali Amar Bouzid-** Finite Element Analysis of a Slope Stability by Incrementally Increasing the Mobilized Principal Stress Deviator. <https://orcid.org/0000-0003-2991-6533>  
*Geotechnique*, 49(3), 387-403.
9. **Griffiths, D.V. and Lane, P.A. (1999).** *Slope Stability Analysis by Finite Elements*,
10. **J.M. Duncan.** State of art ;Limit equilibrium and finite element analysis of slopes. *J.Geotech, GeoenvEng, ASCE*, 107;691-693.
11. **Krabbenhoft, K., Karim, M. R., Lyamin, A. V. & Sloan, S. W. (2012).** Associated computational plasticity schemes for nonassociated frictional material. *Int. J. Numer. Methods Engng* 90, No. 9, 1089–1117.
12. **Lyamin, A. V. & Sloan, S. W. (2002a).** Lower bound limit analysis using nonlinear programming. *Int. J. Numer. Methods Engng* 55, No. 5, 573–611.
13. **Lyamin, A. V. & Sloan, S. W. (2002b).** Upper bound limit analysis using linear finite elements and nonlinear programming. *Int. J. Numer. Analyt. Methods Geomech.* 26, No. 2, 181–216.
14. **Mamadou Doudou NGOM,** Études numériques et expérimentales de l’état initial des contraintes dans une pente.Thèse.
15. **Naylor, D.J., 1981.** Finite elements and slope stability. Proceedings of the NATO Advanced Study Institute, Lisbon, Portugal. [http://dx.doi.org/10.1007/978-94-009-7895-9\\_10](http://dx.doi.org/10.1007/978-94-009-7895-9_10).
16. **Nordal, S., 2008.** Can we trust numerical collapse load simulations using non-associated flow rules?. *International Association for Computer Methods and Advances in Geomechanics (IACMAG)*, 1, India.



17. **Potts, D. M. & Zdravkovic, L. (2012).** Accounting for partial factors of safety in numerical analysis. *Geotechnique* 62, No. 12, 1053– 1065, <http://dx.doi.org/10.1680/geot.11.P.057>.
18. **SLIDE 6.0.** Stability analysis for soil and rock slopes. User's Guide, Geomechanics Software Solutions, Rocscience Inc., Canada. [www.rocscience.com](http://www.rocscience.com).
19. **Sloan, S. W. & Randolph, M. F. (1982).** Numerical prediction of collapse loads using finite element methods. *Int. J. Numer. Analyt. Methods Geomech.* 6, No. 1, 47–76.
20. **Sloan, S.W., 2013. 51<sup>st</sup> Rankine lecture:** geotechnical stability analysis. *Géotechnique*, 63(7), 531-572. <http://dx.doi.org/10.1680/geot.12.RL.001>.
21. **Smith, I.M., Griffiths, D.V. and Margetts, L., 2014.** *Programming the finite element method.* 5<sup>th</sup> edition, John Wiley and Sons, Chichester, UK.
22. **SPENCER, E. (1967).** “A Method of Analysis of the Stability of Embankments Assuming Parallel Inter-Slice Forces,” *Geotechnique*, Vol. 17, No. 1, 11–26.
23. **Tamotsy Matsui and Ka-ching San:**Finite element slope stability analysis by shear strength reduction technique.12 page.
24. **TERZAGHI, K., and PECK, R. B. (1967).** *Soil Mechanics in Engineering Practice*, 2nd ed., Wiley, New York.
25. **US Army Corps of Engineers "Slope Stability"** (PDF).. Retrieved 15 April 2015.
26. **Zienkiewicz, O.C. and Corneau, I.C., 1974.** Visco-plasticity-plasticity and creep in elastic solids-a unified numerical solution approach. *International Journal for Numerical Methods in Engineering*, 8, 821-845. <https://doi.org/10.1002/nme.1620080411>.